



Proceedings
of the
6th International Geologica Belgica Congress

GB2018 GEOLOGY SERVING SOCIETY

KU Leuven, Belgium

12-14 September 2018



KU LEUVEN



Geologica Belgica

Geologica Belgica Conference Proceedings

VOLUME 3 (2018)
date of publication September 2018

6th International Geologica Belgica Congress
12-14 September 2018 – Leuven, Belgium

GB2018 GEOLOGY SERVING SOCIETY
Conference program & abstract book

Volume editors

Jan ELSSEN, Niels HULSBOSCH and Peter STASSEN

KU Leuven, Division of Geology
Celestijnenlaan 200E, 3001 Leuven-Heverlee, Belgium (jan.elsen@kuleuven.be)

ISBN 978-2-9601402-2-4

Available online <https://doi.org/10.20341/gbcp.vol3>

Journal editor

Annick ANCEAU – University of Liege, Dep. ARGENCO / Gemme-Geo3
Bât. B52/3 – 4000 Liège, Belgium (a.anceau@uliege.be)

Publication address: Geologica Belgica, Jenner street 13, B-1000 Brussels, Belgium
© Geologica Belgica

ISSN (online) 2593-6670

Verantwoordelijke uitgever:
A. ANCEAU
Jennerstraat 13
1000 Brussel

Editeur responsable :
A. ANCEAU
Rue Jenner 13
1000 Bruxelles

INTRODUCTION

The organisation of the Congress

The ‘6th Geologica Belgica 2016’ congress was held at the University of Leuven, from the 12th to the 14th of September 2018. This congress was organised under the supervision of the scientific association ‘Geologica Belgica’. It aimed to gather Belgian and international researchers active in Earth Science disciplines in Belgium. This 6th Geologica Belgica international congress was organized under the general theme “Geology serving society”. Nevertheless, a wide range of Earth Science disciplines has been covered during the congress, including, but not restricted to paleoclimatology, geo-energy & reservoirs, hydrogeology, geomaterials and ore geology, geoenvironment, geohazards, deep geological processes, stratigraphy and sedimentary geology, early and past life, plate tectonics and structural geology, geoheritage, geoeducation and geoarcheology.

The scientific committee of the congress was composed by:

- Jean-Marc Baele (Université de Mons, Belgium)
- David Lagrou (Vlaamse Instelling voor Technologisch Onderzoek, Belgium)
- Thierry Camelbeeck (Observatoire Royal de Belgique, Belgium)
- Philippe Claeys (Université Libre de Bruxelles, Belgium)
- Marc De Batist (Universiteit Gent, Belgium)
- Mieke De Craen (Studiecentrum Mol, Belgium)
- Sophie Decrée (Royal Belgian Institute of Natural Sciences, Belgium)
- Jan Elsen (Katholieke Universiteit Leuven, Belgium)
- Jacqueline Vander Auwera (Université de Liège, Belgium)
- Johan Yans (Université de Namur, Belgium)

The organizing committee of the congress was composed by:

- Rudy Swennen Professor KULeuven
- Gert Jan Weltje Professor KULeuven
- Robert Speijer Professor KULeuven
- Philippe Muchez Professor KULeuven
- Jan Elsen Professor KULeuven
- Rieko Adriaens Post-doc KULeuven
- Hannes Claes Post-doc KULeuven
- Niels Hulsbosch Post-doc KULeuven
- Peter Stassen Post-doc KULeuven
- Jeroen Soete Post-doc KULeuven

This event was a real success. During the three days of the congress, 86 scientific talks and 74 posters were presented by national and international researchers, 156 participants have registered for the congress.

The best student poster of the congress was awarded to Alexander Clark (KU Leuven; Fig. 1) for his poster on ‘*Campanile giganteum* (Lamarck, 1804) from the middle Lutetian (~45 Ma) Paris basin: a potential seasonality archive?’ with co-authors Johan Vellekoop, Niels De Winter, Philippe Claeys, Peter Stassen & Robert P. Speijer.

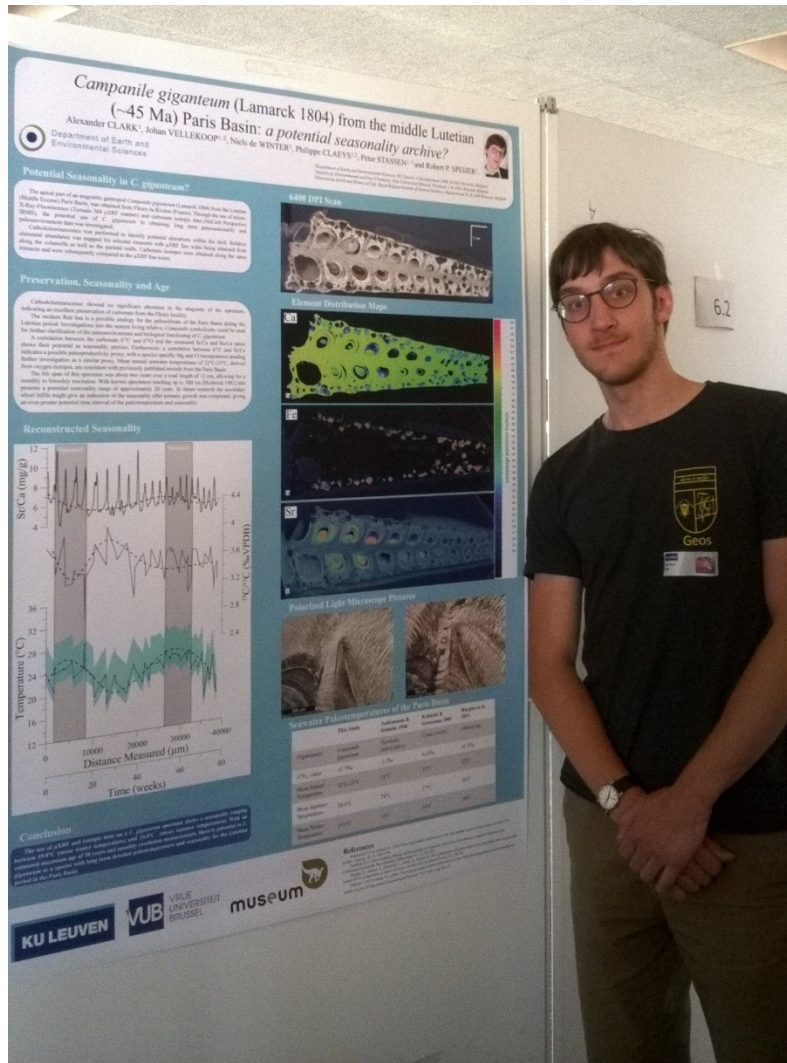


Figure 1. Alexander Clark (winner of the best poster award) and his poster.

GEOLOGICA BELGICA MEETING 2018 PROGRAMME

Each Session of the GB Meeting was devoted to one of the seven following themes.

Theme 1. Visualizing and monitoring the earth: natural and anthropogenic processes

During the last decade, improvement and miniaturization of geophysical instruments and techniques together with improved computer facilities helped analyzing huge amount of data, allowing for 3-D to 4-D visualization and monitoring of processes at the Earth's surface.

We propose to convene a session on: "Geophysical and geodetic monitoring of natural and man-induced processes". The session welcome contributions devoted to the use of geophysical and geodetic methods to image and monitor natural or man-induced processes like those involving earthquakes, volcanoes, geothermal or hydrological systems, landslides or rock mass movements, etc.

Theme 2. Understanding planets through magmatic differentiation

Magmatic differentiation processes, such as crystal fractionation, mixing, assimilation or immiscibility modify the composition of primary magmas that were produced by partial melting of their source. These processes produce distinctive geochemical signatures characterized by marked elemental enrichments and/or depletions as well as specific isotopic compositions. As such, parts of the crustal rocks are among the most fractionated on Earth.

The session will combine case studies of magmatic differentiation observed during the full evolutionary range starting from the formation of the solar system and meteorites, the partial melting of the upper mantle and lower crust, up to the formation of upper crustal melts. Particular attention will be given to the identification of mechanisms responsible for the elemental and isotopic signatures of melts and for the establishment of distinct chemical reservoirs in planetary systems, to results from experimental petrology, and to mechanisms involving fluids.

Theme 3. New developments in geology and their role in future research

New developments in analytical techniques and experimental research, new insights in mathematical and computer models and new sampling and imaging techniques had and will continue to have a major impact of our understanding of geological processes. In this theme these new developments and their possible role in different fields of geology and closely related fields such as archaeometry and physical geography are presented.

Theme 4. Geo-resources, -materials and –energy in a circular economy

The steady increase in the world's population urges us to produce more and more geological resources that serve as the basis for life in our modern-day, sustainable society. There is not only a growing demand for rare or exotic elements, used in high-tech applications, but also for resources, which were thus far considered as common (e.g., Mg-minerals, fluorite, etc.). The supply of many of these materials may become problematic in the near future, which stimulates both geological

exploration and mining industry, even in EU countries. This theme of the conference is aimed at promoting discussion of strategies to address challenges in innovating and developing geo-energy and geo-resources extraction, and greenhouse mitigation measures. Chain strategies and innovative technologies are key aspects of a sustainable economy. Supporting the cradle to cradle loop scientifically is imperative to lower our environmental footprint and to sustain utility and material reserves for society. Building a better future starts with being front runners in recycling and with actively expanding our circular economy.

Theme 5. Hydrology and environmental geology for the future

Studies on hydrogeology and environmental geology serve society in multiple ways, contributing to sustainable management and use of both soil and groundwater. Contributions about soil and shallow groundwater as well as studies on deep groundwater are thus warmly invited for this session. In addition, field studies, characterization techniques, advances in numerical modeling and management studies are of high interest.

The following main topics will be addressed:

Groundwater and soil in a changing environment: consequences of land use and climate change, sustainable use and management of soil and groundwater

Soil and groundwater pollution and environmental geochemistry

Shallow and deep geothermal applications and its relation to groundwater

Advances in characterization and modeling methods in hydrogeology and environmental geology

Groundwater in complex settings: heterogeneous aquifers, such as karstified and fissured reservoirs, transboundary aquifers a.o.

Theme 6. Biotic and climatic evolution and paleoenvironments through time

Environmental and climate changes are a pervasive part of Earth's history and illustrate how the biosphere and geosphere operate on geological time scales. Earth's surface processes are thus not static entities as these react dynamically to biotic and abiotic forcing related to e.g. major devastating events, geo-hazards, evolutionary innovations and adaptations to paleoceanographic or climate changes. Documenting these dynamics in a multidisciplinary approach is essential to understand the evolution of natural processes during various climate states and time scales. This session is open for all contributions involving the integration of biotic, geochemical and lithological data through time and space, which can also provide insight into possible future trajectories during the present millennium.

Theme 7. Lessons to be learned from geoarchaeology

The field of geoarchaeology focuses on the development and application of exact scientific techniques on a wide range of archaeological questions and materials. Providing analytical data for archaeology is an application oriented field for geoscientists which enhances our understanding of the dynamic interactions between environmental changes and the evolution of human cultures and economies. The session aims to present the full spectrum of geological activities in the field

including, but not limited to, material characterisation, provenance studies, reconstruction of production technologies, archaeochronometry, geophysical prospection, remote sensing, earthquake archaeology, human-environment interactions, paleoenvironment, and palaeoclimate studies.

SESSION PROGRAM

Wednesday 12 September: ice breaker party

Thursday 13 September

8.15 Welcome Participants

9.00 Introducing the conference

9.15 Invited speaker 1; **Frank Melcher** (Leoben – Austria)

“Certification of conflict minerals in the Great Lakes Region: Theory and the Truth”

Session 1 A Theme 5 (chair: Marijke Huysmans)

10.00 Mathias Possemiers: Validating an ATES feasibility map and studies using operational and field data.

10.20 Kevin Gonze: Flow and heat transfer numerical modelling in the Hainaut limestone geothermal reservoir: study at local and regional scales.

10.40 Hannes Claes: Towards arsenic background and remediation threshold values in rocks, sediments and soils of southwest Luxembourg.

Session 1 C Theme 2 (chair: Niels Hulsbosch)

10.00 Bernard Charlier: Crystallization of the lunar magma ocean and the primordial mantle-crust differentiation of the Moon.

10.20 Hugues Beunon: Zinc behavior during mantle melting: a reappraisal of natural and experimental observations.

10.40 Jacqueline Van der Auwera: Where and how magma differentiated at La Picada stratovolcano (CSVZ, Chile).

Session 1 D Theme 6 (chair: Peter Stassen)

10.00 Alain Blicq: From Ediacaran to Devonian - The Great Early-Middle Palaeozoic Biodiversification as a ‘Half-Horst’ Model.

10.20 Julien Denayer: An Eifelian story of reefs and reef builders: the Belgian case re-investigated.

10.40 Valentin Fisher: Evolution of the Cretaceous short-necked plesiosaurians.

11.00 Coffee break

Session 2 A Theme 5 (chair: Hannes Claes)

11.30 Ilse Van Keer: Approach of a regional heavy metal pollution caused by non-ferrous industry in the Campine area of Belgium.

11.50 Richard Hoffman: The double porosity of chalk and its influence on solute and heat transport.

12.10 Stijn Bos: The Balmatt project: Deep geothermal energy from the Dinantian in Mol-Donk.

Session 2 C Theme 2 (chair: Vinciane Debaille)

11.30 Olivier Bolle: Late-tectonic evolution of the Sveconorwegian (Grenvillian) orogen in Southern Norway: what do granites tell us?

11.50 Niels Hulsbosch: Mechanism for fractionation of Ta-Nb, Sn and W in granite-related metallogenic systems based on observations from the Karagwe-Ankole Belt of Central Africa.

12.10 Damien Delvaux: Late Neoproterozoic (Pan-African) reactivations in the Mesoproterozoic Karagwe-Ankole Belt (KAB) in Kivu (RDC), Rwanda and Burundi: chronological framework and paleostress field.

Session 2 D Theme 6 (chair: Robert Speijer)

11.30 Sébastien Wouters: Progressive increase in organic-matter burial and preservation from the “Weissert” event to the Faraoni event in Umbria-Marche (central Italy).

11.50 Meriem Moulana: Weathering pattern of Messinian Lithothamnium limestones: implication about paleoclimatic conditions.

12.10 Peter Stassen: Foraminiferal response to early Eocene climate variability in the North Sea Basin.

12.30 Lunch

Session 3 A Theme 7 (chair: Veerle Cnudde)

13.40 Laurent Fontaine & Géraldine Patigny: Stylistic study of a tondo portraying Charles V supported by isotope fingerprinting (alabaster) and thin-section petrography (black marble).

14.00 Sophie Verheyden: Speleothems as chronostratigraphic tool in archaeological cave sites, the Mishin Kamik (Bulgaria) cave site.

14.20 Maikel De Clercq: Drowned landscapes of the Belgian Continental Shelf: implications for northwest European landscape evolution and preservation potential for submerged heritage.

14.40 Shu Changxue: Lime-earth in China: From traditional to modern and contemporary times.

Session 3 C Theme 2 (chair: Jacqueline Van der Auwera)

13.40 Olivier Namur: Petrology of the 2015 eruption of Calbuco volcano, Chile.

14.00 Pim Kaskes: Mode of emplacement of the Chicxulub impact breccia.

14.20 Sietze De Graaff: Making sense of destruction: A geochemical investigation into the impact generated melt rocks of the Chicxulub impact structure, Yucatán, recovered during IODP-ICDP Expedition 364.

14.40 Thomas Déhais: Comparative petrographic, geochemical, and isotopic characterization of distal ejecta layers.

Session 3 D Theme 6 (chair: Marc De Batist)

13.40 Koen Beerten: Reconstructing Holocene water table dynamics from small-scale buried depressions in NE Belgium: pedological, lithological and botanical evidence.

14.00 Nore Praet: Landslide and turbidite records reveal a 2 kyr history of frequent seismic shaking in Eklutna Lake, Alaska.

14.20 Nathalie Fagel: Geochemical record of Lake Jeinimeni and environmental variability over the last centuries in Northern Chilean Patagonia.

14.40 Philipp Kempf: Sedimentary evolution of the Sagara coastal area in Japan and its potential to preserve extreme wave deposits.

15.00 POSTER SESSION

18.30 DINNER - Voltaire

Friday 14 September

8.30 Welcome Participants

9.00 Invited speaker 2; **Oli Shorttle** (Cambridge – UK)

“Preservation of geochemical variability in basalts: From source to storage”

Session 4 A Theme 7 (chair: Patrick Degryse)

9.45 Sarah Dillis: Antimony as a raw material in metal and vitreous materials making: from the Bronze Age to the Roman period.

10.05 Géraldine Fiers: Characterisation and weathering of flint from prehistoric sites in NW Belgium.

10.25 Alicia Van Ham-Meert: Sasanian lead coins – elemental and isotopic analysis.

Session 4 C Theme 1 (chair: Thierry Camelbeek)

9.45 Benoît Smets: Significant improvements provided by SfM-MVS photogrammetry for the study of active volcanism and related hazards and risks in the Virunga Volcanic Province.

10.05 Antoine Dille: Characterising drivers and mechanisms of landsliding in a tropical context – Ikoma landslide, DR Congo.

10.25 Aurelia Hubert-Ferrari: Characteristics and frequency of large submarine landslides at the western tip of the Gulf of Corinth based on a grid of 600 km high-resolution seismic profiles.

Session 4 D Theme 3 (chair: Philippe Muchez)

9.45 Timo Seemann: Resolving the Pore Structure and Phase Behavior of supercritical CD4 in Hardened Cement Pastes and Mudrocks by means of CD4 Contrast Matching Experiments: A Small Angle Neutron Scattering Study.

10.05 Laurent Lemmen: Microstructure generation and effective property estimation of materials used as radioactive waste confinement barriers.

10.25 Maxim Deprez: Using μ CT to investigate water migration during freeze-thaw experiments.

Session 5 A Theme 4 (chair: Jean-Marc Baele)

11.15 Dominique Jacques: W-Sn vein-type mineralisation in the Iberian Metallogenic Province: a kinematic relationship with oroclinal buckling.

11.35 Michèle Verhaert: The unexpected presence of supergene Cu-Pb-Ca-Zn-Fe arsenates and vanadates in Agoujgal Cu-mine (Anti-Atlas, Morocco).

11.55 Sander Wouters: Petrographic study of gold mineralization in the Karagwe-Ankole belt (Byumba, Rwanda).

Session 5 C Theme 1 (chair: Mieke Decraen)

11.15 Anne-Sophie Mreyen: Geophysical reconnaissance of an ancient landslide in the region of Malmedy– visualised by a 3D geomodel.

11.35 Pierre-Yves Declercq: 25 years of ground subsidence related to groundwater pumping for breweries in Belgium.

11.55 Jan Walstra: The GEPATAR project: GEotechnical and Patrimonial Archives Toolbox for ARchitectural conservation in Belgium.

Session 5 D Theme 3 (chair: Philippe Claeys)

11.15 Sam Poppe - An unusual patient: imaging and quantifying volcano deformation in laboratory experiments by using X-ray Computed Tomography.

11.35 Jean-Marc Baele - Laser-Induced Breakdown Spectroscopy (LIBS) for fast geochemical analysis of rocks and minerals – current state of the technique and example applications.

11.55 Rieko Adriaens: How quantitative are mineralogical data? Outcomes of the 9th Reynolds Cup contest.

12.15 Lunch

13.15 Invited speaker 3; **Rick Donselaar** (Delft – NL)

“Geogenic arsenic pollution: geological control on the occurrence and spatial distribution in the shallow aquifer domain”

Session 6 A Theme 4 (chair: Jeroen Soete)

14.00 Ruben Snellings: Transforming waste into resources: inspirational cases from Flanders.

14.20 Katrien De Nil: Explore the subsurface of Flanders with the Virtual Borehole.

14.40 Elke Jacobs: How do petrophysical and petrographical properties influence transport parameters? Examples for the Boom Clay and Eigenbilzen Sands.

Session 6 C Theme 4 (chair: Rudy Swennen)

14.00 Olivier Vopat: Geothermal use of old mines: hydrogeological challenges for predicting efficiency and impacts.

14.20 Hocine Djouder: The Silurian graptolitic black shales of the Tassili n’Ajjer plateau (Algeria): Thermal maturity evolution and origin-timing of late diagenetic illite.

14.40 Kris Welkenhuysen: Economic and environmental comparison of CO₂ storage and enhanced oil recovery project configurations in the North Sea.

Session 6 D Theme 3 (chair: Rieko Adriaens)

14.00 Gert-Jan Weltje: Porosity of uniform sands and gravels as a function of packing state and particle properties (size, roundness and sphericity).

14.20 Bram Paredis: Numerical modeling of sediment generation: characterizing parent rock's properties by digital petrography.

14.40 Koen Van Noten: Anisotropy of thermal conductivity in pelitic rock.

15.00 Coffee break

Session 7 A Theme 4 (chair: Rudy Swennen)

15.30 Michiel Duser: The demise of the natural building stone industry in Belgian Limburg, a case study on the last underground quarries of Maastricht stone.

15.50 Augustin Dekoninck: Formation of the oxidized manganiferous rocks of the Les Plattes Member (Otré Formation, Salm Group) in the Stavelot Massif: timing and weathering processes.

16.10 Johanna Van Daele: Pressure-temperature evolution during the Mesoproterozoic in the Western Domain of the Karagwe-Ankole Belt, Central-Africa.

Session 7 C Theme 4 (chair: Johan Yans)

15.30 Kris Piessens: Geological Economics: Economics, Geology and Ecosystem Earth.

15.50 Zahra Mohammadi: Petrophysical characterization associated with lithotypes in tabular travertine geobody (case study from the Cakmak quarry, Turkey).

16.10 Hannes Claes: DETECT - Determining the risk of CO₂ leakage along fractures of the primary caprock using an integrated monitoring and hydro-mechanical-chemical approach.

Session 7 D Theme 3 (chair: Gert-Jan Weltje)

15.30 Bernd Rombaut: The first regional 3D acoustic velocity model for the eastern part of Flanders (Belgium).

15.50 Pieter Haest: PyDOV brings the data back to the future.

16.10 Timothy Debacker: Subsurface mapping using gravity data during construction of the new 3D model of the Flemish subsurface (G3Dv3).

16.30 Closing session

LIST OF ABSTRACTS

Theme 1: Visualizing and monitoring the earth: natural and anthropogenic processes

- Morphometric analysis of relict patterned ground in the Campine area, NE Belgium
- 25 years of ground subsidence related to groundwater pumping for breweries in Belgium.
- Enhanced In Situ Soil Analysis: a combination of the membrane interphase probe with GCMS detection for on site component specific detection of VOC's
- Characterising drivers and mechanisms of landsliding in a tropical context – Ikoma landslide, DR Congo.
- The Ghent urban heat island effect on freeze-thaw weathering of building stones
- Characteristics and frequency of large submarine landslides at the western tip of the Gulf of Corinth based on a grid of 600 km high-resolution seismic profiles.
- Future geophysical prospections for the development of deep geothermal energy in Hainaut, Belgium
- Geophysical reconnaissance of an ancient landslide in the region of Malmedy– visualised by a 3D geomodel.
- Landslide distribution in a changing environment: focus on the Ruzizi gorges located between DR Congo and Rwanda
- Significant improvements provided by SfM-MVS photogrammetry for the study of active volcanism and related hazards and risks in the Virunga Volcanic Province.
- Tracking magma movements in the Virunga volcanic province using seismic Amplitude Ratio Analysis (SARA)
- Electric and passive seismic geophysical survey in a protected cave environment: the Bruniquel cave (France)
- The GEPATAR project: GEotechnical and Patrimonial Archives Toolbox for ARchitectural conservation in Belgium.
- NiphNet: a self-governing environmental monitoring network

Theme 2: Understanding planets through magmatic differentiation

- Zinc behavior during mantle melting: a reappraisal of natural and experimental observations.
- Crystallization of the lunar magma ocean and the primordial mantle-crust differentiation of the Moon.
- Making sense of destruction: A geochemical investigation into the impact generated melt rocks of the Chicxulub impact structure, Yucatán, recovered during IODP-ICDP Expedition 364.

- Comparative petrographic, geochemical, and isotopic characterization of distal ejecta layers.
- Late Neoproterozoic (Pan-African) reactivations in the Mesoproterozoic Karagwe-Ankole Belt (KAB) in Kivu (RDC), Rwanda and Burundi: chronological framework and paleostress field.
- Mechanism for fractionation of Ta-Nb, Sn and W in granite-related metallogenic systems based on observations from the Karagwe-Ankole Belt of Central Africa.
- Where and how magma differentiated at La Picada stratovolcano (CSVZ, Chile).
- Petrography and geochemistry of Nyiragongo volcano lavas: Implication on viscosity, velocity and associated risks in Goma city (Virunga, East African Rift)
- Mode of emplacement of the Chicxulub impact breccia.
- Petrology of the 2015 eruption of Calbuco volcano, Chile.
- Late-tectonic evolution of the Sveconorwegian (Grenvillian) orogen in Southern Norway: what do granites tell us?

Theme 3: New developments in geology and their role in future research

- How quantitative are mineralogical data? Outcomes of the 9th Reynolds Cup contest.
- Characterizing and sourcing quartz phenocrysts using cathodoluminescence: a case study in the Upper Silurian – Lower Devonian of the Rocroi inlier, Ardennes, Belgium
- Laser-Induced Breakdown Spectroscopy (LIBS) for fast geochemical analysis of rocks and minerals – current state of the technique and example applications.
- Subsurface mapping using gravity data during construction of the new 3D model of the Flemish subsurface (G3Dv3).
- Using μ CT to investigate water migration during freeze-thaw experiments.
- Tracing ancient DNA of foraminifera in tsunami deposits (GEN-EX).
- High-temperature XRD investigations of phase transformation in mineralogy: examples for clay used in ceramics and phosphate minerals.
- Belgian paleontological heritage: time for action?
- PyDOV brings the data back to the future.
- Microstructure generation and effective property estimation of materials used as radioactive waste confinement barriers.

- Stochastic image correction for pore collapse in dried Boom Clay samples.
- Numerical modeling of sediment generation: characterizing parent rock's properties by digital petrography.
- An unusual patient: imaging and quantifying volcano deformation in laboratory experiments by using X-ray Computed Tomography.
- The first regional 3D acoustic velocity model for the eastern part of Flanders (Belgium).
- Resolving the Pore Structure and Phase Behavior of supercritical CO₂ in Hardened Cement Pastes and Mudrocks by means of CO₂ Contrast Matching Experiments: A Small Angle Neutron Scattering Study.
- New Insights on Low-Temperature Redox Reactions of Hydrogen with Hematite (α -Fe₂O₃)
- Anisotropy of thermal conductivity in pelitic rock.
- Stratigraphy of the Lower Palaeozoic of the Anglo-Brabant Deformation Belt, Belgium (Part III): The Silurian of the Orneau Group in the Brabant Massif and the Ordovician-Silurian in the Condroz Inlier.
- Roughness description and characterisation of major fractures in Coniacian chalk at Wellington quarry (Arras, France).
- Porosity of uniform sands and gravels as a function of packing state and particle properties (size, roundness and sphericity).
- Microfacies analysis of a middle to upper Frasnian succession at the Lompret quarry (SW Belgium) documenting a transition from the Lion reef to deep marine Neuville and Matagne environments

Theme 4: Geo-resources, -materials and –energy in a circular economy

- Petrography and geochemistry of Cu-Zn VMS deposits of the Troodos ophiolite, Cyprus
- Relationship between continental carbonate lithotypes and their petrophysical characteristics: a case-study from the Denizli basin (Turkey)
- The radionuclide sorption potential of Neogene glauconite sands in the disposal of radioactive waste: ¹³⁷Cs sorption
- Upper stability limit of authigenic monazite in the Rocroi Inlier
- Geothermal use of old mines: hydrogeological challenges for predicting efficiency and impacts.
- DETECT - Determining the risk of CO₂ leakage along fractures of the primary caprock using an integrated monitoring and hydro-mechanical-chemical approach.

- Formation of the oxidized manganese rocks of the Les Plattes Member (Otré Formation, Salm Group) in the Stavelot Massif: timing and weathering processes.
- Explore the subsurface of Flanders with the Virtual Borehole.
- Geochemical fractionation of pegmatites from the Kabarore-Mparamirundi area (Burundi) as pathfinder to Sn-Ta-Nb pegmatites.
- Mineralogy and geochemistry of the oolitic iron ore deposit, south of tebessa- northeast algeria
- The Silurian graptolitic black shales of the Tassili n'Ajjer plateau (Algeria): Thermal maturity evolution and origin-timing of late diagenetic illite.
- The demise of the natural building stone industry in Belgian Limburg, a case study on the last underground quarries of Maastricht stone.
- How do petrophysical and petrographical properties influence transport parameters? Examples for the Boom Clay and Eigenbilzen Sands.
- Metallogeny of the Kundelungu Group in the Lufilian arc (Congo Copperbelt): insight of fluid evolution and its geodynamic context
- Origin of Cu mineralization in sedimentary breccias (Shangoluwe deposit, Democratic Republic of Congo): brittle tectonics and fluid flow related to the late to post-Lufilian orogeny
- Petrophysical characterization associated with lithotypes in tabular travertine geobody (case study from the Cakmak quarry, Turkey).
- Towards better exploitation of the shallow geothermal potential in the Brussels region
- Cation exchange properties of the Boom Clay, a study on bulk rock and fractionated samples
- W-Sn vein-type mineralisation in the Iberian Metallogenic Province: a kinematic relationship with oroclinal buckling.
- Belgian clay geo-resources and their use for making compressed earth bricks
- Clay resources in the Zeramdine basin (NE Tunisia): Physico-chemical characterization and industrial applications
- Collecting and organizing geological and mining data of the abandoned Monceau-Fontaine coal mine in order to assess geological resources
- The Q16-Maas field as geological buffer in a CCUS network
- Evaluation of mineralogical and radiological data obtained at the geothermal plant in Mol, Belgium

- Understanding the Earth for the people that inhabit it: Belgian and Flemish institutes joining hands in the framework of GeoERA
- Geological Economics: Economics, Geology and Ecosystem Earth.
- Transforming waste into resources: inspirational cases from Flanders.
- Fracturation of Lower Carboniferous carbonates in the Namur-Dinant area as analogues to the Campine-Brabant Basin
- Phyllosilicate Ar-Ar and Rb-Sr geochronology in the Gitarama-Gatumba area (Rwanda): an important Neoproterozoic influence in the Karagwe-Ankole Belt
- Pressure-temperature evolution during the Mesoproterozoic in the Western Domain of the Karagwe-Ankole Belt, Central-Africa.
- The unexpected presence of supergene Cu-Pb-Ca-Zn-Fe arsenates and vanadates in Agoujgal Cu-mine (Anti-Atlas, Morocco).
- Economic and environmental comparison of CO₂ storage and enhanced oil recovery project configurations in the North Sea.
- Petrographic study of gold mineralization in the Karagwe-Ankole belt (Byumba, Rwanda).

Theme 5: Hydrogeology and environmental geology for the future

- Seawater intrusion in coastal areas of arid and semi-arid regions
- Clays in drilling muds: technical considerations and environmental implications
- Water Balance of Beles Basin
- Hydrogeochemical characteristics of shallow groundwater in volcanic rock aquifer systems in the western and northern flanks of Mount Meru, Tanzania
- Groundwater assessment and its dynamics in Mekelle Outlier: Preliminary results, N. Ethiopia
- Investigation of zero-valent iron nanoparticle transport for groundwater remediation by means of lab-scale flow experiments
- The Balmatt project: Deep geothermal energy from the Dinantian in Mol-Donk.
- Approach of a regional heavy metal pollution caused by non-ferrous industry in the Campine area of Belgium.
- Towards arsenic background and remediation threshold values in rocks, sediments and soils of southwest Luxembourg.

- Flow and heat transfer numerical modelling in the Hainaut limestone geothermal reservoir: study at local and regional scales.
- The double porosity of chalk and its influence on solute and heat transport.
- Heavy metal contamination in thermal water springs (case study from the Babagor area, Western Iran)
- Validating an ATEs feasibility map and studies using operational and field data.
- BIMWAM Project: Building an integrated methodology for water resource assessment and management in urban coastal areas of Mindanao Island, southern Philippines
- The RESPONSE project: Reactive transport modelling of point source contamination in soils and groundwater
- Hydrogeological characterization and surface-groundwater interaction of Lake Tana basin, northwestern Ethiopia

Theme 6: The biotic and climatic evolution and the paleo-environment through time

- Depositional reconstruction of Quaternary continental carbonates in Tunceli Region (East of Turkey)
- Reconstructing Holocene water table dynamics from small-scale buried depressions in NE Belgium: pedological, lithological and botanical evidence.
- From Ediacaran to Devonian - The Great Early-Middle Palaeozoic Biodiversification as a 'Half-Horst' Model.
- Stratigraphical, palaeoecological and geochemical consequences resulting from the ostracod study close to the Frasnian / Famennian boundary in the type region for the definition of these two stages
- *Campanile giganteum* (Lamarck 1804) from the middle Lutetian (~45 Ma) Paris Basin: a potential seasonality archive?
- Palaeoecology of the Upper Tournaisian "Petit Granit": much more than crinoids!
- An Eifelian story of reefs and reef builders: the Belgian case re-investigated.
- Shelf ecosystems prior and during the PETM along the US Atlantic Coastal Plain
- Geochemical record of Lake Jeinimeni and environmental variability over the last centuries in Northern Chilean Patagonia.
- Evolution of the Cretaceous short-necked plesiosaurians.
- Sedimentary evolution of the Sagara coastal area in Japan and its potential to preserve extreme wave deposits.

- Geochemistry of Nummulites as a proxy for the Eocene paleotemperature evolution in the Southern North Sea Basin: an Ypresian test case
- A stratigraphic re-evaluation of the Maaseik Member
- Weathering pattern of Messinian Lithothamnium limestones: implication about paleoclimatic conditions.
- Landslide and turbidite records reveal a 2 kyr history of frequent seismic shaking in Eklutna Lake, Alaska.
- Sedimentological study of the Ypresian carbonate platform in Tunisian Atlas and south Pyrenean foreland basin
- Foraminiferal response to early Eocene climate variability in the North Sea Basin.
- An acme of the dinoflagellate cyst *Palynodinium grallator*, Gocht, 1970; a marker for the late Maastrichtian warming event at Northern mid-latitudes?
- Progressive increase in organic-matter burial and preservation from the “Weissert” event to the Faraoni event in Umbria-Marche (central Italy).

Theme 7: Lessons to be learned from geo-archaeology

- Drowned landscapes of the Belgian Continental Shelf: implications for northwest European landscape evolution and preservation potential for submerged heritage.
- Antimony as a raw material in metal and vitreous materials making: from the Bronze Age to the Roman period.
- Update of the natural building stone atlas for Belgian Limburg
- Historical glazes (14th-16th century CE) characterization for the development of adapted restoration materials in Morocco
- Characterisation and weathering of flint from prehistoric sites in NW Belgium.
- Stylistic study of a tondo portraying Charles V supported by isotope fingerprinting (alabaster) and thin-section petrography (black marble).
- Lime-earth in China: From traditional to modern and contemporary times.
- Provenancing Pre-Colonial Pottery in the Lesser Antilles
- Sasanian lead coins – elemental and isotopic analysis.
- Speleothems as chronostratigraphic tool in archaeological cave sites, the Mishin Kamik (Bulgaria) cave site.

ABSTRACTS

Theme 1

Visualizing and monitoring the earth: natural and anthropogenic processes

Morphometric analysis of relict patterned ground in the Campine area, NE Belgium

Koen BEERTEN¹, Erwin MEYLEMANS², Thomas MESTDAGH³, David VAN ROOIJ³, Cornelius KASSE⁴ & Jan BASTIAENS²

¹ *SCK•CEN Belgian Nuclear Research Centre, Waste and Disposal, Engineered and Geosystems Analysis, Boeretang 200, 2400 Mol, Belgium*

² *Flanders Heritage Agency, Havenlaan 88, bus 5, 1000 Brussels, Belgium*

³ *Ghent University, Department of Geology, Renard Centre of Marine Geology, Krijgslaan 281 s.8, 9000 Ghent, Belgium*

⁴ *VU University Amsterdam, Department of Earth Sciences, De Boelelaan 1085, 1081 HV Amsterdam, the Netherlands*

The Campine area (NE Belgium) is characterised by soils that mainly developed in Pleistocene sands. It is widely accepted that the region has witnessed several episodes of permafrost build-up during glacial periods. Geomorphological reconstructions applied during the last few decades aimed at determining the duration of and the climate during permafrost episodes. These reconstructions were mainly based on in-situ periglacial deformation phenomena in the shallow subsoil, such as cryoturbations and ice-wedge casts.

Recently published high-resolution LiDAR (Light Detection and Ranging) images of the Campine area revealed the presence of soil polygon networks which resemble those that can be observed in permafrost regions today. The topographic signature consists of shallow troughs, several decimeter deep, that are organised into polygons with a diameter of several decameters up to 100 m (Figure 1). The shape and size suggests that the networks consist of relict thermal contraction crack polygons or patterned ground that developed during past permafrost. In this study, we aim at determining the morphometric characteristics of the polygon networks, in order to compare them with modern analogues and ultimately obtain information on past permafrost characteristics. Understanding past permafrost would greatly help to assess the future evolution of the Campine, in view of the assessment of geological disposal systems for radioactive waste where time frames of 1 Ma are considered. Radioactive waste management in Belgium is performed by ONDRAF/NIRAS.

An area of ca. 300 km² was visually surveyed on the DEM (Digital Elevation Model), which led to the selection of a series of networks for further analysis. Individual polygons of each network were digitised using very narrow binning for altitude, and the average area of the polygons and percentage of 4-ray and orthogonal intersections within individual networks were calculated. The results were then compared with pedological and geological properties, and the obtained metrics were evaluated against those of published modern and fossil analogues. Finally, several polygon boundaries were surveyed with GPR (Ground Penetrating Radar), in order to characterise the subsoil expression of the presumed fossil contraction cracks.

The first results suggest that the characteristics of individual networks in the Campine area (mean polygon area and percentage of 4-ray and orthogonal intersections) are only weakly related to subsoil characteristics. Strikingly, the mean polygon area (ca. 3000 m²) is much higher than any of

the analogues. In addition, the percentage of 4-ray and orthogonal intersections is fairly low in comparison with the analogues. Finally, the subsoil signature of the polygon boundaries is only weakly expressed on shallow GPR images.

Several explanations can be put forward to understand this discrepancy between Campine polygon networks and their analogues. One possibility is that the observed networks represent an immature stage of ice-poor permafrost – this explanation is in line with the morphometric analysis. Another explanation would involve the detection method. The analogues, whether modern or fossil, are all systematically mapped using aerial imagery or field observations, whereas the Campine polygons are mapped using LiDAR images. It thus cannot be excluded that the topographic expression of so-called higher order polygons inside the main polygon is obliterated by posterior earth surface processes. In the absence of a clear subsoil expression on GPR images, which is likely due to the very weak difference in dielectric properties between wedge and host material, we conclude that trenching is needed as ultimate verification tool.



Figure 1. Mapped polygons at site Tikkebroeken (Kasterlee, NE Belgium).

25 years of ground subsidence related to groundwater pumping for breweries in Belgium

Pierre-Yves DECLERCQ, Jan WALSTRA & Xavier DEVLEESCHOUWER

Geological Survey of Belgium, OD Earth & History of Life, Royal Belgian Institute of Natural Sciences, Jennerstraat 13, B-1000 Brussels, Belgium

Persistent Scatterer Interferometry (PSI) is a valuable technique for studying ground deformation in Belgium and providing more information on their spatial and temporal patterns. In this work, about 700 SAR images of different tracks from the European satellites ERS (1992-2001), ENVISAT (2003-2010), SENTINEL 1 (2014-2018) were processed. TerraSAR-X data covering the time span 2012-2014 and the area of Brussels were processed as well. A mapping of the annual average velocity of the PS of the entire period highlighted already known ground movements discovered during country scale levelling campaigns. But thanks to its millimetre precision, it permitted to highlight new movements that were not identified before.

Seven large subsidence or uplifting areas can be spotted from the velocity map. From north to south, the regions facing ground movements are: The West-Coast, Antwerp and along the Schelde river and estuary, the Limburg Campine coal mines basin, Merchtem-Londerzeel, the cities of Brussels and Liège as well as a large area related to the Tournai-Mons-Charleroi coal mines basin. The purpose of this work is to make an overview of the situation (observations, first interpretations) of these ground movements. The highest positive (uplift), 20 to 25 mm/year and negative (subsidence) -17 to -20 mm/year velocity values are recorded around the former Limburg coal mines areas. The movements are closely linked to the groundwater extraction needed during the exploitation time and the recharge of the mining aquifer occurring at the end of the pumping.

Among the seven highlighted zones, in Merchtem 25 Km NW of Brussels, a ground subsidence (-3 mm/year on average) is occurring since the beginning of the ERS acquisitions in 1992. Through the time (ERS, ENVISAT, TerraSAR-X and SENTINEL 1) the subsidence pattern reduces his extent and is replaced by an uplift due to the raise of the water table. Piezometers located in the deep Cambro-Silurian aquifer show a clear recharge of this aquifer since the late 1990's. The subsidence is finally reduced to a zone where three breweries are very active and pumping groundwater for the production in the Ledo-Paniselian aquifer and in the Cambro-Silurian as process water. The Stella Artois brewery located in Leuven 30 km E of Brussels is facing a ground subsidence as well clearly visible with the PSI data.

Enhanced In Situ Soil Analysis: a combination of the membrane interphase probe with GCMS detection for on site component specific detection of VOC's

Pieter BUFFEL¹, Samuel VAN HERREWEGHE², Martijn NAERT³ & Caroline DE SCHAETZEN⁴

¹⁻³. *EnISSA, Steenokkerzeel, Belgium.*

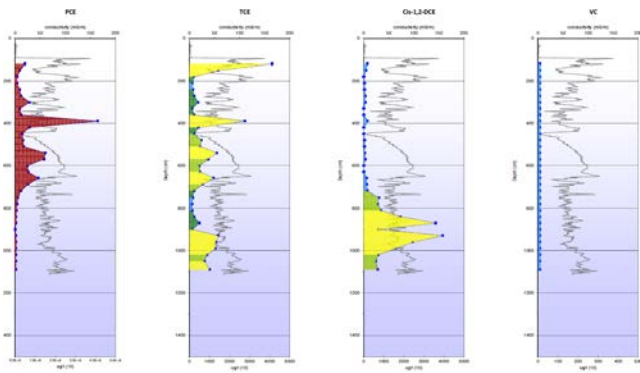
⁴. *Witteveen+Bos Belgium N.V., Steenokkerzeel, Belgium*

The success of soil investigations and remediation designs is highly depended on a solid and constantly adjusted conceptual site model (CSM). The CSM is built by collecting data from the site under investigation. The applied sampling methods and techniques of the investigation will determine the quality and accuracy of the compiled CSM.

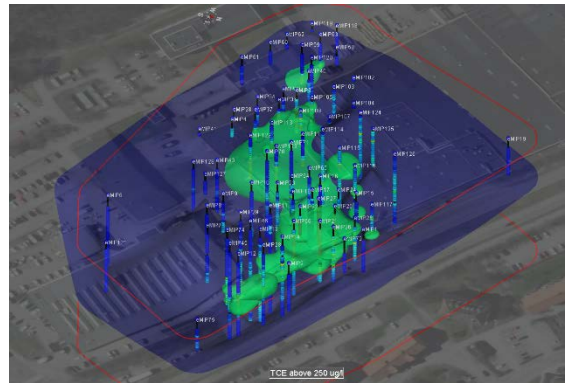
Traditional sampling methods are characterized by low detection levels and a broad and accurate analysis spectrum but despite the high accuracy and precision of the analysis at the certified labs, a large portion of the accuracy is already lost during the sampling, handling and conservation in the field. Furthermore the number of data points (samples) is often very low compared to the investigated area and volume leaving many data gaps and uncertainties. Since the soil is a very heterogeneous medium, hydrogeology and contaminant distribution can vary on a small scale (centimeters). When the scale of the applied measurement methodology does not match the small scale of heterogeneity, results will be confusing and the CSM will not reflect reality. An underestimation of the contaminated area and or pollutant load will lead to an inadequate remediation design resulting in project failure, budget overshooting and residual risks. To lower the uncertainty and improve the CSM a higher data density (and more accurate, on-site sampling and analysis methods) should be achieved. On site investigation methods, such as the well known membrane interface probe (MIP) developed by Geoprobe®, are frequently used in addition to traditional sampling methods to provide a higher data density. The MIP is used to provide a screening of semi(volatiles) over the whole profile and make on-site, real time characterization possible. Additionally, parameters describing the geology such as electrical conductivity, cone resistance and local friction can be logged at cm scale. Newer MIP probes also integrate the hydraulic profiling tool (HPT- which injects water at a constant flow and logs the pressure to achieve this. The pressure is a measure of soil permeability and the recorded data can be empirically correlated to the hydraulic permeability in m/day.

The standard MIP detector setup that is generally applied, limits the application of the MIP. The applied detectors (PID, FID, DELC or XSD) often fall short on sensitivity and specificity limiting the application to source zones. Because of the use of this summation detectors, interpretation and quantification of the signals can be difficult and frustrating. The aim of the EnISSA-MIP is to find a better balance between analytical uncertainty and spatial uncertainty by bringing high quality lab detectors to the field. To increase sensitivity and selectivity of the conventional MIP system, the EnISSA method uses a modified GCMS system which is connected to the MIP. The advantages of using a GCMS detector, are the low intrinsic detection limits of the detector and the capabilities to measure individual compounds. Field evaluations demonstrated that the EnISSA MIP is capable of measuring soil profiles for individual compounds with detection limits near 10-20 µg/l. Since

individual components are measured below the soil remediation standards, the applicability of the membrane interphase probe has substantially increased. Both source and plume delineation are possible. The component specific soil profiles allow reliable “on site” decisions and a dynamic sampling strategy. EnISSA is capable of enhancing the conceptual site model (CSM) resulting in more accurate decision making and a higher Return on Investigation (ROI).



2 EnISSA-MIP results for PCE/TCE/DCE/VC



1 TCE plume Based on EnISSA-MIP results

Characterising drivers and mechanisms of landsliding in a tropical context – Ikoma landslide, DR Congo

Antoine DILLE^{1,2}, François KERVYN¹, Gloire Bamulezi GANZA³, Guy Mawe ILOMBE³, Christian Buzera KALIKONE³, Toussaint Mugaruka BIBENTYO³, Evelyne Safari MAKITO³, Elise MONSIEURS^{1,4,5}, Damien DELVAUX¹, Benoit SMETS¹, Matthieu KERVYN² and Olivier DEWITTE¹

¹ *Department of Earth Sciences, Royal Museum for Central Africa, Leuvensesteenweg 13, 3080 Tervuren, Belgium*

² *Department of Geography, Earth System Science, Vrije Universiteit Brussel, Pleinlaan 2, 1050 Brussels, Belgium*

³ *Department of Geology, Université Officielle de Bukavu, Site Universitaire de Karhale, Kadutu, 570 Bukavu, DR Congo*

⁴ *Department of Geography, University of Liège, Clos Mercator 3, 4000, Liège, Belgium*

⁵ *Fonds de la Recherche Scientifique - FNRS, Rue d'Egmont, 5, 1000, Brussels, Belgium*

Understanding slope evolution and their related hazards relies on accurate landslide process characterisation. This ideally needs knowledge on the timing of slope deformation phases as it allows to understand the link between slope instability and environmental drivers such as seismicity and climate for instance. However, for many regions, especially in tropical environments where vegetation growth can be very quick and low-capacity data collection policy is commonplace, such information remains rare. Here we focus on a large deep-seated landslide in the landslide-prone and data-scarce Kivu rift, in eastern DR Congo. This landslide, developed in (weathered) basalt and regolith, is known for having undergone large deformations during the recent years. The location of this landslide in a seismically active tropical context, as well as the presence of recent and highly apparent deformation features at its surface make it a perfect natural laboratory to study landslide processes. Using high-resolution topography and orthomosaic obtained from Unmanned Aerial Vehicle (UAV) and Structure from Motion (SfM) photogrammetry in addition to detailed field investigations and satellite imagery allows the identification of three different landslide kinematic units that show contrasting movement styles. The presence of these different sectors highlights interactions within the landslide body (e.g. destabilisation due to material accumulation or support removal) but also the occurrence of multiple deformation episodes. The study of the evolution of the slope stability over the past two decades supports the interpretation of the landslide mechanisms. By confronting rainfall time series and major earthquake sequences to the slope evolution, we also show that the relation between instability triggers and slope deformations is not straightforward; e.g. the largest instability occurred at the end of a dry season during a period of relatively low seismicity. Instead of direct influence of external triggers, we show that some phases of instability (and related slope failures) may ultimately be caused by the intrinsic evolution of the hillslope associated with strength degradation of the slope material through time. Our results question the relative weight of the commonly recognized causes and drivers of slope instability, highlighting the relevance of considering interactions between dynamic earth processes, as well as the likely particularity of landslide processes in such tropical environment. The analysis of the landslide processes provided here will help in the evaluation of the landslide hazard in the particular

data-scarce Kivu Rift, but also across other regions of subtropical Africa and elsewhere where similar environmental conditions are met.



Figure 1. Ikoma Landslide (05.2017). Three zones representing different kinematic units are highlighted.

The Ghent urban heat island effect on freeze-thaw weathering of building stones

Daphne GUILBERT¹, Steven CALUWAERTS² & Tim DE KOCK¹

¹ PProGResS, Department of Geology, Ghent University, Belgium

² Atmospheric Physics, Department of Physics and astronomy, Ghent University, Belgium

Introduction

Climate plays a major role in the weathering of natural building stones. Many studies have focused on its impact in the past (e.g. Brimblecombe & Grossi 2009) as well as its potential impact in the future (e.g. Grossi *et al.* 2007), often with special attention for our valuable heritage which has been exposed for the longest time (e.g. Brimblecombe, 2010). This work specifically investigates the influence of the urban heat island in Ghent on the weathering of Savonnières limestone by climatic analysis and both laboratory and computational simulations.

Climatic analysis

The climatic data of six places in and around the city of Ghent, situated in the northwest of Belgium, is provided by the MOCCA project (Caluwaerts and Termonia 2016) from 01/07/2016 until 30/06/2017. Parameterization of this climatic data leads to the evaluation of the difference in climate between urban and rural locations in Ghent. The main difference between both environments is the higher temperature, due to the urban heat island, and the lower wind speed in the city centre. The higher temperatures result in a decrease in the number of freeze-thaw cycles, the intensity of these cycles and the number of wet-frost days, thereby evidencing the decrease of freeze-thaw weathering potential in urban environments for moderate Cfb climates. The numbers are very comparable to what has been reported for a changing climate by Grossi *et al.* (2007). The lower wind speed leads to a lower wind-driven precipitation load and thus to less deep penetration of precipitation in the stone.

Laboratory simulations

Different freeze-thaw cycles were simulated in a climatic chamber for Melle (rural) and the Sint-Bavo School (urban), on an isolated wet and oven-dried Savonnières limestone sample. The temperature in the wet stone shows a zero curtain effect, which is due to the release of latent heat as a consequence of the phase transition of liquid water to ice. Only at Melle, this zero-curtain effect is breached and the stone cools further below zero, illustrating the intensity difference (Fig. 1a). Moreover, these simulations reveal that the impact of the urban heat island is biggest for freeze-thaw cycles under an open sky (UV-radiation as a proxy), where the higher intensity of a rural environment is tempered by the urban heat.

Delphin Simulations

Full year simulations of the Melle and Sint-Bavo School climates on Savonnières in the HAM-simulation program Delphin indicate differences in terms of temperature, moisture content, ice crystallization and freeze-thaw cycles. The outcome of these simulations is in accordance with the

previous analysis, indicating shallower and less freeze-thaw cycles inside an urban stone (Fig. 1b). The higher moisture content in the Melle stone is a consequence of the higher amount of wind-driven precipitation at this location, which leads in combination with a lower temperature, to more and deeper ice crystallization, resulting in a higher probability of ice damage in this rural stone.

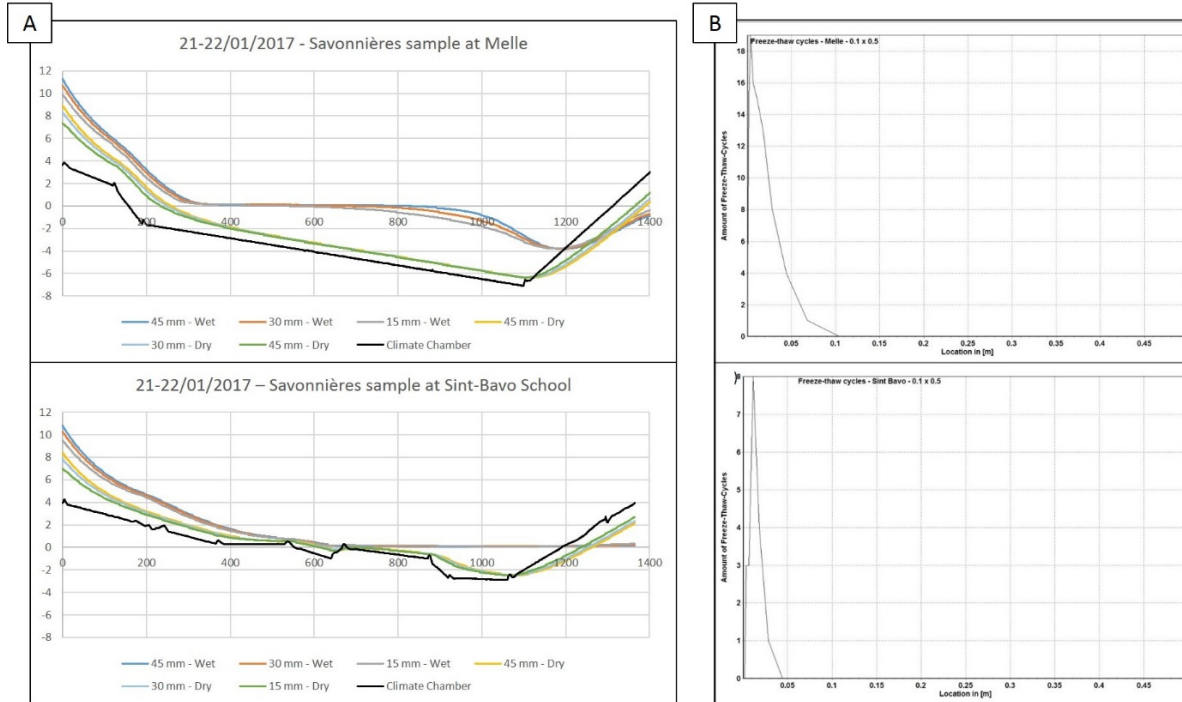


Figure 1. A) Temperature evolution of the climate chamber and inside both an isolated wet and dry Savonnières sample during the 21-22/01/2017 freeze-thaw cycle in Melle (rural, top) and at Sint-Bavo School (urban, bottom); B) Number of freeze-thaw cycles during the 2016-2017 winter in Savonnières limestone in Melle (top) and at Sint-Bavo School (bottom).

Conclusion

The climate analysis, experimental observations and computational simulations lead to the general conclusion that building stones in urban environments in a Cfb climate experience less freeze-thaw cycles and ice crystallization compared to stones in rural environments. The use of more years, or generation of reference years for both environments will allow further quantification of this effect. Moreover, since the obtained numbers are comparable to the projected impact of climate change reported in literature, it shows that the urban heat should be considered as very relevant in future work considering building stone weathering.

References

Brimblecombe, P., 2010. "Heritage Climatology." P. 7 in Climate change and cultural heritage, edited by R. Lefevre and C. Sabbioni. Bari.

- Brimblecombe, P. & Carlota M. G., 2009. "Millennium-Long Damage to Building Materials in London." *Science of The Total Environment* 407(4), 1354–61. Retrieved <http://linkinghub.elsevier.com/retrieve/pii/S0048969708010206>.
- Caluwaerts, S. & Termonia, P., 2016. "Urban Projects Monitoring the Urban Climate of the City of Ghent, Belgium." *International Association for Urban Climate*, 16, 15–20.
- Grossi, C. M., Brimblecombe P. & Harris, I., 2007. "Predicting Long Term Freeze–thaw Risks on Europe Built Heritage and Archaeological Sites in a Changing Climate." *Science of the Total Environment*, 377, 273–81.

Characteristics and frequency of large submarine landslides at the western tip of the Gulf of Corinth based on a grid of 600 km high-resolution seismic profiles

Aurelia HUBERT-FERRARI¹, Arnaud BECKERS², Christian BECK³, George PAPANICOLAOU⁴, Marc de BATIST⁵, Dimitris SAKELLARIOU⁶, Efthymios TRIPSANAS⁷ & Alain DEMOULIN¹

¹*Department of Geography, University of Liège, allée du 6 août 2, 4000 Liège, Belgium.*

²*CSD Engineers, Namur Office Park 2, Avenue des dessus de Lives, 5101 Namur, Belgium*

³*ISTerre, CNRS UMR 5275, University of Savoie, F-73376 Le Bourget du Lac, France.*

⁴*Department of Geology, University of Patras, Patras, Greece*

⁵*Department of Geology and Soil Science, Ghent University, Ghent, Belgium*

⁶*Institute of Oceanography, Hellenic Center for Marine Research, GR-19013 Anavyssos, Greece*

⁷*Hellenic Petroleum, Exploration and Production of Hydrocarbons, Marousi, Greece*

Coastal and submarine landslides are frequent at the western tip of the Gulf of Corinth, where small to medium failure events (10^6 - 10^7 m³) occur on average every 30-50 years. These large sliding events mainly result from slope failures in, or close to, the submarine Gilbert-type fan-deltas. These deltas are 400m high, have steep 15° to 35° delta fronts incised by gullies and bordered by active faults running along or near the coastline (Becker et al., 2015). Slope failure trigger tsunamis, and consequently represent a significant hazard.

We realize here an inventory of the large mass transport deposits (MTDs) that result from submarine landslides based on geophysical data acquired by the Renard Center of Marine Geology of the University of Ghent with a "CENTIPEDE" Sparker seismic source combined with a single-channel high-resolution streamer as receiver. In the high-resolution seismic profiles, mass transport deposits have been identified based on their typical seismic facies made of discontinuous to chaotic reflections

Most of mass wasting deposits are clustered and are defining multi-MTDs temporal "events", based on common un-deformed underlying or overlying reflections that can be followed across the basin. Six large sliding events are identified, and their associated deposits locally represent 30% of the sedimentation since 130ka in the main western Basin. The definition of sliding events reflects here a clustering of submarine landslides in a relatively short period of time. The most recent sliding event demonstrates that MTDs grouped within the same event may not occur at the same moment. By contrast, the synchronicity of different submarine landslides has been suggested for 3 other sliding events from the complex shape of the large MTDs they include and suggests an earthquake triggering. The average recurrence interval for large earthquakes (Mw 6-7) has been estimated in the central part of the Gulf of Corinth at ~500 yr during the Holocene, and ~400 yr for the period 12-17 ka (Campos et al., 2013). Therefore, large sliding events in the westernmost Gulf of Corinth were less frequent than Mw 6-7 earthquakes, during both the Holocene and the last glacial period. Consequently, while large earthquakes could have triggered some sliding events, other factors contributed to the occurrence of such large sliding events.

Processes that might have "pre-conditioned" or triggered sliding events in the Gulf of Corinth need to show a return period of at least 2.5 ka over the last 12 ka in order to fit the sliding event frequency. Two likely main pre-conditioning factors have been identified. The first one is the reloading time of slopes, which varied with the sedimentation rate. Average sedimentation rate (excluding the thickness of MTDs) reaches ~2.4 mm/yr for the Holocene and ~ 0.4 mm/yr for the previous 120 kyrs. This is in line with the fact that only one large sliding event was recorded during the ~60 ky-long Last Glacial. In addition, sedimentation supply was not constant during the Holocene. Fuchs (2007) identified two main phases of land degradation between 6.5 and 8.5 ka, and from ~4 ka onwards. Two sliding events occurred at the end of these periods of high sediment supply. The second pre-conditioning factor is sea level changes and the associated modification in water circulation. At 10-12 ka, the rising waters in the Ionian Sea flooded the "Lake Corinth", the sea level continued to increase from ca. -60 m to its present elevation until 5.5-6 ka, and bottom currents appeared in the study area (Beckers et al., 2016). The deposition of sliding event occurred at 10-12 ka, when these dramatic changes in water depth and water circulation that occurred. We conclude that the overall temporal distribution of MTDs result from the time-dependent evolution of pre-conditioning factors, rather than from the recurrence of external triggers.

Finally, it is likely that these sliding events have triggered large tsunami waves in the whole Gulf of Corinth, in some cases much larger than those reported in historical sources. Indeed one MTD stands out as a particularly large feature (a little less than 1 km³ in volume). This is about two orders of magnitude larger than the range previously proposed for the size of submarine landslides in the westernmost Gulf of Corinth.

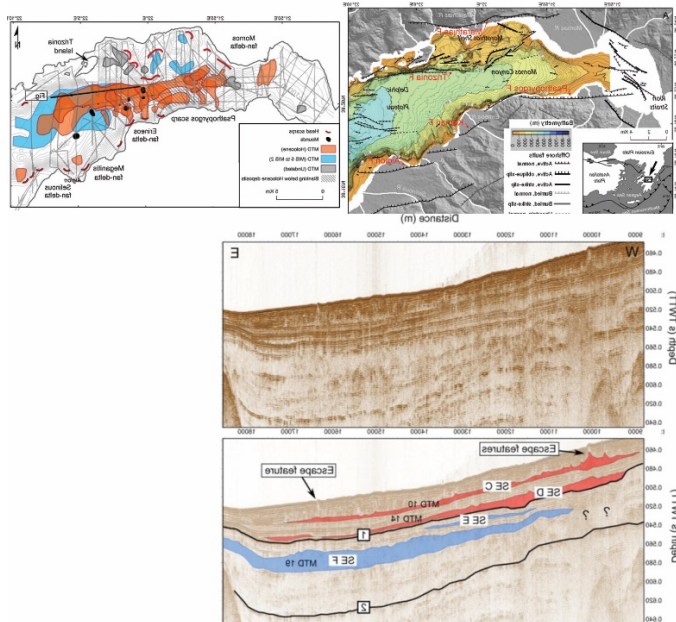


Figure. Top left: Study area; Top right: Inventory of mass transport deposits (MTDs) at the westernmost Gulf of Corinth for the last ca. 130 ka; Bottom: E-W Sparker seismic profile showing the mass transport deposits imaged.

References

- Beckers, A., Hubert-Ferrari, A., Beck, C., Bodeux, S., Tripsanas, E., Sakellariou, D., & De Batist, M., 2015. Active faulting at the western tip of the Gulf of Corinth, Greece, from high-resolution seismic data. *Marine Geology*, 360, 55-69.
- Beckers, A., Beck, C., Hubert-Ferrari, A., Tripsanas, E., Crouzet, C., Sakellariou, D., Papatheodorou, G. & De Batist, M., 2016. Influence of bottom currents on the sedimentary processes at the western tip of the Gulf of Corinth, Greece. *Marine Geology*, 378, 312-332.
- Campos, C., Beck, C., Crouzet, C., Carrillo, E., Welden, A. V., & Tripsanas, E., 2013. Late Quaternary paleoseismic sedimentary archive from deep central Gulf of Corinth: time distribution of inferred earthquake-induced layer. *Annals of Geophysics*, 56 (6), 1-15.
- Fuchs, M., 2007. An assessment of human versus climatic impacts on Holocene soil erosion in NE Peloponnese, Greece. *Quaternary Research*, 67 (3), 349-356.

Future geophysical prospections for the development of deep geothermal energy in Hainaut, Belgium

Frank MARTIN¹, Nicolas DUPONT¹, Kevin GONZE¹, Pascal GODERNIAUX¹, Thierry MARTIN¹, Michel EVERAERTS¹, David CHARLET², Frederic HABILS² & Olivier KAUFMANN¹.

¹*Geology and Applied Geology, University of Mons, Rue de Houdain 9, 7000 Mons, Belgium*

²*IDEA (“Intercommunale de Développement Economique et d’Aménagement du Coeur du Hainaut”), Rue de Nimy 53, 7000 Mons, Belgium*

Few years ago, in 2014, the EU launched new financing funds called ERDF whose role was to strengthen economic and social cohesion in the European Union and, more importantly, make a step forward in the low-carbon economy and greenhouse gas emissions. Project MORE-GEO belongs to this movement. This is a research project on deep geothermal energy designed for district heating in the surroundings of Mons, Belgium (project GEOTHERWALL_DOUBLET 1). The project targets the geothermal resources of the Carboniferous limestone formations. It aims at developing the knowledge on this geothermal reservoir, improving the prediction of the behaviour of the geothermal resource over time and support the drilling of new wells in Mons.

In this paper, the geophysical aspects covered in the project will be exposed as well as the context in which they take place. On the one hand, seismic reflexion and gravimetry surveys are planned in order to better characterize the reservoir at the regional scale, thus leading to better constraining the geothermal reservoir model. On the other hand, a more local focus in the whereabouts of the geothermal wells and will aim at implementing solutions for the microseismic monitoring during the geothermal plant operations.

Even if former coal mining operations lead to accumulate a large amount of data about this area's underground, the knowledge about its deep geology, more specifically below the coal bearing formations, is still quite limited and is not sufficient to characterise with some precision the reservoir. Therefore, several geophysical surveys (Seismic refraction, seismic reflexion and gravimetry) are planned to characterize as accurately as possible the geometry of the geothermal reservoir and, thereafter, to design a dynamic model of the area. In the future, it will allow providing an efficient management tool for developing additional geothermal wells and optimizing the position of the injection and production wells in the reservoir.

These geophysical surveys will cover the “Coeur du Hainaut” area, around the City of Mons (South Belgium). Firstly, five 14 km long North-South seismic reflection lines distributed from Bernissart (Western line) to Obourg (Eastern line) will be carried out. Each line will be separated by intervals of approximately 5 km. This layout allows covering the entire area of interest considering the previous seismic acquisitions in this area.

Indeed, several 2D seismic reflexion lines were already carried out such as the 1986 Belcorp survey. However, the recovered data and processing were not set for a deep reservoir characterisation. In 2012, 2 seismic lines covering Mons and Estinnes from North to South were

surveyed and analysed by the same method (Dupont N. et al., 2016) and operators also reprocessed the Belcorp 1986 dataset to improve the imaging of the reservoir. To supplement these, the new seismic reflexion campaign will come first. As data will be acquired on a broader scale, these new lines will hopefully contribute to improve the understanding of the geometry and structure of the deep geothermal reservoir. The seismic reflexion campaign will be preceded by a Low Velocity Layers (LVL) acquisition along the same profiles to derive the static corrections to apply to the 2D seismic reflection dataset.

A new gravimetry survey is also planned along the seismic survey. In 2016, a preliminary work by Everaets et al (2016) consisted in building 2D density models along the 2012 seismic lines, in order to fit the Bouguer anomalies. It led to test and propose several structural interpretations but it also highlighted the low gravimetric data density along the lines. A better coverage would certainly allow more in depth processing and interpretation. Therefore, a new gravimetric prospection with data collection and processing will be performed along the seismic lines with spatial density of one measurement every vibrating point (1s/250m). A Scintrex CG-5 is planned to be used for the operations. These data will allow to complement the seismic data and better constrain the interpretations at a larger scale.

Concerning the geophysical applications focused on the geothermal doublet, they consist in the deployment of a microseismic monitoring network, in a perimeter of up to 3 km around the geothermal doublet. The reason for this installation lies in the fact that the impacts of this new exploitation by a doublet should be monitored considering the deep geothermal context. This will be a surveillance tool to quantify the possible impact of the water extraction and injection on the local microseismicity. The network will include 6 broadband seismometers, two within a 1 km radius and the 4 others within a 3 km radius of the geothermal plant. The localization of each station was based on the approach proposed by T.Kraft et al. (2013) involving geographical and seismic noise parameters. The network and processing chain will be implemented to detect and to locate micro-events in the vicinity of the doublet. In this way the monitoring of potential microseismic impacts of the geothermal production of the doublet will be highly ensured.

To conclude with, the main scope of the seismic reflexion and gravimetric campaigns is to acquire enough data to improve the reservoir modelling, especially regarding its geometry and structure. Finally, the installation of a local seismic network will ensure the monitoring of this exploitation aiming at a secured geothermal energy production.

References

- Dupont N., Kaufmann O., 2016. Exploration of the geothermal reservoirs of Hainaut (Belgium): preliminary results of the 2DMons2012 seismic survey. New deep structures revealed in the Brabant Parautochton. in 5th International Geologica Belgica Meeting, Mons, Belgium. Geologica Belgica Meeting, Mons, Belgium.
- Everaerts M., Dupont N. and Kaufmann O., 2016. Collecte et mise en forme des données gravimétriques, modélisation gravimétrique à l'échelle du territoire du Cœur du Hainaut. Internal study report. Faculté Polytechnique de Mons, Mons, Belgium.
- Kraft, T., Mignan A. and Giardini D., 2013. Optimization of a large-scale microseismic monitoring network in northern Switzerland. In Geophysical Journal International n°195 (Oxford University Press). ETH-Zurich, Switzerland, 474-490. microseismic monitoring network in northern Switzerland. In Geophysical Journal International n°195 (Oxford University Press). ETH-Zurich, Switzerland, 474-490.

Geophysical reconnaissance of an ancient landslide in the region of Malmedy – visualised by a 3D geomodel

Anne-Sophie MREYEN^{1*}, Alain DEMOULIN² & Hans-Balder HAVENITH¹

¹University of Liege, Department of Geology, Allée du six Août 14, B18, 4000 Liege, Belgium.

²University of Liege, Department of Physical Geography, Clos Mercator 3, B11, 4000 Liege, Belgium.

*Corresponding author: AS.Mreyen@uliege.be

1. Introduction

In the frame of the relaunched geological mapping project of the Walloon region, formerly unknown geomorphological structures have been discovered on the southern slopes of the Warche valley in Bévercé (region of Malmedy): a steep scarp, of 20 m height and ~ 100 m length, next to two landslides (Mreyen et al., accepted). These features developed in a Permian conglomerate formation, the *Poudingue de Malmedy*, that occupies the Malmedy Graben and lies discordant on top of Cambro-Ordovician bedrock. Roughly perpendicular to the graben axis, the scarp has a N330°E orientation similar to that of the seismotectonically active Hockai Fault Zone (HFZ) that crosses the region (Demoulin, 2006). Here, we present a detailed geophysical field survey of the bigger landslide that lies directly adjacent to the scarp. Results are integrated in a 3D model of the slope and serve as input information to remodel its subsurface in terms of structural and/or geological interfaces and volumes.

2. Methods

In order to vary exploration depth and resolution, but also to guarantee validation of results, several geophysical techniques were combined: (1) passive seismics, i.e. H/V method, recording the ambient noise of soil with a single seismic station in order to determine its resonance frequency that can be used to calculate the 1D thickness of soft soil overlying the bedrock (several tens of meters can be reached depending on the geophysical properties of subsoil); (2) active seismics, i.e. seismic refraction along a profile line (115 m, i.e. 24 geophones spaced by 5 m, reaching depths of ~ 30-40 m), analysed in terms of P-wave tomography (SRT) and 1D surface wave analysis (MASW); and (3) electrical measurements, i.e. electrical resistivity tomography (ERT), illustrating resistivity contrasts of the subsoil along a profile line (315 m, i.e. 64 electrodes spaced by 5 m, reaching depths of max. 50 m). H/V, in particular, is increasingly used in landslide studies as it can provide useful applications such as the detection of basal slip surfaces (e.g. Pazzi et al., 2016).

3. Results

Results of data interpretation were compiled in a 3D geological-geophysical model supported by high resolution remote sensing data of the ground surface (i.e. 1 m resolution LiDAR-data provided by the Walloon region). By the interpolation of such information, we are able to characterise the soil of the study area in depth.

Fig. 1 represents the surface- (with projected orthophoto) and geomodel of the bigger Bévercé landslide, together with interpolated surfaces based on H/V measurements (detected interfaces in the subsoil deduced by measured impedance contrasts) and seismic as well as electric tomographies

(due to significant contrasts in velocity or resistivity, respectively). Also, on the scarp and in its prolongation, a supposedly tectonic shift of bedrock could be imaged and was integrated as fault plane in the geomodel. On the basis of the constructed surfaces, volumes representing stratigraphic or geological units were computed. We could thereby differentiate between in-situ rock, i.e. conglomerate lying on top of the bedrock, and the supposed mass of landslide (i.e. failed mass) that is marked by reduced seismic velocities (in terms of both, P-wave and S-wave velocity).

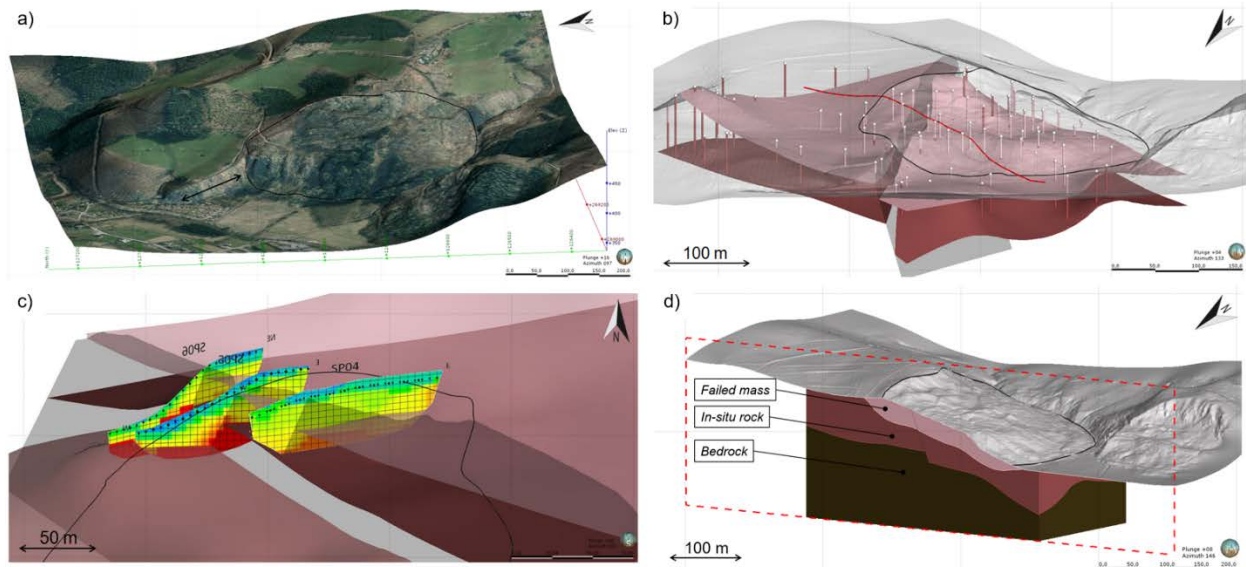


Figure 1. Geomodel of the Bévercé slope: a) surface model with projected orthophoto; b) interpolated surfaces on the basis of H/V measurements; c) modelled fault plane in line with seismic velocity contrasts; d) section of modelled volumes along red line shown in b.

4. Acknowledgements

We thank the Fund for Research Training in Industry and Agriculture (FRIA/F.R.S.-FNRS, Belgium) for supporting Anne-Sophie Mreyen with a PhD fellowship.

5. References

- Demoulin, A., 2006. La néotectonique de l'Ardenne-Eifel et des régions avoisinantes. Acad. R. Belg., Mém. Classe Sci., 25, 252.
- Mreyen, A.-S., Demoulin, A. & Havenith, H.-B. Seismotectonic activity in East Belgium: relevance of a major scarp and two associated landslides in the region of Malmedy. *Geologica Belgica*, accepted.
- Pazzi, V., Tanteri, L., Bicchocchi, G., D'Ambrosio, M., Caselli, A., & Fanti, R., 2016. H/V measurements as an effective tool for the reliable detection of landslide slip surfaces: Case studies of Castagnola (La Spezia, Italy) and Roccalbegna (Grosseto, Italy). *Physics and Chemistry of the Earth, Parts A/B/C*.

Landslide distribution in a changing environment: focus on the Ruzizi gorges located between DR Congo and Rwanda

Toussaint MUGARUKA BIBENTYO^{1,2}, Antoine DILLE³, Matthias VANMAERCKE¹ & Olivier DEWITTE³

¹*University of Liège*

²*Université Officielle de Bukavu*

³*Royal Museum for Central Africa*

The conversion of natural ecosystems into agricultural or urban areas can be accompanied by changes in geomorphological processes. This is common in areas where environmental conditions naturally predispose landscapes to landslides. Here we focus on the Ruzizi gorges, a region of the western branch of the East African Rift known for being affected by landslides and where the development of the city of Bukavu (DR Congo) and the establishment of regional hydroelectric dams have disturbed the landscape over the last decades. The aim of this research is to understand the regional spatio-temporal distribution of landslides in this context where the scarcity of information on geomorphological processes is commonplace. Data from field observations, historical aerial photographs, satellite imagery and archive analysis are combined to produce a multi-temporal inventory of 149 landslides over an area of 94 km². The largest (up to 2 km²) and oldest landslides precede clearly human induced-changes of the last 60 years. There are made of slides (planer and rotational) and topography, lithology (through weathering of volcanic formations) and river incision linked to Lake Kivu formation (~10 kyr BP) explain their distribution. The other landslides (52% of the inventory) have occurred in the last six decades. Most are flow-like landslides including flow slides, earthflows, debris avalanches and debris flows; the remaining being rotational and planer slides. These most recent (and often less deep) landslides are mostly controlled by topography. For the shallow ones, a regional control of land use is also identified. These recent landslides are either triggered by rainfall or the result of slope evolution (potentially human-disturbed) where a clear trigger is absent. Further work will be needed to decipher in a more quantitative way the impact of human disturbance on recent landslide occurrence.

Significant improvements provided by SfM-MVS photogrammetry for the study of active volcanism and related hazards and risks in the Virunga Volcanic Province.

Benoît SMETS¹, Lore STEYAERT², Caroline MICHELLIER¹, Adalbert M. SYAVULISEMBO^{1,3,4}, Gustave MUNGUNGA⁵, Julien BARRIÈRE⁶, Nicolas D'OREYE^{6,7} & François KERVYN¹

¹Royal Museum for Central Africa, 13 Leuvensesteenweg, B-3080 Tervuren, Belgium.

²Vrije Universiteit Brussel, 2 Pleinlaan, B-1050 Brussels, Belgium.

³Université Libre de Bruxelles, 50 Avenue Roosevelt, B-1050 Brussels, Belgium.

⁴Goma Volcano Observatory, 142 Avenue Rond-Point, Goma, D.R. Congo.

⁵Institut Géographique du Congo, 142 Avenue Rond-Point, Goma, D.R. Congo.

⁶European Center for Geodynamics & Seismology, Walferdange, Luxembourg.

⁷National Museum of Natural History, Walferdange, Luxembourg.

Satellite remote sensing is sometimes the best way to get information on areas where no field data exist and where the socio-political instability recurrently prevents the use of ground-based approaches. This is for example the case in the North Kivu province, D.R. Congo. The ~800,000 inhabitants of the city of Goma are directly threatened by one of the most active volcanoes on Earth, i.e., Mount Nyiragongo. The scientific knowledge on this volcano remains limited compared to other hazardous volcanoes and the direct observation of its current eruptive activity, which corresponds to the presence of a persistent lava lake in its summit crater, is difficult to implement. Consequently, the proper assessment of volcanic hazards and risks in this region remains also limited. If remote sensing is already used to study and monitor Nyiragongo, the tropical environment of this region of Central Africa strongly restricts its proper application. The frequent cloud cover and the volcanic gas emissions most of the time prevent the use of optical imagery, such as Sentinel-2, Landsat, SPOT or Pléiades products. In addition, the dense vegetation on the flanks of the volcano limits the observation of ground deformation by SAR interferometry (InSAR) to some parts of the volcanic field. Since 2013, we have taken advantage of the UAS (or “drone”) technology and the helicopter support provided by the United Nations (UN) to the Goma Volcano Observatory (OVG) and the Congolese Geographic Institute (IGC) to acquire different sets of cloud-free optical images at low altitude, over Nyiragongo and the surrounding inhabited areas. In this work, we present the main applications developed using ground-based and airborne Structure-from-Motion Multi-View Stereo (SfM-MVS) photogrammetry.

Using time-lapse camera systems temporarily installed on top of Nyiragongo, annual airborne photogrammetric surveys and innovative SAR measurements, we are able to measure the Nyiragongo lava lake level fluctuations at different time scales, allowing the description and interpretation of different types of lake level variation, such as gas piston cyclic variations (Smets et al., 2017), sporadic magma pressure-driven level changes and long-term trend changes (Smets, 2016). The annual 3D modelling of the Nyiragongo crater performed since 2013 using helicopter- or drone-based SfM-MVS photogrammetry allows us to quantify the ground deformation

associated with the lava lake activity, the volume of lava accumulated in the crater and some erosion processes along the crater flanks (Smets, 2016; Fig. 1).

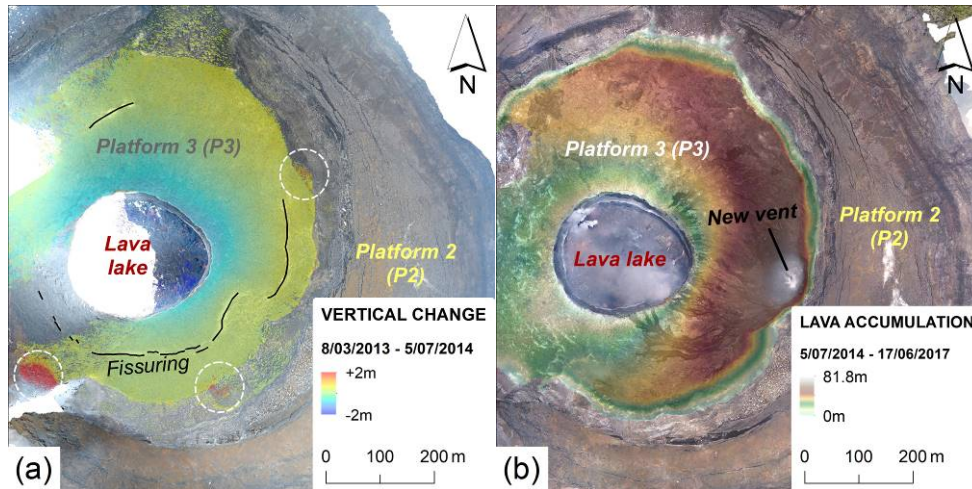


Figure 1. Volume changes detected at the bottom of the Nyiragongo crater, by comparison of digital elevation models. (a) Ground subsidence associated with a 2-year long lava lake level drop. White dashed circles highlight debris deposits. (b) 2014-2017 lava flow accumulation in the Nyiragongo crater.

For the city of Goma and its vicinity, we took advantage of the UN helicopter support to fly over the urbanized areas and test the feasibility of acquiring a very-high resolution (VHR) orthomosaic with consumer-grade cameras and SfM-MVS photogrammetry. The result led to an orthomosaic (17.5 cm/pixel) and a digital elevation model (35 cm/pixel) over an area of ~ 140 km² (Smets et al., 2018). The VHR orthomosaic is already used by the staff of the OVG and IGC for the development of a wide range of mapping applications, including cadaster delimitation, building and road type identification, population distribution, etc., hence contributing to improve urban planning and volcanic risk management. Here, we show that the orthomosaic can also be exploited to improve the mapping and interpretation of volcanic features, including mazuku, i.e., lethal diffuse dry gas vents located in urbanized areas along the Lake Kivu northern shoreline.

References

- Smets, B., 2016. Dynamics of volcanic activity in a youthful extensional setting studied by means of remote sensing and ground-based monitoring techniques: Nyiragongo and Nyamulagira volcanoes (North Kivu, D.R. Congo). Unpublished Ph.D Thesis. Vrije Universiteit Brussel, Belgium, 240 p.
- Smets, B., d'Oreye, N., Kervyn, M., Kervyn, F., 2017. Gas piston activity of the Nyiragongo lava lake: first insights from a Stereographic Time-Lapse-Camera system. *Journal of African Earth Sciences*, 134, 874-887. doi:10.1016/j.jafrearsci.2016.04.010
- Smets, B., Michellier, C., Syavulisembo, A.M., Munganga, G., d'Oreye, N., Kervyn, F., 2018. Very high-resolution imaging of the city of Goma (North Kivu, D.R. Congo) using SfM-MVS photogrammetry. *Proceedings of IGARSS 2018*. (Accepted)

Tracking magma movements in the Virunga volcanic province using seismic Amplitude Ratio Analysis (SARA)

Josué SUBIRA¹, Corentin CAUDRON², Aurélia HUBERT-FERRARI³, Julien BARRIÈRE⁴, Adrien OTH⁴ & François KERVYN⁵

¹*Environmental Sciences and Management Department, University of Liège, Belgium, jsubira@student.uliege.be*

²*Department of Geology, Ghent University*

³*Institut de Géographie, Université de Liège, Belgium*

⁴*European Center for Geodynamics and Seismology*

⁵*Département de Géorisques, Musée Royal d'Afrique Centrale (Tervuren), Belgium*

Volcanic eruptions are often characterized by the emission of magma at the surface. Prior to the extrusion, magma rises or moves laterally in the crust releasing seismic energy. These movements can be tracked using seismic waves recorded by a network of seismometers deployed around the studied volcano. A new methodology called the Seismic Amplitude Ratio Analysis (SARA) has been designed to detect and locate magma migrations in the subsurface at volcano observatories and for research purposes (Taisne et al. 2011). By analyzing the evolution of seismic amplitude ratios recorded at different pairs of stations corrected for site effects, the location of magma can be assessed without picking any earthquake; the most traditional way to detect melt movements.

This study tests the potential of this technique using a seismic network, the KivuNet, deployed in the Virunga Volcanic Province. The Virunga Volcanic Province is located in eastern DRC in a transition zone between Lake Eduard and Lake Kivu where the western branch of the East African Rift changes direction from N-S to NNE-SSW. Two out of the eight volcanoes, i.e., Nyamulagira and Nyiragongo, are currently active and considered as the most active volcanoes in Africa. The presence of the Nyiragongo volcano near the cities of Goma and Gisenyi makes this area with its complex socio-political context among the most vulnerable areas to eruption risk.

Given the high risk in the area, the seismic surveillance in the Virunga region started in the 1960s, but an operational network only emerged after the 2002 Nyiragongo eruption. Most of the seismic studies (Lukaya et al. 1992; Wafula et al. 1992; Mavonga et al. 2006, 2010; Tuluka 2010) have been dedicated to the location of long-period (LP) and volcano-tectonic (VT) events recorded during earthquake swarms preceding eruptions using classical methods. However, these methods are not efficient in the presence of emergent volcanic signals, especially with small seismic networks, resulting in large uncertainties with LP locations. A new network has been developed in the area since 2013, which permitted new initiatives to track the magmatic activity with seismic approaches. Recent efforts successfully located volcanic tremor using cross correlation functions (Barrière et al. 2017).

In our study we apply the SARA method that successfully tracked magma migration at the Piton de la Fournaise (La Réunion), Tolbachik (Russia) and Bardarbunga (Iceland) volcanoes. The

advantage of this technique compared to the approach developed by Barrière et al. (2017) concerns its better temporal resolution that would offer the possibility to automatically locate volcanic tremor thereby allowing to locate magma in real-time, possibly before an eruption occurs.

We used more than 3 years of high-quality seismic data recorded by ~15 telemetered seismic stations of the broadband network KivuSNet. The 0.3-1 Hz frequency band was selected because it corresponds to coherent volcanic tremor sources from the Nyiragongo and Nyamulagira volcanoes, and is thus representative of the magmatic activity in the region (Barrière et al. 2017). To constrain magmatic intrusions, the 3D location requires a preliminary estimate of site amplification factors. The MSNoise software (Lecocq et al. 2014) was used to process the seismic data and calculate amplitude ratios. We then validate the methodology by comparing our seismic amplitude ratio and locations with tremor locations using the cross-correlation approach, earthquake activity, SO₂ emissions.

Preliminary results show good correlation of main observations of magmatic evolution during the period from October 2015 to February 2017 made by Julien and it suggests good ability of the SARA method to track the magmatic intrusions in the VVP.

References

- Barrière J, Oth A, Theys N, et al (2017) Long-term monitoring of long-period seismicity and space-based SO₂ observations at African lava lake volcanoes Nyiragongo and Nyamulagira (DR Congo). *Geophys Res Lett* 44:6020–6029. doi: 10.1002/2017GL073348
- Lecocq T, Caudron C, Brenguier F (2014) MSNoise, a Python Package for Monitoring Seismic Velocity Changes Using Ambient Seismic Noise. *Seismol Res Lett* 85:715–726. doi: 10.1785/0220130073
- Lukaya N, Ciraba M, Mavonga T, Wafula M (1992) Main pattern of waveforms observed in the Virunga volcanic zone, Western rift valley of Africa. *Tectonophysics* 209:261–265. doi: 10.1016/0040-1951(92)90031-Z
- Mavonga T, Kavotha SK, Lukaya N, et al (2006) Seismic activity prior to the May 8, 2004 eruption of volcano Nyamuragira, Western Rift Valley of Africa. *J Volcanol Geotherm Res* 158:355–360. doi: 10.1016/j.jvolgeores.2006.06.021
- Mavonga T, Zana N, Durrheim RJ (2010) Studies of crustal structure, seismic precursors to volcanic eruptions and earthquake hazard in the eastern provinces of the Democratic Republic of Congo. doi: 10.1016/j.jafrearsci.2010.08.008
- Taisne B, Brenguier F, Shapiro NM, Ferrazzini V (2011) Imaging the dynamics of magma propagation using radiated seismic intensity. *Geophys Res Lett* 38:2–6. doi: 10.1029/2010GL046068
- Tuluka GM (2010) Crustal structure beneath two seismic broadband stations revealed from teleseismic P-wave receiver function analysis in the Virunga volcanic area, Western Rift Valley of Africa. doi: 10.1016/j.jafrearsci.2009.11.003
- Wafula M, Zana N, Mavonga T, Sassa M (1992) Recent Seismicity of the Virunga volcanic zone, Western rift, Zaire. *Tectonophysics* 209:259–260. doi: 10.1016/0040-1951(92)90030-A

Electric and passive seismic geophysical survey in a protected cave environment: the Bruniquel cave (France)

Koen VAN NOTEN¹, Christian BURLET¹, Serge DELABY², Thomas LECOCQ³, Jacques JAUBERT⁴ and Sophie VERHEYDEN^{1,5}

¹*Geological Survey of Belgium, Royal Belgian Institute of Natural Sciences, Jennerstraat 13, 1000 Brussels, Belgium. koen.vannoten@naturalsciences.be*

²*Geopark Famenne-Ardennes*

³*Seismology-Gravimetry, Royal Observatory of Belgium, Ringlaan 3, 1180 Brussels, Belgium*

⁴*PACEA- UMR- Bordeaux Allée Geoffroy Saint Hilaire CS 50023; 33615 Pessac cedex*

⁵*Federaal Wetenschapsbeleid, BELSPO, Louizalaan 231, 1050 Brussels.*

1. Geophysics in protected caves

The study of detrital cave sediments is a powerful tool to obtain information on cave development, environmental and climatic context and evolution as well as of anthropogenic perturbations in cave sediments. Amongst geophysical methods applicable in caves, H/V spectral ratio analysis (HVSR) of ambient seismic noise is of particular interest to study a cave's infill as the soft, detrital nature of cave infills usually presents a good seismic velocity contrast with the underlying carbonate bedrock. Electrical Resistivity Tomography (ERT) is usually also considered as a non-invasive technique, however, as iron electrodes need to be planted in the cave floor, destructive drillings (strongly forbidden in protected caves) are still required to penetrate calcite deposits that cover cave floors. Hence, other ERT innovations need to be developed to overcome these protective actions.

In this contribution we present the results of a combined passive seismic (HVSR) and ERT geophysical survey conducted in May 2018 in the Bruniquel cave (Tarn-et-Garonne department, South of France) to investigate detrital clay infill, gallery shape and thickness of calcite covering the cave floor. The Bruniquel cave is world renowned for the discovery of the oldest underground Neanderthal constructions; i.e. circular gatherings of broken stalagmites with fire pit burning marks found in a deep gallery of the cave (*Salle de la Structure*, Jaubert et al. 2016). In this contribution methods and solutions are discussed to work in difficult accessible caves and the first geophysical results are presented.

2. Methods

To avoid cave floor penetrating, surface contact electrodes were constructed at the Geological Survey of Belgium. We tested and used circular medical electrode pads (contact area 28 cm²) made of conductive rubber (non-adhesive) which were glued to 350 g rock cylinders used as weight. The contact resistance of the pads was measured on a steel sheet and comprised between 80 and 100 Ohms, with few outliers of 200 Ohms (marked, for possible post-processing). In a clayey environment this contact resistivity can generate artificial effects, however, due to the high resistivity of the calcite deposited on the Bruniquel cave floor, these additional effects are rather

negligible. To avoid using too long ERT cables, we also constructed a new cable with a maximum electrode spacing of 50 cm.

Three acquisition systems (Cityshark II), each connected to a 1s Lennartz LE-3Dlite seismometer, were used to record ambient noise. Short 20 minutes individual station records as well as synchronous overnight array measurements were performed at 42 locations in the cave. Resonance frequency at every station was determined from HVSR analysis of ambient noise and was subsequently converted to depth to investigate the cave infill. As the Citysharks were not synchronised, all three instruments were launched ~simultaneously manually. Small shifts in timing were corrected before the array measurements could be processed to depth-velocity profiles.

To reach the difficult accessible *Salle de la Structure*, all geophysical equipment (one ABEM terrameter, 64 pad electrodes, three seismometers and acquisition systems, two ERT and three seismometer cables) needed first to be dragged through the narrow ~25 m-long entrance tunnel and then transported to the middle gallery of the cave during a 20 min walk.

3. Preliminary results and discussion on the Bruniquel cave infill

Three ERT profiles were conducted in the gallery: one E-W profile (31.5 m) along the length axis of the main cave and two perpendicular N-S profiles (20 m and 17 m length). On the calcite floor ERT did not allow to detect the bedrock as the calcite was too resistive and electric current could not sufficiently penetrate the clay below the calcite floor. ERT however still provides very useful information on calcite thickness variations (up to more than one metre) of the cave floor that can be further linked to variations in calcite precipitation in the cave.

ERT provided good results below places where electrodes were placed directly on the clay infill. At these places, ERT analysis tentatively suggests a bedrock depth of ~2 m. As caves provide a quiet environment, HVSR is particularly suited to investigate the cave infill if the shear wave velocity (V_s) of the infill is known. HVSR analysis of stations placed directly on the clay infill indicate clear resonance frequency peaks around ~12-13 Hz. This resonance frequency and the 2 m depth indicate a rather slow V_s of the clay of ~100 m/s. Using this V_s allowed inverting other single station measurements to depth which resulted in bedrock depth variations between 1.5 to 3 m in the middle part of the *Salle de la Structure*. This V_s however needs to be confirmed after inverting the array measurements in the cave.

Complementary seismic analysis was performed to deduce the azimuthal direction in which the H/V resonance peak has its maximum peak amplitude. In the central part of the gallery, the polarization is dominantly N150°E to N-S oriented, which is oblique to the main N100E orientation of the cave. This dominant polarization is currently in debate because it can be linked to (i) the geometry and shape the eroded/original cave floor below the clayey infill, (ii) the orientation of main geological faults in the region, (iii) joint orientation, or (iv) main bedding dip of the host rock in which the cave developed.

4. Conclusion

This survey demonstrates an innovative use of surface electrode pads and non-invasive geophysical techniques in a challenging environment of an underground archaeological site. In the particular

configuration of the Bruniquel cave, the combined electric-seismic geophysical analysis is complementary as the superficial cave floor thickness could be detected by using ERT whereas HVSR analysis provided thickness of the cave infill.

5. Reference

Jaubert, J. et al. 2016. Early Neanderthal constructions deep in Bruniquel Cave in southwestern France. *Nature* 534, 111-114.

The GEPATAR project: GEotechnical and Patrimonial Archives Toolbox for ARchitectural conservation in Belgium

Jan WALSTRA¹, Pierre-Yves DECLERCQ¹, Christian BARBIER², Leidy BEJARANO-URREGO³, Thibault CROONENBORGH⁵, Dominique DERAUW², Anastasios DROUGKAS³, Roald HAYEN⁴, Francois-Philippe HOCQUET⁴, Michal SHIMONI⁵, Koen VAN BALEN³ & Els VERSTRYNGE³

¹ *Geological Survey of Belgium, OD Earth & History of Life, Royal Belgian Institute of Natural Sciences, Jennerstraat 13, B-1000 Brussels, Belgium*

² *Centre Spatial de Liège, Avenue du Pré Aily, B-4031, Liège, Belgium*

³ *Building Materials and Building Technology Division, Department of Civil Engineering, Katholieke Universiteit Leuven, Kasteelpark Arenberg 40, B-3001 Heverlee, Belgium*

⁴ *Royal Institute for Cultural Heritage, Jubelpark 1, B-1000 Brussels, Belgium*

⁵ *Signal and Image Centre, Belgian Royal Military Academy, Hobbemastraat 8, B-1000 Brussels, Belgium*

Belgium is well known for its diverse collection of built heritage, visited every year by millions of people. Because of its cultural and economic importance, conservation is a priority at both federal and regional levels. Monuments may suffer from structural instabilities related to industrial and urban development, such as groundwater extraction,

mining and excavation activities. Adequate protection and preservation requires an integrated analysis of environmental, architectural and historical parameters.

The aim of the GEPATAR project is to create an online interactive geo-information tool that integrates information about Belgian heritage buildings and the occurrence of ground movements. The toolbox will allow the user to view and be informed about buildings potentially at risk due to differential ground movements and thus help improving the management of built patrimony.

Countrywide deformation maps spanning nearly 25 years were produced by applying advanced multi-temporal InSAR techniques to time-series of SAR data. We used StaMPS (Stanford Method for Persistent Scatterers; Hooper et al. 2012) to process ERS-1/2 and Envisat archive data and MSBAS (Multidimensional Small Baseline Subsets; Samsonov & d'Oreye 2012) to combine both ascending and descending tracks of Sentinel-1. High-resolution deformation maps of selected urban centres were obtained by processing VHR SAR data (TerraSAR-X and CosmoSkyMed).

Within the GEPATAR toolbox, the country-scale deformation maps are integrated with other geo-data layers such as geology, land-use and the location of the built heritage; feature-based data fusion techniques and decision rules based on geomechanical expertise are combined to create ground movement risk maps. At the local scale the fusion process is more complicated due to the inclusion of non-spatial datasets, such as photographic and historical surveys, architectural and geotechnical data; at this scale decision rules are provided by engineering and architectural

expertise. The output risk maps will be regularly updated with the availability of new SAR acquisitions.

Some selected case-studies will be investigated at high resolution by means of on-site monitoring techniques as well as stability analysis to evaluate the applied approaches.

References

- Hooper, A., Bekaert D., Spaans, K. & Arikan, M. (2012). Recent advances in SAR interferometry time series analysis for measuring crustal deformation. *Tectonophysics*, 514-517, 1-13.
- Samsonov, S. & d'Oreye, N. (2012). Multidimensional time series analysis of ground deformation from multiple InSAR data sets applied to Virunga Volcanic Province. *Geophysical Journal International*, 191 (3), 1095-1108.

Acknowledgements

The GEPATAR project is funded by the Belgian Science Policy within the framework of the BRAIN-be programme (contract BR/132/A6/GEPATAR). ERS-1/2 and Envisat data were provided by ESA (proposals 32381 & 34984), TerraSAR-X data by DLR (proposal GEO3185), Cosmo-SkyMed data by ASI (proposal 445), and Sentinel-1 data by the Copernicus program.

NiphNet: a self-governing environmental monitoring network

Kris WELKENHUYSEN¹, Kris PIESENS¹, Yves VANBRABANT¹, Sophie VERHEYDEN¹, Christian BURLET¹

¹ *Geological Survey of Belgium – Royal Belgian Institute of Natural Sciences, Jennerstraat 13, 1000 Brussels, Belgium*

A high-precision and low-cost temperature and humidity logging device, called Niphargus and originally intended for environmental monitoring in caves, was developed at the Geological Survey of Belgium (Burlet et al., 2015). The Niphargus is designed as a stand-alone logger, with data to be retrieved manually whenever needed. This allows for a very small and simple electronic design, low power consumption and flexible placement. There are, however, a number of disadvantages for specific applications. For example, there is no feedback possible on malfunction or battery lifetime. To avoid loss of data during long-term measurement campaigns, regular inspection and data retrieval are necessary. Apart from the inconvenience, this manipulation also causes disturbance in the measurements.

A new version of the Niphargus was therefore developed, including a wireless Digi XBee DigiMesh module. These modules communicate on a 868 MHz radio frequency, in a self-governing mesh network (Fig. 1). In such a network, every device is able to communicate to any other device within range. For data transmission, the most optimal pathway is chosen between transmitter and receiver. As such, in case of a single device malfunction, the connection between the other nodes can still be guaranteed.

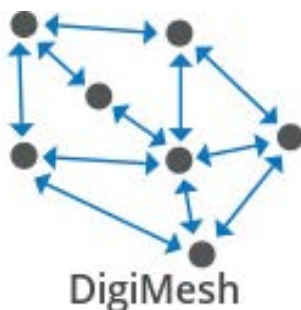


Figure 1. Example of the DigiMesh self-governing mesh network (www.digi.com).

In case of the NiphNet, the receiving end includes a single-board computer with cellular network connectivity, from which data is uploaded to a cloud repository. From there, live monitoring data can be displayed online, downloaded and processed. A first successful test was conducted with a NiphNet of 5 devices in waterproof containers (Fig. 2) and online display at the GeoEnergy Test Bed in Nottingham, UK, in March 2018. Current and future efforts focus on the enclosure design and the automation of data readout over the network.

There is a large array of possible applications. For environmental monitoring in caves, the individual nodes can ensure data transmission from a network of environmental sensors inside the cave to a station outside, allowing for continuous access to measurements and minimising the need for regular field inspection. This is currently being installed in the caves of Han.

The geological storage of CO₂ requires long-term monitoring to establish a baseline and detect leakage from the reservoir, both below and above ground. Such monitoring activities need to be maintained for several decades, and therefore need to be low effort and low cost. Near the surface, temperature is expected to be a good proxy for CO₂ leakage when a network is set-up that can detect temperature anomalies in the range of 0.01°C. This is possible with a network of shallow buried Niphargus nodes. Then, wireless access to these devices is not only a matter of long-term and maintenance-free coverage of a large area. Detection of small temperature differences depends on not disturbing the shallow subsurface, and therefore on being able to download the data remotely.



Figure 2. NiphNet node, as a wireless Niphargus inside a waterproof, stainless steel container.

Reference

Burlet, C., Vanbrabant, Y., Piessens, K., Welkenhuysen, K. & Verheyden, S., 2015. Niphargus: A silicon band-gap sensor temperature logger for High-precision environmental monitoring. *Computers & Geosciences*, 74, p. 50-59.

Theme 2

Understanding planets through magmatic differentiation

Zinc behavior during mantle melting: a reappraisal of natural and experimental observations

Hugues BEUNON¹, Nadine MATTIELLI¹, Luc-Serge DOUCET², Baptiste DEBRET¹ & Bertrand MOINE³

¹ *Laboratoire G-Time, Université Libre de Bruxelles, Belgium*

² *TiGeR, Earth Dynamics Group, Curtin University, Australia*

³ *Laboratoire Magmas et Volcans, St Etienne, France*

Mantle stable isotope heterogeneities resulting from hightemperature processes have been reported for a growing number of elements. Among them, Zn is of great interest due to its single valence state (Zn^{2+}) in compounds or complex ions which makes it insensitive to redox conditions. Zn isotopic compositions ($\delta^{66}\text{Zn}$, relative to JMC-Lyon) in igneous rocks vary up to $\sim 0.3\%$ from ultramafic rocks ($\delta^{66}\text{Zn} = +0.10$ to $+0.30\%$, Doucet et al., 2016, Wang et al., 2017, Sossi et al., 2018) to isotopically heavier mantle-derived melts ($\delta^{66}\text{Zn} = +0.25$ to $+0.40\%$, Wang et al., 2017, Ben Othman et al., 2003, Chen et al., 2013, Herzog et al., 2009).

Yet, there is a major controversy about the behaviour of Zn and its isotopes during mantle partial melting: some authors suggest that high degrees of melt extraction may fractionate Zn isotopes up to $\sim 0.15\%$ (Doucet et al., 2016, Wang et al., 2017) while others find no resolvable Zn isotope variations ($< 0.015\%$) in melting residues (Sossi et al., 2018). Considering a bulk partition coefficient close to unity ($D^{\text{mantle-melt}} \sim 1$) and focusing on the role of pressure during partial melting (e.g. spinel vs garnet stability field), previous modeling studies have failed in reproducing Zn concentrations and Zn isotope compositions in both mantle peridotites and mantle-derived basalts (Doucet et al., 2016, Wang et al., 2017, Sossi et al., 2018). Here, we explore the role of temperature on Zn behavior during mantle melting.

Through (1) a comprehensive review of Zn elemental and isotopic compositions in mantle-related rocks and (2) an exhaustive compilation of relevant experimental works, we show strong evidences of a thermal control on Zn partitioning at melting conditions. Results are incorporated into a mantle melting model which successfully reproduces Zn concentrations and isotopic compositions in basaltic and ultramafic rocks. Major implications for Zn elemental and isotopic heterogeneities in the Earth's mantle and new potential applications of Zn isotopes as tracers of source lithology are further discussed.

References

- Doucet, L. S., Mattielli, N., Ionov, D. A., Debouge, W., & Golovin, A. V. (2016). Zn isotopic heterogeneity in the mantle: A melting control?. *Earth and Planetary Science Letters*, 451, 232-240.
- Wang, Z. Z., Liu, S. A., Liu, J., Huang, J., Xiao, Y., Chu, Z. Y., ... & Tang, L. (2017). Zinc isotope fractionation during mantle melting and constraints on the Zn isotope composition of Earth's upper mantle. *Geochimica et Cosmochimica Acta*, 198, 151-167.
- Sossi, P. A., Nebel, O., O'Neill, H. S. C., & Moynier, F. (2018). Zinc isotope composition of the Earth and its behaviour during planetary accretion. *Chemical Geology*, 477, 73-84.

- Ben Othman, D., Luck, J. M., Tchalikian, A., & Albarède, F. (2003, April). Cu-Zn isotope systematics in terrestrial basalts. In EGS-AGU-EUG Joint Assembly.
- Chen, H., Savage, P. S., Teng, F. Z., Helz, R. T., & Moynier, F. (2013). Zinc isotope fractionation during magmatic differentiation and the isotopic composition of the bulk Earth. *Earth and Planetary Science Letters*, 369, 34-42.
- Herzog, G. F., Moynier, F., Albarède, F., & Berezhnoy, A. A. (2009). Isotopic and elemental abundances of copper and zinc in lunar samples, Zagami, Pele's hairs, and a terrestrial basalt. *Geochimica et Cosmochimica Acta*, 73(19), 5884-5904.

Crystallization of the lunar magma ocean and the primordial mantle-crust differentiation of the Moon

Bernard CHARLIER^{1,2,3}, Timothy L. GROVE², Olivier NAMUR⁴ & Francois HOLTZ³

¹ *Department of Geology, University of Liège, 4000 Sart Tilman, Belgium*

² *Massachusetts Institute of Technology, Department of Earth, Atmospheric, and Planetary Sciences, Cambridge, MA 02139 USA*

³ *Institut für Mineralogie, Leibniz Universität Hannover, 30167 Hannover, Germany*

⁴ *Department of Earth and Environmental Sciences, KU Leuven, 3000 Leuven, Belgium*

We present crystallization experiments on silicate melt compositions related to the lunar magma ocean (LMO) and its evolution with cooling. Our approach aims at constraining the primordial internal differentiation of the Moon into mantle and crust. We used graphite capsules in piston cylinder (1.35-0.80 GPa) and internally-heated pressure vessels (< 0.50 GPa), over 1580 to 1020°C, and produced melt compositions using a stepwise approach that reproduces fractional crystallization. Using our new experimental dataset, we define phase equilibria and equations predicting the saturation of liquidus phases, magma temperature, and crystal/melt partitioning for major elements relevant for the crystallization of the LMO. These empirical expressions are then used in a forward model that predicts the liquid line of descent and crystallization products of a 600 km-thick magma ocean. Our results show that the effects of changes in the bulk composition on the sequence of crystallization are minor. Our experiments also show the crystallization of a silica phase at ca. 1080°C and we suggest that this phase might have contributed to the building of the lower anorthositic crust. Calculation of crustal thickness clearly shows that a thin crust similar to that revealed by GRAIL cannot have been generated through solidification of whole Moon magma ocean. We discuss the role of magma ocean depth, trapped liquid fraction (with implication for the alumina budget in the mantle and the crust), and the efficiency of plagioclase flotation in producing the thin crust. We also constrain the potential range of pyroxene compositions that could be incorporated into the crust and show that delayed crustal building during ca. 4% LMO crystallization on the nearside of the Moon may explain the dichotomy for Mg-number. Finally, we show that the LMO can produce magnesian anorthosites during the first stages of plagioclase crystallization.

Making sense of destruction: A geochemical investigation into the impact generated melt rocks of the Chicxulub impact structure, Yucatán, recovered during IODP-ICDP Expedition 364.

Sietze J. DE GRAAFF¹, Ruben VANDIJCK², Pim KASKES¹, Thomas DÉHAIS¹, Steven GODERIS¹ & Philippe CLAEYS¹

¹*Research unit: Analytical, Environmental and Geo-chemistry, Vrije Universiteit Brussel, Pleinlaan 2, 1050 Elsene, Belgium*

²*Department of Earth and Environmental Sciences, Katholieke Universiteit Leuven, Celestijnenlaan 200E, B-3001, Leuven, Belgium.*

In 2016 the International Ocean Discovery Program (IODP) and International Continental Scientific Drilling Program (ICDP) Expedition 364 sampled the peak-ring of the Chicxulub impact structure, Yucatán (Morgan et al., 2016). This impact structure is famously linked to the Cretaceous-Palaeogene event, which led to the extinction of the non-avian dinosaurs (Alvarez et al., 1980, Smit and Hertogen, 1980, Schulte et al. 2010). The IODP-ICDP 364 Expedition cored the peak ring of the crater, recovering ± 110 m of Paleogene sediments, ± 130 m of breccia containing impact melt fragments (suevite) and clast poor impact melt rocks, and ± 590 m of granitoid basement material, containing impact melt rocks (Morgan et al., 2016). The impact melt rocks can be subdivided in the upper (between $\pm 721 - 747$ meters below seafloor (mbsf)) and lower melt rocks (between $\pm 1209 - 1316$ mbsf). This study focused on the recovered impact melt rocks. Impact generated melt rocks essentially represent the molten, quenched state of the target rock (Belza et al., 2014) and their geochemical and isotopic signatures provide a unique fingerprint that characterizes the impact site (Premo and Izett, 1992). Thus, impact melts hold the key to understanding the formation of an impact crater.

The dynamic collapse model is the currently accepted model to have formed the Chicxulub impact structure (Morgan et al., 2016; Fig.1). Visually this model suggests the formation of a uniform, single impact melt sheet formed from the different target lithologies (Fig. 1). However, geochemical variations of the impact melt rocks do not agree with this observation. The upper melt sheet shows higher Al_2O_3 (up to 18 wt%) and CaO (up to 20 wt%) and generally lower Fe_2O_3 and MgO (around 5 and 2 wt% respectively) when compared to the lower melt rocks. Moreover, the lower melt rocks show trace elemental compositions more comparable to crustal basement target rocks with notable enrichment in Sr isotopic composition ($^{87}\text{Sr}/^{86}\text{Sr}$ up to 0.7083, compared to ± 0.7077 of the basement). This shows the upper melt rocks to be more comparable to the carbonate target rock, while the lower melt rocks are more similar to the crustal target rocks. This suggests that the formation of the upper and lower melt rocks was to some extent decoupled. Whether this implies discrete melt formation or the immiscibility of carbonaceous (upper) and more siliceous (lower) melts is yet to be determined.

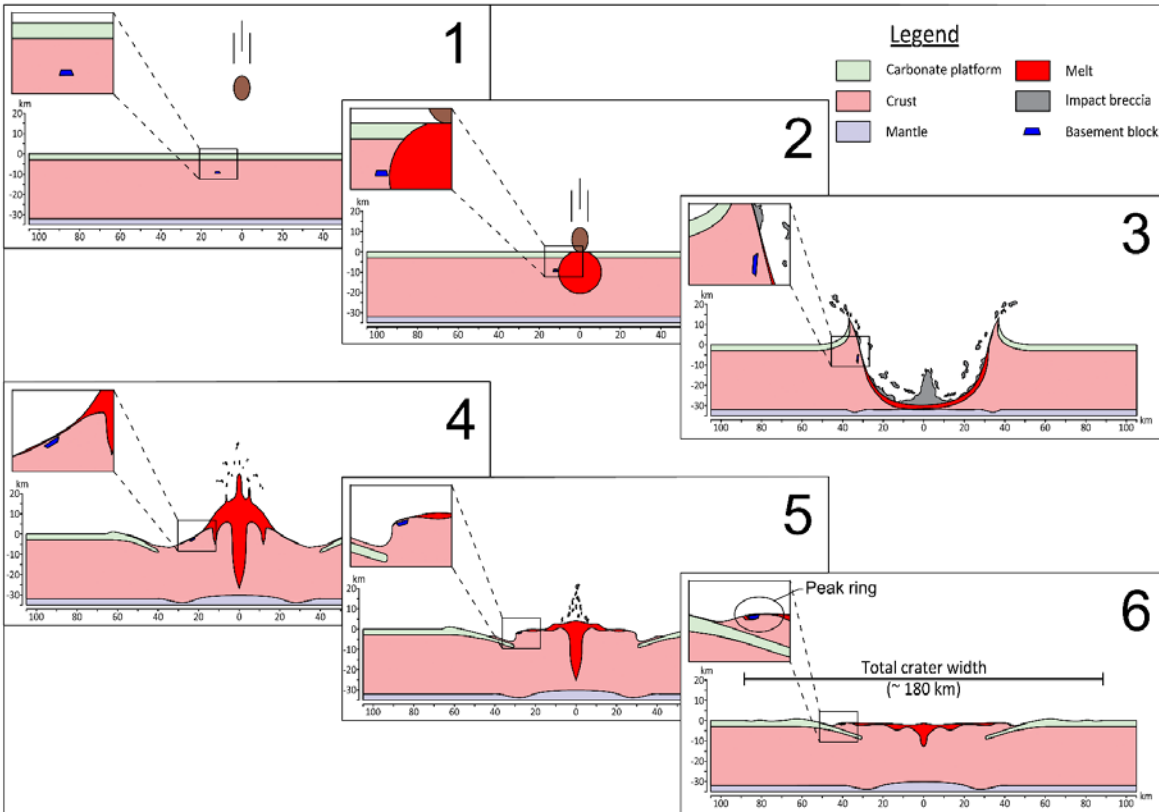


Figure 1. Chicxulub crater formation according to the dynamic collapse model showing the formation of a peak ring and the emplacement of mid-crustal basement at shallow depths. Box 2 displays the impact zone at time of impact ($T = 0$ min), Box 6 displays the impact zone at 10 minutes after impact ($T = 10$ min) when no suevite sequence and sedimentary cover was deposited yet (redrawn by R. Vandijck after Morgan, et al., 2016).

References

- Alvarez, L. W., Alvarez, W., Asaro, F., & Michel, H. V., 1980. Extraterrestrial cause for the Cretaceous-Tertiary extinction. *Science*, 208(4448), 1095-1108.
- Belza, J., Goderis, S., Smit, J., Vanhaecke, F., Baert, K., Terryn, H., & Claeys, P., 2015. High spatial resolution geochemistry and textural characteristics of 'microtektite' glass spherules in proximal Cretaceous–Paleogene sections: insights into glass alteration patterns and precursor melt lithologies. *Geochimica et Cosmochimica Acta*, 152, 1-38.
- Morgan, J. V., Gulick, S. P., Bralower, T., Chenot, E., Christeson, G., Claeys, P., & Gebhardt, C., 2016. The formation of peak rings in large impact craters. *Science*, 354(6314), 878-882.
- Premo, W. R., & Izett, G. A., 1992. Isotopic signatures of black tektites from the K-T boundary on Haiti: Implications for the age and type of source material. *Meteoritics & Planetary Science*, 27(4), 413-423.
- Schulte, P., Alegret, L., Arenillas, I., Arz, J.A., Barton, P.J., Bown, P.R., Bralower, T.J., Christeson, G.L., Claeys, P., Cockell, C.S. and Collins, G.S., 2010. The Chicxulub asteroid impact and mass extinction at the Cretaceous–Paleogene boundary. *Science*, 327(5970), pp.1214-1218.
- Smit, J., & Hertogen, J., 1980. An extraterrestrial event at the Cretaceous–Tertiary boundary. *Nature*, 285(5762), 198.

Comparative petrographic, geochemical, and isotopic characterization of distal ejecta layers

Thomas DÉHAIS¹, Pim KASKES¹, Sietze J. DE GRAAFF¹, Steven GODERIS¹ & Philippe CLAEYS¹

¹*Analytical, Environmental and Geo-Chemistry, Vrije Universiteit Brussel, Pleinlaan 2, 1050 Elsene, Belgium*

Collision and impact crater formation represent one of the most fundamental geological processes in the Solar System, with important consequences for the formation and the evolution of the surface and/or the atmosphere of planetary bodies. In the case of the Earth, these high-energy phenomena can also affect life on a local and/or global scale (e.g., the Chicxulub impact; Renne et al., 2015). During hypervelocity impact events, target lithologies are vaporized, melted and fractured as well as mixed with projectile (i.e., meteoritic) matter. The formation of large impact structures can be accompanied by the production of a specific type of deposits called ejecta, often distributed over vast areas. These layers are largely composed of crushed and melted dust and rock fragments. More than 2.5 crater diameters away from the source crater, these layers are called distal ejecta (Glass & Simonson, 2012), which are not commonly preserved. Beyond 10 crater diameters from the source crater, the ejecta layer is primarily composed of glassy impact spherules of less than 1 mm, which represent solidified melt droplets and vapour-condensates. If primary crystals are present within the spherules, these impact spherules are called microkrystites, otherwise they are called microtektites. Compared to the 190 confirmed impact structures on Earth, only roughly 30 distal ejecta layers are currently known, and only c. 7 impact structures have been directly linked to distal ejecta layers (Glass & Simonson, 2012).

To verify the impact origin of terrestrial spherules layers, petrographic (e.g., glassy and altered spherules, Ni-rich spinel crystals, shock-metamorphosed mineral grains), geochemical (e.g., Ir anomalies and other siderophile element enrichments), and isotopic (e.g., Cr and Os isotopic data) characteristics are mostly used. Together with tectonic, stratigraphic, and geochronological information, these indicators for impact cratering have also been used to group different spherules layers together (e.g., Paraburdoo-Reivilo; Goderis et al., 2013) and to suggest potential source craters (e.g., spherules in the Zaonega Formation may be linked to the Vredefort impact structure, Huber et al., 2014). However, the products of ejecta formation can be highly diverse, as well-illustrated by the Chicxulub case, where crushed, melted and condensed material was deposited in different types and proportions across the globe.

This work focuses on the extensive collection of proximal and distal ejecta from various locations and time intervals available at the Vrije Universiteit Brussel by using petrography and Scanning Electron Microscopy with Energy Dispersive Spectroscopy (SEM-EDS) coupled with novel geochemical techniques such as micro X-ray fluorescence (μ XRF), which is non-destructive and provides semi-quantitative trace elements mapping and quantitative point analyses with a 25 μ m resolution (de Winter et al., 2017), and Laser Ablation (or MultiCollector) Inductively Coupled Plasma Mass Spectrometry (LA-(MC-)ICP-MS), which gives precise additional major and trace elemental analyses. This way we aim to provide better constraints on impact spherule formation

through time and to confirm or disprove the links between specific spherule layers and with particular impact structures.

References

- Glass, B. P. & Simonson, B. M., 2012. Distal Impact Ejecta Layers: Spherules and More. *Elements*, 8, 43–48.
- Goderis, S., Simonson, B. M., McDonald, I., Hassler, S. W., Izmer, A., Belza, J., Terryn, H., Vanhaecke, F. and Claeys, P., 2013. Ni-rich spinels and platinum group element nuggets condensed from a Late Archean impact vapour cloud. *Earth & Planetary Science Letters*, 376, 87–98.
- Huber, M. S., Črnc, A. E., McDonald, I., Hecht, L., Melezhik, V. A. and Koeberl, C., 2014. Impact spherules from Karelia, Russia: Possible ejecta from the 2.02 Ga Vredefort impact event. *Geology*, 42, 375–378.
- Renne, P. R., Sprain, C. J., Richards, M. A., Self, S., Vanderkluysen, L. and Pande, K., 2015. State shift in Deccan volcanism at the Cretaceous-Paleogene boundary, possibly induced by impact. *Science*, 350, 76–78.
- de Winter, N. J., Sinnesael, M., Makarona, C., Vansteenberge, S. & Claeys, P., 2017. Trace element analyses of carbonates using portable and micro-X-ray fluorescence: performance and optimization of measurement parameters and strategies. *Journal of Analytical Atomic Spectrometry*, 32, 1211-1223.

Late Neoproterozoic (Pan-African) reactivations in the Mesoproterozoic Karagwe-Ankole Belt (KAB) in Kivu (RDC), Rwanda and Burundi: chronological framework and paleostress field.

Damien DELVAUX¹, Max FERNANDEZ-ALONSO¹, Stijn DEWAELE¹, Mohamed LAGHMOUCH¹, Gloire B. GANZA², Guy M. ILOMBE², Christian B. KALIKONE², Espoir B. MUGISHO², Yogolelo M. MUKOKYA², Toussaint MUSHAMALIRWA², Charles NZOLANG², Evelyne N. SAFARI² & Robert N. WAZI²

1. Royal Museum for Central Africa, Tervuren, Belgium (damien.delvaux @africamuseum.be)

2. Université Officielle de Bukavu, Bukavu, R.D. Congo

The Karagwe-Ankole Belt (KAB) in the Kivus of the Democratic Republic of the Congo (DRC), Rwanda and Burundi is generally considered as a Mesoproterozoic belt, with a geodynamic evolution governed by the 1375 Ma Kibaran magmatic event, the ± 1.0 Ga Rodinia and the ± 550 Ma Gondwana (Pan-African) amalgamation events (Tack et al., 2010). Here we focus on the ± 550 Ma Gondwana event, which has been generally underestimated in previous works. This last event was first detected by “anomalously” young ages interpreted as isotopic rehomogenisations of “Lufilian” age in the granites of Rwanda, including the ± 980 Ma Tin granites which have been frequently cataclased (Gerards and Ledent, 1970). Similar ages were obtained also for Pb/Pb, Rb/Sr on microcline from pegmatites (Monteyne-Poulaert, 1962), U/Pb on hydrothermal muscovite (Walemba, 2001) and U/Pb on monazite in a tectonic breccia in Burundi (Brinckmann et al., 2001).

We compiled the existing chronological datasets for the Karagwe-Ankole belt from the Paleoproterozoic to the late Cenozoic rifting. It evidences a multistage evolution (magmatism, mineralization, sedimentation, metamorphism, ductile and brittle deformation) and, in particular, the importance of Pan-African reactivations. In parallel, recent work in the neighboring areas (e.g. in Tanzania, Uganda and Kenya) showed that East-Central Africa appears much more unstable than previously thought as a consequence of the east Gondwana amalgamation. Fritz et al. (2013) evidenced early Pan-African formation of the East African Orogen between 650 and 615 Ma due to the collision and closure of the Mozambique ocean. Further E-W convergence occurred between 590 and 570 Ma (Fritz et al., 2013; Saalman et al., 2016), together with interaction between the Tanzania Craton and the Bangweulu Block between 590 and 550 Ma (Boniface & Appel, 2018). Late Pan-African reactivations under E-W shortening were caused by the Tanzania–Congo / Dharwar Cratons convergence at about 530 Ma (Fritz et al., 2013).

Field observations at various sectors of the KAB belt evidence brittle faulting that appear unrelated to and younger than the previous “Kibaran” magmatic, deformation and mineralization events (1.375 Ga or ~ 1.0 Ga), but contemporaneous with the deformation of the Neoproterozoic (Cryogenian-Ediacaran) Itombwe series. Paleostress inversion allowed to reconstruct an older and widely expressed tectonic stress field characterized by a general E-W horizontal compression in a strike-slip to thrust faulting regime, and a younger brittle reactivation under N-S horizontal compression. The first brittle event occurred in brittle-ductile conditions and is interpreted as

related to the late Pan-African event that affected the entire belt. The second brittle event is restricted to a few area and whiteness younger deformations. This finding opens important perspectives for a revision of the regional geological map and also for the better understanding of the mineral resources.

References

- Boniface, N. & Appel, P., 2018. Stenian - Tonian and Ediacaran metamorphic imprints in the southern Paleoproterozoic Ubendian Belt, Tanzania: Constraints from in situ monazite ages. *Journal of African Earth Sciences*, 133, 25-35.
- Brinckmann J., Lehmann, B., Hein, U., Höhndorf, A., Mussallam, K., Weiser, T. & Timm, F., 2001. La géologie et la minéralisation primaire de l'or de la chaîne Kibarienne, nord-ouest du Burundi, Afrique orientale. *Geologische Jahrbuch Reihe, D 101*: 3-195.
- Cahen, L., Gerards, M., Theunissen, K., Lavreau, J., Villeneuve, M. Frautschi, J.M., 1976. Réunion de travail des 1, 2, et 3 septembre 1975: La géologie des terrains précambriens voisins du fossé tectonique occidental, spécialement dans les régions cises et part et d'autre de la partie sud du lac Kivu et du nord du lac Tanganyika au Kivu, au Rwanda et au Burundi. *Mus. roy. Afr. centr., Tervuren (Belg.)*; Dept. Geol. Min., Rapp. ann. 1975, 143/170.
- Fritz, H., Abdelsalam, M., Ali, K., Bingen, B., Collins, A., Fowler, A., Ghebreab, W., Hauzenberger, C., Johnson, P., Kusky, T., Macey, P., Muhongo, S., Stern, R. & Viola, G., 2013. Orogen styles in the East African orogen: a review of the Neoproterozoic to cambrian tectonic evolution. *Journal of African Earth Sciences*, 86, 65-106.
- Gerards, J. & Ledent, D., 1970. Grands traits de la géologie du Rwanda, différents types de roches granitiques et premières données sur l'âge de ces roches. *Annales de la Société géologique de Belgique*, 93; 477-489.
- Monteyne-Poulaert, G., Delwiche, R., Cahen, L. & Safiannikoff, A., 1962. Ages de minéralisations pegmatitiques et filoniennes du Kivu méridional (Congo oriental), Indications préliminaires sur les âges de phases pegmatitiques successives, *Bulletin de la Société belge de Géologie, Paléontologie et Hydrologie*, 71(2), 272-295.
- Saalmann, K., Manttari, I., Nyakecho, C. & Isabirye, E., 2016. Age, tectonic evolution and origin of the Aswa Shear Zone in Uganda: Activation of an oblique ramp during convergence in the East African Orogen *Journal of African Earth Sciences*, 117, 303-330
- Tack, L., Wingate, M.T.D., De Waele, B., Meert, J., Belousova, E., Griffin, A., Tahon, A. & Fernandez-Alonso, M., 2010. The 1375 Ma "Kibaran event" in Central Africa: prominent emplacement of bimodal magmatism under extensional regime. *Precambrian Research*, 180, 63-84.
- Walembe, K.M.A., 2001. Geology, geochemistry, and tectono-metallogenic evolution of Neoproterozoic Gold deposits in the Kaduba area, Kivu, Democratic Republic of Congo. Ph.D Thesis University of the Witwatersrand, Johannesburg, South Africa, 491 p.

Mechanism for fractionation of Ta-Nb, Sn and W in granite-related metallogenic systems based on observations from the Karagwe-Ankole Belt of Central Africa

Niels HULSBOSCH¹, Stijn DEWAELE² & Philippe MUCHEZ¹

¹ *Division of Geology, Department of Earth and Environmental Sciences, KU Leuven, Celestijnenlaan 200E, 3001 Leuven, Belgium. *niels.hulsbosch@kuleuven.be*

² *Mineralogy and Petrology, Department of Geology, Ghent University, Krijgslaan 281 S8, 9000 Ghent, Belgium.*

Tantalum, niobium, tin and tungsten mineralization occurs worldwide in close proximity to fractionated peraluminous leucogranites. These granite-related ore deposits show a diversity of mineralization modes, ranging from plutonic-hosted breccia and hydrothermal vein-stockwork systems to (peri)batholithic greisens, skarns, pegmatites and hydrothermal veins. In the Mesoproterozoic Karagwe-Ankole orogenic belt (KAB) of Central-Africa numerous early-Neoproterozoic Nb-Ta-Sn-W rare-metal deposits formed as primary mineralization in hydrothermal quartz veins, magmatic lithium-cesium-tantalum family pegmatites and associated intra-pegmatitic greisens (Fig. 1). These deposits are on a belt-scale spatially and temporally related to ilmenite-series, peraluminous, S-type leucogranites, which are generally defined in the KAB as the Kibara Sn granite generation with an intrusion age of $\sim 986 \pm 10$ Ma (SHRIMP U-Pb on zircon; Tack et al., 2010).

This study reviews the petro- and metallogenesis of Nb-Ta-Sn-W granite-related ore deposits, as they occur in the Rwandese part of the KAB, and provides a general overview of the geochemical mechanisms behind the formation of pegmatite- and quartz vein-hosted deposits and the distribution and enrichment of the ore elements Nb, Ta, Sn and W in the different metallogenic subsystems (i.e. granites, pegmatites and veins). Moreover, the observed close spatiotemporally association between leucogranites, pegmatites and quartz veins is assessed in terms of a direct genetic link between the mineralization and the felsic magmatism. Based on this review and element distribution calculations, an integrated orthomagmatic metallogenic model for Nb-Ta-Sn-W mineralization in the KAB is demonstrated. Rayleigh-type fractional crystallization acted as the main mechanism by which pegmatitic magmas differentiate from a parental leucogranitic melt and by which incompatible elements Nb, Ta, Sn and W initially are enriched. However, early aqueous fluid immiscibility has been identified to occur during differentiation of this B-rich, F-poor melt system, which greatly effects W depletion in the melt by preferential partitioning of W into the mobile fluid phase. Sn retains dominantly in the melt phase and becomes, by high degrees of fractional crystallization, enriched in late-stage magmatic fluids. Element-specific melt-fluid-crystal fractionation together with element-specific and lithological-controlled precipitation conditions are the key enrichment processes and are all responsible for the decoupling of Nb-Ta, Sn and W and their subsequent precipitation in pegmatite, hydrothermal quartz vein and greisen deposits. This formation model for the KAB system can form a major tool in the exploration for granite-related ore deposits in general.

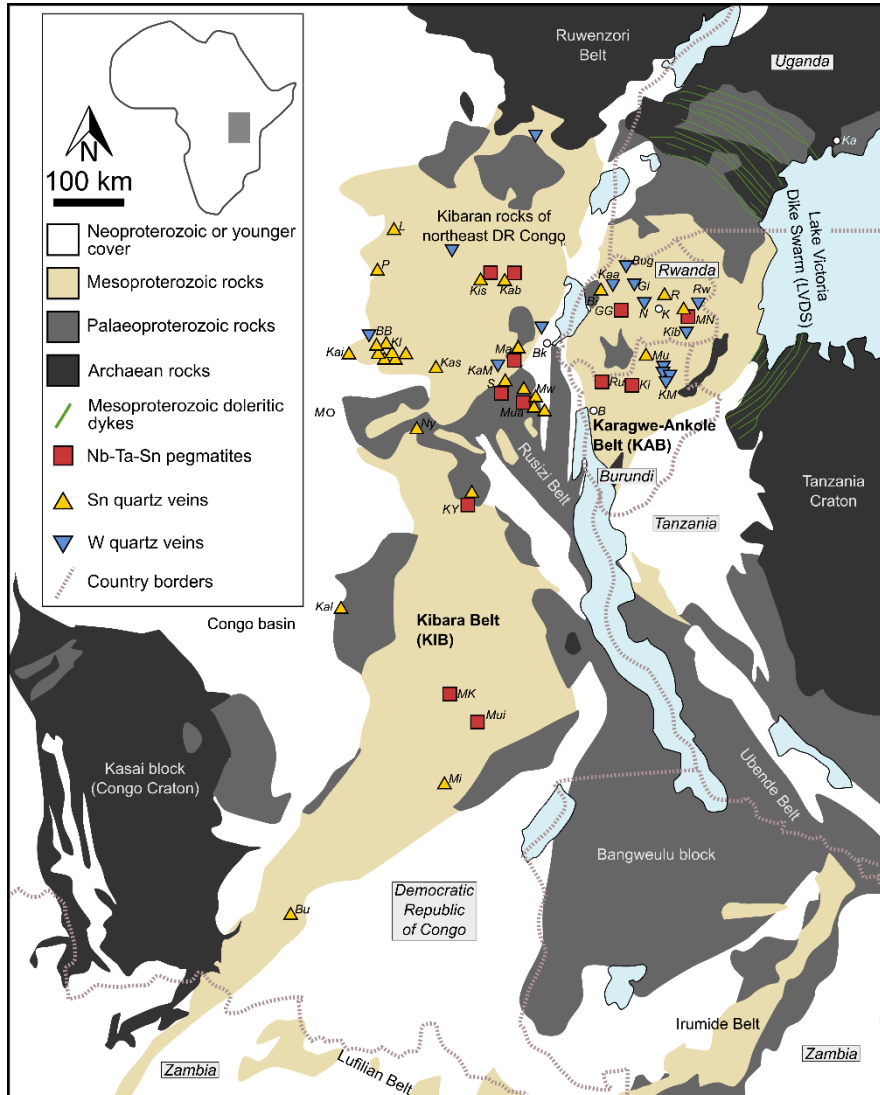


Figure 1. Conceptual outline of the geographical and geological setting of the major rare-metal deposits of the Karagwe-Ankole (KAB) and neighboring Kibara (KIB) belts in Central African Great Lakes region. B: Bujumbura, BB: Bengo-Biri, Bi: Bisesero, Bk: Bukavu, Bu: Busanga, Bug: Bugarama, GG: Gatumba-Gitarama pegmatite field, Gi: Gifurwe K: Kigali, Ka: Kampala, Kaa: Kabaya, Kab: Kabunga, Kai: Kailo, Kal: Kalanda, Kas: Kasese, Kl: Kalima, Ki: Kivuvu, Kib: Kibungo, KaM: Kamituga-Mobale, KM: Kirundo-Muyinga, KY: Kabambare – Yungwe, L: Lowa, Kis: Kiseke, Ma: Matala, Mi: Mitwaba, MK: Manono-Kitotolo, MN: Musha-Ntunga, Mu: Mulehe, Mua: Muana, Mui: Muika, Mw: Mwenga, N: Nyakabingo, Ny: Nyangulube P: Punia, R: Ruhembe, Rw: Rwinkwavu, S: Sasa. After Hulsbosch (in press).

References

- Hulsbosch, N, In press. Nb-Ta-Sn-W distribution in granite-related ore systems: fractionation mechanisms and examples from the Karagwe-Ankole Belt of Central Africa. In Decrée, S. & Robb, L. (eds), *Ore Deposits Origin Exploration and Exploitation*. Wiley. In press.
- Tack, L., Wingate, M.T.D., De Waele, B., Meert, J., Belousova, E., Griffin, B., Tahon, A. & Fernandez-Alonso, M., 2010. The 1375 Ma “Kibaran event” in Central Africa: Prominent emplacement of bimodal magmatism under extensional regime. *Precambrian Research*, 180, 63-84.

Where and how magma differentiated at La Picada stratovolcano (CSVZ, Chile)

Jacqueline VANDER AUWERA¹, Olivier NAMUR¹⁻³, Adeline DUTRIEUX^{1 4}, Camilla M. WILKINSON⁵, Morgan GANERØD⁵, Valentin COUMONT¹, Olivier BOLLE¹

¹ *Université de Liège, Département de géologie (Belgium)*

² *Leibniz Universität Hannover, Institute of Mineralogy (Germany)*

³ *KU Leuven, Department of Earth and Environmental Sciences (Belgium)*

⁴ *University of Southampton, Ocean and Earth Science (UK)*

⁵ *Geological Survey of Norway (Norway)*

La Picada stratovolcano (41°S) belongs to the Andean Central Southern Volcanic Zone (CSVZ) (38°S-41.5°S, Chile) that results from the subduction of the Nazca plate beneath the western margin of the South American continent. Forty-seven representative samples collected in different units of the volcano define a differentiation trend from basalt to basaltic andesite and dacite (50.9 to 65.6 wt. % SiO₂). This trend straddles the tholeiitic and calc-alkaline fields and displays a conspicuous compositional (Daly) gap between 57.0 (most evolved basaltic andesite) and 62.7 wt. % SiO₂ (dacite). Interstitial, mostly dacitic glass pockets extend the trend to 76.0 wt. % SiO₂. Basalts and basaltic andesites (50.9 to 57.0 wt. % SiO₂) are lavas with macrocrysts of plagioclase (An₉₃₋₂₈), olivine (Fo₈₆₋₅₁), clinopyroxene (Mg# = 82.8-55.2) and orthopyroxene (Mg# = 74.1-56.1), plagioclase being the dominant phase. On the contrary, the dacites were only observed in dykes and are poor in macrocrysts of plagioclase (An₆₈₋₄₆), clinopyroxene (Mg# = 72.2-60.3) and orthopyroxene (Mg# = 63).

A collection of geothermobarometers and hygrometers based on crystal and lava compositions were used to quantify the conditions of differentiation. They indicate that the parent magma(s) had low to moderate H₂O content (1.1-2.5 wt. %) and an oxygen fugacity close to NNO. This latter agrees with experimental data on basalts that straddle the tholeiitic/calc-alkaline boundary. Moreover, clinopyroxene-melt equilibria show that differentiation took place at shallow depth (~ 0.2 GPa). This low pressure is supported by the bulk rock geochemistry and corresponds to an intracrustal discontinuity separating the lower and upper crust.

As mineral and bulk rock compositions don't show the trace of an intermediate fractionation stage in the lower crust, the observed Daly gap likely results from upper crustal magmatic processes. Samples from both sides of the Daly gap show contrasting textures: basalts and basaltic andesites are rich in macrocrysts (18-54 vol %), whereas dacites, only observed in crosscutting dikes, are very poor in macrocrysts (<10 vol %). Moreover, modelling of the fractional crystallization process indicates a total fractionation of 43% to reach the most evolved basaltic andesites. This proportion of crystals in the main storage region is close to the value at which crystals start to form a connecting network (critical crystallinity). The Daly gap is thus interpreted as resulting from critical crystallinity that was reached in the basaltic andesites, thus precluding eruption of more evolved lavas. Some interstitial dacitic melt was extracted from the crystal mush and emplaced as dikes possibly connected to small dacitic domes, now eroded away. However, because of the occurrence of immiscible globules in the matrix, silicate-liquid immiscibility is an alternative hypothesis that needs to be further tested.

Petrography and geochemistry of Nyiragongo volcano lavas: Implication on viscosity, velocity and associated risks in Goma city (Virunga, East African Rift)

Ephrem K. KAMATE¹⁻⁴, Benoit SMETS³, Olivier NAMUR⁴⁻⁵, Jaqueline V. AUWERA⁴, Aurélia H. FERRARI⁶ & François KERVYN³

¹*Département des Sciences et Gestion de l'Environnement, Université de Liège, Belgium ; ephremkamathe@gmail.com*

²*Observatoire Volcanologique de Goma, D.R. Congo*

³*Département de Géorisques, Musée Royal d'Afrique Centrale (Tervuren), Belgium*

⁴*Département de Géologie, Université de Liège, Belgium*

⁵*Department of Earth and Environmental Sciences, Katholieke Universiteit Leuven, Belgium*

⁶*Département de Géographie, Université de Liège, Belgium*

Nyiragongo volcano is located in the western branch of the East African rift system, about 15 km from the city of Goma in the Democratic Republic of Congo. Its summit crater culminates at 3470 m with a diameter of 1.3 km and hosts the largest persistent lava lake on Earth (e.g. Smets et al., 2017).

The main threat of the Nyiragongo volcano on the city of Goma is the lava flows produced during flank eruptions, as attested by the 1977 and 2002 eruptions, which both led to a human, environmental and socio-economic disasters (e.g. Demant, 1994 and Komorowski, 2002/2003). A detailed knowledge of the chemical composition, texture and rheological properties of the Nyiragongo lavas, which are parameters influencing the lava flowing behaviour, is essential to better manage and mitigate future volcanic risks in the city of Goma. Most of the Nyiragongo rocks correspond to a pyroxene-nephelinitic melt, which evolved to melilite nephelinite and melilitite by fractionation of leucite, together with varying amounts of nepheline (Platz, 2004).

In this study, we investigate a new set of samples from the 1977 and 2002 flank eruptions and the 2016-present intra-crater eruptive activity. The first part of the present work consists in the petrological and geochemical (major and minor elements) analyses of the samples. In the second part, these results are used to estimate the melt viscosity with the experimentally-regressed predictive model of Giordano (2008) that is based on melt chemistry and temperature. Viscosity is required as a key parameter influencing the velocity and spreading of lava flows (Tallarico, 2006). In the third and final part, we assess the influence of the calculated viscosity values on both the lava flow velocity according to the slope and the maximum length and spreading of lava flows. The latter has been assessed using the FLOWGO lava flow simulation model (Harris and Rowland, 2001) implemented in Q-LAVHA (Massoux et al., 2016).

Preliminary petrographic results for the 2016 eruption indicate an abundance of nepheline, generally phenocrysts, a moderate proportion of pyroxene and little olivine. Leucite and melilitite are very rare. All samples show high concentrations of alkalis, with K₂O/Na₂O ratios very close to 1 and less than 40 wt.% SiO₂. These results allow us to classify these rocks in nepheline-rich foidites as revealed in previous studies of Nyiragongo volcano rocks (Dement et al., 1994; Barette et al., 2017). Compared to the 1977 samples, the 2002 and 2016 lavas show a lower Al₂O₃ content;

and higher Rb and Ba contents. In fact, at low pressure, high Al₂O₃ concentrations influence the increase of magma velocity (Ohira et al., 2016). The increase in Rb concentrations influences the increasing evolution of eruptive dynamism of volcanoes (Michaud, 1991) while the Ba / Nb ratio can help to understand the geodynamic context (Shuguang, 1995). At 1200°C, the average temperature of liquidus of Nyiragongo lavas (Giordano et al., 2007; Morrison, 2016), the calculated viscosity (Log_n) is on average 2.06 Pa.s (for 2002 lavas) which is low and close to that obtained by Giordano (2007) for lavas of the 2002 eruption (≈ 2 Pa.s). For the 1977 and 2016 lavas, we calculated a viscosity of 1.99 Pa.s and 2.15 Pa.s respectively. It should be noted that the density values calculated at 1200 °C show a stability around 2431 Kg/m³ for the three eruptions considered for this study.

Lava flow simulations were performed on the southernmost 2002 lava flow (Munigi event). Using the 2-D flow model given by Tallarico et al. (2006), taking into account the viscosity, density, average thickness and width of 2002 lava flows, and topographic parameters, we show that a small decrease in the logarithmic viscosity of about 0.015 Pa.s increases by approximately 130 m³/s of effusion rate and by 0.5 m/s the velocity. Simultaneously, the simulations indicate that this increase of effusion rate and velocity, due to the decrease of viscosity, improves the fitness index of the simulation. A high fitness index demonstrates the use of main optimal parameters for the simulation and whose result is close to the real lava flow.

References

- Demant, A., Lestrade, P., Lubala, R.T., Kampunzu, A.B. & Durieux, J., 1994, Volcanological and petrological evolution of Nyiragongo volcano, Virunga volcanic field, Zaire. *Bulletin of Volcanology*, Volume 56, Issue 1, 47-61.
- Komorowski, J.C.; Tedesco, D., Kasereka, M., Allard, P., Papale, P., Vaselli, O., Durieux, J., Baxter, P., Halbwachs, M., Akumbe, M., Baluku, B., Briole, P., Ciraba, M., Dupin, J-C., Etoy, O., Garcin, D., Hamaguchi, H., Houlié, N., Kavotha, K. S., Lemarchand, A., Lockwood, J., Lukaya, N., Mavonga, G., de Michele, M., Mpore, S., Mukambilwa, K., Munyololo, F., Newhall, C., Ruch, J., M. Yalire, M., & Wafula, M., 2002/2003. The January 2002 flank eruption of Nyiragongo volcano (Democratic Republic of Congo): chronology, evidence for a tectonic rift trigger, and major impact of lava flows on the city of Goma. *Acta Vulcanologica*, Volumes 12 (1-2), 15 (1-2), 27-62.
- Smets, B., D'Oreye, N., Kervyn, M. & Kervyn, F., 2017. Gas piston of the Nyiragongo lava lake: First insights from a stereographic Time-Lapse-Camera system, *Journal of African Earth Sciences*, 134, 877-884.
- Platz, T., Foley, S.F. & André, L., 2004. Low-pressure fractionation of the Nyiragongo volcanic rocks, Virunga Province, D.R. Congo. *Journal of Volcanology and Geothermal Research*. Volume 136, Issue 3-4, 269– 295.
- Harris, A. J. L., & Rowland, S., 2001. FLOWGO : A kinematic thermo-rheological model for lava flowing in a channel. *Bulletin of Volcanology*, Volume 63, Issue 1, 20–44.
- Giordano, D., Polacci, M., Longo, A., Papale, P., Dingwell, D.B. , Boschi, E., & Kasereka, M. 2007, Thermo-rheological magma control on the impact of highly fluid lava flows at Mt. Nyiragongo, *Geophysical Research Letters*, Volume 34, Issue 6.
- Giordano, D., Russell, J.K. & Dingwell, D.B., 2008, Viscosity of magmatic liquids : A model. *Earth and Planetary Science letters*, Volume 271, Issues 1-4, 123-134.
- Tallarico, A., Dragoni, M., & Zito, G., 2006, Evaluation of lava effusion rate and viscosity from other flow parameters. *Journal of Geophysical Research : Solid Earth banner*. volume 111, Issue B11205.
- Mossoux, S., Saey, M., Bartolini, S., Poppe, S., Canters, F., & Kervyn, M., 2016. Q-LAVHA: A flexible GIS plugin to simulate lava flows, *Computers & Geosciences* 97, 98–109.

- Barette, F., Poppe, S., Smets, B., Benbakkar, M. & Kervyn, M., 2017. Spatial variation of volcanic rock geochemistry in the Virunga Volcanic Province: Statistical analysis of an integrated database, *Journal of African Earth Sciences* 134, 888-903.
- Ohira, I., Murakami, M., Kohara, S., Ohara, K., & Ohtani, E., 2016. Ultrahigh-pressure acoustic wave velocities of SiO₂-Al₂O₃ glasses up to 200 GPa, *Progress in Earth and Planetary Science*, 10p.
- Li Shuguang, 1995. Implications of ENd-La/ Nb, Ba/Nb, Nb/Th Diagrams to Mantle Heterogeneity Classification of Island-arc Basalts and Decomposition of EMII Component, *Chinese Journal Of Geochemistry*, Vol.14, No.2, pp.117-127.

Mode of emplacement of the Chicxulub impact breccia

Pim KASKES¹, Sietze J. DE GRAAFF¹, Sander OP DE BEECK², Niels J. DE WINTER¹, Thomas DÉHAIS¹, Jan SMIT³, Steven GODERIS¹ & Philippe CLAEYS¹

¹*Analytical, Environmental and Geo-Chemistry, Vrije Universiteit Brussel, Pleinlaan 2, B1050, Brussels, Belgium.*

²*Department of Earth and Environmental Sciences, Katholieke Universiteit Leuven, Celestijnenlaan 200E, B-3001, Leuven, Belgium.*

³*Faculty of Sciences, Vrije Universiteit Amsterdam, De Boelelaan 1085, 1081 HV, Amsterdam, the Netherlands.*

The joint IODP-ICDP 364 expedition in 2016 extracted a unique, continuous sequence of upper peak ring material from the Chicxulub impact structure in Mexico. The interval between core section 40R-1 and 95R-3 consists of a c. 130 m thick succession of suevite and impact melt rock that holds important clues about the composition and modification of the Chicxulub target lithologies (Morgan et al., 2017). The suevite unit is characterized as a melt-bearing polymict impact breccia with a clastic matrix that displays a generally gradual fining and a more well-sorted upward trend. This trend is most likely caused by the gradual decrease in settling velocity of ejecta after the asteroid impact. More subtle changes in the suevite succession, such as the transition between the fallback of ejecta material and the wash-back by tsunamis into the crater, are difficult to recognize. High resolution chemostratigraphy along the entire suevite sequence is therefore essential to identify the provenance of the various clasts and to link them to different formational processes.

Micro X-ray fluorescence (μ XRF) is an ideal technique for such a task, since it combines rapid, non-destructive elemental analysis such as semi-quantitative trace element mapping and quantitative line and point measurements at a 25 μ m resolution (de Winter et al., 2017). Laser Ablation Inductively Coupled Plasma Mass Spectrometry (LA-ICP-MS) provides additional highly sensitive major and trace elemental analyses, which can be coupled to petrographic observations to further distinguish between different types of clasts and matrix.

The main end-members discovered inside the Chicxulub suevite are (sub)angular clasts of fossiliferous limestone and chert in the top part versus clasts of granite and fragments of mafic lithologies that dominate the lower part. These clasts are remnants of a mixed target composed of a 2-3 km thick Mesozoic carbonate and evaporite platform and a Pan-African gneissic-granitic basement. The suevite matrix changes upward from green to grayish brown and represents a mixture of calcite and a clay component dominated by smectite (Morgan et al., 2017). Another important observation is the clear lack of sulfur in the entire suevite interval, which is suggested to be caused by the shock vaporization of major parts of the pre-impact evaporite platform on the Yucatán Peninsula. The only sulfuric components in the core are linked to pyrite crystals, as verified by petrography and μ XRF. By integrating the μ XRF and LA-ICP-MS results with XRF and Computed Tomography scan data of the different core sections, it is possible to extrapolate

microscopic data on the studied samples towards the entire core. This may shed light on the ongoing debate about emplacement mechanisms of suevite and on the relative contributions of the various lithologies to the Chicxulub pre-impact target.

References

- de Winter N., et al., 2017. Trace element analyses of carbonates using portable and micro-X-ray fluorescence: Performance and optimization of measurement parameters and strategies. *J. Anal. At. Spectrom.*, 2017, 32, 1211.
- Morgan, J., et al., 2017. *Chicxulub: Drilling the K-Pg Impact Crater*. Proceedings of IODP, 364. <https://doi.org/10.14379/iodp.proc.364.2017>.

Petrology of the 2015 eruption of Calbuco volcano, Chile

Olivier NAMUR¹, Jacqueline VANDER AUWERA², Olivier BOLLE², Salvatrice MONTALBANO²

¹KU Leuven, Department of Earth and Environmental Sciences

²ULiege, Department of Geology

The Calbuco volcano (41°20'S-72°37'W) is one of the ~ 20 historically active stratovolcanoes in the Southern Volcanic Zone (SVZ; 33-46°S) of the Andes. It is represented by a truncated cone that covers an area of 150 km². Twelve historical eruptions have been described since 1792, including the recent eruption of April 22-23, 2015. In addition, more than 40 major deposits from pyroclastic density currents and pumice fallouts were recognized intercalated in sedimentary rocks from postglacial times (< 13 ky). The activity of Calbuco is divided into 4 stages during which eruptive products alternated between basaltic andesite, andesite and dacite.

On April 22nd 2015, an intense explosive eruption was observed with a (sub)plinian column of 15 km above the crater level. Another more energetic eruption occurred on April 23rd 2015 and lasted for 6 hours. The erupted volume is estimated at 0.38 km³ (0.15 km³ dense rock equivalent), with approximately 90% corresponding to tephra fall deposits and the other 10% to pyroclastic density current deposits. The tephra fallout deposits were distributed mainly to the NE of the volcano and reached a thickness of 52 cm at 6 km from the vent. Pyroclastic density currents were generated in the main valleys around the volcano, reaching up to 6 km from the vent.

We collected 27 samples in the NE and SW of the volcano. Most samples are beige-brown scoria lapillis with particle sizes ranging from less than 1 mm to 3 mm. Pumiceous bombs, up to 25 cm in size, were also collected in the pyroclastic density current deposits. Under the microscope, samples are fresh, highly vacuolar and crystal-rich. Crystals are strongly dominated by plagioclase, olivine and pyroxenes. Fe-Ti oxide minerals are subordinate and amphibole was observed in a single sample. Some samples contain minor olivine represented by highly corroded and partly dissolved anhedral crystals. The matrix is either fined-grained and dominated by plagioclase, pyroxene and Fe-Ti oxides, or quenched as a glass.

Bulk-rock compositions were obtained for major and trace elements. They show little variability, as expressed by the SiO₂ content that ranges between 53 and 58 wt.%. All samples plot at the limit between basaltic andesite and andesite in classification diagrams. Trace elements also show little variability. In many samples, it was possible to measure the glass composition in situ for major and trace elements. The glass is significantly enriched (61-76 wt.% SiO₂) compared to bulk-rock data. However, it should be noted that the most evolved compositions were observed as small pockets of glass between crystals and most probably represent the very late-stage of crystallization.

Crystal compositions were obtained for plagioclase, clinopyroxene and orthopyroxene. Plagioclase compositions show a strong bimodal distribution with crystal cores ranging from An₈₀

to An₉₂ [An = molar Ca/(Ca+Na)] and crystal rims ranging from An₃₀ to An₈₀. Clinopyroxene crystals show a unimodal distribution between Mg#70 and 80 [Mg# = molar Mg/(Mg+ Fe²⁺)] while orthopyroxene displays a more complicated distribution with three different modes at Mg#67, Mg#69 and Mg#72. Trace elements also show intra-crystal variability but further work is needed to fully interpret the data.

In the following part of this project, we will use the relationship between bulk-rock and glass compositions, as well as the mineral compositions to estimate the conditions of magma storage prior to eruption. We will also use these data to estimate how the plumbing system beneath Calbuco might look like. Finally, we will address an important question in petrology that concerns the formation of andesite: Do andesitic samples represent melt compositions or do they form by crystal accumulation in a dacitic melt?

Late-tectonic evolution of the Sveconorwegian (Grenvillian) orogen in Southern Norway: what do granites tell us?

Olivier BOLLE¹, Hervé DIOT², Jacqueline VANDER AUWERA¹

¹ *Université de Liège, Département de géologie (Belgium)*

² *Université de La Rochelle, Faculté de Sciences et Technologie (France)*

Granites *s.l.* (granitoids) occupy an important volume of the continental crust, especially in orogenic belts, and they represent key markers of the Earth's crust evolution. In particular, it is now well established that despite their massive aspect, granitoids commonly display homogeneous fabrics that mimic the tectonic pattern of their country rocks. This means that granitic bodies are capable of recording tectonic strain in the course of their crystallization and may be used as markers of crustal deformation.

In the Precambrian basement of Southern Norway and Southwest Sweden, abundant granitic plutons were emplaced at 0.99-0.92 Ga (Bingen et al., 2008b; Vander Auwera et al., 2011; and references therein), during the last stage of evolution of the Sveconorwegian (Grenvillian) orogen. These plutons are classically regarded as post-tectonic bodies, emplaced in an extensional context related either to gravitational collapse of the orogenic belt, considering the conventional, collisional model admitted for the Sveconorwegian orogen (Bingen et al., 2008b) or to steepening of the subducting slab, considering a challenging, accretionary model proposed recently (Slagstad et al., 2013). An alternative tectonic context to extension is discussed here, based on published structural maps, using the anisotropy of magnetic susceptibility (AMS) technique, of three late-Sveconorwegian plutons of Southern Norway (Bolle et al., 2003, 2018): the Holum granite, and the Kleivan and Sjelset granitic complexes. The Holum granite is a homogeneous, biotite+hornblende granite dated at 957 ± 7 Ma (zircon U-Pb age; Bingen et al., 2006). The Kleivan and Sjelset granitic complexes are two composite plutons, containing both biotite (\pm hornblende) and orthopyroxene granitic facies that are almost coeval in the Kleivan complex (U-Pb ages of single zircons from 936.94 ± 0.42 Ma to 935.62 ± 0.67 Ma; Bolle et al., 2018), but correspond to magmatic pulses with a significant age difference in the Sjelset complex (935.67 ± 0.37 Ma and 932.43 ± 0.75 Ma; Bolle et al., 2018).

The three plutons are elongated parallel to the regional tectonic framework defined by several generations of superimposed folds developed along *ca.* N-S-trending axes. The Holum granite and the Kleivan complex crop out, respectively, along strike and in the core of a large-scale fold. Their magnetic lineations are parallel to the axis of these folds, as well as to lineations measured in the country rocks. Magnetic lineations in the Sjelset complex are also parallel to fold axes and lineations in the country rocks. These results demonstrate that regional-scale folding was still active in the area at the time of emplacement of the three plutons (957-932.5 Ma) and probably shortly after, *i.e.* up to *ca.* 40 Ma after the peak of regional metamorphism dated at 1.035-0.97 Ga (Bingen et al., 2008a; Drüppel et al., 2013; and references therein).

The mean magnetic lineation calculated for the Holum granite, and the Kleivan and Sjelset granitic complexes points to a *ca.* N-S and low-angle (<45°) regional axis of stretching (*X* axis). Folding around this axis implies a *ca.* E-W and low-angle direction of shortening (*Z* axis). Such regional *X* and *Z* axes approximate the pattern of finite strain that would be produced either by a strike-slip deformation or by a strike-slip-dominated, homogeneous (i.e. not or weakly partitioned) transpression or transtension at low to moderate magnitude of strain. The strike-slip explanation being probably irrelevant in the late-Sveconorwegian context, we propose that transpression is a viable alternative to extension or transtension since this regime can also promote the emplacement of granitoids, as well as the exhumation of deep crustal rocks causing extensional movements.

References

- Bingen, B., Davis, W.J., Hamilton, M.A., Engvik, A.K., Stein, H.J., Skår, Ø. & Nordgulen, Ø., 2008a. Geochronology of high-grade metamorphism in the Sveconorwegian belt, S. Norway: U-Pb, Th-Pb and Re-Os data. *Norwegian Journal of Geology*, 88, 13-42.
- Bingen, B., Nordgulen, Ø. & Viola, G., 2008b. A four-phase model for the Sveconorwegian orogeny, SW Scandinavia. *Norwegian Journal of Geology*, 88, 43-72.
- Bingen, B., Stein, H.J., Bogaerts, M., Bolle, O. & Mansfeld, J., 2006. Molybdenite Re-Os dating constrains gravitational collapse of the Sveconorwegian orogen, SW Scandinavia. *Lithos*, 87, 328-346.
- Bolle, O., Diot, H. & Trindade, R.I.F., 2003. Magnetic fabrics in the Holum granite (Vest-Agder, southernmost Norway): implications for the late evolution of the Sveconorwegian (Grenvillian) orogen of SW Scandinavia. *Precambrian Research*, 121, 221-249.
- Bolle, O., Diot, H., Vander Auwera, J., Dembele, A., Schittekat, J., Spassov, S., Ovtcharova, M. & Schaltegger, U., 2018. Pluton construction and deformation in the Sveconorwegian crust of SW Norway: magnetic fabric and U-Pb geochronology of the Kleivan and Sjelset granitic complexes. *Precambrian Research*, 305, 247-267.
- Drüppel, K., Elsäßer, L., Brandt, S. & Gerdes, A., 2013. Sveconorwegian mid-crustal ultrahigh-temperature metamorphism in Rogaland, Norway: U-Pb LA-ICP-MS geochronology and pseudosections of sapphirine granulites and associated paragneisses. *Journal of Petrology*, 54, 305-350.
- Slagstad, T., Roberts, N.M.W., Marker, M., Røhr, T.S. & Schiellerup, H., 2013. A non-collisional, accretionary Sveconorwegian orogen. *Terra Nova*, 25, 30-37.
- Vander Auwera, J., Bolle, O., Bingen, B., Liégeois, J.P., Bogaerts, M., Duchesne, J.C., De Waele, B. & Longhi, J., 2011. Sveconorwegian massif-type anorthosites and related granitoids result from post-collisional melting of a continental arc root. *Earth-Science Reviews*, 107, 375-397.

Theme 3

New developments in geology and their role in future research

How quantitative are mineralogical data? Outcomes of the 9th Reynolds Cup contest.

Rieko ADRIAENS^{1,2}, Gilles MERTENS²

¹ *KU Leuven, Departement of Earth and Environmental Sciences, Celestijnenlaan 200 E, 3000 Leuven*

² *QMineral, Analysis & Consulting, Gaston Geenslaan 1, 3001 Heverlee*

The Reynolds Cup competition is an international renowned round robin event for quantitative mineralogy and clay mineralogy, open for scientists active in academia, research institutions, industries or commercial consulting agencies. Unlike other round-robin events, the Reynolds Cup competition issues three mixtures of pure mineral standards that represent realistic rock compositions. The participants can use any method or a combination of methods to obtain the most accurate quantitative phase analysis and, apart from the winners, remain anonymous. The quantification of mineral mixtures is very often performed by the aid of X-ray diffraction, infrared spectroscopy or thermal analysis methods but each method requires a human interpretation to decide on the correct identification and quantification. The primary goal of the contest is therefore to inspire and stimulate researchers to improve their analytical techniques and individual interpretation skills.

The Reynolds Cup was named after Bob Reynolds for his pioneering work in quantitative clay mineralogy and his great contributions to clay science and was established in 2000 by Douglas McCarty and Jan Srodon of ChevronTexaco and Dennis Eberl of the United States Geological Survey (USGS). The first RC competition was started in 2002 and is currently funded by the Clay Minerals Society CMS and the German-Austrian-Swiss Clay Group DTTG. The success of this competition encouraged the founders to make it a biennial event so that in 2018 already the 9th edition of the Reynolds Cup was organized.

Gilles Mertens and Rieko Adriaens won the edition of 2016 and therefore were privileged, parallel to the Eurovision song contest, to organize the latest 2018 Reynolds Cup competition. The organizers prepared ca. 100 sample sets to distribute amongst the different participants. The three samples were prepared to match a specific rock type: (1) a sabkha deposit, (2) a weathered marine deposit and, (3) a carbonatite deposit. The samples consist of powder mixtures of minerals that were carefully selected and tested for their purity. The pure minerals were passively hand ground and where necessary sieved to minus 0.125 mm (or finer for minor components) prior to mixing. Some minerals were milled in a centrifugal mill using a 0.08 mm screen. All materials were equilibrated at 22°C and a relative humidity of 37-39% before weighing out the individual phases. The homogenization of the mixtures was performed by 24h overhead tumbling, then passing the mixture through a 0.2 mm screen to destroy aggregates, and final mixing for 24 hours by overhead tumbling in 1.2 L bottles with a few mixing balls with different density.

In total, 88 participants registered for the competition representing universities, national and private research institutions, industrial and consulting companies from 28 different countries. After 3

months at the final deadline, 73 participants submitted their best quantitative result, of which all but 3 used X-ray diffraction as a primary technique.

It is clear from the 2018 results, parallel to the results of previous contests, that huge differences exist between the results of different participants, regardless of the used equipment and software packages. The Reynolds Cup results of the different editions show that there is not a unique successful approach towards accurate quantification. The winners of past Reynolds Cup competitions have often used different procedures in preparation but also different software. For instance some Reynolds Cup winners have used Rietveld-based software whereas others were very successful using pattern summation software. Both approaches have clear advantages and disadvantages and both can be successfully applied but also do not guarantee in any way an accurate quantification. The Reynolds Cup has shown that the competence and experience of the participant itself is much more crucial. The optimal strategy to follow in preparation, X-ray measurements, interpretation and additional analyses very much depend on the matrix, i.e. the sample composition and thus cannot be easily formalized in a set of hard and fast rules.

The TOP-3-finishers of the 2018 Reynolds Cup were announced at the 55th Annual meeting of the Clay Minerals Society in Urbana-Champaign (USA) in June.

Characterizing and sourcing quartz phenocrysts using cathodoluminescence: a case study in the Upper Silurian – Lower Devonian of the Rocroi inlier, Ardennes, Belgium

Jean-Marc BAELE¹, Corentin COBERT¹, Antoine TRIANTAFYLLOU² and Frédéric LACQUEMENT³

¹*University of Mons, Geology and Applied Geology, 9 rue de Houdain, 7000 Mons, Belgium*

²*UNantes, Laboratory of Planetology and Geodynamics (CNRS UMR 6112), Nantes, France*

³*BRGM (French Geological Survey), GeoRessources Division, Orléans, France*

A cathodoluminescence (CL) study showed that the “roches à quartz dihexahédriques” (*sensu* Beugnies, 1969) or “porphyroïdes” in the Willerzie area (easternmost Rocroi inlier) are rhyolitic meta-tuffs and meta-ignimbrites deposited in an aquatic environment. More than 40 samples were investigated from different localities, including the Willerzie borehole, Rocher des Ruchons, Ruisseau des Rousseries valley (incl. Marotelle), Hauts-Buttés, Laifour and other sites. In the Willerzie borehole, remarkable shale breccias up to 7 m thick include rhyolite lapilli and clasts with various volcanic textures and quartz phenocrysts/splinters. These ones attest for the close vicinity of a fossil volcanic center with explosive eruptions. The volcanogenic horizons are interbedded within Upper Silurian to Lower Devonian metasediments (Roche et al., 1986; Meilliez, 1988).

Quartz phenocrysts and glomerocrysts in these rocks exhibit a ubiquitous red CL emission with a rounded growth zoning, which is typical for (sub)volcanic quartz (Fig. 1). A similar red CL was observed in quartz phenocrysts in Silurian rhyolitic lava flow from “Piroy volcano” (Malonne) but not in other well-known subvolcanic rocks in Belgium, where the CL is blue (Lessines, Quenast). However, quartz grains from Upper Silurian to Lower Devonian siliciclastics overlying the Rocroi inlier, have a different cathodofacies with blue to brown CL colors and abundant internal textures such as “spiders” and “cobweb” (Boggs & Krinsley, 2006), which would suggest a deeper (subvolcanic to plutonic) origin. The source area of these quartz grains is unknown. The investigated series included the “Fépin Conglomerate”, “Arkose” and “Grès d’Haybes” (Fépin Fm.), “Arkose de Willerzie”, quartzitic to arkosic rocks from Oignies Fm., etc. Some sandstone units in the Willerzie borehole, are also devoid of or extremely poor in red-luminescent quartz phenocrysts. All this points to local episodic production of volcanic material in the vicinity of the eruptive center of Willerzie.

Our study also demonstrated that CL is more reliable in discriminating/sourcing quartz phenocrysts than do conventional optical petrography as it reveals primary and secondary geochemical/microstructural characteristics that are otherwise hardly or not visible. Primary characteristics include growth zoning, enigmatic cylindrical features with blue CL possibly related to former inclusions now resorbed and irregular dark-CL patterns (“cobweb” and other related textures). Secondary CL characteristics of the phenocrysts include overgrowths and the development of a dark-blue CL rimming cracks due to fast cooling and forming a streak pattern inside the phenocrysts, especially around pressure shadows. A bright-green short-lived CL similar to that in adjacent quartz veins induced by (Variscan) tectonic stress is also observed in microfractures. CL also highlights various rhyolitic textures in the groundmass such as flow

banding, perlites, spherulites, pumiceous structures and “snowflake” devitrification textures, as well as alteration (kaolinite) and abundant irradiation haloes due to REE/U/Th-bearing minerals, especially in As-Pb-Zn-Cu(-Au?) SedEx mineralized zones.

The contemporaneity between bimodal magmatism in the Rocroi inlier and Willerzie volcanites, first hypothesized by Beugnies & Charlet (1970) has recently been confirmed based on new geochronological data (Cobert et al., 2018). However, quartz phenocrysts from Mairupt and Grande-Commune microgranites display a blue CL color, which is typical of magmatic quartz. Interestingly, quartz phenocrysts in rocks from the top of Laifour plateau and Hauts-Buttés, which are supposed to originate from an intermediate emplacement depth, have quartz phenocrysts with both blue and red CL colors. This suggests that the red CL in quartz phenocrysts could provide a record of particular conditions or processes of felsic magma emplacement to the surface that still need to be elucidated.

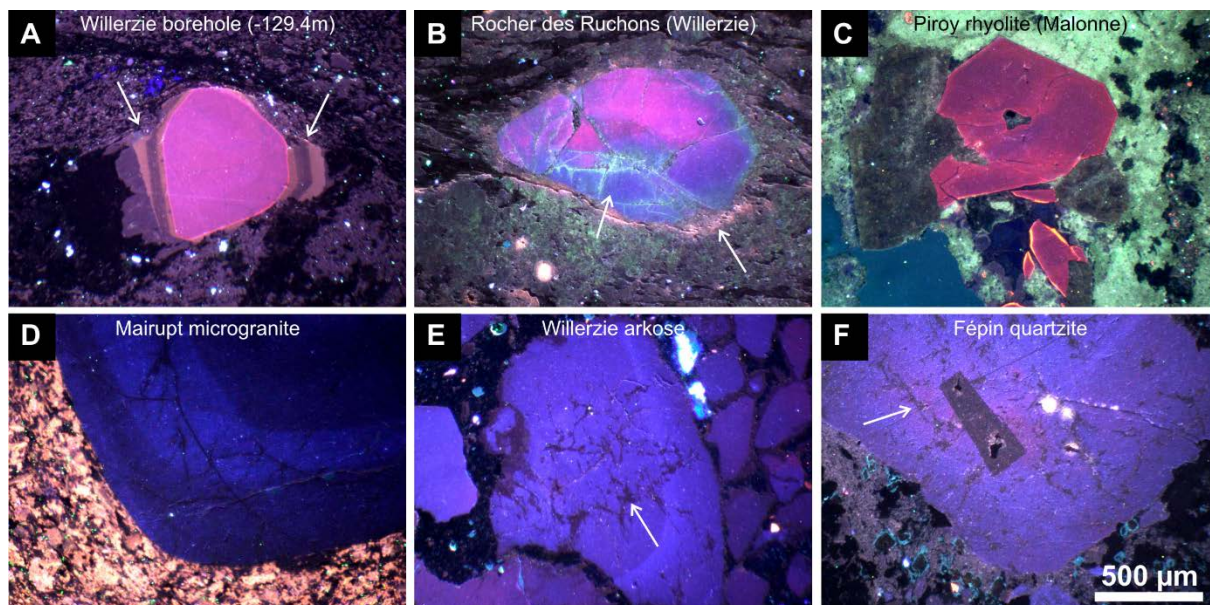


Figure 1. Cathodoluminescence (CL) micrographs of quartz phenocrysts in magmatic and sedimentary rocks from different locations described in the text. In (A), arrows point to quartz overgrowth with banded-brown CL within pressure shadows. In (B), left arrow shows the development of dark blue and bright green CL as secondary features related to deformation and associated fluids. Right arrow points to irradiation haloes. In (E) and (F), arrows show a dark CL “cobweb” texture, which is typical of more plutonic quartz.

References

- Beugnies, A., 1969. Les roches à quartz dihexaédriques du Franc-Bois de Willerzie. *Bull. Soc. Belge Géol.*, 77, 311-329.
- Beugnies, A. & Charlet, J.-M., 1970. Sur l'âge hercynien des microgranites du Massif cambrien de Rocroi (données pétrographiques et analyse par thermoluminescence). *Ann. Soc. géol. Belgique*, 93, 431-452.
- Cobert, C., Baele, J.-M., Boulvais, Ph., Poujol, M. & Decrée, S., 2018. Petrogenesis of the Mairupt microgranite: a witness of an uppermost Silurian magmatism in the Rocroi Inlier, Ardenne Allochton. *C. R. Geoscience*, 350, 89-99.
- Meilliez, F., 1988. Le sondage de Willerzie, en bordure orientale du massif de Rocroi. *Bull. Soc. Hist. Nat. Ardennes*, 78, 49-58.
- Roche, M., Sabir, M., Steemans, P. & Vanguetaine, M., 1986. Palynologie du sondage et de la région de Willerzie. *Aardkundige Mededelingen*, 3, 149-190.

Laser-Induced Breakdown Spectroscopy (LIBS) for fast geochemical analysis of rocks and minerals – current state of the technique and example applications

Jean-Marc BAELE¹

¹*University of Mons, Geology and Applied Geology, 9 rue de Houdain, 7000 Mons, Belgium*

LIBS (Laser-Induced Breakdown Spectroscopy) is a versatile analytical technique based on atomic emission spectroscopy of laser-induced plasmas. It allows fast chemical analysis of solids, liquids and gases with no or minimal sample preparation and is virtually non-destructive (Miziolek et al., 2006; Musazzi & Perini, 2014; Galbács, 2015). Application of LIBS to earth sciences is a rapidly growing field (e.g. Senesi, 2014) and diverse geological and environmental materials can be interrogated with a rather simple equipment both in the laboratory, for macro- to microanalysis, and in the field, where remote analysis is even possible. The ability of LIBS to simultaneously detect all elements (especially light to very light elements) down to trace levels is another attractive attribute, and routine isotope analysis could become a reality in the next future.

Despite all these advantages, LIBS has a major drawback: its rather poor analytical performances, especially in chemometric terms. The LIBS signal results from a complex interplay between several factors pertaining to the analytical system and the chemical and physical properties of the sample. Laser-matter interaction, plasma generation and their influence on the experimental data are not yet fully understood, which, among others, results in poor reproducibility and complicates quantitative analysis. However, raw LIBS spectra provide geochemical fingerprints that can readily be used for material identification, discrimination and provenance analysis in several industrial, geological and archeological problems such as real-time monitoring/sorting of ores and sourcing raw materials.

In its current state, LIBS do not compete with well-established techniques such as LA-ICP-MS in terms of accuracy, precision and detection level. Instead, it should be regarded as an exploratory technique, typically in situations where the number of samples is so large that conventional techniques will be exceedingly expensive or time-consuming. LIBS can also be advantageously used for screening large sample sets for preparing further geochemical analysis of smaller subsets. In this case, subsampling can be optimized as it has a firm, geochemical basis. LIBS can also expand the capabilities of other analytical systems such as LA-ICP-MS for analyzing major elements, XRF for light elements, and Raman spectroscopy, for combining elemental and molecular (vibrational) spectroscopy.

Depending on its design, a LIBS system can be very versatile, allowing point, line, surface and even 3D analysis of samples with a wide variety of sizes, shapes and preparation types. For example, geochemical logging of long core sections and fast mapping of hand-sample are possible on the same system with minimal efforts and costs (Fig. 1). The laser beam can also be shaped as a line instead of the common circular spot, which greatly accelerates the scanning of finely layered rocks while keeping a high stratigraphic resolution. The laboratory system developed at UMONS can also use three different laser wavelengths (alone or in combination): UV (266 nm), VIS (532

nm) and NIR (1064 nm) for optimal laser-matter coupling. Ongoing developments include micro-LIBS capability using a dedicated optical microscope and implementation of Raman spectroscopy in the 532 nm LIBS line.

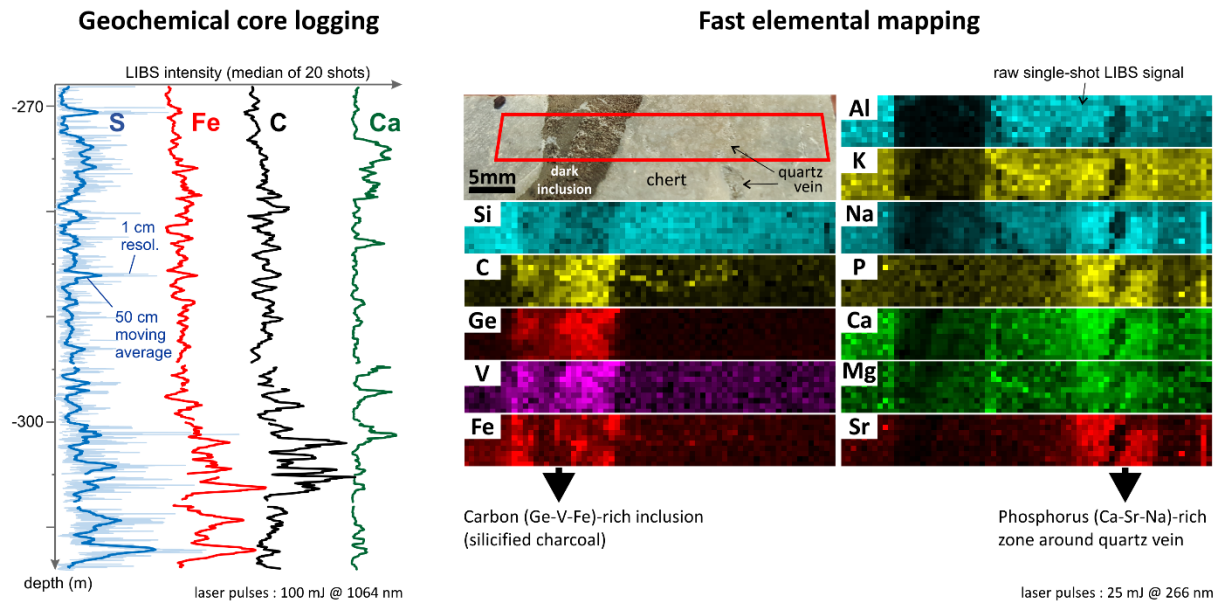


Figure 1. Two example applications of LIBS. Left : geochemical core logging of selected elements in the ~50 m-thick Cretaceous lacustrine clay sequence in Ber3 borehole, Bernissart, showing some cyclicity and an enrichment in pyrite and (total) carbon in the lower part. Right: low-resolution single-shot LIBS mapping performed on a sawn surface of a Cretaceous chert from the Mons Basin to quickly investigate a dark-brown fibrous inclusion (70 s acquisition time, no data processing). The absence of P and Ca indicates that the inclusion is not a fossil bone as expected but silicified carbonaceous matter interpreted as silicified charcoal. An unexpected phosphate-bearing zone is detected to the right.

References

- Gálbács, G., 2015. A critical review of recent progress in analytical laser-induced breakdown spectroscopy. *Analytical Bioanalytical Chemistry*, 407(25), 7537-62.
- Harmon, R.S., Russo, R.E. & Hark, R.R., 2013. Applications of laser-induced breakdown spectroscopy for geochemical and environmental analysis: A comprehensive review. *Spectrochimica Acta Part B*, 87, 11-26.
- Miziolek, A.W., Palleschini V. & Schechter, I., 2006. *Laser-Induced Breakdown Spectroscopy (LIBS). Fundamentals and Applications*, New York, Cambridge University Press, 620 p.
- Musazzi, S. & Perini, U., 2014. *Laser-Induced Breakdown Spectroscopy. Theory and applications*. Heidelberg, Springer, 565 p.
- Senesi, G.S., 2014. Laser-Induced Breakdown Spectroscopy (LIBS) applied to terrestrial and extraterrestrial analogue materials with emphasis to minerals and rocks. *Earth-Science Reviews*, 139, 231-267.

Subsurface mapping using gravity data during construction of the new 3D model of the Flemish subsurface (G3Dv3)

Timothy N. DEBACKER¹, Jef DECKERS², Bernd ROMBAUT², Matsen BROOTHAERS², Helga FERKET¹, Paul WILLIAMSON³

¹. VPO, Bureau for Environment and Spatial Development – Flanders, Koning Albert II-laan 20, 1000 Brussels; timothy.debacker@vlaanderen.be

². VITO, Flemish Institute for Technological Research, Boeretang 200, BE-2400 Mol, Belgium

³. BGS, British Geological Survey, Environmental Science Centre, Keyworth, Nottingham, NG12 5GG UK

1. Introduction

In the framework of the construction of the new 3D geological model of Flanders (G3Dv3) by VITO, we tested the use of gravity data for mapping at a subregional level in the Campine Basin, hereby focusing on faults.

For fault mapping, VITO has mainly relied on 2D seismic data, and where available used additional data such as coal mining and borehole data, surface expressions, electric resistivity profiles and jumps in hydraulic head (Matthijs et al., 2013; cf. Deckers et al., 2018). Because of the focus on seismic data, there is a considerable (seismic) data driven bias in fault density. In addition, it is often difficult to correlate faults between - often widely spaced - 2D seismic sections, in particular in the presence of fault splays and relay zones. Also fault terminations (lateral tip lines) are difficult to position. Because of these uncertainties, the regional structural framework is often obscured.

The additional use of potential field data can overcome many of these uncertainties. For the Campine Basin, conventional aeromagnetic data do not provide much extra information because of the relatively large depth to basement and the apparently, virtually non-magnetic nature of both basin sediments and basement in this area. However, density contrasts between basement and sediments, and the presence of intrabasinal high-density and low-density units are promising for the use of gravity data.

2. Data and method

In 2004 the British Geological Survey (BGS) reinterpreted the gravity data of the Brabant Massif as part of a commissioned study managed by GF Consult bvba on behalf of the Flemish government (VLA04-3.1; Chacksfield et al., 2004). For this purpose, BGS constructed a new, high-resolution (point distance ≤ 1 km) Bouguer gravity map of Flanders, using gravity data from the Geological Survey of Belgium. A variable density Bouguer reduction was used for the construction of this map, and, for interpretation purposes several short-wavelength gravity filters were produced. Since 2003 no new publicly available gravity data have been acquired in Belgium (cf. Everaerts & De Vos, 2012).

For this study, first, a regional gravity lineament map of Flanders was constructed by VPO using BGS Bouguer gravity and filters (VLA04-3.1; Chacksfield et al., 2004). This was done completely independent from the mainly seismic data based fault mapping by VITO. In a second step, VPO

compared the faults mapped by VITO with the gravity data. This was done consecutively for three subareas within the Campine Basin. Feedback was provided on the mapped faults in terms of fault trace and trend, cross-cutting relationships and fault terminations. Also at this stage no gravity data or gravity interpretations were passed on to VITO. In a third step, the resulting fault map of the Campine Basin was interpreted together by VPO and VITO, checking all available data against the gravity data. This resulted in the final fault map for G3Dv3.

3. Results and conclusion

The incorporation of gravity data allows extending and mapping fault traces outside of the areas covered by seismic and mine data. Individual Palaeozoic sub-basins, horsts and rift-structures can be recognized, and can often be mapped using the gravity data. The incorporation of gravity data at a very early stage in the interpretation process quickly results in a much better constrained regional fault framework, and in turn highlights interpretation issues. Also the nature and significance of specific, sometimes controversial, fault structures (e.g. Donderslag lineament) become much better understood.

As this study illustrates, even at a sub-regional level, potential field data – in this case gravity data - should be regarded as a standard mapping tool in unexposed terrains, with a level of hierarchy quite similar to that of seismic data.

4. References

- Chacksfield, B.C., Williamson, J.P., Pharaoh, T.C. & McEvoy, F.M., 2004. *Reinterpretation of gravity anomalies over the Brabant Massif in southern Flanders (Belgium)*. British geological survey commissioned Report, CR/04/215. 47 p.
- Deckers, J., Van Noten, K., Schiltz, M., Lecocq, T & Vanneste, K., 2018. Integrated study on the topographic and shallow subsurface expression of the Grote Brogel Fault at the boundary of the Roer Valley Graben, Belgium. *Tectonophysics*, **722**, 486-506.
- Everaerts, M. & De Vos, W., 2012. Gravity acquisition in Belgium and the resulting Bouguer anomaly map. *Memoirs of the Geological Survey of Belgium*, **58**, 55 p.
- Matthijs, J., Lanckacker, T., De Koninck, R., Deckers, J., Lagrou, D. & Broothaers, M., 2013. Geologisch 3D lagenmodel van Vlaanderen en het Brussels Hoofdstedelijk Gewest - versie 2, G3Dv2. Studie uitgevoerd door VITO in opdracht van de Vlaamse overheid, Departement Leefmilieu, Natuur en Energie, Afdeling Land en Bodembescherming, Ondergrond, Natuurlijke Rijkdommen, *VITO-rapport2013/R/ETE/43*.

Using μ CT to investigate water migration during freeze-thaw experiments

Maxim DEPRez¹, Tim DE KOCK¹, Geert DE SCHUTTER² & Veerle CNUUDE¹

¹ PProGRess/UGCT, Department of Geology, Ghent University, Krijgslaan 281, S8, 9000 Ghent

² Magnel Laboratory for Concrete Research, Department of Structural Engineering, Ghent University, Technologiepark 904, 9052 Zwijnaarde.

1. Introduction

The degree of water saturation is an important factor to freeze-thaw (FT) weathering. There is even a material-specific critical saturation level above which the host will suffer immediate damage when subjected to a FT cycle (Prick, 1997). Up to today, it is not fully clear which process, accompanying crystallization in the pores, is responsible for the stress build-up. Hence, the link between the pressure mechanism and the critical saturation degree is not fully understood. It is believed moisture is drawn towards growing crystals (Everett, 1961; Walder and Hallet, 1985), which enables the crystals to remain growing as long as water is able to move to the site. Consequently, crystallization pressure on the pore walls is supposed to be the main damaging mechanism (Scherer, 1999). However, in highly saturated rocks, there could be an influence of trapped water in the smaller pores of the system, and hydraulic pressures could be generated (e.g. Powers, 1945) for high rates of freezing and low permeabilities. However, the latter is unlikely to occur within *in situ* building materials (Scherer and Valenza, 2005). These theories can be supported by measuring the length change of samples subject to a FT experiment. However, such observations only result in indirect evidence which could lead to misinterpretations (e.g. Powers & Helmuth, 1953). Therefore, *in situ* monitoring water transport during one or more FT-cycles, could deliver an extra clue in the search for the damaging mechanisms. Cyclic FT weathering tests were performed both on laboratory scale and on the micro-scale using X-ray computed tomography (μ CT) on samples with different degrees of saturation. Laboratory samples were monitored for length changes and long-term decay pattern. μ CT time-lapse imaging of the freezing process, was used to study the repositioning of water/ice. Afterwards, these microscopic observations were compared with the macroscopic weathering pattern, with a link to the saturation degree.

2. Materials and Methods

Savonnières limestone (Upper Jurassic) is a French natural building stone composed of oolites and shell fragments. Bentheimer sandstone (Lower Cretaceous) is found at the German-Dutch border and is a well-sorted, homogeneous quartz arenite. FT resistivity largely depends on the pore characteristics of a certain material. Therefore, these two stones, which are known to have totally different pore characteristics, were selected for the experiments.

The weathering behaviour of the two natural stones was investigated in function of the degree of water saturation. After applying 140 FT cycles to differently saturated samples, the damage was assessed visually, microscopically and by porosity measurements. Monitoring some proxies of the internal processes during the FT cycles (i.e. temperature evolution and length change) were added to comprehend the internal processes.

To assess the processes within the pores, μ CT was used. This technique has proven its value within geoscience as a non-destructive imaging method (Cnudde and Boone, 2013). At the Ghent University Centre for Tomography (UGCT) it has been possible to image a sample subjected to FT cycles (De Kock et al., 2015) by implementing a custom-made freezing stage (De Schryver et al., 2014). To check the feasibility of the technique and the duration of an appropriate FT process, a Savonnières sample was imaged at several defined temperatures during cooling. To investigate the preferred location of water/ice crystals and whether these locations shift during the process, samples with certain defined saturations were subjected to FT cycles on the μ CT device. The samples of interest were imaged both unfrozen and frozen and this for several FT cycles.

3. Results and discussion

Results of the weathering test show that Bentheimer sandstone and Savonnières limestone have a different weathering pattern, independent of the saturation degree. At saturation degrees larger than 80 %, Bentheimer will burst from the inside out, while Savonnières will lose large parts of its edges. At lower saturation degrees, both stones remain unaffected after 140 FT cycles.

An exotherm in temperature measurements during FT cycles shows that crystallization does occur in all samples when cooled to $-15\text{ }^{\circ}\text{C}$. Similar to the temperature, length change curves illustrate the crystallization event. For low saturations, the length change curve follows the temperature curve, while for high saturations, it is clear that more stress is developed within the pores. The way this is pronounced is however slightly different for both stones. Both, temperature and length change curve indicate a different effect of processes in the pores for both stones while a similar FT test is performed.

A first μ CT test on a Savonnières sample shows that it is possible to monitor the change between the unfrozen and frozen scan. When the behaviour of the pore water/ice is monitored after several cycles, a shift is seen in the positions of the ice. Combining the results of μ CT with the proxies for ice crystallization could lead to a more uniform idea of what happens during ice crystallization and melting within these rocks and what the influence of the saturation degree is on the acting processes.

4. References

- Cnudde, V., & Boone, M. N. (2013). High-resolution X-ray computed tomography in geosciences: A review of the current technology and applications. *Earth-Science Reviews*, 123, 1–17.
- De Kock, T., Boone, M. A., De Schryver, T., Stappen, J. Van, Derluyn, H., Masschaele, B., De Schutter, G., & Cnudde, V. (2015). A Pore-Scale Study of Fracture Dynamics in Rock Using X-ray Micro-CT Under Ambient Freeze–Thaw Cycling. *Environmental Science & Technology*, 49, 2867–2874.
- De Schryver, T., Boone, M. A., De Kock, T., Duquenne, B., Christaki, M., Masschaele, B., Dierick, M., Boone, M. N., & Van Hoorebeke, L. (2014). A compact low cost cooling stage for lab based x-ray micro-CT setups. In *AIP Conf. Proc.* (Vol. 1696, pp. 1–5).
- Everett, D. H. (1961). The thermodynamics of frost damage to porous solids. *Transactions of the Faraday Society*, 57(0), 1541.
- Powers, T. C. (1945). A Working Hypothesis for Further Studies of Frost Resistance of Concrete. In *Journal Proceedings- American Concrete Institute* (Vol. 41, p. 245).
- Powers, T. C., & Helmuth, R. A. (1953). Theory of volume changes in hardened portland-cement paste during freezing. *Highway Research Board Proceedings*, 32.

- Prick, A. (1997). Critical Degree of Saturation as a Threshold Moisture Level in Frost Weathering of Limestones. *Permafrost and Periglacial Processes*, 8(1), 91–99.
- Scherer, G. W. (1999). Crystallization in pores. *Cement and Concrete Research*, 29(8), 1347–1358.
- Scherer, G. W., & Valenza, J. J. (2005). Mechanisms of Frost Damage. *Materials Science of Concrete*, VII, 209–246.
- Walder, J., & Hallet, B. (1985). A theoretical model of the fracture of rock during freezing. *Geological Society of America Bulletin*, 96, 336–346.

Tracing ancient DNA of foraminifera in tsunami deposits (GEN-EX)

Max ENGEL¹, Isa SCHÖN², Tasnim PATEL², Sue DAWSON³, Ed GARRETT^{1,4}, Witold SZCZUCIŃSKI⁵, Philipp KEMPF¹ & Vanessa M.A. HEYVAERT^{1,6}

¹*Royal Belgian Institute of Natural Sciences, OD Earth and History of Life, Geological Survey of Belgium, Jennerstraat 13, 1000 Brussels, Belgium*

²*Royal Belgian Institute of Natural Sciences, OD Nature, ATECO, Freshwater Biology, Vautierstraat 29, 1000 Brussels, Belgium*

³*University of Dundee, Department of Geography, Tower Building, Nethergate, Dundee DD1 4HN, UK*

⁴*Durham University, Department of Geography, South Road, Durham, DH1 3LE, UK*

⁵*Adam Mickiewicz University in Poznań, Institute of Geology, Bogumiła Krygowskiego 12, 61-680 Poznań, Poland*

⁶*Ghent University, Department of Geology, Krijgslaan 281, 9000 Ghent, Belgium*

1. Background

Tsunami deposits provide information on the long-term frequency-magnitude patterns of events, which may not be covered by the historical and instrumental record. Such information is crucial for the assessment of coastal hazards and mitigation measures against the loss of life and assets. In order to identify tsunami deposits in the coastal sedimentary record and to infer tsunami characteristics, a wide range of proxies has been established based on studies of recent tsunami deposits. Microfossils (e.g. foraminifera, ostracods, diatoms) are often used to recognize tsunami deposits, and to differentiate them from those of other processes. In terms of foraminifera, tsunami deposits mostly contain allochthonous associations dominated by benthic intertidal to inner shelf taxa. Specimens may originate from outer shelf to bathyal depths; even planktonic forms may occur. Furthermore, changes in test numbers, taphonomy, size or adult/juvenile ratios compared to background sedimentation are common (Pilarczyk et al., 2014; Engel et al., 2016). However, dissolution of microfossils often prevent identification and diminish their value as a proxy (Yawsangratt et al., 2012).

2. Study goals and concept

To address the problem of post-depositional alteration of microfossil associations in tsunami deposits, high-throughput metagenomic sequencing techniques are applied by the GEN-EX project to identify marine organisms in onshore sand layers based on their DNA remains. Metagenomics (or environmental genomics) is related to sequencing DNA directly from the environmental samples, where the genetic material may have been preserved in sedimentary records covering tens of thousands of years. Metagenomics is an emerging technique in environmental research and is used to characterize the diversity of bacterial communities but also higher organisms such as animals, plants and fungi of recent and ancient origin in a variety of settings, including ice, lake sediments, soils, cave deposits, and various types of surface waters. Metagenomics can also be used to detect cryptic diversity, ultimately providing more accurate estimates of biodiversity

(Pedersen et al., 2015). Among the broad range of organisms, foraminifera (single-celled protists) show a water depth-related zonation in subtidal environments, and are the first to have been identified successfully in palaeo-tsunami deposits by their DNA (Szczuciński et al., 2016).

The main objectives of GEN-EX include: quantifying the relationship between water depth and the distribution of different foraminiferal taxa where known tsunami deposits are present, using a comparative classic micropalaeontological and metagenomic approach; assessing the potential (based on both approaches) for identifying key indicator species in tsunami deposits in different coastal settings; and establishing how metagenomic approaches can contribute to the differentiation between storm and tsunami deposits.

3. DNA extraction

DNA will be analysed in two types of material – modern extant foraminifera and sediments (tsunami deposits and adjacent layers). DNA extracted from single foraminiferal specimens will be followed by whole genome amplification to obtain sufficient DNA concentrations. Either part of the nuclear 18S rRNA region or the mitochondrial genome (mtDNA) will be amplified, before high-throughput sequencing of the amplicons. Sequences will be edited and aligned, and their identity verified by BLAST (Altschul et al., 1990) searches in Genbank and the Forambarcoding project (<http://forambarcoding.unige.ch>). A project-specific database of 18S and mtDNA data of the identified recent foraminifera will be constructed.

Sampling of tsunami deposits and DNA extraction follows the protocol of Szczuciński et al. (2016). Suitable primers will be developed from our reference database of recent foraminifera to amplify overlapping short fragments of 18S or mtDNA of the target species. Amplicon concentration will be quantified and prepared for high-throughput sequencing. Sequence data will be analysed with different bioinformatics pipelines (e.g. QIIME), including quality control, removal of barcodes and adaptors, identification and removal of chimeric and redundant sequences, and comparisons with our own and open access databases of 18S data for defining Operational Taxonomic Units with 95% and 97% similarity cut-offs.

4. Study area

One of the study areas, where the eDNA approach is applied, are the Shetland Islands, exposed to the mega-tsunami triggered by the early Holocene Storegga submarine slide off the coast of Norway. Sediment run-up of more than 25 m left a distinct landward-thinning sand layer with an erosive lower contact, large rip-up clasts, fining-upward sequences and marine diatoms in near-shore lakes and coastal peat lowlands. In addition to sediments associated with the Storegga tsunami, two younger tsunami deposits dated to c. 5 and 1.5 ka (Bondevik et al., 2005) are investigated. Sampling for the planned foraminiferal analyses and eDNA extraction of the deposits and their source area, comprising along the beach and subtidal area to the central shelf area is scheduled for the second half of March 2018.

5. Acknowledgements

Funding is kindly provided by a BELSPO BRAIN-be pioneer grant (BR/175/PI/GEN-EX).

6. References

- Altschul, S.F., Gish, W., Miller, W., Myers, E.W. & Lipman, D.J., 1990. Basic local alignment search tool. *Journal of Molecular Biology*, 215, 403–410.
- Bondevik, S., Mangerud, J., Dawson, S., Dawson, A. & Lohne, Ø., 2005. Evidence for three North Sea tsunamis at the Shetland Islands between 8000 and 1500 years ago. *Quaternary Science Reviews*, 24, 1757–1775.
- Engel, M., Oetjen, J., May, S.M. & Brückner, H., 2016. Tsunami deposits of the Caribbean – Towards an improved coastal hazard assessment. *Earth-Science Reviews*, 163, 260–296.
- Pedersen, M.W., Overballe-Petersen, S., Ermini, L., Sarkissian, C.D., Haile, J., Hellstrom, M., Spens, J., Thomsen, P.F., Bohmann, K., Cappellini, E., Bærholm Schnell, I., Wales, N.A., Carøe, C., Campos, P.F., Schmidt, A.M.Z., Gilbert, M.T.P., Hansen, A.J., Orlando, L. & Willerslev, E., 2015. Ancient and modern environmental DNA. *Philosophical Transactions of the Royal Society B*, 370, 20130383.
- Pilarczyk, J.E., Dura, T., Horton, B.P., Engelhart, S.E., Kemp, A.C. & Sawai, Y., 2014. Microfossils in coastal environments as indicators of paleo-earthquakes, tsunamis and storms. *Palaeogeography, Palaeoclimatology, Palaeoecology*, 413, 144–157.
- Szczuciński, W., Pawłowska, J., Lejzerowicz, F., Nishimura, Y., Kokociński, M., Majewski, W., Nakamura, Y. & Pawłowski, J., 2016. Ancient sedimentary DNA reveals past tsunami deposits. *Marine Geology*, 381, 29–33.
- Yawsangratt, S., Szczuciński, W., Chaimanee, N., Chatprasert, S., Majewski, W. & Lorenc, S., 2012. Evidence of probable paleotsunami deposits on Kho Khao Island, Phang Nga Province, Thailand. *Natural Hazards*, 63, 151–163.

High-temperature XRD investigations of phase transformation in mineralogy: examples for clay used in ceramics and phosphate minerals

François FONTAINE¹, Frédéric HATERT², Pascal PILATE³, Nathalie FAGEL¹

¹AGEs, Argiles, Géochimie et Environnement sédimentaires, ULiège, Belgium

²LMC, Laboratoire de Minéralogie et Cristallogéologie, ULiège, Belgium

³INISMa-CRIBC, Mons, Belgium

1. Introduction

High-temperature X-ray diffraction is a technique used to determine the mineralogy of a sample at various, non-ambient, temperatures. It allows the measurement and visualisation of dehydration and oxidation processes, phase transformations (Wahl *et al.*, 1961; Montanari, 2004; Zampori *et al.*, 2012), reaction processes and crystallite growth (Natter *et al.*, 2001). The approach was tested on two distinct materials, i.e. raw clays used for ceramic production and phosphate minerals. Four clay samples from Westerwald (Germany) were chosen: a Fe-rich illite clay, a red, a yellow and a white clay. In addition, two natural phosphate samples were selected: alluaudite [$\text{Na}_2\text{MnFe}^{2+}\text{Fe}^{3+}(\text{PO}_4)_3$] from Townsite, Pringle, South Dakota, USA (sample TOW-01; Hatert, 2002), and triphylite [$\text{LiFe}^{2+}(\text{PO}_4)$] from the Palermo pegmatite, New Hampshire, USA. Mineral transformation and vitrification processes were followed from 30 to 1250 °C.

2. Methods

The *in situ* HT-XRD experiments were performed with a Bruker D8 Advance Eco instrument equipped with a Linxeye XE detector and a modular temperature chamber (MTC). Each powdered sample was placed directly on a platinum rhodium (PtRh) alloy strip combined with a thermocouple. XRD patterns were recorded in the 8-70° 2 θ range with a step width of 0.02°. Samples were heated with a rate of 30 °C/min and were kept at the desired temperature for 5 minutes before analysis. Each sample was first analysed at room temperature and then heated at 300, 600, 900, 1100, 1150, 1200 and 1250 °C. Mineral proportions were then quantified using Topas software.

3. Results

The difference between the white, yellow and red clays lies in the temperature of appearance and the abundance of some minerals (Fig. 1). The white clay does not contain any Fe-bearing minerals. It is composed of kaolinite, illite, quartz and rutile. The red and yellow clay contain hematite and goethite respectively. During the heating process, the first mineral transformation observed in Fe-bearing clays is the dehydration of goethite to hematite occurring between 30 and 300 °C. The second transformation, observed in all studied clays, is related to the dehydroxylation of kaolinite into metakaolin (amorphous) between 300 and 600 °C. At 1100 °C, the illite totally disappeared and a large amount of mullite is formed. At higher temperature cristobalite is formed at 1100 °C for the red clay and at 1200°C for the yellow clay but it is not observed in the white clay. Fe-rich illite clay, used for its good vitrification properties at low temperature is different from the three

other samples. It is less stable, resulting in a lower dehydroxylation temperature (between 600 and 900 °C). At higher temperature spinel was observed from 1100 °C in this sample.

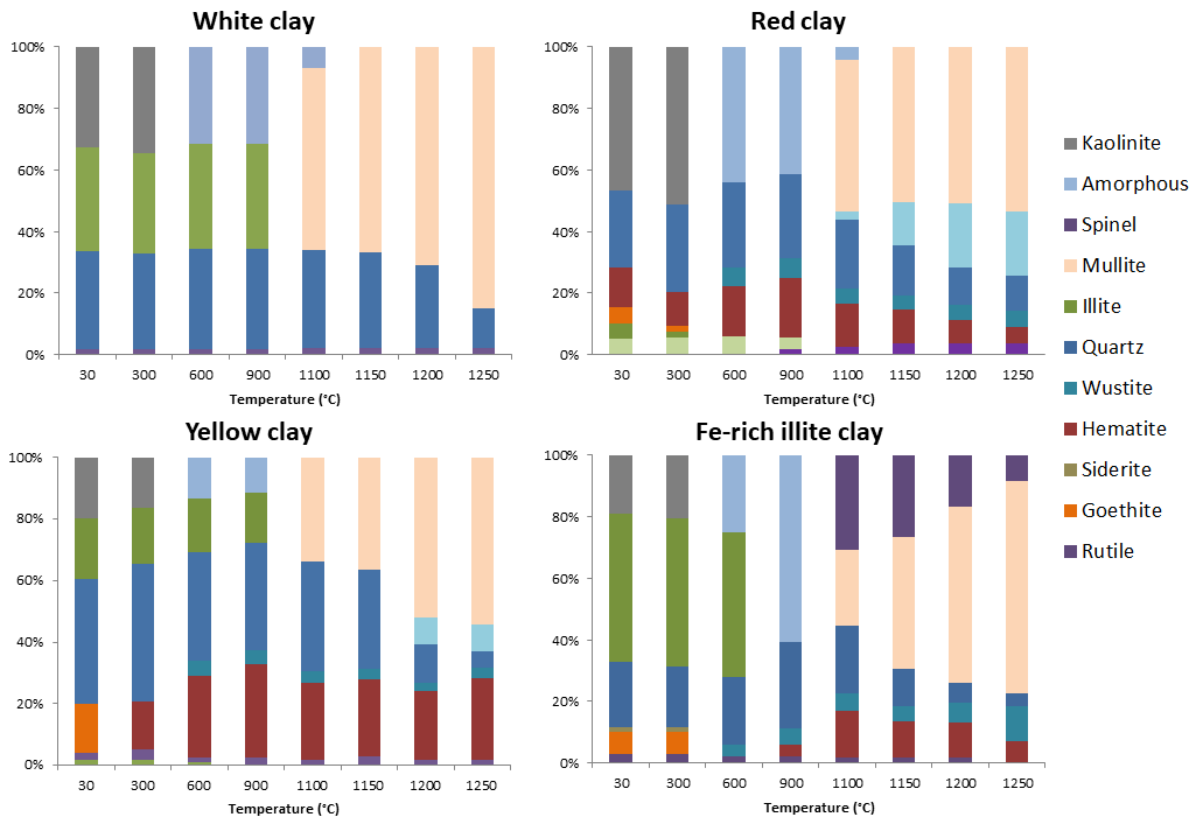


Figure 1. Evolution of mineral proportions of clay samples with temperature.

Heating experiments on phosphates are currently being processed. They will allow to shed some light on the variation of unit-cell parameters of alluaudite- and triphylite-type phosphates over heating. Moreover, accurate determination of phosphate proportions at different temperatures will help us to better understand the stability features of these minerals.

4. References

- Hatert, F., 2002. Cristallochimie et synthèse hydrothermale d'alluaudites dans le système Na-Mn-Fe-P-O: contribution au problème de la genèse de ces phosphates dans les pegmatites granitiques. Unpublished PhD thesis, University of Liège, 247 p.
- Montanari, R., 2004. High-temperature XRD investigations on phase transformations. *La Metallurgia Italiana*, 2, 23-30.
- Wahl, F.M., Grim, R.E. & Graf, R.B., 1961. Phase transformations in silica-alumina mixtures as examined by continuous X-ray diffraction. *The American Mineralogist*, 46, 196-208
- Zamporti, L., Dotelli, G., Gallo Stampino, P., Cristiani, C. & Zorzi, F., 2012 Thermal characterization of a montmorillonite, modified with polyethylene-glycols (PEG1500 and PEG4000), by in situ HT-XRD and FTIR: Formation of a high-temperature phase. *Applied Clay Science*, 59-60, 140-147.

Belgian paleontological heritage: time for action?

Stijn GOOLAERTS

Royal Belgian Institute of Natural Sciences, Vautierstraat 29, B-1000 Brussels, Belgium, stijn.goolaerts@naturalsciences.be

1. Fossils not protected by law

In Belgium, fossils are not protected by law (Gerrienne, 1999) leading to the unfortunate situation that in active quarries and at building sites, thousands of fossils are destroyed every day. Many of those are relatively insignificant finds, but they also may include possible major scientific discoveries. With no government organization dealing with it, assessing and saving Belgium's paleontological heritage is in the hands of a small number of highly motivated professional and citizen paleontologists who are scouring active quarries and building sites after hours and during the weekends.

2. Many important finds although no support

In the past two decades, this small group of highly motivated paleontologists was responsible for an impressive number of important new discoveries. To cite only some of their discoveries: more than a dozen cetacean skeletons, many of them leading to the description of new species, several new finds of decapod crustaceans, amongst them also several species new to science, many first recordings of species of shark teeth and some new species, a very large number of new species of trilobites, the oldest known Belgian mosasaur skeleton, new finds of Frasnian placoderm fish, the largest collection of bed-by-bed collected upper Frasnian cephalopods, a new crinoid Lagerstätte and so on and on. Each of these motivated paleontologists will however tell you that what they were able to rescue was only a small portion of what they had been able to rescue if a bit more support was on hand. This support could have been a better status to discuss with contractors at building sites or quarry operators, some financial support during excavation (cf. professionalism), and not unimportantly, more help of professional paleontologists quickly identifying important finds from less important ones, or supplying skills and know-how to e.g. excavate complete vertebrate skeletons.

3. Time for action?

A major question to tackle is whether or not we leave the situation as it currently is. This is, do we leave the saving of important Belgian paleontological heritage only in the hands of volunteers? From the money point of view, one could argue that still a large number of important specimens are rescued from destruction at no cost. But on the other hand, a much larger amount of important specimens got irreversibly lost, or, and by lack of professional support, parts or even whole specimens became lost by inadequate excavation and conservation.

Isn't it time that the Belgian geo and paleo communities unite themselves to stand up and ask for more attention for the safekeeping and safeguarding of Belgian paleontological heritage? And shouldn't we ourselves explore the best possible options to propose to our policy makers,

instead of waiting until the policy makers awake themselves? To stimulate the discussion, the author proposes to change nothing to the existing laws, but to ask our government(s) to supply funds for the hiring of two or more professional paleontologists whose major task would be to rescue and to facilitate the rescue (e.g. with the help of volunteers) of important paleontological specimens in quarries and on building sites. Considering where today the know-how of fossil excavation, identification and conservation is found, next to the already existing networks for working with volunteers, doing outreach and press communications, the author proposes the RBINS as the best possible workplace.

4. Reference

Gerrienne, P., 1999. International laws: collecting, transporting and ownership of fossils – Belgium. In Jones, T.P. & Rowe, N.P. (eds), *Fossil Plants and Spores: Modern Techniques*. The Geological Society, London, 324.

PyDOV brings the data back to the future

Pieter J. HAEST^{1,2}, Roel HUYBRECHTS³, Stijn VAN HOEY⁴, Johan VAN DE WAUW⁵, Marijke HUYSMANS^{2,7}, Hervé VAN BAELEN⁸, Marleen VAN DAMME⁶

¹ *AGT – Advanced Groundwater Techniques, Kontichsesteenweg 38, 2630 Aartselaar, Belgium*

² *Geology Division, Department of Earth and Environmental Sciences, KU Leuven, Celestijnenlaan 200E, 3001 Heverlee, Belgium*

³ *Real Dolmen, A. Vaucampslaan 42, 1654 Huizingen, Belgium*

⁴ *Research Institute Nature and Forest (INBO). Havenlaan 88 bus 73, 1000 Brussels, Belgium*

⁵ *Gisky – scientific programming, Christine D’haenhof 7, 9040 Gent*

⁶ *Department of Environment & Spatial Development, Koning Albert II laan 20, 1000 Brussels, Belgium*

⁷ *Department of Hydrology and Hydraulic Engineering, VUB, Pleinlaan 2, 1050 Brussels, Belgium*

⁸ *ONDRAF/NIRAS – Belgian agency for Management of Radioactive Waste and Enriched Fissile Material, Kunstlaan 14, 1210 Brussels, Belgium*

1. Introduction

DOV (Flanders Soil and Subsurface Database, <https://www.dov.vlaanderen.be>) is a unique partnership of different departments within the Flemish Government, initiated in 1996. Together with other actors they contribute from their expertise to an extensive database with information about the subsoil. These data can range from geotechnics to geology and groundwater. The webservice DOV explorer is continuously expanded with new features, such as the ‘Virtual Borehole’.

However, the above mentioned services focus on the interactive and human-readable querying and visualization of the data. In this new era of data science it was deemed appropriate to create an API in addition that supports machine-based extraction and conversion of the data. This enables the integration of DOV data in larger data processing pipelines and supports the reproducibility and/or repeatability of research studies. This API is being developed in a community effort, coordinated by DOV, and is called pyDOV.

2. PyDOV

2.1. General information

The pyDOV API is a Python package hosted on GitHub [online: <https://github.com/DOV-Vlaanderen/pydov>]. PyDOV provides in the first place a convenient wrapper around the XML export of the DOV explorer and related applications, in combination with the available DOV webservices. By combining the information of these web services, different data request use cases can be automated. Currently the API is being developed for the following data types [*In Dutch*]: *boringen* (102741), *sonderingen* (74667), *formele stratigrafie* (98021), *gecodeerde lithologie* (10396), *geotechnische coderingen* (11051), *hydrogeologische stratigrafie* (9911), *informele hydrogeologische stratigrafie* (16), *informele stratigrafie* (65946), *lithologische beschrijvingen* (92475), *quartaire stratigrafie* (14580), and groundwater screens (7361). The numbers indicate the xml permlinks that are currently present for each data type. PyDOV can be further expanded to include the data of the 67082 records of subsoil samples, unlocking a vast amount of analysis data.

2.2. Example use case

PyDOV gives access to borehole data and related (hydro)geological interpretations. One can for example retrieve all the hydrogeological interpretations available for the Ypresian aquitard system

to examine if and how much difference there could exist between interpretations. This illustrates the uncertainty of the depth-interval where the Ypresian aquitard system is defined (see Figure 1). Apparently only 12 of the 1790 boreholes present in the Ypresian aquitard system in Flanders have had more than 1 hydrogeological interpretation. The uncertainty on the position of the top of the Kortrijk Formation is largest with a median of about 6.5 m. A more detailed (spatial) analysis can be performed but in this case it is deemed more appropriate to point to the possibility of including another data source provided by DOV: the (hydro)geological models.

The presence of the Ypresian aquitard system in Flanders is defined following the Hydrogeological code of the subsoil in Flanders (HCOV). One can quantify the uncertainty related to the depth interval of the aquitard system by making use of pyDOV in combination with other Python packages for spatial analysis. Figure 2 shows the difference between the top, respectively bottom of the model definition and the interpretations from borehole data. Such information can be used in a first step of data exploration to highlight knowledge gaps and focus attention to these problem areas (code: <https://gist.github.com/pjhaest/aaab1f7a323feece08868541395236e.js>)

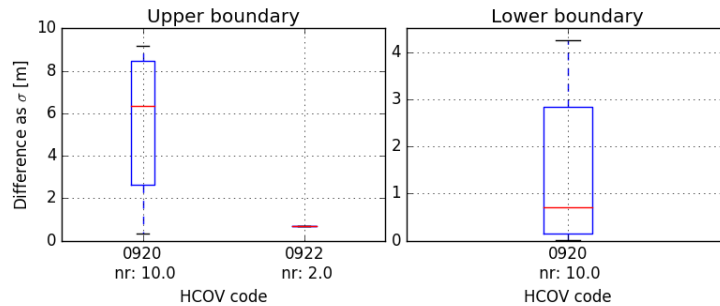


Figure 1. The difference (as standard deviation σ) of the upper boundary, respectively lower boundary between hydrostratigraphical interpretations of the same borehole.

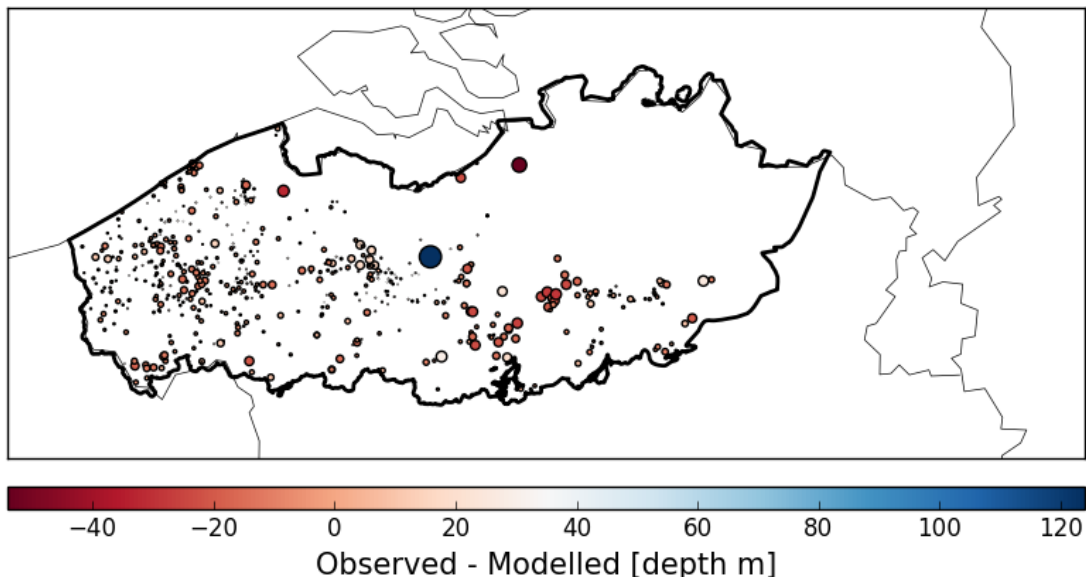


Figure 2. The locations of the boreholes with a hydrostratigraphical interpretation of the Ypresian aquitard system (indicated by the black solid line). The size and color of the dots indicate the difference in depth between the interpretations from borehole data and the model following the HCOV code.

3. Conclusions

The machine-based availability of the data hosted by DOV can potentially serve a diverse community of researchers, consultants, modelers, and students. As such, a community-based effort is deemed most appropriate to develop and maintain these functionalities as an open source package. Everybody is welcome to contribute.

Microstructure generation and effective property estimation of materials used as radioactive waste confinement barriers

Laurent LEMMENS^{1,2}, Bart ROGIERS¹, Eric LALOY¹, Mieke DE CRAEN¹, Diederik JACQUES¹, Rudy SWENNEN², Janos L. URAI³, Guillaume DESBOIS³, Marijke HUYSMANS².

¹ *Waste and Disposal, Belgian Nuclear Research Centre, SCK•CEN, Mol, Belgium.*

² *KU Leuven, Department of Earth and Environmental Sciences, Belgium.*

³ *Institute of Structural Geology, Tectonics and Geomechanics, RWTH Aachen University, Germany.*

1. Introduction

Transport through materials potentially used in radioactive confinement barriers (Boom Clay, cement paste) depends strongly on their 3D microstructure. To predict transport and related processes at time and spatial scales beyond experimental data, numerical simulations are necessary. This, requires an accurate description of the 3D microstructures involved. For Boom clay and cement paste, 3D imaging by μ CT does not have sufficient resolution to describe the microstructure in a needed quality. In the last years, various microstructure modeling platforms have been developed, such as HYMOSTRUC and CEMHYD3D to model cement paste. While those modelling platforms provide accurate estimates of the evolution of the material in 3D over time, they do not describe the microstructure well (Ravi Patel et al., 2016). We present a new hierarchical-multiresolution-multiphase simulated annealing algorithm for porous media reconstruction, which uses 2D-SEM images to generate 3D microstructure realizations (Lemmens et al., in preparation). We evaluate the reconstruction methodology by calculating diffusion coefficients with a pore-scale transport model through the 3D structures using a lattice Boltzmann approach.

2. Methodology

The basic simulated annealing (SA) reconstruction of Yeong and Torquato (1998) uses a simulated annealing process to minimize the energy, E , of a system. In the context of porous media reconstruction, E encodes the deviations of the generated image from the Training Image (TI) based on one or more structural descriptor values. To generate the reconstructions within this work we use the two-point probability function and the lineal-path function (Torquato, 2013).

The SA reconstruction process starts with a random structure that honors the different phase fractions found in the TI. Once the energy E of the system is determined, the algorithm starts to swap pixels from various phases. After each swap, the energy E' of the new state is determined and the energy difference $\Delta E = E' - E$ is calculated accordingly. The new state is then accepted with the Metropolis probability $p(\Delta E)$.

SA classically suffers from a large computational demand, due to the pixel switching process. This problem becomes more prominent when there are more than 2 phases considered in the reconstruction process. Therefore, it is often not possible to do multiphase reconstructions with SA. To make SA feasible for multiphase reconstruction, our algorithm combines two different approaches. Firstly, the algorithm uses a hierarchal approach which simulates one phase after

another and is represented in Fig. 1a. Once a phase is simulated, the corresponding pixels are frozen and cannot be swapped anymore. Secondly, the algorithm uses a multiresolution approach to speed up the reconstruction (Fig. 1b). By doing so, the TI is coarsened and reconstructed on a lower resolution first. Hence, the individual pixels are grouped into clasts within fewer iterations. Once the structure has been generated on the coarse resolution, the structure is refined. At the fine resolution, only changes at the interface of particles are necessary to account for the difference in resolution.

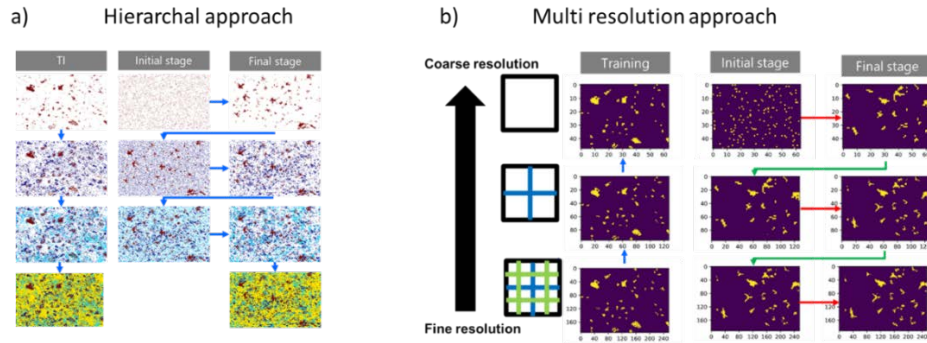


Figure 1. Approaches to make multiphase reconstruction feasible with simulated annealing. a) Hierarchical approach: In this approach one phases is simulated after another. b) Multi resolution approach: In this approach the TI is initially coarsened and first reconstructed at a coarse resolution and refined afterwards.

To generate 3D reconstructions from a single SEM image an isotropic medium is assumed. Using this assumption the structural descriptor for the third dimension can be deduced, from taking the average of the other two main directions. To validate the quality of the simulation results, the generated 3D microstructures are used for diffusivity calculations using a Lattice Boltzmann approach (Ravi Patel, 2016) and compared to values measured in the laboratory.

3. Findings

The presented algorithm can be used to efficiently generate 3D structures of cement-based materials (Fig. 2b) using a single SEM image as TI (Fig. 2a). The suggested hierarchical-multiresolution approach does not only increase the computational performance of the algorithm by up to one order of magnitude, but it also improves the reconstruction quality. The reconstructions are especially characterized by proper continuity between consecutive slices (Fig. 2c), which is often problematic in other approaches. Preliminary diffusion simulation results, based on the generated 3D model, show a good agreement to values measured in the laboratory.

While the method works well for homogenous materials, further development is need for heterogeneous materials such as Boom Clay, as the algorithm struggles in reconstructing the bedding behavior.

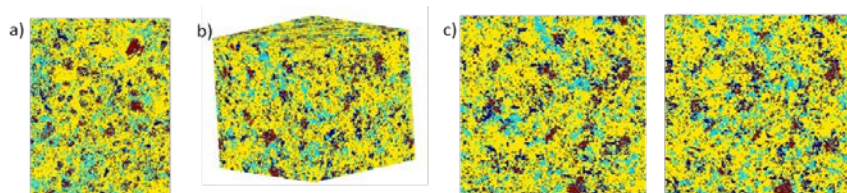


Figure 2. Cement paste images a) Training image. b) 3D reconstruction, c) 2 consecutive slices.

References

- Patel, R. (2016). *Lattice Boltzmann method based framework for simulating physico-chemical processes in heterogeneous porous media and its application to cement paste*. Ghent University,
- Patel, R., Perko, J., Jacques, D., De Schutter, G., Ye, G., & Van Breugel, K. (2016). *Can a reliable prediction of cement paste transport properties be made using microstructure models?* Paper presented at the Int. Conference on Materials, Systems and Structures in Civil Engineering 2016-Segment on Service Life of Cement-Based Materials and Structures.
- Torquato, S. (2013). *Random heterogeneous materials: microstructure and macroscopic properties* (Vol. 16): Springer Science & Business Media.
- Yeong, C., & Torquato, S. (1998). Reconstructing random media. *Physical Review E*, 57(1), 495.

Stochastic image correction for pore collapse in dried Boom Clay samples

Laurent LEMMENS^{1,2}, Bart ROGIERS¹, Guillaume DESBOIS³, Eric LALOY¹, Mieke DE CRAEN¹, Diederik JACQUES¹, Rudy SWENNEN², Janos L. URAI³, Marijke HUYSMANS².

¹ Waste and Disposal, Belgian Nuclear Research Centre, SCK•CEN, Mol, Belgium.

² Department of Earth and Environmental Sciences, KU Leuven, Belgium.

³ Institute of Structural Geology, Tectonics and Geomechanics, RWTH Aachen University, Germany.

The Boom Clay is considered to be a potential host rock for the geological disposal of radioactive waste. To predict the transport, and related processes, of radionuclides through such waste confinement barriers, numerical simulation is necessary for performance assessment at temporal and spatial scales beyond those of experimental data, and the demonstration of in-depth process understanding. This does require an accurate and realistic description of the 3D microstructures involved, however.

For Boom Clay, 3D imaging by μ CT does not provide sufficient resolution to describe neither the porosity, nor the pore connectivity. To obtain a 3D representation of the microstructure at higher resolution, it is therefore necessary to use 3D FIB-SEM tomography, or generate statistically representative 3D reconstructions based on 2D BIB-SEM images (Lemmens *et al.*, in preparation). Imaging methods based on SEM require drying of the samples, which can damage the clay-rich micro-fabrics. Desbois *et al.* (2009, 2017) however developed the use of FIB-cryo-SEM and BIB-cryo-SEM to investigate wet-preserved micro-fabrics in clay-rich geomaterials by quenching the original fluids by cryogeny. Preliminary comparison between wet-preserved and dried 2D micro-fabrics imaged by BIB-cryo-SEM suggests the drying induces a collapse of the inter clay aggregate porosity (Desbois *et al.*, 2017). Therefore, we assume that the pore collapse observed in 2D by Desbois *et al.* (2017) affects (i) the 3D-microstructure and potentially also (ii) the transport properties of Boom Clay.

This contribution presents a first attempt at relating the images of wet-preserved and dried states of a sample, targeting the development of a correction procedure. Such a procedure would allow to assess the effects of the pore collapse on the transport properties numerically, by 3D reconstruction and simulating effective properties for both states of a single sample.

We construct a multivariate training image (TI) here, and test the use of multivariate multiple point statistics simulations by direct sampling DS (Mariethoz *et al.*, 2010), to reconstruct the wet-preserved state conditional to the dried sample image. The multivariate TI features two different variables. The first variable is an image of a wet preserved sample and the second variable the corresponding image at the dried state. The individual patterns within the wet state TI and the relationship between the 2 variables are then used to generate the representation of the wet state. In the reconstruction process the secondary variable (dry stated image) is already known and DS uses this information as indirect conditioning data to guide the simulation of the wet state representation.

References

- Desbois G., Urai J.L. and Kukla P.A. (2009). Morphology of the pore space in claystones - evidence from BIB/FIB ion beam sectioning and cryo-SEM observations. *E-Earth*, 4:15-22.
- Desbois G., Schmatz S., Klaver J. and Urai J.L. (2017). Micro-fabric damages in Boom Clay inferred from cryo-BIB-SEM experiment: recent results. 19th EGU General Assembly, Vienna, Austria.
- Lemmens, L., Rogiers, B., Laloy, E., De Craen, M., Jacques, D., Swennen, R. and Huysmans, M. (in preparation). A hierarchical multiresolution multiphase simulated annealing algorithm for porous media reconstruction. *Physical Review E*.
- Mariethoz, G., P. Renard, and J. Straubhaar (2010), The Direct Sampling method to perform multiple-point geostatistical simulations, *Water Resources. Res.*, 46.

Numerical modeling of sediment generation: characterizing parent rock's properties by digital petrography

Bram PAREDIS¹, Gert Jan WELTJE¹

¹*Department of Earth and Environmental Sciences, KU Leuven, Celestijnenlaan 200E, 3001 Leuven, Belgium.*

In light of the numerical modeling of sediment generation project, aimed at simulating the chemical and mechanical weathering of crystalline parent rocks to sediments, digital petrography has been applied to characterize parent rock's properties such as grain size distribution and texture. Such a characterization is necessary to initialize a parent rock in the sediment generation model (SedGen) after which it weathers to sediment.

By using circular polarized light, grain outlines as well as mineral identity are more clearly distinguishable, not only by eye but also by image analysis software (Higgins, 2010). Circular polarized light is obtained by inserting two quarter lambda plates into a petrographic microscope perpendicular to each other and at 45° of the polarizers. Resulting interference colors are at their maximum for the respective section through the crystal. Due to the circular occurrence of the polarized light, extinction does not take place, except for minerals with their optical axis perpendicular to the thin section surface. By taking multiple images at low magnification (e.g. 32x) and stitching them together afterwards, a high resolution image of the entire thin section can be obtained while minimizing time spent. The images can then be analyzed on a computer with minimal further petrography work at a microscope required. This allows for faster observation of principal minerals' identity, crystal boundaries and texture in general. It also enables the user to create a digital archive of thin sections. With image analysis software a specified number of crystals within a digitized thin section can be outlined and analyzed for 2D grain size parameters. Modal mineralogy can also be analyzed.

The digital petrography approach has been applied to thin sections of granitoid parent rocks (Heins, 1992). Two dimensional grain size data could be obtained for 300 crystals per thin section (50 per mineral class) which allows for an estimation of the 2D crystal size distribution. These data will allow a reanalysis of interfacial frequency data gathered by Heins and will enable a characterization of crystal size distributions for granitoid rocks which will serve an important purpose in the initialization of parent rock during the Sediment Generation model (SedGen). Granitoid rocks have been selected as test data for SedGen, as they represent the most common type of igneous rock at the Earth's surface and tend to produce large quantities of sand. Digital petrography can of course be applied to a whole range of parent rocks as well as to the resulting sediments. More modern microscopes would even enable a semi-automated setup of the approach described here.

References

- Heins, 1992. The effect of climate and topography on the composition of modern, plutoniclastic sand. PhD Thesis, Los Angeles, University of California, 465 p.
- Higgins, 2010. Imaging birefringent minerals without extinction using circularly polarized light. *The Canadian Mineralogist*, 48, 231-235.

An unusual patient: imaging and quantifying volcano deformation in laboratory experiments by using X-ray Computed Tomography

Sam POPPE¹, Nico BULS², Gert VAN GOMPEL², Dave HOLLIS³, Alex NILA³, Joost BRANCART⁴, Olivier GALLAND⁵, Eoghan P. HOLOHAN⁶, & Matthieu KERVYN¹

¹ *Physical Geography, Department of Geography, Vrije Universiteit Brussel, Pleinlaan 2, 1050 Brussels, Belgium.*

² *Radiology Department, UZBrussel, Vrije Universiteit Brussel, Brussels, Belgium.*

³ *LaVision UK Ltd, Oxford, UK.*

⁴ *Physical Chemistry and Polymer Science (FYSC), Vrije Universiteit Brussel, Brussels, Belgium*

⁵ *Physics of Geological Processes, University of Oslo, Oslo, Norway*

⁶ *UCD School of Earth Sciences, University College Dublin, Dublin, Ireland*

1. Introduction

Geological deformation processes have been studied traditionally by observing the surface expression of the resultant structures, complemented since several decades with remote sensing and subsurface imaging by e.g. drilling and geophysical techniques. Scaled laboratory modeling is a common technique to simulate deformation processes and study their dynamics in a controlled environment. Whereas early efforts focused on qualitative descriptions of observed structures, model deformation is increasingly quantified by using advanced imaging and image analysis (laser scanning, Structure-from-Motion (SfM) photogrammetry and Digital Image Correlation (DIC); Galland et al., 2016).

For granular crustal analogues, typical laboratory monitoring techniques are limited to quantifying 3D deformation at the model surface, to recording the final deformation state in sliced and digitized model cross-sections (e.g. Ravaglia et al., 2004), or to quantifying 2D deformation along a quasi-interior vertical cross-section at the model side-wall where friction effects could affect deformation rates (e.g. Ruch et al., 2012). The use of transparent gelatin as a crustal analogue enables an interior view, but this limits the model rheology to idealized elastic deformation (Kavanagh et al., 2013). Granular materials enable simulation of elasto-plastic crustal behavior, but the model interior itself remains a black box, its deformation studied only through indirect inferences, similar to nature.

To surmount this issue, we used X-ray Computed Tomography (XCT) to dynamically image and quantify the interior deformation of laboratory experiments in 4D (i.e. 3D + time), as applied to analogue magma intrusion.

2. Methodology and results

We constructed a model with contrast-rich X-ray CT images by characterising the physical properties of a range of analogue materials. We use golden syrup as a magma analogue, and granular sand-plaster mixtures at varying mixture ratios to represent upper crustal rocks of varying strengths. We dynamically image ongoing fluid intrusion in the granular host in 4D by using wide beam X-ray Computed Tomography at UZ Brussel, and visualise the geometric development of the induced deformation structures. We then use advanced Digital Volume Correlation to calculate incremental and cumulative volume displacements and strains throughout the experimental space and time, as was done for compressive tectonics experiments by Adam et al. (2013).

We demonstrate that the characterised physical properties of our granular sand-plaster mixtures display complex elasto-plastic rheology. Our experiments show how golden syrup intrusions of contrasting geometries are formed in granular host material of varying strength. These

laccoliths, cup-shaped sheet intrusions and dykes induce contrasting surface deformation and strain field characteristics in 4D.

3. Discussion and conclusion

By imaging laboratory experiments of analogue magma intrusion in an elasto-plastic granular host material, we gain an unprecedented insight in the structural and dynamic aspects of intrusion-induced deformation of the Earth's upper crust. Our experiments confirm the dominant role of host rock strength and rheology on the geometry and dynamics of magma intrusion in the Earth's upper crust, similar to the findings of Schmiedel et al. (2017).

The major novelty of our approach is that it extends 4D monitoring and quantification of structural deformation beyond the model surface by enabling a full quantification of the entire model volume over time. The presented methodology makes it now possible to observe the temporal development of fracture systems in the host material in 3D. Importantly, the displacement and strain fields can be monitored throughout the model volume over time, and not only at the model surface.

This unprecedented internal perspective helps understanding how tectonic and volcanic processes affect their host material of varying strength, and shed light on the mechanical behavior of the heterogenic upper crust. We demonstrate that this technique helps validating more idealized geodetic and inversion models currently used to interpret tectonic and volcanic geodetic data, or a more complete comparison with passive mapping of subsurface structures, such as sills and dykes in sedimentary basins.

4. References

- Adam, J., Klinkmüller, M., Schreurs, G. & Wieneke, B., 2013. Quantitative 3D strain analysis in analogue experiments simulating tectonic deformation: Integration of X-ray computed tomography and digital volume correlation techniques. *Journal of Structural Geology*, 55, 127–149.
- Burchardt, S. & Walter, T. R., 2010. Propagation, linkage, and interaction of caldera ring-faults: Comparison between analogue experiments and caldera collapse at Miyakejima, Japan, in 2000. *Bulletin of Volcanology*, 72(3), 297–308.
- Galland, O., Bertelsen, H. S., Guldstrand, F., Girod, L., Johannessen, R. F., Bjugger, F., Burchardt, S. & Mair, K., 2016. Application of open-source photogrammetric software MicMac for monitoring surface deformation in laboratory models. *Journal of Geophysical Research-Solid Earth*, (2), 1–21.
- Kavanagh, J. L., Menand, T. & Daniels, K. A., 2013. Gelatine as a crustal analogue: Determining elastic properties for modelling magmatic intrusions. *Tectonophysics*, 582, 101–111.
- Ravaglia, A., Turrini, C. & Seno, S., 2004. Mechanical stratigraphy as a factor controlling the development of a sandbox transfer zone: A three-dimensional analysis. *Journal of Structural Geology*, 26(12), 2269–2283.
- Ruch, J., Acocella, V., Geshi, N., Nobile, A. & Corbi, F., 2012. Kinematic analysis of vertical collapse on volcanoes using experimental models time series. *Journal of Geophysical Research*, 117(B7), B07301.
- Schmiedel, T., Galland, O. & Breitzkreuz, C., 2017. Dynamics of Sill and Laccolith Emplacement in the Brittle Crust: Role of Host Rock Strength and Deformation Mode. *Journal of Geophysical Research: Solid Earth*, 122(11), 8860–8871.

The first regional 3D acoustic velocity model for the eastern part of Flanders (Belgium)

Bernd ROMBAUT¹, Katrijn DIRIX¹, Jef DECKERS¹

¹VITO, Flemish Institute for Technological Research. Boeretang 200, BE-2400 Mol, Belgium

1. Introduction

VITO is currently building a new 3D geological model, called G3Dv3-model, ordered by the Bureau for Environment and Spatial Development – Flanders. The model will cover all the different Late Paleozoic to recent (hydro)geological units that are present in Flanders. In the eastern part of Flanders, the strata are strongly faulted and deformed by multiple tectonic phases of both compression and extension. To model this geologically complex area, large amounts of existing 2D seismic and borehole data were combined, locally supported by 20th century coal mining information and topographic and gravimetric data. Based on these datasets, horizons and faults were interpreted on seismic sections and modelled into 3D horizons and fault planes in the time-domain.

2. Methodology

In a next step, the horizons and fault planes had to be converted from the time-domain towards the depth-domain. To accomplish this, the first comprehensive 3D velocity model of Flanders was developed. The workflow to construct the model was based on the “V0-k method” (Japsen, 1993), which assumes a linear increase in acoustic velocity with depth. To make the model as accurate as possible, suitable velocity functions and – maps were constructed for each of the modeled geologic horizons. Based on these maps, a 3D velocity cube was then derived and used to convert the faults to the depth domain.

2.1. Time-depth conversion of the horizons

Two different data sources can be used to derive acoustic velocity maps for the horizons. First, they can be based on rough acoustic velocity data (such as sonic logs and well shoots) measured along boreholes within a specific stratigraphic unit. Secondly, they can be calculated based on the ratio of the depth of the stratigraphic unit in boreholes and the two-way-travel time of the same unit on the seismic data. Depending on the data-availability for the different units, one of these two methods was applied:

- For the uppermost Paleozoic to Cenozoic units, there are a lot of borehole data and relatively few acoustic velocity data. The seismic interpretation of these units is furthermore quite reliable due to the limited structural complexity and strong control by the many borehole data. Therefore, we used the time-surfaces and depths of the different layers in the boreholes to extract interval velocities at each borehole location and to create the acoustic velocity maps for the uppermost Paleozoic to Cenozoic units.

- For the Upper Paleozoic (Carboniferous) interval, there are less boreholes and a relatively large number of acoustic data. The seismic interpretations of these units are furthermore less reliable due to the high structural complexity and limited control by the few borehole data. Therefore, we used sonic and well shoot interval velocities to create velocity maps.

In addition, previous studies have shown that the Carboniferous strata are currently overcompacted in most of the study area, meaning that they were once buried deeper than they are now (Muechez et al., 1987; Langenaeker, 1992; Fermont et al., 1994; Van Keer et al., 1998; Helsen and Langenaeker, 1999; Langenaeker, 2000; Hildenbrand et al., 2004). Since deeper burial implies higher compaction and acoustic velocities, overcompaction has to be taken into account in the acoustic velocity models. This was accomplished by first adding the difference between the current and maximum burial depth for the different boreholes (extracted from Ferket, 2006; Ferket et al., 2010) to the current burial depth and thereafter correcting this to account for later decompaction. These corrected depths were subsequently used to derive the velocity model for the Carboniferous.

2.2. Time-depth conversion of the faults planes

In a second step, the velocity maps for the different horizons were linearly interpolated into a 3D velocity cube to convert the fault planes from the time-domain to the depth-domain. This 3D voxel - with a resolution of 500 m x 500 m x 10 milliseconds two-way-travel time - was first divided in units restricted to the horizon boundaries. Next, a linear function defining the instantaneous velocity as a function of time was applied to interpolate the velocities for each unit and assign the calculated values to the correct voxels.

3. Conclusion

The combined 3D velocity model can now be used to directly convert geological horizons and fault planes in Flanders from the time- to the depth domain, while guaranteeing a perfect fit between both.

4. References

- Ferket, H., 2006. "Begravingsgeschiedenis Kempens bekken". Internal study / concept report of VITO, Mol, Belgium.
- Ferket, H., Laenen, B. and Van Tongeren, P., 2010. Basin modeling of the Campine Basin; can we complete the puzzle? Schriftenreihe der Deutschen Gesellschaft für Geowissenschaften (SDGG), 68, 166 p.
- Fermont, W., Jegers, L. & Dusar, M., 1994. A model study of coal bed methane generation in well Peer (KB206), Belgium. Rijks Geologische Dienst, Haarlem, internal paper, 67 p.
- Helsen, S. & Langenaeker, V., 1999. Burial history and coalification modeling of Westphalian strata in the eastern Campine Basin (Northern Belgium). Professional paper, Geological Survey of Belgium, Brussels, Belgium, 1999/1, 289, 23 p.
- Hildenbrand, A., Laenen, B. & Van Tongeren, P., 2004. The burial history of the Upper Carboniferous strata of the Belgian Campine Basin – a re-evaluation. VITO intern rapport 2004/MAT/R/081.
- Japsen, P., 1993. Influence of lithology and Neogene uplift on seismic velocities in Denmark: implications for depth conversion of maps. AAPG Bulletin, 77(2), 194-211.
- Langenaeker, V., 1992. Coalification maps for the Westphalian of the Campine Coal Basin. Professional paper, Geological Survey of Belgium, Brussels, Belgium, 256, 38 p.
- Langenaeker, V., 2000. The Campine Basin. Stratigraphy, structural geology, coalification and hydrocarbon potential for the Devonian to Jurassic. Aardkundige Mededelingen, 10, 142 p.
- Muechez, Ph., Viaene, W., Wolf, M. & Bouckaert, J., 1987. Sedimentology, coalification pattern and paleogeography of the Campine-Brabant Basin during the Viséan. Geologie en Mijnbouw, 66, 313-326.
- Van Keer, I., Ondrak, R., Muechez, Ph., Bayer, U., Dusar, M. & Viaene, W., 1998a. Burial history and thermal evolution of Westphalian coal-bearing strata in the Campine Basin (NE Belgium). Geologie en Mijnbouw, 76, 301-310.

Resolving the Pore Structure and Phase Behavior of supercritical CD₄ in Hardened Cement Pastes and Mudrocks by means of CD₄ Contrast Matching Experiments:

A Small Angle Neutron Scattering Study

Timo SEEMANN^{1,2}, Pieter BERTIER³, Andreas BUSCH⁴, Amirsaman REZAEYAN⁴, Norbert MAES¹, Seif Ben HADJ HASSINE⁵, Severine LEVASSEUR⁵, Veerle CNUUDE²

¹ Waste and Disposal, Belgian Nuclear Research Centre, SCK•CEN, Mol, Belgium.

² PProGress-UGCT, Department of Geology, Ghent University, Belgium.

³ RWTH Aachen University, Clay and Interface Mineralogy, Bunsenstr.8, 52072 Aachen, Germany.

⁴ Heriot-Watt University, The Lyell Centre, Geo-Energy Research Group, Research Avenue 5 South, Edinburgh, UK.

⁵ ONDRAF/NIRAS, Belgian National Agency for Radioactive Waste and enriched Fissile Material, Belgium.

1. Introduction

Fundamental understanding of the pore network of cementitious materials and mudrocks is key to understanding transport processes, solid-fluid interactions and their intrinsic controls. While transport is influenced by the accessibility and interconnectivity of the pore system, gas storage is affected by the phase- and sorption behavior of supercritical fluids in confined space. Various analytical methods exist to study pore networks but the simultaneous assessment of pore structure accessibility and phase behavior at different pore sizes is reserved to a small number of techniques like neutron scattering. Small angle neutron scattering (SANS) is an interface phenomenon which results from the difference in phase density and associated scattering length density. This technique is capable of covering length scales from nano- to micrometers, and is not restricted to the fluid-accessible pore space like fluid invasion techniques. These attributes make the technique attractive to combine with supercritical fluid penetration into pore space because it allows to study the mutual dependence of pore structure, pore size and phase behavior. This contribution provides insight into the accessible pore space of cementitious materials and mudrocks and the phase behavior of supercritical deuterated methane as a function of pressure and pore size.

2. Theory

The coherent scattering cross section ($I(Q)$) is measured as a function of the momentum transfer vector (Q) and it is directly proportional to the neutron scattering contrast ($\Delta\rho^2$). For the materials studied here, this contrast is the difference in scattering between pores and matrix. When pores are filled with a substance, like deuterated methane, the scattering contrast changes. Empty or air-filled pores have very low contrast while the contrast of CD₄ filled pores depends on its density. For an ideal porous material, a continuous decrease in coherent scattering cross section is expected, when the scattering length density (SLD) of the CD₄ in the pores approaches that of the matrix, i.e. at the matching point (Fig. 1). Furthermore, the proportionality $I(Q) \sim \Delta\rho^2$ predicts a linear variation of the square root of $I(Q)$ with fluid density for a homogeneous two-phase system. According to Melnichenko et al. (2006) any deviation from this linear relationship indicates the presence of a third, either higher or lower density phase. This observation can thus be used to discriminate a two-

phase system from a three-phase system and essentially the phase behaviour at different Q-ranges and associated pore sizes (Radlinsky et al., 2000).

3. Methodology

Two cement- (OPC-I) and five mudrock thick-sections (1 x Opalinus Clay, 3 x Posidonia shale and 1 x Eagleford shale) were investigated by means of combined small angle neutron scattering gas sorption experiments at the KWS3 and KWS1 instruments of the Jülich Center for Neutron Science at Garching, Germany. The samples were fitted into a high-pressure cell and the scattering behaviour was recorded as function of pressure between 1 and 460 bar at 30°C and 50°C. The data of both instruments were merged after buffer and background correction resulting in a continuous scattering curve. For the assessment of phase behaviour, the individual scattering length densities of the samples were calculated based on quantitative XRD data, for the matrix, whereas the SLD of the gas was calculated from the equation of state provided by NIST.

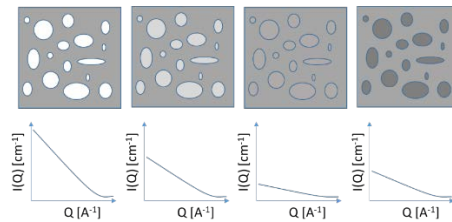


Figure 1. Sketches demonstrating the qualitative relationship between the structure of fluid saturated porous media and associated SANS patterns as a function of pressure ($P_1 < P_2 < P_3 < P_4$). $I(Q)$ gradually reduces with increased fluid pressure (density) due to decreasing neutron contrast between the fluid saturated pores and the solid matrix (left to right). At pressure P_3 the fluid SLD matches that of the solid matrix resulting in $I(Q) \approx 0$ independent of the Q -value. At P_4 the scattering contrast rises again due to increasing densification and resulting scattering contrast (cf. Melnichenko et al., 2012).

4. Findings

The preliminary analysis reveals a clear, but sample dependent relationship between phase density and Q -range. The formation of a third phase is observed from a deviation of data from the predicted linear relationship of the square root of $I(Q)$ and ρ_{CD_4} (Fig. 2A). This third phase is considered to be an adsorbed phase characterized by a higher fluid density in the system providing new interfaces resulting in no apparent contrast match. However, the Q -dependence demonstrates the influence of the pore size on phase behaviour which is likely to be associated with a change in mechanism as a function of pressure and pore size (Fig. 2B). Thus, this observation may have considerable implications on the gas storage capacity and how such systems should be understood in future.

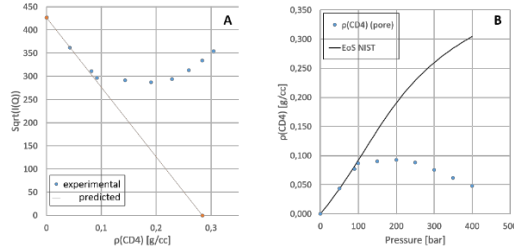


Figure 2. (A) Representative plot of $I(Q)^{-1/2}$ vs. ρ_{CD_4} of hardened cement paste ($w/c = 0.5$); (B) Comparison of bulk density (ρ_{pore}) of CD₄ as a function of pressure as predicted from the EoS and the experimental results in a hardened cement paste ($w/c = 0.5$).

References

- Melnichenko, Yuri B., Lilin He, Richard Sakurovs, Arkady L. Kholodenko, Tomasz Blach, Maria Mastalerz, Andrzej P. Radliński, Gang Cheng, and David FR Mildner (2012). "Accessibility of pores in coal to methane and carbon dioxide." *Fuel* 91, no. 1, 200-208.
- Melnichenko, Y. B., Wignall, G. D., Cole, D. R., & Frielinghaus, H. (2006). Adsorption of supercritical CO₂ in aerogels as studied by small-angle neutron scattering and neutron transmission techniques. *The Journal of chemical physics*, 124(20), 204711.
- Radliński, A. P., Boreham, C. J., Lindner, P., Randl, O., Wignall, G. D., Hinde, A., & Hope, J. M. (2000). Small angle neutron scattering signature of oil generation in artificially and naturally matured hydrocarbon source rocks. *Organic Geochemistry*, 31(1), 1-14.

New Insights on Low-Temperature Redox Reactions of Hydrogen with Hematite (α -Fe₂O₃)

Nicolai M. THÜNS^{1,*}, Pieter BERTIER¹, Bernhard M. KROOSS², Helge H.-G. STANJEK¹

¹RWTH Aachen University, Institute of Clay and Interface Mineralogy, Bunsenstr. 8, 52072 Aachen

²RWTH Aachen University, Institute of Geology and Geochemistry of Petroleum and Coal, Lochnerstr. 4-20, 52056 Aachen

*nicolai.thuens@emr.rwth-aachen.de

1. Scientific Importance

Molecular hydrogen (H₂) is under recurrent investigation as a replacement for metallurgical coke as a reducing agent in steel production. This technology would combine economic and ecologic benefits: (1) H₂ can be readily produced by hydrolysis of water, ensuring a broad availability; (2) the costs of H₂ generation may be reduced by using surplus renewable energy during periods of low demand; (3) process-bound emission of greenhouse gases (CO₂ and CO) can be avoided; (4) direct reduction of iron ore by H₂ allows production of low carbon steels (Pineau et al., 2006, 2007). Furthermore, temporary underground storage of hydrogen in depleted oil and gas reservoirs is likely to become increasingly important for chemical industry demands and peak-shaving in the energy supply grid (Reitenbach et al., 2015). Mineral coatings of hematite are a very common feature in conventional (sandstone) oil and gas reservoirs. A thorough understanding of the reactivity of the hematite-H₂ reaction system is of paramount importance for both of the aforementioned applications.

Reduction of hematite to elemental iron has been studied extensively, yet the use of hydrogen gas has not often been addressed, and only few studies have investigated this process at temperatures below 400°C. Earlier studies on the kinetics of the hematite-H₂ reaction system relied almost exclusively on thermo-gravimetric analysis (TGA). TGA yields little to no information on the driving mechanism of the reactions and the pressure dependence of the reaction cannot be addressed by open system experiments at atmospheric pressure. Moreover, TGA experiments do not allow unambiguous distinction of the different reduction steps (i.e. hematite → magnetite → wustite → native Fe).

This study aims at making precise predictions on the technical feasibility of new applications for hydrogen gas and to obtain a better fundamental understanding of the kinetics of each of the reaction steps using novel experimental approaches. This research is part of the H₂_ReacT project (BMBF Geo:N 03G0870).

2. Experimental Approach and Results

The experimental data is collected from two different setups, the first consisting of stainless steel batch reactors connected to a H₂ pressure regulator (closed system), and the second setup containing a flow through reactor system linked to a gas chromatograph (open system). Both setups are temperature-controlled up to 350°C and designed for isobaric batch experiments (first setup) and continuous H₂ flow experiments (second setup). The reactants used are high-purity hematite and magnetite. Mineral phases of the reactants and the reduction products are characterized

quantitatively by X-ray powder diffraction. Changes in specific surface area and pore characteristics are analyzed by N₂ physisorption.

At temperatures below 400°C, the reaction is considered to proceed by a consecutive two-step mechanism, i.e. hematite → magnetite → elemental Fe. However, first results of our low-temperature tests in the batch and flow reactor systems show that both reactions proceed simultaneously. Additionally, the back reaction of magnetite with the produced water appears to occur in parts of the reaction vessels, affecting the overall reaction progress. Variation of the flow rate in flow through experiments as well as the pressure in batch experiments showed that the reduction reaction is very sensitive to the H₂ and water vapor pressure (fugacity). Unless the water produced from hematite is removed from the system, only one reduction step from hematite to magnetite can be observed. Chemical removal of the water (e.g. by admixture of CaO reacting to portlandite, Ca(OH)₂) increases the rate of the initial reduction reaction to values much faster than previously reported by e.g. Nabi & Lu (1974), Shimokawabe et al. (1979), Sastri et al. (1982) or Pineau et al. (2006).

3. Conclusion and Future Investigations

Our experiments on the hematite-H₂ reaction system show that water fugacity exerts a major control on reaction progress. To the best of our knowledge, there is currently no literature that addresses this effect in any detail. Reaction rates can be increased substantially by keeping the fugacity of the produced water vapor low. Specific experimental observations suggest that different reductions steps proceed (at least to some extent) simultaneously rather than consecutively, and that a back reaction of produced water with the reaction products controls the apparent kinetics of the system.

Our future research on this topic will focus on: (1) the effect of H₂ and water partial pressure on the reaction kinetics; (2) the quantification of the reagent/product composition in-situ and with a high time resolution.

4. References

- Nabi, G., & Lu, W. K. (1974). The kinetics of hematite to magnetite reduction in hydrogen-water and hydrogen-water-nitrogen mixtures. *Industrial & Engineering Chemistry Fundamentals*, 13(4), 311-316.
- Pineau, A., Kanari, N., & Gaballah, I. (2006). Kinetics of reduction of iron oxides by H₂: Part I: Low temperature reduction of hematite. *Thermochimica acta*, 447(1), 89-100.
- Pineau, A., Kanari, N., & Gaballah, I. (2007). Kinetics of reduction of iron oxides by H₂: Part II. Low temperature reduction of magnetite. *Thermochimica Acta*, 456(2), 75-88.
- Reitenbach, V., Ganzer, L., Albrecht, D., & Hagemann, B. (2015). Influence of added hydrogen on underground gas storage: a review of key issues. *Environmental Earth Sciences*, 73(11), 6927-6937.
- Sastri, M. V. C., Viswanath, R. P., & Viswanathan, B. (1982). Studies on the reduction of iron oxide with $\frac{1}{2}$ hydrogen. *International Journal of Hydrogen Energy*, 7(12), 951-955.
- Shimokawabe, M., Furuichi, R., & Ishii, T. (1979). Influence of the preparation history of α -Fe₂O₃ on its reactivity for hydrogen reduction. *Thermochimica Acta*, 28(2), 287-305.

Anisotropy of thermal conductivity in pelitic rock

Koen VAN NOTEN¹, Ben NEEFS² & Kris PIESENS¹

¹*Geological Survey of Belgium, Royal Belgian Institute of Natural Sciences, Jennerstraat 13, 1000 Brussels, Belgium. koen.vannoten@naturalsciences.be*

²*Division of Geology, Earth and Environmental Sciences, KU Leuven, Celestijnenlaan 200E, 3001 Leuven, Belgium*

1. Thermal conductivity

Thermal conductivity (TC) [W/m.K] is a quantitative sediment/rock property that determines where and how much heat flows through a rock/reservoir. In geothermal exploitation, TC determines the efficiency of heat transport in a reservoir, with high values being preferential for good production. In middle- to high nuclear waste storage, the knowledge of TC of pelitic host rock is of prime importance to determine the spacing necessary between waste batches. Storage galleries need to be sufficiently spaced to allow the released heat to be sufficiently dispersed, thus avoiding temperature increase above detrimental levels. Rock or sediments with higher TC are thus preferred.

TC is a tensor property and depending on the rock material studied and its mineralogy, it may exhibit a strong anisotropy, especially in clay-rich rocks. TC anisotropy is a function of primary (mineralogy, deposition) and secondary (compaction, tectonic deformation) features affecting rock fabric (Davis et al. 2007). The knowledge of TC anisotropy of laminated and pelitic rock (that potentially may be useful as host rock for nuclear waste in Belgium) is however rather poor and forms the subject of this study.

2. Aim

We aim to develop a methodology beyond the state-of-the-art to measure, investigate and explain the 3D anisotropy of thermal conductivity in pelitic rock. A petrophysical study is performed on four pelitic rock formations (Fm): i.e. the Deerlijk Fm (DEE, Silurian cover), Fauquez Fm (FAU, Ordovician) and Asquempont Member of the Oisquercq Fm (OIS, Cambrian) in the SW part of the Brabant Massif (Belgium) and the Ronquières Fm (RON) in the northern part of the Brabant Massif. Samples were selected from borehole cores available at the core store of the Geological Survey of Belgium (GSB).

3. Methodology

TC measurements were made using the Thermal Conductivity Scanner (TCS; Popov et al., 1983) available at the GSB. The TCS employs a moving heat source that is preceded and followed by two temperature infrared sensors, respectively referred to as cold and hot sensors. When the TCS moves along a straight line below a cut rock sample (painted black to ensure homogeneous absorption of heat) heat is conducted in a plane normal to the scanline. The cold and hot sensors measure initial and heated rock sample temperature, respectively. An apparent TC of the plane normal to the line scan is calculated from the sample temperature gradient and the gradient produced between standards with known TC. Three repetitive measurements along the sample line

ensure statistical accuracy and reproducibility of the apparent TC value. The TCS accurately samples TC values at mm resolution making it possible to study and isolate layering, inhomogeneities and mineral layers.

Each core was cut in two orthogonal sections perpendicular to bedding and oriented parallel to either dip or strike. For samples in which bedding was not obvious to detect (e.g. Oisquercq Fm), microCT scanning was used to detect subtle bedding indications. To study TC in 3D, samples were measured along three perpendicular line scans: one oriented (sub)normal to bedding and two within the bedding plane. Knowledge of the angle between the line scan and the bedding plane allows conversion of measured apparent TC values along the three linescans into the true 3D principal axes of the TC tensor. Developing and applying this conversion in 3D and visualising the outcome of the TC tensor is advised in the TCS manual but is hardly ever applied in thermal conductivity research and hence is innovative.

4. Results

No matter the difference in lithology, all samples of the five formations show a strong anisotropy with significant lower (up to 60%) TC values perpendicular to bedding than in the bedding plane. Bedding normal TC varies between 1.5-2.7 (OIS), 2.2-2.8 (FAU), 2.2-2.9 (RON) and 2.8-3.9 W/m.K (DEE) whereas bedding parallel TC ranges between 2.9-4.9 (OIS), 2.6-3.8 (FAU), 3.3-4.5 (DEE) and 2.7-4.3 W/m.K (RON). Largest anisotropy factor is detected for OIS. Anisotropy within in the bedding plane is also detected, yet these TC variations (up to max ~30% difference) are significantly smaller than the bedding normal parallel versus bedding parallel TC anisotropy. Whether TC is higher along dip or strike within the bedding plane depends on texture and microscopic fabric of the pelitic formations rather than on mineralogy.

To investigate the relationship between mineral orientation and the TC tensor, small cubes cut out of the cores were analysed in a Agico KappaBridge to measure the anisotropy of magnetic susceptibility (AMS). For samples in the SW part of the Brabant Massif, the susceptibility tensor has a dominant oblate shape indicative of a compaction fabric with minimum susceptibility normal to bedding and alternating intermediate and maximum susceptibility axes parallel to strike and dip in the bedding plane. The similarity of susceptibility and TC tensors suggests that the mineralogical fabric, which in the SW part of the Brabant Massif is mainly caused by compaction, controls the anisotropy and orientation of the TC tensor.

5. Conclusions

In the studied mineralogically nearly identical but texturally different pelitic rock formations, the compaction texture results in a thermal conductivity anisotropy with the bedding TC significantly higher than the TC normal to bedding. The TC anisotropy in pelitic rock is much higher than in fine- or coarse-grained (reservoir) rock. Although anisotropy effects in sands or sandstones (i.e. reservoir rock) are generally expected to be rather minor due to the dominant isotropic packing of quartz grains, the influence of mud drapes, clay or silt layers, clasts and bedding parallel diagenetic alteration can still introduce a preferred thermal conductivity anisotropy. Hence applying the described innovative 3D methodology for measuring thermal conductivity in host rock or in reservoir rock should always be considered.

6. References

- Davis, M.G., Chapman, D.S., Van Wagoner, T.M., Armstrong, P. 2007. Thermal conductivity anisotropy of metasedimentary and igneous rocks. *Journal of Geophysical Research: Solid Earth*, 112, 1-7.
- Popov, Y.A., V.G. Semionov, V.M. Korosteliov, and V.V. Berezin. 1983. Non-contact evaluation of thermal conductivity of rocks with the aid of a mobile heat source, *Izvestiya, Phys. Solid Earth*, 19, 563-567.

Stratigraphy of the Lower Palaeozoic of the Anglo-Brabant Deformation Belt, Belgium (Part III): The Silurian of the Orneau Group in the Brabant Massif and the Ordovician-Silurian in the Condroz Inlier

Jacques VERNIERS¹, Alain HERBOSCH², Jan VANMEIRHAEGHE^{1,3}, Jan MORTIER¹ and Tim DEBACKER⁴

¹ Ghent University, Krijgslaan 281 S8, 9000 Ghent, Belgium.

² Université Libre de Bruxelles, D.G.E.S. 50 av. F.D. Roosevelt. 1050 Bruxelles, Belgium.

³ Kapel Ter Bede 121, 8500 Kortrijk, Belgium.

⁴ Bureau for Environment and Spatial Development – Flanders, Koning Albert II-laan 20, 1000 Brussels, Belgium.

Multidisciplinary research on the Lower Palaeozoic rocks in Belgium during the last 40 years considerably advanced our understanding of the Belgian part of the Anglo-Brabant Deformation belt. This research includes structural geology, geophysical data analysis, detailed geological mapping, lithostratigraphy, sedimentology and biostratigraphical dating using chitinozoans, acritarchs and graptolites, both in outcrop and on borehole rock. Combined with the aforementioned data, recent provenance studies of the sediments and geochemical analysis of the magmatic units have allowed refining the basin evolution, and magmatic history, contributing to a better understanding of the tectonic evolution of the Brabant Massif (cf. Linnemann et al., 2012).

It is now well established that the outcrop area of the Lower Palaeozoic in the Brabant Massif contains a more than 13 km thick sedimentary succession. More accurately, it is a composite succession, of which only some parts in outcrops have been described in detail, and for which the total thickness assumes a vertical succession from Cambrian to Silurian. In most parts, it is accurately dated biostratigraphically with graptolites, chitinozoans, acritarchs, and other macrofossil groups. Hence, it represents the visible and well-studied Lower Palaeozoic stratigraphical succession for the otherwise largely concealed eastern part of Eastern Avalonia.

In two previous publications, the stratigraphy of this thick pile of sediments has been synthesized and reviewed in the light of all recent studies on the Cambrian of the Brabant Massif (Herbosch & Verniers, 2013) and on the Ordovician of the Brabant Massif (Herbosch & Verniers, 2014).

The present study on the Brabant Massif, the third one in a series, brings together all recent stratigraphical studies on the Silurian strata, the Orneau Group. In an addition we summarize all recent stratigraphical studies on the Ordovician and Silurian of the different parts of the Condroz Inlier, especially the partly unpublished studies on the Ordovician and on the Silurian (Jan Vanmeirhaeghe, ms. PhD 2006, Jan Mortier, ms. PhD. 2014).

References

- Herbosch, A. & Verniers, J., 2013. Stratigraphy of the Lower Palaeozoic of the Brabant Massif, Belgium. Part I: The Cambro-Ordovician from the Halle and Ottignies groups. *Geologica Belgica*, 16, 49-65.
- Herbosch, A. & Verniers, J., 2014. Stratigraphy of the Lower Palaeozoic of the Brabant Massif, Belgium. Part II: The Middle Ordovician to lowest Silurian of the Rebecq Group. *Geologica Belgica*, 17, 115-136.
- Linnemann, U., Herbosch, A., Liégeois, J.P., Pin, C., Gärtner A. & Hofmann, M., 2012. The Cambrian to Devonian odyssey of the Brabant Massif within Avalonia: A review with new zircon ages, geochemistry, Sm-Nd isotopes, stratigraphy and palaeogeography. *Earth-Science Reviews*, 112, 126-154.

Porosity of uniform sands and gravels as a function of packing state and particle properties (size, roundness and sphericity)

Gert Jan WELTJE

KU Leuven, Department of Earth and Environmental Sciences, Celestijnenlaan 200E, 3001 Heverlee.

1. Problem

The ability to predict the porosity of sediments with arbitrary size-roundness-sphericity (D,R,S) distributions has remained one of the elusive goals of sedimentology. It is proposed that this complex problem may be broken down into a series of sub-problems, which must be resolved sequentially: (1) predict the porosity of arbitrary uniform particle assemblages (i.e., particles with fixed size, roundness and sphericity) under specified experimental conditions; (2) predict the porosity of arbitrary mixtures of uniform particle assemblages under specified experimental conditions (this is where grain-size and -shape distributions come in); (3) relate the experimental conditions to the evolution of boundary conditions over the course of geological time and use this to predict how porosity will evolve (this is where burial history and diagenesis come in). Not much is known about the first sub-problem, although a considerable amount of empirical data relevant to its resolution are available in the field of geotechnical engineering (e.g. Cho et al., 2006), and an equation has been proposed for smooth spheres (Yu et al., 2003), which is consistent with the range of stable packing states of coarse uniform sphere assemblages (Weltje & Alberts, 2011). The second sub-problem has been extensively studied in the field of powder technology (e.g. Yu & Standish, 1991, 1993). The third poses many problems. In geology, it has been dealt with in a highly generic way only, i.e. without specification of the properties of particle assemblages (e.g. Gluyas & Cade, 1997; Paxton et al, 2002), and is therefore regarded as essentially unresolved.

2. Solution to the first sub-problem

In this contribution a solution to the first sub-problem will be presented. Legacy data were culled from a range of mostly geotechnical sources, published between 1938 and 2017, and analysed in the light of a new porosity model. Analysis of this heterogeneous data set has ($n = 284$) been carried out by capturing the variability among experimental conditions with a single number, termed the packing state of a particle assemblage (E). The porosity of uniform particle assemblages corresponding to a given packing state has been termed the intrinsic porosity. Available data permit an intrinsic porosity function to be derived for grain assemblages in the sand-to-gravel range with any combination of roundness and sphericity values, which have been deposited in air. With this function, the porosity of arbitrary uniform particle assemblages can be predicted quite accurately (within about 5% relative error) if E is known. The geological significance of the packing state E lies with the fact that it reflects the conditions under which deposition occurs. The new porosity model treats particle properties (D,R,S) independent from packing state. It is thus now possible to separate these effects, and to characterize a specific set of conditions under which deposition occurs (in the lab or the real world) in terms of a single parameter which is independent of particle properties. This is a significant improvement over all previously proposed porosity functions, which opens the way to rigorous prediction of initial porosities for improved modelling of sandstone diagenesis.

3. Future work: the second sub-problem

Accurate and precise porosity prediction requires knowledge of the characteristic packing states of depositional (sub) environments. Such knowledge is presently unavailable, despite its obvious relevance to sedimentological, diagenetic and hydrogeological studies. Existing data-acquisition technology may be used to establish a library of characteristic packing states of specific environments. Measurement of resinated samples to obtain in-situ porosities in combination with the size-roundness-sphericity distributions of the particle assemblages may be carried out by micro-CT scanning. The quality of partitioning will improve if unconsolidated samples are taken adjacent to resinated ones. These may be used to establish average grain density to refine the porosity estimate of the micro-CT scan. Their joint roundness-sphericity distribution as a function of size may be characterized in more detail by means of dynamic image analysis techniques, and their size distribution by means of laser-diffraction particle size analysis. Data integration may be carried out with dedicated multivariate calibration algorithms (Weltje et al., 2015). Integration of the data obtained with these three techniques on a fair number of samples from any given (sub)environment within a single sedimentary system provides sufficient information to resolve the second (sub)problem identified above. The data will be used to fit the parameters of the porosity model presented in this paper, using experiments in which the porosities of samples with different grain-size distributions have been measured (e.g. Beard & Weyl, 1973). This part of the research program, in which the second sub-problem is resolved, will be presented in a follow-up study.

References

- Beard, D.C., Weyl, P.K., 1973. Influence of texture on porosity and permeability of unconsolidated sand. *American Association of Petroleum Geologists Bulletin*, 57, 349-369.
- Cho, G.C., Dodds, J., Santamarina, J.C., 2006. Particle shape effects on packing density, stiffness, and strength: natural and crushed sands. *Journal of Geotechnical and Geoenvironmental Engineering*, 132, 591-602.
- Gluyas, J., Cade, C.A., 1997. Prediction of porosity in compacted sands. In: Kupecz, J.A., Gluyas, J., Bloch, S. (Eds.), *Reservoir Quality Prediction in Sandstones and Carbonates*. American Association of Petroleum Geologists Memoir 69, p. 19-28.
- Paxton, S.T., Szabo, J.O., Ajdukiewicz, J.M., Klimentidis, R.E., 2002. Construction of an intergranular volume compaction curve for evaluating and predicting compaction and porosity loss in rigid-grain sandstone reservoirs. *American Association of Petroleum Geologists Bulletin*, 86, 2047-2067.
- Weltje, G.J., Alberts, L.J.H., 2011. Packing states of ideal reservoir sands: insights from simulation of porosity reduction by grain rearrangement. *Sedimentary Geology*, 242, 52-64.
- Weltje, G.J., Bloemsma, M.R., Tjallingii, R., Heslop, D., Röhl, U., Croudace, I.W., 2015. Prediction of geochemical composition from XRF-core-scanner data: A new multivariate approach including automatic selection of calibration samples and quantification of uncertainties. *Developments in Paleoenvironmental Research* 17, pp. 507-534.
- Yu, A.B., Feng, C.L., Zou, R.P., Yang, R.Y., 2003. On the relationship between porosity and interparticle forces. *Powder Technology*, 130, 70-76.
- Yu, A.B., Standish, N., 1991. Estimation of the porosity of particle mixtures by a linear-mixture packing model. *Industrial and Engineering Chemistry Research*, 30, 1372-1385.
- Yu, A.B., Standish, N., 1993. Limitation of proposed mathematical models for the porosity estimation of nonspherical particle mixtures. *Industrial and Engineering Chemistry Research*, 32, 2179-2182.

Microfacies analysis of a middle to upper Frasnian succession at the Lompret quarry (SW Belgium) documenting a transition from the Lion reef to deep marine Neuville and Matagne environments

Marc-Aurèle WYNANTS¹, Stijn GOOLAERTS², Sofie GOUWY³, Thomas GOOVAERTS², Frédéric BOULVAIN¹, Xavier DEVLEESCHOUWER²

¹*Université de Liège, Pétrologie sédimentaire, B20, Géologie, Université de Liège, Sart Tilman, B-4000 Liège, Belgium*

²*Royal Belgian Institute of Natural Sciences, Rue Vautier 29, B-1000 Brussels, Belgium*

³*Geological Survey of Canada, 3303, 33rd St. NW, Calgary, Alberta, Canada*

1. Introduction

When in 2011 quarrying extended northward at the ‘Carrière de Lompret’, Lompret, SE Belgium, a middle to upper Frasnian succession from the Grands Breux up to Matagne Formation became progressively accessible. Although slightly hampered by the large number of faults with two major intersecting directions, and over a period of several years, we succeeded in logging almost the entire stratigraphic interval. We collected a large number of samples for microfossil, sedimentological and geochemical analyses, plus a very large number of macrofossils. Amongst the latter are many ammonoid and nautiloid cephalopods, crinoids, brachiopods, corals and trilobites (Ginter et al., 2017; Goolaerts & Gouwy, 2015; Goolaerts et al. 2018; Gouwy & Goolaerts, 2015). For microfacies analysis, we sampled and studied three sections in detail: LOK, LOL and LOM. The transition from the reefal settings of the upper part of the Lion Member (Grands Breux Formation) to the coral and crinoid rich lower part of the Neuville Formation was studied in the LOL section. LOK allowed to study the upper half of the Neuville Formation and the lower part of the Matagne Formation, and LOM several meters of nearly black Matagne Formation shales stratigraphically upwards of the LOK sequence. The goal of the study is to establish the sedimentary paleo-environments using microfacies analysis.

2. Deep water marine paleo-environments after deposition of the Lion reefal sediments

Almost the entire Neuville Formation succession is characterized by nodular limestone beds. Their microfacies reveals a deep marine sedimentation environment in which sponges were very common. Because several of the odd-shaped nodules have well-preserved sponge remains in them, it is possible that the nodular character of the Neuville beds at Lompret directly relates to well preserved sponges (the spicule network is generally extremely well preserved). The sponges are predominantly abundant in the deeper environments in between the Lion Member reefal facies. The sponge facies are occasionally affected by storm deposits directly overlying the sponge facies and locally disturbing the assemblage of sponges and filling the spaces in between the sponges by coarse-grained bioclastic packstones composed of fragments of bivalves, ostracods, crinoids, trilobites, algae, brachiopods, sponge spicules and calcimicrobes. The change from thick (pluricentimetric) bioclastic layers towards thinner (plurimillimetric) storm deposits indicate a rise in sea-level and a transition from proximal to distal storm layers.

The microfacies of the sparse limestone beds in the Matagne Formation correspond to an argillaceous mudstone containing small fragments of bivalves, ostracods, goniatites and tentaculitids. It is also enriched in organic matter and opaque minerals. A detrital fraction is underlined by the presence of clay minerals and silty quartz. These microfacies represent the deepest environments and are observed in the Matagne Formation indicating a water depth below the storm wave base.

The preliminary results of our microfacies analysis suggest that the entire stratigraphic succession was deposited on a middle to outer ramp setting at proximity of a reef mound. The sponge facies were regularly affected by storm events. The rounded morphology of the sponges as seen from microfacies could suggest that part of the sponge nodules were reworked by storms and transported further offshore.

3. References

- Ginter, M., Gouwy, S & Goolaerts, S., 2017. A classic Late Frasnian chondrichthyan assemblage from southern Belgium. *Acta Geologica Polonica*, 67(3), 381-382.
- Goolaerts, S. & Gouwy, S., 2015. The Lahonry quarry at Lompret, Belgium: an extraordinary new site to study Upper Frasnian cephalopods during the onset of anoxia in the Dinant Basin. *STRATA série 1: communications*, 16, 61-62.
- Goolaerts, S., Gouwy, S., Houben, K., Wynants, M.A. & Devleeschouwer, X., 2018. Frasnian cephalopods from the newly discovered Carrière de Lompret section, Lompret, Belgium. *Münstersche Forschungen zur Geologie und Paläontologie*, 110, 32-33.
- Gouwy, S. & Goolaerts, S., 2015. Upper Frasnian deposits at the Lahonry quarry (Lompret, Belgium): conodont biostratigraphy, microvertebrates and bentonites. *STRATA série 1: communications*, 16, 63.
- Humblet, M. & Boulvain F., 2001. Sedimentology of the Bieumont Member: influence of the Lion Member Carbonate mounds (Frasnian, Belgium) on their sedimentary environment. *Geologica Belgica*, 3 (1-2), 97-118.

Theme 4

Geo-resources, -materials and -energy in a circular economy

Relationship between continental carbonate lithotypes and their petrophysical characteristics: a case-study from the Denizli basin (Turkey)

Cihan ARATMAN^{1, 2, 3}, Rochelle TAYLOR³, Cathy HOLLIS³, Zahra MOHAMMADI², Mehmet ÖZKUL¹ and Rudy SWENNEN²

¹ *Engineering Faculty, Department of Geological Engineering, Pamukkale University, Turkey.*

² *Geodynamic and Geofluids Research Group, Department of Earth and Environmental Sciences, KU Leuven, Belgium.*

³ *Basin Studies and Petroleum Geoscience Group, University of Manchester, UK.*

1. Introduction

Continental carbonates have recently received a lot of interest due to the presence of large volumes of hydrocarbons in these strata, for example in the Santos and Campos Basin (e.g. Tupi, Carioca, Guara, and Lara Fields; Wright, 2012; Herlinger et al., 2017) and in the Namibe, Congo and Kwanza Basins, offshore Angola (Schröder et al., 2012; Saller et al., 2016). Travertine outcrops in the Denizli Basin as well as in Italy and Hungary serve as outcrop analogues since they present several similarities to continental carbonate reservoirs (Terra et al., 2010; Erthal et al., 2017) in terms of microfacies components. However, no clear relationship between travertine/tufa-like lithotypes and porosity and permeability has been established because these lithologies are made up of complex sedimentary fabrics containing lithic peloids, peloidal shrubs and micro- or macrophytes encrusted by calcite. The latter relate to shallow- or deep-circulated fluids with varying temperatures from 20 to 40°C under low to high alkalinity and CO₂ degassing (Ford and Pedley, 1996; Pentecost, 2005). This detailed study of sedimentary fabrics and lithotypes however allows to refine the relationship of continental carbonates in the Denizli Basin (Turkey) to petrophysical parameters, such as porosity, permeability and acoustic velocities. In addition, it aims to address facies heterogeneity at the basin scale, by defining lithotypes formed under varying environmental conditions as suggested by Lopez et al. (2017).

2. Results

Helium porosity and permeability analyses as well as acoustic-wave velocity measurements under dry-saturated and ambient conditions were carried out on 165 cores, each up to 7 cm length and 2.5cm diameter. Field analysis identified three different lithotypes based on the quantity of lime mud, carbonate and coated grains, the different types of skeletal organisms, and the importance of lamination. The following lithotypes were differentiated: (i) microsparite wackestone, (ii) intraclast packstone, (iii) massive shrubby grainstone, and (iv) boundstone. In addition, in the boundstone lithotype, shrubby, granular shrubby, laminated, coated reed, and phyto sub-lithotypes can be differentiated. Petrographical studies allow discrimination of each lithotype or sub-lithotype using their sedimentary fabrics according to the packing and organization of lithic peloids and peloidal shrubs. The compressional-wave (V_p) and shear-wave (V_s) velocities of the studied travertine lithotypes vary between 4192 m/s to 6077 m/s, and 2207 m/s to 3873 m/s, respectively. They show a porosity ranging from 2.78% to 36.54%, and a permeability ranging from 0.002 mD to 58060 mD. The V_p/V_s ratio ranges from 2.19 to 1.5. Each lithotype indicates various dynamic elastic moduli including bulk, shear and young's modulus that were calculated from the measured acoustic-wave velocities and bulk density because the link of geological parameters of the lithotypes to seismic properties helps to infer their complex micro facies properties from

velocity/porosity data. The microsparite wackestone, shrubby and phyto boundstone lithotypes are differently clustered in the plot of the elastic moduli *versus* porosity. Furthermore, with respect to porosity and bulk modulus, the phyto boundstone clearly distinguished from other lithotypes that have similar seismic properties. As porosity increases, the elastic moduli decreases in all lithotypes, however, it increases in the shrubby boundstone sub-lithotype. The microsparite wackestone and the laminated boundstone as well as phyto boundstone (sub-) lithotypes display the best correlation between porosity and V_p due to their massive sparite, clotted to mesh-work, and spherulite fabrics that are associated with the highest degree of cementation and dissolution. Consequently, this study points out that differences in petrophysical parameters occur between lithotypes. Furthermore, each lithotype exhibits a relationship between porosity and permeability ($R^2 > 0.5$) while having an inversely proportional relationship with acoustic-wave velocities.

References

- Erthal, M.M., Capezzuoli, E., Mancini, A., Claes, H., Soete, J., Swennen, R., 2017. Shrub morpho-types as indicator for the water flow energy - Tivoli travertine case (Central Italy). *Sedimentary Geology*, 347, 79-99.
- Ford, T.D., Pedley, H.M., 1996. A review of tufa and travertine deposits of the World, *Earth Science Review*, 41, 117 – 175.
- Herlinger, R., Zambonato, E.E., Los, L.F.D., 2017. Influence of Diagenesis on The Quality of Lower Cretaceous Pre-Salt Lacustrine Carbonate Reservoirs from Northern Campos Basin, Offshore Brazil. *Journal of Sedimentary Research*, 87, 1285-1313.
- Lopez, B., Camoin, G., Ozkul, M., Swennen, R., Virgone, A., 2017. Sedimentology of coexisting travertine and tufa deposits in a mounded geothermal spring carbonate system, Obruktepe, Turkey. *Sedimentology*, doi: 10.1111/sed.12284.
- Pentecost, A., 2005. *Travertine*, Springer, Berlin.
- Schroder, S., Ibekwe, A., Saunders, M., Dixon, R., and Fisher, A., 2015. Algal-microbial carbonates of the Namibe Basin (Albian, Angola): implications for microbial carbonate mound development in the South Atlantic. *Petroleum Geoscience*, 22, 71-90.
- Terra, G.J.S., Spadini, A.R., Franca, A.B., Sombra, C.L., Zambonato, E.E., Juschaks, L.C.d.S., Arienti, L.M., Erthal, M.M., Blauth, M., Franco, P.P., Matsuda, N.S., da Silva, N.G.C., Junior, P.A.M., D'Avila, R.S.F., deSouza, R.S., Tonietto, S.N., dos Anjos, S.M.C., Campinho, V.S.? Winter, W.R., 2010. Classificac~ao de rochas carbonaticasaplicacavel as bacias sedimentares brasileiras. Carbonate rock classification applied to brazilian sedimentary basins. *Bulletin Geoscience, Petrobras*, Rio de Janeiro, 18, p. 9–29.
- Wright, P. V., 2012. Lacustrine carbonates in rift settings: The interaction of volcanic and microbial processes on carbonate deposition, *Geological Society London Special Publications*, 370, p. 1–39.

The radionuclide sorption potential of Neogene glauconite sands in the disposal of radioactive waste: ^{137}Cs sorption

Yaana BRUNEEL^{1,2}, Liesbeth VAN LAER¹, Erik SMOLDERS², Stéphane BRASSINNES³

¹ *Belgian Nuclear Research Centre (SCK•CEN), Expert Group Waste & Disposal*

² *Department of Earth and Environmental Sciences, Division of Soil and Water Management, KULeuven*

³ *ONDRAF/NIRAS, the Belgian Agency for Radioactive Waste and Fissile Materials*

1. Introduction

In Belgium, surface disposal is considered in Dessel for low and intermediate short lived radioactive waste. For the disposal of long-lived, intermediate and high level waste geological disposal is considered, though no formation and or location has been selected. Most of the research has focused on the poorly indurated Boom Clay. In the NE of Belgium, the 100 m thick Boom Clay layer at a depth below 200 m (in Mol) is situated between glauconite rich sands with glauconite contents up to 70 wt%. The general objective of the PhD is to study the sorption behaviour of radionuclides on these glauconite sands to check whether they can be regarded as a possible sorption sink next to the Boom Clay. Moreover, this mineral is presently considered as one of the potential complementary sorption sinks to be added in the sandy embankment of the surface disposal facility for low and intermediate short lived radioactive waste.

Though low sorption potentials are generally expected in sands, the Neogene sands are interesting due to the high glauconite content. Glauconite has the appearance of a green sand grain, however, glauconite is a clay. Glauconite is described as an iron (Fe) - potassium (K) phyllosilicate $((\text{K},\text{Na})(\text{Fe}^{3+}\text{Fe}^{2+},\text{Al},\text{Mg})_2(\text{Si},\text{Al})_4\text{O}_{10}(\text{OH})_2)$, comparable to an Fe-rich illite with K^+ the main interlayer cation. The structure contains both Fe^{2+} and Fe^{3+} due to formation in alternating oxidizing reducing conditions in marine shelf environment. Due to weathering the mineral can evolve, to a smectite-like structure with lower K content and a rim of oxides may develop. Leaching the interlayer cations opens the edges of the layers creating specific sorption sites for K, Cs or ammonium (NH_4).

2. Materials and methods

The sands used in the radiocesium sorption experiments originate from different sections in the Neogene formations. In Mol the Neogene sands have a thickness of 156 m (between 3 and 159 m deep, respectively 22 and -134 mTAW – reference height). Over this section, over the different formations, nine Neogene sands samples were selected for the Cs sorption experiments. To understand the reaction of the complete sand it was chosen to study the individual fractions. By centrifugation in a double chamber system the pore water was extracted. With magnetic separation glauconite can be separated from the sediment in fractions with particle sizes larger than 32 μm . Good separation becomes more difficult with decreasing particle size. In fractions smaller than 250 μm the glauconite pellets can never be extracted completely.

^{137}Cs sorption is tested through a batch sorption experiment on the complete sands and on the glauconite fraction. In this experiment the sorption potential is determined in a solution with a 0.5 mM K and 100 mM Ca concentration (Radiocesium Interception Protocol (RIP) (Wauters et

al., 1996)). The cation composition is important in the case of Cs^+ sorption due to the competition for sorption sites with K^+ and NH_4^+ in natural systems.

3. Results

The ^{137}Cs sorption test has proven that the Neogene glauconite sands sorb Cs strongly with sorption potentials (distribution coefficient K_d) between 850 and 4900 mmol/kg at 0.5 mM K^+ (complete sands), similar to ^{137}Cs sorption potentials in the Boom Clay. In the glauconite fraction sorption potentials range from 3500 to 5500 mmol/kg under these conditions, comparable to illite with K_d 's of 6000 – 7000 mmol/kg.

The size of the glauconite pellets does limit the Cs sorption and clay sized glauconite has larger sorption potentials. However, between large ($>500\ \mu\text{m}$) and small (125-32 μm) glauconite pellets no significant differences in sorption potential exist. Sorption potential variations among the glauconite sands of Diest, Berchem and Voort are limited, though there is a compositional diversity and a large difference in glauconite content. Glauconite sands with about 20% glauconite content from the upper Diest Fm have similar sorption potentials as samples of the Berchem Fm (containing about 75% GL) indicating that other factors might play a role.

There is a strong indication that these sorption differences are related to the weathering state of the glauconite pellet. More weathered glauconite, as can be found in the Upper Diest Fm, are associated with iron oxides and with a decrease in K content. The K is the 'glue' between the clay layers. Decreasing the K content causes the formation of more frayed edges and a larger charge defect. The validity of this hypothesis has to be tested by more mineralogical and chemical analysis.

^{137}Cs sorption is expressed as the sorption potential due to the competition with K^+ . When calculating K_d using the K concentrations in the extracted pore solutions, the estimated sorption decreases up to 1.3 log K_d units (L/kg). In the waters pumped from the observation wells (aquifer water) the average concentration is 0.2 mM K, causing an increase of the estimated sorption up to 0.5 log K_d units. The extracted pore water concentrations can be seen as the worst case scenario, while the aquifer concentrations are better representations of the competing cation concentration in the Neogene glauconite sands today.

4. Conclusions

The Neogene glauconite sands have shown sorption potentials for Cs comparable to the sorption potential in the Boom Clay. Glauconite sands can thus be considered a good sorbent, however, sands have very high permeabilities compared to clay layers. Therefore the kinetics of Cs sorption and exchange by competing cations in a natural system will be of vital importance.

Reference

Wauters, J, et al., 1996. Prediction of Solid/Liquid Distribution Coefficients of Radiocaesium in Soils and Sediments. Part One: A Simplified Procedure for the Solid Phase Characterisation. Applied Geochemistry 11.4, 589-94.

Upper stability limit of authigenic monazite in the Rocroi Inlier

Corentin COBERT¹, Jean-Marc BAELE¹, Sophie DECREE² and Olivier BEYSSAC³

¹*Geology and Applied Geology, University of Mons, 9, rue de Houdain, 7000 Mons, Belgium.*

²*Royal Belgian Institute of Natural Sciences, Brussels, Belgium.*

³*Institut de Minéralogie et de Physique des Milieux Condensés (IMPMC), CNRS-Université Pierre et Marie Curie, Case Courrier 115, 4 place Jussieu, 75005 Paris, France.*

Authigenic monazite (also called “grey” or “dark” monazite) is a Rare Earth Elements (REE) orthophosphate, which is Eu-rich and Th-poor compared to the more common “yellow” monazite of magmatic or high-grade metamorphic origin. This mineral is believed to form under late diagenesis to very low metamorphism conditions (250-400 °C and P~2-10 kbar) in carbonate-poor and organic matter(OM)-rich shales (e.g. Burnotte et al., 1989; Janots et al., 2006; Wan et al., 2007). Investigation on the potential economical interest of authigenic monazite is motivated by the worldwide distribution of this mineral and the occurrence of secondary concentration in (paleo-)placer (e.g. Rosenblum and Mosier, 1983; Cobert et al., 2016). In Belgium, authigenic monazite has been reported in Lower Paleozoic rocks of the Rocroi inlier, Brabant massif and Stavelot-Venn inlier.

In the Rocroi inlier, Nonnon (1984) firstly documented dark monazite in stream sediments in the Croix-Scaille massif before tracing to its source rock in shales of the Revin Group (middle Cambrian to Ordovician). Due to its structure, the Rocroi inlier offers an extensive outcrop of the Revin group. In addition, it is affected by a North to South prograde metamorphism (anchizone to epizone). Therefore, the Rocroi inlier is a good natural laboratory to carry out a petrographical and geochemical study on the behaviour of authigenic monazite during prograde metamorphism.

Cathodoluminescence imaging (CL) and Scanning Electron Microscopy with Energy-Dispersive Spectroscopy (SEM-EDS) of the Revin Group shales reveal the presence of authigenic monazite in the northern and central part of the Rocroi inlier (Fig.1a), along the “Eau Noire” stream and at Revin, respectively. At Mairupt, in the southern part of the inlier, CL show images of nodules alike authigenic monazite with their typical irradiation haloes around but with different luminescence characteristics inside. SEM-EDS analysis indicate the presence of allanite (LREE-rich epidote), xenotime (HREE-rich phosphate) and LREE, Th-rich monazite assemblages in these nodules (Fig.1b). Raman Spectroscopy on Carbon Material (RSCM) showed that the local maximum temperature that was reached by the host rock is 500 ± 50 °C, while at Revin and in the “Eau Noire” valley, <300°C is reported in the literature (Beugnies, 1986). A few authors (e.g. Janots et al., 2008) have discussed the conditions for the destabilization of monazite and its transformation into allanite, which occur at 420–450 °C. Allanite can later be partially or totally destabilized in metamorphic monazite and xenotime at 550–575 °C and >585 °C, respectively, or by retrograde metamorphism only if the CaO/Na₂O ratio < 0.54. Based on literature data, our results would indicate a breakdown of authigenic monazite at Mairupt and its transformation into allanite.

Therefore, in the Rocroi inlier, the required conditions to form authigenic monazite have been reached and the upper stability limit of this mineral was crossed to the south, which would indicate a minimum temperature of 420°C if we use this limit as a geothermometer.

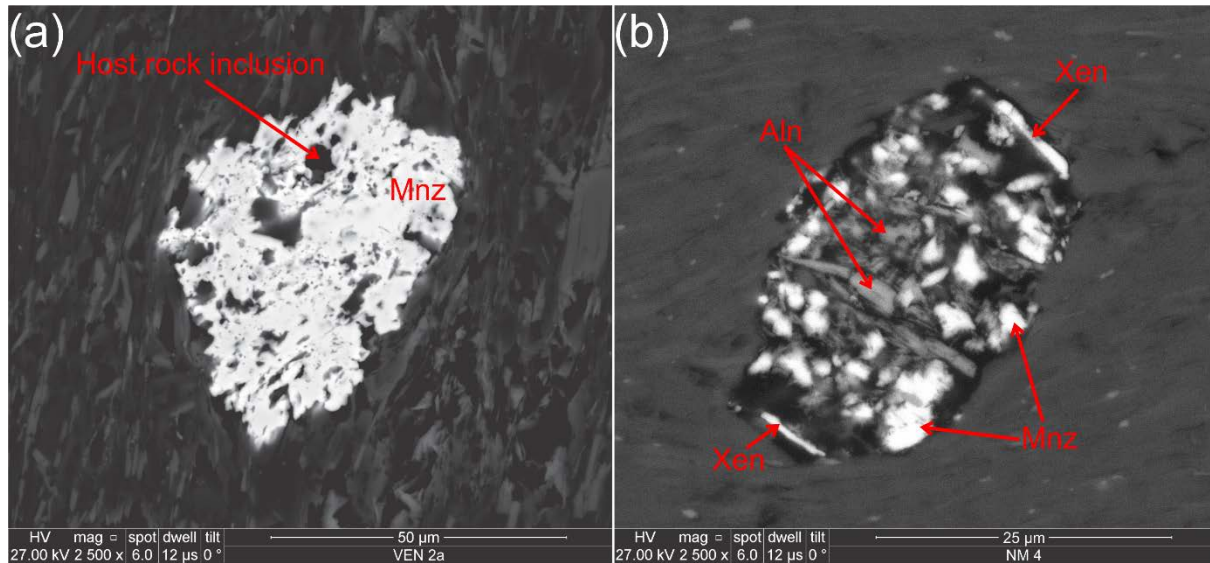


Figure 1. SEM imaging of (a) authigenic monazite nodule in shale of the northern part of the Rocroi inlier; (b) allanite (grey) / monazite (light white) / xenotime (light white stretched mineral) assemblage in shale of the southern part of the Rocroi inlier. Abbreviations: Mnz, Monazite; Aln, Allanite; Xen, Xenotime.

References

- Beugnies, A., 1986. Le métamorphisme de l'aire anticlinale de l'Ardenne. *Hercynica II* (1), 17-33.
- Burnotte, E., Pirard, E. & Michel, G., 1989. Genesis of gray monazites; evidence from the Paleozoic of Belgium. *Economic Geology*, 84(5), 1417-1429.
- Cobert, C., Baele, J.M., Boulvais, Ph., Decrée, S., Dupont, N. & Spagna, P., 2015. Grey Monazite Paleoplacers in Lower Cretaceous Continental Formations in the Mons Basin, Belgium. 13th SGA Biennial Meeting, Nancy, France, 2015. Abstract book. 703-706.
- Janots, E., Negro, F., Brunet, F., Goffé, B., Engi, M. & Bouybaouene, M.L., 2006. Evolution of the REE mineralogy in HP-LT metapelites of the Sebide complex, Rif, Morocco: monazite stability and geochronology. *Lithos*, 87(3-4), 214-234.
- Janots, E., Engi, M., Berger, A., Allaz, J., Schwarz, J. O. & Spandler, C., 2008. Prograde metamorphic sequence of REE minerals in pelitic rocks of the Central Alps: implications for allanite–monazite–xenotime phase relations from 250 to 610 C. *Journal of Metamorphic Geology*, 26(5), 509-526.
- Nonnon, M., 1984. Découverte de monazite grise en nodules et d'or alluvionnaire dans le massif de la Croix-Scaille. *Bulletin de la société belge de géologie*, 93(4), 307-314.
- Rosenblum, S. & Mosier, E.L., 1983. Mineralogy and occurrence of europium-rich dark monazite. U.S. Geological Survey Professional Paper 1181 67 pp.
- Wan, Y., Song, T., Liu, D., Yang, T., Yin, X., Chen, Z. & Zhang, Q., 2007. Mesozoic monazite in Neoproterozoic metasediments: evidence for low-grade metamorphism of Sinian sediments during Triassic continental collision, Liaodong Peninsula, NE China. *Geochemical Journal* 41, 47–55.

DETECT - Determining the risk of CO₂ leakage along fractures of the primary caprock using an integrated monitoring and hydro-mechanical-chemical approach

Marcella DEAN¹, Jeroen SNIPPE¹, Niko KAMPMAN¹, Kevin BISDOM¹, Stephanie ZIHMS², Andreas BUSCH², Florian DOSTER², Sebastian GEIGER², Pieter BERTIER³, Hannes CLAES^{3,*}, Alexandra AMANN-HILDENBERAND³, Reinhard FINK³, Bernhard M. KROOSS³, Sheryl HURST⁴, Andy LIDSTONE⁴ & Paul VAN ROSSUM⁴

¹ *Shell Global Solutions B.V., NL*

² *Heriot Watt University, UK*

³ *RWTH Aachen University, GE*

⁴ *Risktec Solutions B.V., NL*

* *Presenter, hannes.claes@emr.rwth-aachen.de*

1. Introduction

In order to verify and demonstrate successful long-term CO₂ storage to the regulators and the public, it is critical to improve our understanding of leakage from CO₂ storage reservoirs along natural pathways. Currently, there are significant gaps in the general understanding of fluid migration along fault zones and fracture networks of the primary caprock, as represented in Figure 1. Leakage rates depend on pressure gradients, fluid densities, fluid saturations, and the flow properties of the fracture networks, which are a complex function of fracture density, connectivity, aperture size and stress regime. The fluid flux is affected by physical and chemical interactions taking place in the fracture system, including mineral dissolution and precipitation, swelling or shrinkage of clay minerals or hydro-mechanically driven propagation of new fractures. These combined effects can result in an increase or decrease in fracture network connectivity and permeability over different temporal and spatial scales. The combination of all these aspects is challenging and although some fundamental laboratory or modelling studies are available in the literature, an integrated study, involving a complete life cycle risk assessment of CO₂ leakage along fractures in caprocks is lacking. Added complexity is given by the fact that a leak can only be detected and quantified when geophysical or chemical monitoring tools are able to distinguish relevant changes in gas saturation, pressures or compositions compared to baseline levels.

2. Aims and strategy

DETECT, co-funded by the ACT program of the European Union and national governments, intends to determine realistic flow rates and geometries across fractured and faulted caprocks, and aims to identify monitoring tools capable of detecting such fluid migration. For this purpose, predicted monitoring performance of state-of-the-art technologies are compared with results from coupled hydro-mechanical flow and reactive transport simulations which in turn have incorporated insights from a comprehensive laboratory study.

This improved understanding of the potential flow rates will feed into an integrated life cycle risk assessment using the established bowtie method to provide an overall picture of the natural paths via which CO₂ leaks could occur from subsurface storage reservoirs. The bowtie model will be

expanded to include quantitative risk assessment, with the goal of calculating the probability/likelihood of leakage across the caprock and estimating the risk reduction provided by monitoring

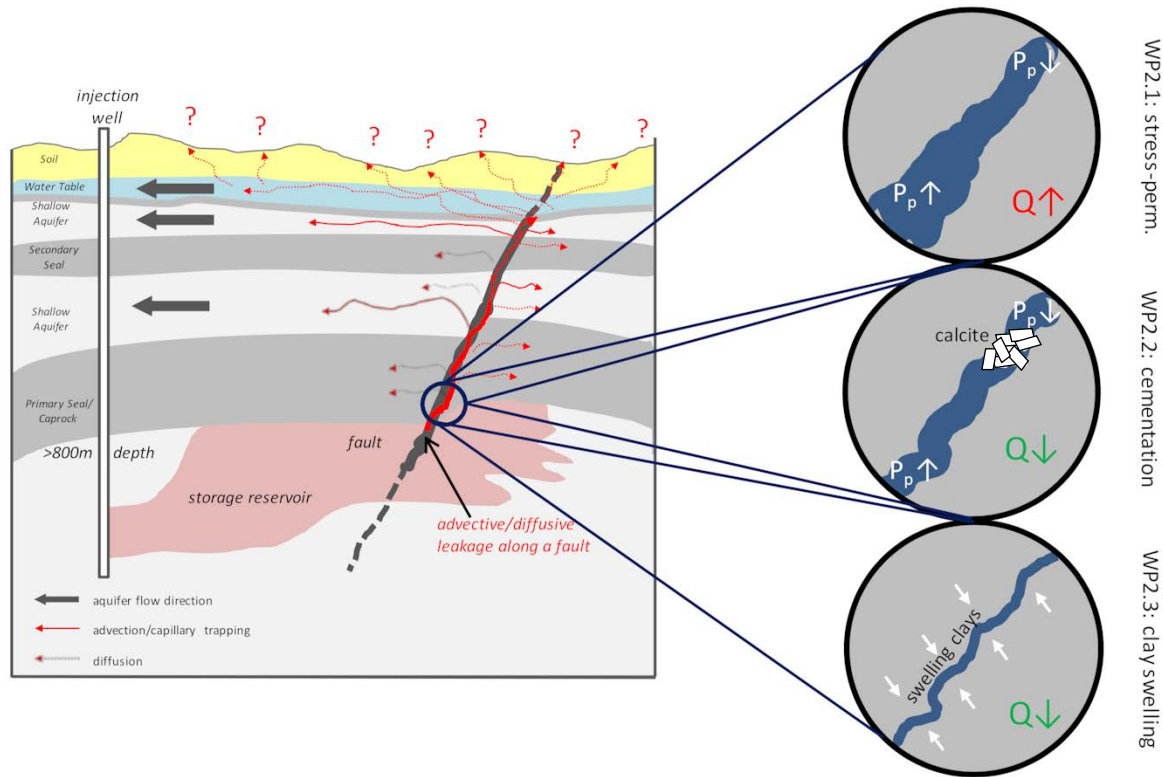


Figure 1. Reservoir model showing a scenario for a leaking fault and highlighting the three processes that will be studied in detail (modified after Busch and Kampman, acc.). T2.1: stress-permeability relations, T2.2: mineralisation in fractures and T2.3: clay swelling affecting fracture apertures. Q is flow rates and arrows indicate an increase or decrease of Q; P_p is pore pressure and arrows indicate high or low values for P_p.

3. Conclusion

The integrated approach (quantitatively) determines the risk of natural leakage across the primary caprock. The combination of state-of-the-art laboratory work with partly unique modelling experience helps to improve Measuring Monitoring and Verification (MMV) plans leading to reasoned risk assessment schemes that are based on the established bowtie method used as a standard in many operations.

Reference

Busch, A. & Kampman, N., accepted, Migration and Leakage of CO₂ from Deep Geological Storage Sites, in Vialle, S., Carey, J.W. and Ajo-Franklin, J.B. (eds.), Caprock Integrity in Geological Caprock Storage, American Geophysical Union.

Formation of the oxidized manganiferous rocks of the Les Plattes Member (Otré Formation, Salm Group) in the Stavelot Massif: timing and weathering processes

Augustin DEKONINCK¹, Patrick MONIÉ², Frédéric HATERT⁴, Sabine BLOCKMANS^{1,3}, Gaëtan ROCHEZ¹, Johan YANS¹

¹ *Institute of Life-Earth-Environment (ILEE), University of Namur, 61 rue de Bruxelles B-5000, Namur Belgium.*

² *Géosciences Montpellier, UMR-CNRS 5243, Université de Montpellier, Montpellier, France*

³ *Service géologique de Wallonie, DGO3, Service public de Wallonie, 14 Avenue Prince de Liège B-5100, Jambes, Belgium.*

⁴ *Laboratoire de Minéralogie, Université de Liège, 14 allée du six août B-4000, Liège, Belgium.*

1. Introduction

Intense and long-term chemical weathering have produced numerous economic manganese deposits worldwide, which have supplied the steel industry for decades. The base of the Lower to Middle Ordovician red and purple slates of the Les Plattes Member (Otré Formation, Salm Group) at the southern part of the Stavelot Massif are particularly enriched in manganese. These levels were mined until the first half of the 21th century, but are known worldwide for their coticule veins, a metasedimentary yellowish rock composed of fine-grained spessartine, quartz and muscovite (e.g. Baijot et al. 2011; Herbosch et al. 2016). These strata have undergone weathering processes leading to the formation of supergene Mn-oxides. The investigation proposed here focuses on the weathering processes and the timing of those sediments.

2. Geological settings

2.1. Tectonic of the Stavelot Massif

The Stavelot Massif is the largest and best-exposed lower Paleozoic inlier of Belgium and belongs to the Ardennes allochthon, which is part of the Rheno-hercynian fold-and-thrust belt. The Massif has been strongly tectonized by the Caledonian and Variscan orogenic cycles. A graben, filled by Permian conglomerates, delimits two structural domains: the southern part of the Massif records an epizonal metamorphism, when the northern part corresponds to an anchizonal zone (e.g. Herbosch et al. 2016). It has been suggested that Tertiary uplift of the Ardennes started with large scale tilting during Paleocene, after a very long period of tectonic quiescence during the Mesozoic (e.g. Demoulin et al. 2018).

2.2. Location and features of the manganiferous levels

Two locations expose the Fe-Mn-bearing strata: in the Salmchâteau syncline (epizonal zone) and the Chevron syncline (anchizonal zone). The Les Plattes Member consists of red and purple slates interbedded with coticule beds. The slates are composed of quartz grains, laminated and disseminated hematite, and variable content of spessartine in a clayey matrix. The yellowish coticule levels are devoid of hematite but contain larger amount of spessartine associated with quartz and clays (Baijot et al. 2011; Herbosch et al. 2016). Metamorphic transformations of the Otré Formation has led to the formation of slates and quartz veins containing spessartine,

rhodochrosite, Mn-chloritoïd, andalusite-kanonaite, pyrophyllite, paragonite, kaolinite and chlorite in the Salmchâteau syncline, as well as manganese oxides, manganese aluminosilicates, and copper sulphides (Hatert, 2003, 2005; Blondieau et al., 2017). Differences exist in the Chevron syncline and are mostly attributed to the variation in metamorphic grades. Therefore, andalusite-kanonaite, pyrophyllite and kaolinite are absent in the northern area (Chevron syncline), when rhodochrosite is scarce in the Salmchâteau area (south).

3. Weathering transformations and timing

Manganese oxides are known as late weathering products of Mn-carbonates and, possibly, Mn-rich silicates. Most of these oxides are often considered together as massive botryoidal “psilomelane” or soft fine-grained “wad” disseminated in the host slates or in quartz veins. The main Mn-oxide phases are cryptomelane and lithiophorite, which are associated with small amounts of manganite, pyrolusite and ramsdellite. Groutite, hausmannite, hollandite-strontiomelane, nsutite and todorokite have also been described (Hatert et al., 2014; Blondiau et al. 2017).

Scanning electron views show that spessartine is poorly or even non-weathered both in coticule and slates. The Mn-oxides are rather located in the clayey matrix. Some of these clay minerals could contain some Fe and Mn in their structure. However, the small amount of Mn substituted in the clayey lattice is probably not sufficient to provide large amount of Mn-oxides. The observation of nsutite by Fransolet (1979) could indicate the presence of primary Mn-carbonates, as nsutite is often associated with Mn-carbonates and results from the weathering of rhodochrosite. New $^{40}\text{Ar}/^{39}\text{Ar}$ dating of pure cryptomelane samples indicate the major weathering period(s) to be Oligocene-Miocene in age. Some older periods (Cretaceous?) cannot be excluded, as they are common in other weathered deposits of the Ardenne (e.g. Demoulin et al. 2018) and suspected in some discordant $^{40}\text{Ar}/^{39}\text{Ar}$ spectra. A recent weathering phase is also reported between 5-1 Ma and could then correspond to the current weathering of the Stavelot Massif.

References

- Baijot, M., Hatert, F. & Fransolet, A.-M., 2011. Mineralogical and geochemical study of pseudocoticule from the Stavelot Massif, Ardennes (Belgium), and redefinition of coticule. *European Journal of Mineralogy*, 23, 633-644.
- Blondieau, M., Puccio, S., Compère, P & Hatert, F., 2017. Données nouvelles sur quelques espèces minérales de Vielsalm et Salmchâteau (Province de Luxembourg, Belgique). *Bulletin de la Société Royale des Sciences de Liège*, 86, 1-48.
- Demoulin, A., Barbier, F., Dekoninck, A., Verhaert, M., Ruffet, G., Dupuis, C. & Yans, J., 2018. Erosion Surfaces in the Ardenne–Oesling and Their Associated Kaolinic Weathering Mantle, in: Demoulin, A. (Ed.), *Landscapes and Landforms of Belgium and Luxembourg*. Springer International Publishing, Cham, pp. 63–84.
- Fransolet, A.-M., 1979. Occurrences de lithiophorite, nsutite et cryptomélane dans le massif de Stavelot, Belgique. *Annales de la Société Géologique de Belgique* 102, 303–312.
- Hatert, F., 2003. Occurrence of sulphides on the bornite-idaite join from Vielsalm, Stavelot Massif, Belgium. *European Journal of Mineralogy*, 15, 1063-1068.
- Hatert, F., 2005. Transformation sequences of copper sulfides at Vielsalm, Stavelot Massif, Belgium. *Canadian Mineralogist*, 43, 623-635.
- Hatert, F., Blondieau, M., Puccio, S., Baijot, M. & Gustine, C., 2014. Le gisement de manganèse de la Vallée de la Liègne, Belgique. *Le Règne Minéral*, 117, 5-24.
- Herbosch, A., Liégeois, J.-P. & Pin, C., 2016. Coticules of the Belgian type area (Stavelot-Venn Massif): Limy turbidites within the nascent Rheic oceanic basin. *Earth-Science Reviews* 159, 186–214.

Explore the subsurface of Flanders with the Virtual Borehole

Katrien DE NIL¹, Roel DE KONINCK², Jan CORLUIY³, Tinne De ROUCK³, Marleen VAN DAMME¹

¹ VPO, Bureau for Environment and Spatial Development – Flanders, Department of Environment & Spatial Development, Koning Albert-II-laan 20, 1000 Brussels

² VITO, Flemish Institute for Technological Research, Boeretang 200, 2400 Mol

³ VMM, Flanders Environment Agency, Dokter De Moorstraat 24-26, 9300 Aalst

A new tool in the DOV Explorer

Flanders Soil and Subsurface Database (DOV, <https://www.dov.vlaanderen.be>) is the public web portal through which regional administrations of Flanders deliver INSPIRE-compliant Open Data, available for re-use, concerning geology, natural resources, soil, hydrogeology, geotechnical characteristics and groundwater licenses. Even though a vast amount of subsurface maps are available for policy makers, it remains difficult for most external users to gain insight in the (hydro)geological structure of the subsurface. Therefore, the ‘Virtual Borehole’ is set up as a tool within the DOV Explorer: one mouse click results in the vertical succession of the (hydro)geological layers together with some basic properties at that location. It is an interactive and visual tool to understand the subsurface of Flanders as it is modelled today.

Geology as a service

This simple visualization of (hydro)geological 3D models helps to understand the subsurface without the need of being an expert in geology. It is a strong educational tool that will contribute to raise awareness concerning our subsurface. Comprehension of the earth beneath our feet is important in facilitating innovation and opportunities in the subsurface. The interaction between surface and subsurface is important in sustainable development and in spatial planning.

The Virtual Borehole is a practical tool preparatory to site investigations by drilling companies and consulting or engineering bureaus. It gives an indication of the (hydro)geological layers to be encountered in a future vertical borehole on a specific location. As the subsurface can be very heterogeneous, especially in the top layers, the tool cannot replace real site investigation. Since 2017 drilling companies are obliged to add qualitative drilling reports to the DOV database. Additionally DOV expands collaboration with other institutes. Over time this will enlarge the amount of observations in the DOV database. These new data will serve in updating the existing 3D models which in turn will lead the Virtual Borehole tool to generate more qualitative results.

Data of the Virtual Borehole are made available as multibeam rasters, ready to be reused in other applications.

Key instruments

The key instruments to build the tool are the Geological 3D Model of Flanders and Brussels-Capital Region - G3Dv2 (Matthijs et al., 2013) of VPO and the results of the hydrogeological HCOV-model (Vancampenhout et al., 2007) of VMM, with units defined by the Hydrogeological Coding of the Subsoil of Flanders (HCOV, acronym in dutch) by Meyus et al. (2000). Lithological information is generalized for each geological unit based on the information of the National

Commission for Stratigraphy on <https://ncs.naturalsciences.be/>. Hydraulic parameters from Lebbe and Vandenbohede (2004) are added to the hydrogeological layers. The actual topography results from the Digital Elevation Model of Flanders II, as published by the Flanders Information Agency.

Use of the results

The models consist of gridded layers, representing the base of the (hydro)geological units with cell sizes of 100 m by 100 m. A (hydro)geological model is a de facto simplified representation of the geological reality (Matthijs et al., 2013). The geological input data for these models (borehole data, seismic data and maps) have been collected for various purposes, were gathered for decades and described and interpreted by different experts. Useful data were selected and interpreted in order to create a consistent base layer for each unit, using suitable geological concepts.

The degree of accuracy is different for each layer of the models and even for each grid cell of the modelled layers. Several issues need to be factored in when estimating the accuracy of the model information: the correctness of the geological interpretation of a borehole, the accuracy of the geographical locations of the data points, the distance to the closest borehole with an interpretation of the height of the base of a specific unit, the accuracy of the used seismic measurements and its interpretation, the data density, the modelling technique and software, the input data and maps, the steepness of the topography and of the layers itself, and the expertise of the modelling team.

Future developments

In the near future, the tool will be made available for mobile devices, so one can visualize the concealed geology in the field. Developments regarding the interaction between the hydrogeological and geological models, both based on the same dataset and with a common modeling process, are well on the way. Future opportunities could be to make vertical sections to visualize the interaction between the layers, to integrate photos of the layers and to display soil information.

References

- Lebbe, L. en A. Vandenbohede, 2004. Ontwikkeling van een lokaal axi-symmetrisch model op basis van de HCOV kartering ter ondersteuning van de adviesverlening voor grondwaterwinningen; Onderzoeksopdracht voor het Ministerie van de Vlaamse Gemeenschap, AMINAL, afdeling Operationeel Waterbeheer.
- Matthijs, J., Lanckacker, T., De Koninck, R., Deckers, J., Lagrou, D., Broothaers, M., 2013. Geologisch 3D lagenmodel van Vlaanderen en het Brussels Hoofdstedelijk Gewest – versie 2, G3Dv2. Studie uitgevoerd door VITO in opdracht van de Vlaamse overheid, Departement Leefmilieu, Natuur en Energie, Afdeling Land en Bodembescherming, Ondergrond, Natuurlijke Rijkdommen, 21p., VITO-rapport 2013/R/ETE/43.
- Meyus Y., Batelaan O., De Smedt F., 2000. Concept Vlaams Grondwater Model (VGM), Technisch concept van het VGM, Deelrapport I: Hydrogeologische Codering van de Ondergrond van Vlaanderen (HCOV). Onderzoeksopdracht voor AMINAL, afdeling Water.
- Vancampenhout P., De Ceukelaire M., Duser M., Declercq P., 2007. Aanpassen van de Hydrogeologische Kartering van de Ondergrond in Vlaanderen (HCOV). Onderzoeksopdracht voor AMINAL, afdeling Water.

Mineralogy and geochemistry of the oolitic iron ore deposit south of Bebesa - northeast Algeria

Hamida DIAB¹, Abdelmadjid CHOUABBI¹, Ernest CHI FRU² & Djamel-Eddine NACER³

¹ *Laboratory of Geodynamics and Natural Resources - LGRN - BADJI Mokhtar University, Annaba, Algeria National Company of Iron Mines SOMIFER, Tebessa, Algeria.*

² *School of Earth and Ocean Sciences, University of Cardiff, United Kingdom.*

³ *Nuclear Research Center Draria -CRND- Algiers, Algeria.*

1. Introduction and geological setting

The Djebel Had Iron Formation (DHIF) is located 60 km southwest of Tebessa and 23 km south-southwest of the Daïra of Chr ea, the administrative division of 1984, locates the DHIF on horseback between the Communes of Telidjene (9 km in the South-East) and that of El Ogla (25 km in the North-West). The DHIF is about 60 km southwest of the phosphate deposit Djebel Onk, Joleaud L. (1932).

The DHIF south of Tebessa in the North-East of Algeria is a distinct stratiform sedimentary iron deposit. Six to eight meters thick, the DHIF forms part of the largest structural units of Algeria, the autochthonous domain of the eastern Saharan Atlas, it is located exactly between two anticlines oriented NE-SW (Atlasic direction): the Bou Kammech anticline and the Kef En Nssour anticline, separated by a syncline of the same orientation (Syncline of Babouche) BRGM and Sn-Repal, (1987), This mining district is part of a vast region, encompassing northeastern Algeria and southwestern Tunisia, where there are many similarities in stratigraphic, lithological, structural and metallogenic characteristics.

2. Results

The iron ore mineralization is in the form of layers of oolitic iron ore and Inter-bedded iron marl within the mid-Eocene gypsiferous marls (middle or upper Lutetian) Vila J. M. (1997).

The iron ore is present in detrital grains of brownish to blackish color, more or less rounded with dimensions varying from a few hundredths of a millimeter to two millimeters. They are oolites and granules of goethite, limonite, hematite and a small amount of magnetite and piemontite, having a smooth outer surface, bound by ferruginous, argilo-ferruginous, carbonate and siliceous cement. On the other hand, this mineralized rock is extremely crumbly.

Chemical analyzes and X-ray diffraction (XRD) analysis of the mineralization of DHIF gave high iron contents: Fet = 53.2%, FeO (OH) = 76.05%, and other elements, such as MnO = 3.69% to 3.47%, Al₂O₃ = 2.83% to 0.87%, SiO₂ = 5.15% to 12.4%, P₂O₅ = 1.5%, TiO₂ = 0.09 %, MgO = 0.47%, CaO = 0.60%, K₂O = 0.02%, Na₂O = 0.22%. These percentages are explained by the nature of the cement, which is essentially siliceous, clayey and calcareous. The low Al₂O₃ and TiO₂ content of the DHIF, suggest a pure chemical origin. Moreover, the presence of the silicate mineral, piemontite and the nobium mineral, pyrochlore, which have a hydrothermal origin, suggest a hydrothermal and/or a chemically leached component of corresponding rocks, as a source of the iron.

The sequential iron extraction data show that the mineralization formed from anoxic water column, which was likely the result of reducing hydrothermal fluids. That is the immediate water column beneath which the sediments formed were ferruginous. Taking into account the extent of

the pyritization of the highly reactive iron basin, the two ratios (FePy / FeHR) and (FeHR / Fe total) (FeHR = highly reactive iron; FeT = total iron; FePy = pyrite iron), in the sediments are an obvious proof of anoxic deposit.

LA-ICP-MS analyzes show that major elements in most bulk samples of oolite ore are generally enriched in: 51V, 59Co, 60Ni, 75As, 66Zn, 65Cu, 85Rb, 90Zr, 93Nb, 137Ba, 178Hf, 53Cr, with a richness in rare earth elements (REE: 89Y, 139La, 140Ce, 146Nd > 100000 ppm, 147Sm, 153Eu, 163Dy > 10000 ppm, and 172Yb, 175Lu > 1000 ppm) associated with goethite.

3. Interpretation and discussion

The results of the analyzes show that there are two sedimentation environments that facilitate the genesis of the mineralization, a deep marine sedimentation medium and a shallow marine environment, The sequential extraction data states that the iron was formed from an anoxic water column under which the sediments formed were anoxic and ferruginous, the sequential extraction data states that iron was formed from a column of anoxic water under which the sediments formed were anoxic and ferruginous. Goethite analyzes by XRD, show the existence of low levels of Al₂O₃ and TiO₂, therefore the derivation by oxidation of silicates is unlikely and the iron must have been precipitated directly in Fe (OH)₃ and gradually oxidized to FeO (OH). This results suggests that goethite is of pure chemical origin "late diagenetic", in addition the presence of silicate minerals, piemontite and niobium, pytochlor, of hydrothermal origin, suggests a hydrothermal component and / or chemically leached rocks corresponding, as a source of iron.

Observations under a microscope converge towards a shallow intertidal deposit medium. The petrographic characteristics of the DHIF, including the symmetrical shape, the presence of broken oolites, and the delicate layer of the oolite cortex exclude the hypothesis of an origin of sediment deposits transported from Further away, oolite fragmentation is probably due to an in situ process due to dehydration (Adeleye, 1975).

Regarding the iron source (s) for the DHIF, we assume that the iron was leached from the underlying rocks, probably affected by hydrothermal mineralization due to a metensomatosis phenomenon probably related to diapirism Rudis (1968).

References

- ADELEYE, D.R. (1975). Derivation of fragmentary oolites and pisolites from dessication cracks. *J. Sediment. Petrol.* 45, 794–798.
- BRGM et SN-REPAL, (1987). La carte des gîtes minéraux au 1/500 000 de l'Algérie "Département Constantine Nord" réalisée et imprimée par l'Institut de Cartographie d'Alger.
- JOLEAUD L. (1932). Les nouvelles découvertes d'ethnologie préhistorique en Afrique orientale. *L'Anthropologie. Paris, t. XLII.*
- RUDIS (1968). Recherche géologiques sur le gisement de fer Ain Babouche, association industrielle et minière, service géologique yougoslave.
- VILA J. M. (1997). La carte géologique d'Ain Télijdjene à l'échelle 1/50.000, avec notice explicative.

The Silurian graptolitic black shales of the Tassili n'Ajjer plateau (Algeria): Thermal maturity evolution and origin-timing of late diagenetic illite

Hocine DJOUDER^{1,2,*}, Tonguç UYSAL³, Julien BOURDET³, Claudio DELLE PIANE³, Andrew TODD³, Peter CROSDALE⁴, Anne-Christine Da Silva¹, Frédéric BOULVAIN¹, Erick RAMANAÏDOU²

¹ *University of Liège, Sedimentary Petrology, B20, Quartier Agora, Allée du Six Août, 12, 4000 Liège, BELGIUM.*

² *CSIRO Mineral Resources Flagship, Australian Resources Research Centre, 26 Dick Perry Ave., Kensington, 6151 Perth, AUSTRALIA.*

³ *CSIRO Energy Flagship, Australian Resources Research Centre, 26 Dick Perry Ave., Kensington, 6151 Perth, AUSTRALIA.*

⁴ *Energy Resources Consulting Pty Ltd, ERC Technologies Pty Ltd, 4/55 Clarence St, Coorparoo, 4151 Queensland, AUSTRALIA.*

* Corresponding author: Hocine.Djouder@doct.uliege.be

Keywords: Silurian, Graptolite-rich black shales, Illite, Graptolite reflectance, Thermal maturity, Tassili n'Ajjer plateau, Algeria

The study area is located in the Tassili n'Ajjer plateau in the south-eastern part of the Algerian Saharan Platform near the Hoggar Massif. Outcrops along the Tassili n'Ajjer plateau offer exceptional exposure of Silurian sections and more specifically the Oued Imihrou 'graptolite-rich black shales' Formation (Djouder et al., 2018). Furthermore, the Tassili n'Ajjer plateau is the southern margin of the largest petroliferous Berkine – Ghadames and Illizi basins (BGI) that provides a critical insight to understand the diagenesis- and thermal maturity-evolution mainly of the lower Silurian shales, which are the major source rock of Paleozoic sourced hydrocarbons in North Africa and the Middle East (MacGregor, 1998; Lüning et al., 2000).

On the basis of sixty-five representative samples from the eastern- and western-Tassili n'Ajjer plateau, the black 'hot' shales, mudstones, siltstones and sandstones in the Oued Imihrou Formation and the Atafaitafa Formation contain high amounts of graptolite organic matter, clay minerals and non-clay minerals such as quartz, muscovite and minor phases such as pyrite, iron oxides and K-feldspar. The clay assemblages show important differences depending on the stratigraphical level, the geographical location and the lithology.

Clay mineralogy characterization and the measurements of illite crystallinity (IC) on the clay fraction (<2µm) were determined from each samples. The identified clay minerals include kaolinite (20–100%), mica-illite (0–20%), and chlorite (0–5%) from the total clay content.

The extreme western Tassili n'Ajjer succession yielded the lowest of all the measured CIS-calibrated IC values, around or less than 0.53 with median of 0.6 $\Delta^{\circ}2\theta$ (n= 22). These lowest values point to abnormally high temperature conditions of the advanced grade diagenesis. Alternatively, these samples may have attained during the illite crystallization the high anchi-metamorphic degree (e.g. Kübler, 1967; Ferreiro Mählmann et al., 2012).

The observations and interpretations reached during this study, both on the inorganic and organic evolution (authigenic clay minerals and graptolites-derived organic matter) are good

evidence of heating events. Thus, influencing later on the hydrocarbon generation/migration, especially near to the Hoggar Massif inherited N-S lineaments mega-shear-zones. The K–Ar illite age data of the extreme western Tassili n’Ajjer suggest fault reactivation at least at two different periods during the Mesozoic (i.e. Middle-Late Triassic and Lias). Our result is the first documentation of the reactivation of Pan-African fault zones in south-eastern Algeria on the basis of illite crystallinity and graptolite reflectance. These reactivation may represent significant transtensional tectonic events coupled with subsequent igneous activity during the opening of the Tethys (Triassic) and the Central Atlantic (Jurassic) oceans in extensive areas of the Saharan Platform (Djouder et al., in prep).

Acknowledgments

H. Djouder gratefully acknowledges the first financial support from the ERASMUS+ programme (2016-2017) and the University of Liège (ARD) for his research stay in Australia.

References

- Djouder, H., Lüning, S., Da Silva, A.C., Abdallah, H. & Boulvain, F., 2018. Silurian Deltaic Progradation, Tassili n’Ajjer Plateau, south-eastern Algeria: Sedimentology, ichnology and sequence stratigraphy. *Journal of African Earth Sciences*, 142, 170-192. <https://lnkd.in/ekzweby>.
- Djouder H., Boulvain, F., Da Silva, A. C., Cornet, P., Lüning, S. & Musial, G., (Oral) 2016. The Siluro – Devonian sedimentary record of the Tassili n’Ajjer (SE Algeria): new insights from sedimentology and stratigraphy. 5th International Geologica Belgica Meeting, GB Mother Earth, 26-29 January 2016, Mons, Belgium. <http://orbi.ulg.ac.be/handle/2268/192622>.
- Djouder, H., Uysal, T., Bourdet, J., Delle Piane, C., Todd, A., Crosdale, P., Da Silva, A.C., Boulvain, F. & Ramanaidou, E. In Prep. The Silurian graptolitic black shales of the Tassili n’Ajjer plateau (Algeria): Thermal maturity evolution and origin-timing of late diagenetic illite.
- Ferreiro Mählmann, R., Bozkaya, Ö., Potel, S., Le Bayon, R., Šegvić, B. & Nieto, F., 2012. The pioneer work of Bernard Kübler and Martin Frey in very low-grade metamorphic terranes: paleo-geothermal potential of variation in Kübler-index/organic matter reflectance correlations. A review, *Swiss Journal of Geosciences*, 105, 153-170.
- Kübler, B., 1967. La cristallinité de l’illite et les zones tout à fait supérieures du métamorphisme: Etages tectoniques, Colloque de Neuchâtel 1966. University of Neuchatel, a la Baconniere, Suisse, 105–121.
- Lüning, S., Craig, J., Loydell, D.K., Štorch, P. & Fitches, B., 2000. Lower Silurian ‘hot shales’ in North Africa and Arabia: regional distribution and depositional model. *Earth-Science Reviews*, 49, 121-200.
- Macgregor, D.S., Moody, R.T.J. & Clark-Lowes, D.D. (Eds.), *Petroleum Geology of North Africa*. Geological Society, London, Special Publication, 132, 155 p.

The demise of the natural building stone industry in Belgian Limburg, a case study on the last underground quarries of Maastricht stone

Michiel DUSAR¹, Ton BREULS², Luck WALSCHOT³ & David LAGROU⁴

¹ *Royal Belgian Institute of Natural Resources – Geological Survey of Belgium; mdusar@naturalsciences.be*

² *Studiegroep Onderaardse Kalksteengroeven (SOK), Kanne; tbreuls@telenet.be*

³ *Stichting Ondergrondse Werken (S.O.W.), Roermond; walschot.luck@telenet.be*

⁴ *VITO, Boeretang 200, 2400 Mol, Belgium; david.lagrou@vito.be*

The Euregio area centred around Maastricht (Mergelland) is built on Cretaceous deposits and has become a reference area for the Maastrichtian chronostratigraphic stage. The Maastricht Formation of latest Maastrichtian age consists of fossiliferous mostly fine grained calcarenites of high porosity, suitable as building stone ‘extremely weak, yet time-resistant’ (Dubelaar et al., 2006). The Maastricht Formation reaches a thickness of up to 50 m and was deposited in a shallowing sea, hence there are subtle differences between the successive members, depending on grain size, degree of compaction and sea-bottom ecosystem variations (Felder & Bosch, 2000). Maastricht stone (locally known as “mergel”) was extracted from ca. 300 underground quarries, between Valkenburg in the east and Heers in the west. Underground quarrying is documented from the late 12th century onwards. Underground quarrying became episodic in the 20th century, with the exception of a single quarry in Sibbe, near Valkenburg, still active today. The quarry history is matched by the use of Maastricht stone in the built environment, which also goes back to the 12th century, exception made for use by the Romans, probably from opencast quarries. Maastricht stone is the dominant building stone from the 13th till 17th century in Belgian Limburg: nearly all churches were constructed in Maastricht stone (Dreesen et al., 2001). In later centuries until the first half of the 20th century Maastricht stone was still widely used, often in combination with bluestone (Meuse limestone). Most Maastricht stone must have been quarried in the Meuse valley south of Maastricht or in the Belgian Limburg part of the Mergelland. However, the quite distinctive Sibbe stone gradually became preponderant from the late 19th century onwards and is also the unique replacement stone in restoration works today.

In this context, it is remarkable that two churches, built or rebuilt in the second half of the 20th century and entirely clad in Maastricht stone around a concrete core deviate from this model and used stones from Belgian Limburg: the St Lutgardis basilica in Tongeren, built in 1953-55 as a Gesamtkunstwerk by architect Jos Ritzen and the hall replacing the central nave of the village church of St.-Huibrechts-Hern reconstructed in 1964-65 by architects Deré & Janssens (Dusar et al., 2017). At the same time two new quarries were opened in Belgian Limburg but had the shortest lifetime of all, the Berg van Haesen in Zichen operated by Herman Haesen from 1948 to 1963 with most productive extraction period in 1951-55, and the Blokberg van Mathus along the Albert canal in Kanne operated by CIBEMARNE from 1948 to 1961 continued by Harrie Vrijens in the succeeding years (Walschot, 2010). These quarries both furnished high-quality building stone for the contemporary monuments but they are distinctive in output and operation method. The Blokberg van Mathus extracted stone following the Sibbe method from the same stratigraphic level

as the Sibbe quarry (Emael member), whereas the Berg van Haesen worked with a patented machine producing blocks of standardised size from the lowest stratigraphic level (combined Valkenburg – Gronsveld member) (Breuls & Walschot, 2006).

Contrary to the practice of the previous centuries these quarries were short-lived, notwithstanding the quality of the product and the efficiency of the extraction. The first reason was the low price, 5 times less than Belgian Bluestone. Mushroom production was more profitable, hence quarrying served to create space for mushroom beds. A second reason was the near-illegality of the quarry operations, not contributing to the stability of the operating enterprises. A third reason was the abandonment of traditional crafts in favour of modernisation of landscape and industry during the years 1960; their low ecological footprint did not count. Finally both quarries fell victim to the cement industry operating at a completely different size of land use and profits.

References

- Breuls, T. & Walschot, L., 2006. De Berg van Haesen te Eben-Emael. Samen met de laatste schachtblok verdween een unieke groeve. *Natuurhistorisch Genootschap in Limburg. SOK Mededelingen* 43, 2-21.
- Dubelaar, C.W., Duser, M., Dreesen, R., Felder, W.M. & Nijland, T.G., 2006. Maastricht limestone: a regionally significant building stone in Belgium and The Netherlands. Extremely weak, yet time-resistant. *Heritage, Weathering and Conservation*, ed. Fort, Alvarez de Buergo, Gomez-Heras & Vazquez-Calvo. Taylor & Francis Group, London, 9-14.
- Dreesen, R., Duser, M. & Doperé, F., 2001. *Atlas Natuursteen in Limburgse monumenten*, Provincie Limburg, 294 p.
- Duser, M., Breuls, T., Walschot, L. & Lagrou, D., 2017. Zoektocht naar de oorsprong van de mergelsteen in het Sint-Lutgardisheiligdom van Tongeren. In: Wido Quist & Hendrik-Jan Tolboom, red. *Natuursteen in Limburg / Natuursteen uit Limburg*. Delftdigitalpress: 123-146.
- Felder, W.M. & Bosch, P.W., 2000. *Geologie van Nederland deel 5: Krijt van Zuid-Limburg*. Nederlands Instituut voor Toegepaste Geowetenschappen TNO, 192 p.
- Walschot, L., 2010. *Over groeve de Keel*. S.O.W. (Stichting Ondergrondse Werken), Roermond, 160 p.

Cation exchange properties of the Boom Clay, a study on bulk rock and fractionated samples

Lander FREDERICKX^{1,2}, Miroslav HONTY¹, Mieke DE CRAEN¹ & Jan ELSSEN²

¹*Belgian Nuclear Research Centre (SCK•CEN), Boeretang 200, 2400 Mol, Belgium*

²*Division Geology, Department of Earth and Environmental Sciences, KU Leuven, Celestijnenlaan 200E, 3001 Leuven, Belgium*

In the context of the geological disposal of radioactive waste, the Boom Clay has been studied intensively for the past decades as a potential host rock. One of the parameters of interest is the cation exchange capacity (CEC), as it is related to the sorption potential of radionuclides to the clay host rock. In the past, a number of studies have been performed to assess the CEC of the Boom Clay (e.g. Baeyens et al., 1985; Maes et al., 2003; Zeelmackers et al., 2015), with a variety of methods being used. A significant variation has been reported on the average CEC in-between these studies (Honty, 2010). The question remains whether these variations can be attributed to methodology, i.e. the complex which was used to perform the cation exchange, or to stratigraphic variations in the Boom Clay.

Our study attempts to settle this ambiguity by (a) collecting a stratigraphically diverse sample set and (b) using a standard methodology complemented by mineralogical data. A sample set covering the entire Boom clay stratigraphy was assembled, after which the CEC was determined. The copper (II) triethylenetetramine method with calcite saturation (Dohrmann & Kaufhold, 2009) was chosen to prevent the dissolution of carbonate minerals. The main sample set was also measured with the cobalt (III) hexamine method with calcite saturation (Dohrmann & Kaufhold, 2009) as a quality control for the results of the former method. The CEC values acquired with both methods are similar, while a significant stratigraphical variation of the CEC is demonstrated. These variations could be linked to variations in the smectite content.

In addition to constraining the CEC of the bulk rock, different size fractions of the Boom Clay were isolated and the CEC of these was determined as well. The CEC of these fractions could then be combined with mineralogical data in an effort to constrain the CEC of the individual clay minerals present in the Boom Clay.

Acknowledgments

The authors would like to thank NIRAS-ONDRAF, the Belgian Agency for Radioactive Waste and Fissile Materials, for providing the clay cores on which the study was executed.

References

- BAEYENS, B., MAES, A., CREMERS, A. & HENRION, P.N. (1985) In situ physico-chemical characterization of boom clay. *Radioactive Waste Management and the Nuclear Fuel Cycle*, 6, 17.
- DOHRMANN, R. & KAUFHOLD, S. (2009): Three new, quick CEC methods for determining the amounts of exchangeable calcium cations in calcareous clays. - *Clays and Clay Minerals*, 57, 338-352.
- HONTY, M. (2010): CEC of the Boom Clay - a review. - SCK•CEN-ER-58, Mol, Belgium, 27 p.

- MAES, A., VANCLUYSEN, J. & BRUGGEMAN, C. (2003) Influence of oxidation on the Cs cation exchange capacity of Boom Clay. Unpublished report of the Catholic University of Leuven, Faculty of Bioscience Engineering, Centre for Surface Chemistry and Catalysis, 16.
- MAZUREK, M., ALT-EPPING, P., GIMI, T., NIKLAUS, W., BATH, A. & GIMMI, T. (2009): Natural tracer profiles across argillaceous formations: The claytrac project.
- ZEELMAEKERS, E., HONTY, M., DERKOWSKI, A., ŚRODOŃ, J., DE CRAEN, M., VANDENBERGHE, N., ADRIAENS, R., UFER, K. & WOUTERS, L. (2015) Qualitative and quantitative mineralogical composition of the Rupelian Boom Clay in Belgium. *Clay Minerals*, 50, 249-272.

How do petrophysical and petrographical properties influence transport parameters? Examples for the Boom Clay and Eigenbilzen Sands

Elke JACOBS^{1,2,3}, Timo SEEMAN¹, Nick JANSSENS², Rudy SWENNEN², Norbert MAES¹, Bernhard KROOSS³, Ralf LITTKE³, Alexandra AMANN-HILDENBRAND³ & Christophe BRUGGEMAN¹

¹ *Belgian Nuclear Research Centre (SCK•CEN), Waste & Disposal Expert Group, Mol, Belgium*

² *KU Leuven, Dept. of Earth & Environmental Sciences, Heverlee, Belgium*

³ *EMR | Energy and Mineral Resources Group, Institute of Geology and Geochemistry of Petroleum and Coal, Aachen, Germany*

Several countries consider clay-rich (argillaceous) rock formations for the safe disposal of high- and intermediate level radioactive waste. In Belgium, the Boom Clay (Oligocene, Rupelian) is under investigation as a potential host rock. It consists of different lithological sub-units with a rhythmic alternation of silty and more clay-rich layers, organic-rich and carbonate-rich layers.

Within a geological repository, the production of gas is unavoidable whereby the dominant process is anaerobic corrosion of metals producing hydrogen. In order to obtain a reliable estimate on the balance between gas generation and gas dissipation, accurate diffusion coefficients for dissolved gases are essential. Therefore, SCK•CEN developed a new technique to measure diffusion coefficients of dissolved gases, by using the double through-diffusion technique (Jacops et al., 2013). From previous work, we know that transport parameters (both hydraulic conductivity and diffusivity) vary with the depth of the formation (Aertsens et al., 2008). Up to now, it is still unclear how variations of petrophysical parameters influence the transport parameters. Samples with a variable clay/silt/sand content were selected, transport parameters were measured and afterwards, a detailed petrophysical study was performed, gathering information on the mineralogical composition, grain size distribution, specific surface area and pore volume distribution. The distribution of the different minerals and pores was investigated by (micro-) computer tomography ((μ -)CT) imaging and light microscopy of thin sections. In the final step, an attempt was made to answer the question “How do petrophysical and petrographical properties influence transport parameters” by coupling transport and petrophysical/petrographical properties.

Hydraulic conductivity and diffusivity (for several gases, such as He, Ne, H₂, Ar, CH₄, Xe, C₂H₆) were measured on several samples of the Boom Clay and overlying Eigenbilzen Sands, and major differences were observed between both formations. Hydraulic conductivity increased by two orders of magnitude, while diffusivity increased by a factor of three in proportion to an increase in quartz content from 25 to 60% (Figure 4).

Large differences in mineralogy and grain size distribution were observed: samples of the Boom Clay are rich in clay minerals and contain a large clay (< 2 μ m) fraction (> 67 wt%), while the samples of the Eigenbilzen Sands are rich in detrital quartz and contain a large (> 43 wt%) sand (> 62 μ m) fraction. Clear correlations were found between the transport parameters and the petrophysical properties, but some open questions remain. A petrographical study revealed that the

differences in composition are also reflected in the micro-structure of the samples. The Boom Clay samples are characterized by a clay-supported matrix with some homogeneously distributed quartz grains; pores are not visible at the resolution of the microphotographs (Figure 5, left). It is likely that the pores are mainly located in the clay matrix and are very small (< 250 nm). These observations are in line with previous studies. In contrast, the quartz-rich samples of the Eigenbilzen Sands show a heterogeneous distribution of clay phases and interparticle porosity adjacent to the quartz grains. Porosity is still partly located in the clay matrix, but there is also an important fraction of larger pores (> 250 nm), which allows enhanced transport of dissolved gases and water (Figure 5, right).

Transport parameters and petrophysical properties are clearly correlated, which is directly reflected in the micro-structure. The petrographical study indicated that not only the composition is important, but also the distribution of the mineral phases as this influences the pore volume distribution. The latter will largely influence the transport parameters, and is considered to be the key factor.

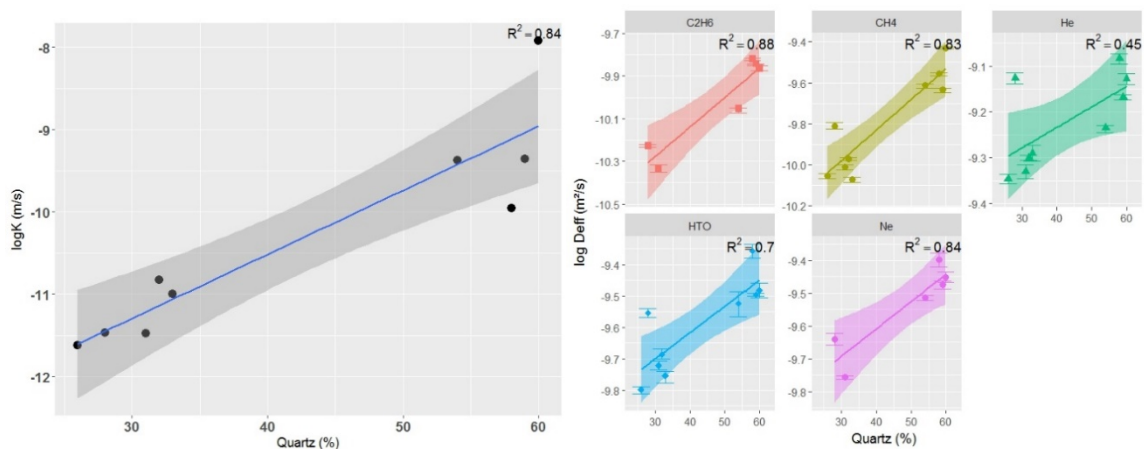


Figure 1. Hydraulic conductivity (left, expressed as $\log K$ (m/s)) and diffusivity (right, expressed as $\log D_{\text{eff}}$ (m^2/s)) increase with quartz content.

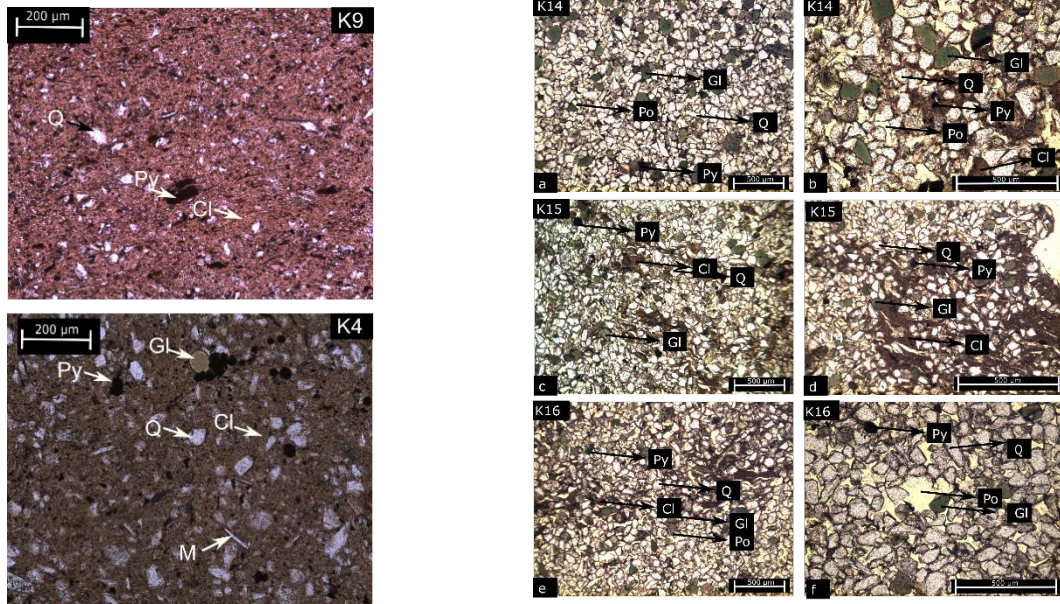


Figure 2. Microphotographs of thin sections of the Boom Clay (left) and Eigenbilzen Sands (right), showing clear differences in the composition and organization of the mineral phases. Py = pyrite, Po = pore, Q = quartz, Gl = glauconite, Cl = clay, M = mica.

References

- Aertsens, M., Van Gompel, M., De Cannière, P., Maes, N., Dierckx, A., 2008. Vertical distribution of transport parameters in Boom Clay in the Mol-1 borehole (Mol, Belgium). *Physics and Chemistry of the Earth, Parts A/B/C*, 33, Supplement 1: S61-S66.
- Jacops, E., Volckaert, G., Maes, N., Weetjens, E., Govaerts, J., 2013. Determination of gas diffusion coefficients in saturated porous media: He and CH₄ diffusion in Boom Clay. *Applied Clay Science*, 83-84(0): 217-223.

W-Sn vein-type mineralisation in the Iberian Metallogenic Province: a kinematic relationship with oroclinal buckling

Dominique JACQUES¹, Philippe MUCHEZ¹, Manuel SINTUBIN¹

¹*Geodynamics and Geofluids Research Group, Department of Earth and Environmental Sciences, KU Leuven, Celestijnenlaan 200E, B-3001 Leuven, Belgium*

1. Introduction

Granite-related W-Sn deposits typically occur in close association with highly specialised S-type granites, which are especially numerous in late- to post-orogenic settings (Cerný et al., 2005). The formation of W-Sn hydrothermal ore deposits has been extensively studied from a geochemical and mineralogical viewpoint. Few studies, however, tend to focus on the geometry and kinematics of the deposits and their overall structural context (e.g. Romer & Kroner, 2016). The latter is especially relevant for W-Sn vein-type deposits, whose geometry is highly dependent on array of brittle-ductile deformation processes. The emplacement of W-Sn bearing vein systems is often stated to hinge on a granite-controlled or post-orogenic extensional stress regime (Jackson et al., 1989; Liu et al., 2014). However, detailed structural analyses to support such a kinematic hypothesis and highlight the relationship with the orogenic framework are typically lacking.

To fill this hiatus, we have performed an integrated structural analysis of different W-Sn vein-type deposits within the southern Central Iberian Zone, part of the Iberian Metallogenic Province. These deposits consist of (i) hydrothermal quartz vein systems (e.g. Panasqueira, Rio de Frades, Queiriga, Argemela) and (ii) late-magmatic aplite-pegmatites (e.g. Lagares). Based on an integrated structural methodology, we formulate a metallotectonic model for the structural emplacement of the W-Sn mineralisation, highlighting the relationship between the regionally observed vein and fracture geometry, the Variscan deformation structure and the late- to post-orogenic geodynamic context.

2. Structure of W-Sn vein systems

Structurally, the studied vein-type deposits can broadly be subdivided in two groups. The first and most significant group consists of subhorizontal quartz and aplite-pegmatite vein systems that are exploiting a regional cross-fold joint system within the metasedimentary host rock (Jacques et al., 2018a, 2018b). This cross-fold joint system is oriented perpendicular to the late-Variscan F_3 fold generation, which is characterised by subvertical fold axes. Subsequent veining reactivated the cross-fold joints through hydraulic fracturing under low differential stresses. The consistent perpendicular orientation of the veins relative to the non-cylindrical F_3 fold axes indicates that this reactivation did not occur during far-field horizontal contraction. Instead, the vein geometry is dictated by a local stress state with the minimum principal stress consistently subparallel to the F_3 fold axis, i.e. in a similar stress regime as the cross-fold joints.

A second but minor group consists of vein systems whose geometry is controlled by a local stress regime induced by granite emplacement and expansion of the underlying magma body.

Granite emplacement was coupled to doming and a local extensional stress regime within the overlying metasedimentary host rock. This stress regime is reflected in (i) the occurrence of concentric, granite-hosted quartz veins, and (ii) subvertical veins hosted by the neighbouring metasedimentary host rock (Jacques et al., 2018a).

3. Kinematic relationship with oroclinal buckling

Despite a wealth of studies, the relationship between oroclinal buckling (ca. 315-297Ma) with the late-Variscan folding stages is still debated. This study demonstrated the existence of two regional fold generations with subvertical fold axes: (i) localised, isoclinal F_1 folds, and (ii) F_3 folds that constrain the structural outline of the major folds (Jacques et al., 2018a). Temporal and kinematic considerations indicate that the F_3 fold generation developed simultaneously with oroclinal buckling. Firstly, the incorporation of Stephanian C metasediments within the F_3 Porto-Sátão syncline demonstrates that D_3 deformation was continuous till at least the early Permian, i.e. 300Ma. Secondly, F_3 folding is associated with dextral, pure-shear dominated transpression, i.e. the expected deformation style within the outer arc and southern limb of the Cantabrian orocline (cf. Gutiérrez-Alonso et al., 2004; Shaw et al., 2015).

To conclude, we can thus state that W-Sn mineralisation and oroclinal buckling appear to not only share their late-Variscan timing, but could also be considered as kinematically related processes.

References

- Cerný, P., Blevin, P.L., Cuney, M. & London, D., 2005. Granite-Related Ore Deposits. *Economic Geology*, 100th Anniversary Volume, 337–370.
- Gutiérrez-Alonso, G., Fernández-Suárez, J. & Weil, A.B., 2004. Orocline triggered lithospheric delamination. In Sussman, A.J., Weil & A.B. (eds), *Orogenic Curvature: Integrating Paleomagnetic and Structural Analyses*. Geological Society of America, Special Papers, 383, 121–131.
- Jackson, N.J., Willis-Richards, J., Manning, D.A.C. & Sams, M.S., 1989. Evolution of the Cornubian ore field, Southwest England; Part II, Mineral deposits and ore-forming processes. *Economic Geology*, 84, 1101–1133.
- Jacques, D., Muechez, P. & Sintubin, M., 2018a. Superimposed folding and W-Sn vein-type mineralisation in the Central Iberian Zone associated with late-Variscan oroclinal buckling: A structural analysis from the Regoufe area (Portugal). *Tectonophysics*, 742–743, 66–83.
- Jacques, D., Vieira, R., Muechez, P. & Sintubin, M., 2018b. Transpressional folding and associated cross-fold jointing controlling the geometry of post-orogenic vein-type W-Sn mineralization: examples from Minas da Panasqueira, Portugal. *Mineralium Deposita*, 53, 171–194.
- Liu, X., Xing, H. & Zhang, D., 2014. Fluid focusing and its link to vertical morphological zonation at the Dajishan vein-type tungsten deposit, South China. *Ore Geology Reviews*, 62, 245–258.
- Romer, R.L. & Kroner, U., 2016. Phanerozoic tin and tungsten mineralization -Tectonic controls on the distribution of enriched protoliths and heat sources for crustal melting. *Gondwana Research*, 31, 60–95.
- Shaw, J., Johnston, S.T. & Gutiérrez-Alonso, G., 2015. Orocline formation at the core of Pangea: A structural study of the Cantabrian orocline, NW Iberian Massif. *Lithosphere*, 7, 653–661.

Clay resources in the Zeramdine basin (NE Tunisia): Physico-chemical characterization and industrial applications

Imen MAALLA¹, Slim BOUSSEN^{1,2}, Nathalie FAGEL³ & Mohamed ESSGHAIER GAIED^{1,4}

¹ *Geosciences, Mineral Resources, Energies and Environment Laboratory GRM2E, University Of Tunis El Manar Faculty Of Sciences Of Tunis, Department Of Geology, University Campus, 2092 Tunis, Tunisia. imenmaala@gmail.com*

² *National Office of Mines, Energy Street No. 24 Z.I. Charguia I, Tunis, Tunisia.*

³ *UR Clay, Geochemistry and Sediment Environment (AGES), Department of Geology, Agora Quarter, Building B18, Allée du 6 Aout, 14, Sart-Tilman, University of Liège, B-4000, Belgium.*

⁴ *Higher Institute of Fine Arts in Sousse, Station Square - 4000 Sousse, Tunis.*

The study area is located in the eastern side of Tunisia (Sahel). It occupies a position of foreland. It is bordered to the North by the overlap of Zaghouan and the Northern Atlas of the Tunisian ridge, to the South by the fault of Gafsa, in the East by the continental shelf of the Pelagian Sea, in the West by the North-South axis. The platform of the Sahel constitutes a vast sedimentary basin named "Zeramedine Basin" (Fig1). The latter shows outcrops of Upper Miocene clays (Kamoun, 1987). Dozens of quarries exploit the clays and sands which constitute the raw materials of red products and pottery. The multidisciplinary study aims to investigate the potential of illite-kaolinite clays, Serravallian-Tortonian in age, of Zeramdine region (Bédir, 1988) and to estimate their uses as ceramics.

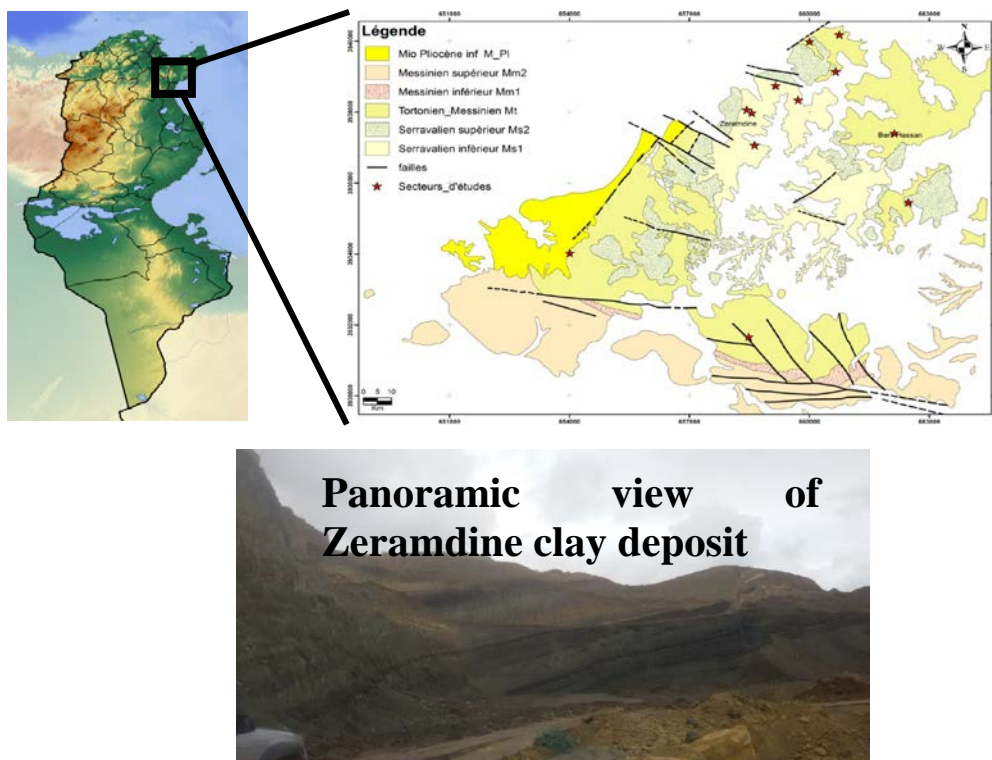


Figure 1. Extract of the map 1/50 000 of Jemmel and Kerker and location of the study area.

This study covers the geological maps 1/50 000 Jemmel (n° 65) and Kerker (n°73). Samples are collected from the region of Zeramdine according to facies variations. The section at the Zeramdine basin (Fig. 2) shows a thick series of brownish black laminated clay with thin intercalations of sandy clays and lignite joints, above this predominantly clay mass.

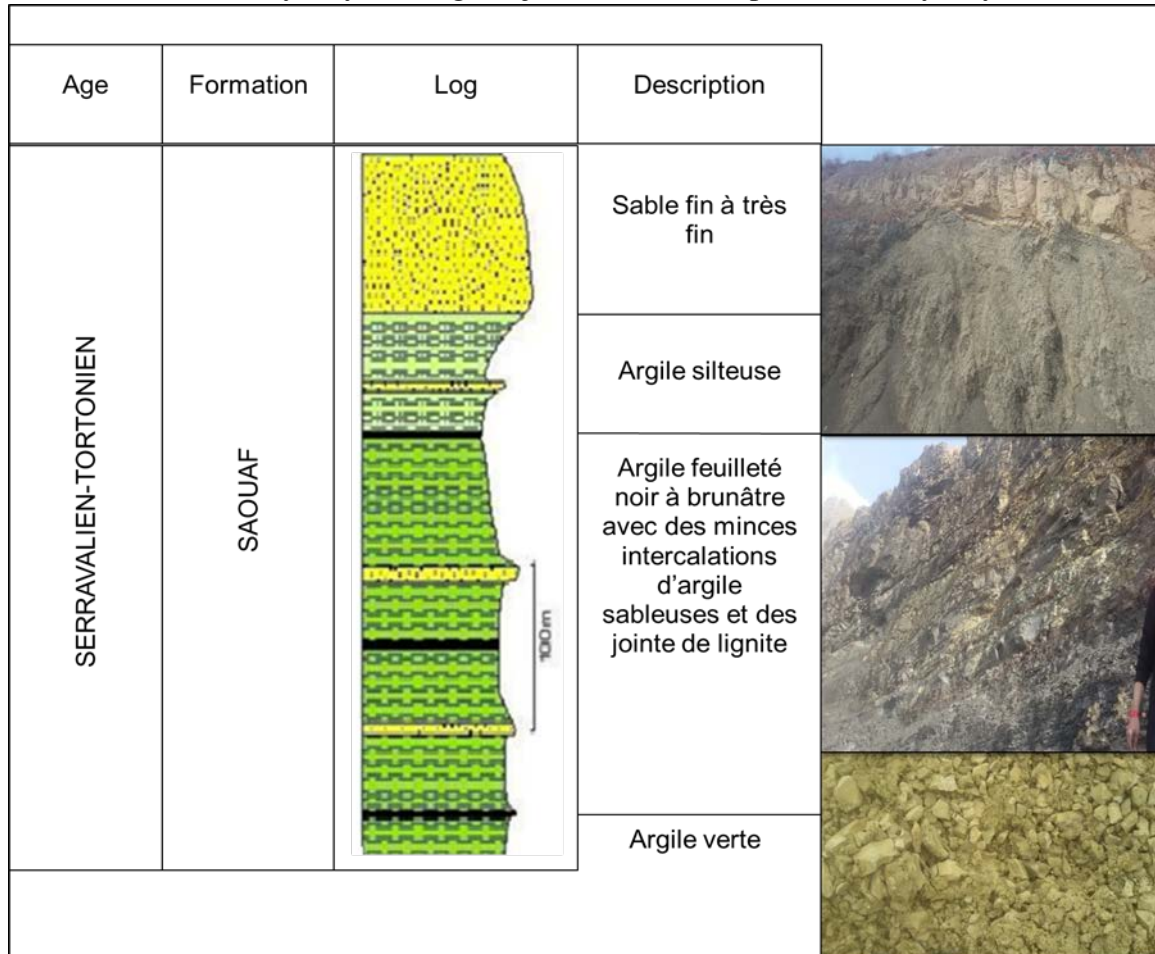


Figure 2. Lithological description of Zeramdine Basin.

The mineralogical study by X-ray diffraction of the total rock and the oriented plates shows that these clays consist essentially of illite, kaolinite and variable percentages in mixed-layers clays. The associated minerals are quartz and calcite. The chemical analysis shows a relatively high content of silica (48-57.5%) and alumina (12-22%), consistent with the kaolinite abundance deduced by XRD. The low contents of CaO (<2%) and iron oxide (<5%) indicate that these clays perfectly meet the required ceramic standards.

The reserves of geological clays identified in the Zeramdine field are very important. From a practical point of view, the various technological tests of these clays show that these characteristics are favorable to red products, faience and manufacturing tiles.

References

- Bédir, M. (1988). Géodynamique des bassins sédimentaires du Sahel de Mahdia (Tunisie orientale) de l'Aptien à l'actuel. Sismo-stratigraphie, sismo-tectonique et structurale.
- Kammoun, Y. (1981). Etude néotectonique dans la région de Monastir Mahdia (Tunisie orientale). Thèse Doc 3ème cycle, FST, 175 p.

Metallogeny of the Kundelungu Group in the Lufilian arc (Congo Copperbelt): insight of fluid evolution and its geodynamic context

Pascal MAMBWE^{1,2}, Stijn DEWAELE^{3,4}, Louis KIPATA² & Philippe MUCHEZ¹

¹*KU Leuven, Department of Earth and Environmental Sciences, Celestijnenlaan 200E, B-3001 Leuven, Belgium*

²*University of Lubumbashi, Department of Geology, Lubumbashi, BP 1825, DR of Congo*

³*Royal Museum for Central Africa, Department of Geology and Mineralogy, Leuvensesteenweg 13B-3080 Tervuren, Belgium*

⁴*Ghent University, Department of Geology, Krijgslaan 281 S8, B-9000 Gent, Belgium*

Corresponding author: p.mambwe@sciencesunilu.ac.cd

Key words: Cu mineralization, Kundelungu Group, Lufilian arc, Katangan Supergroup

The Neoproterozoic Katangan Supergroup in the Central African Copperbelt hosts Cu-Co and vein-type Cu-Ag-Zn-Pb deposits. The Roan Group contains stratiform and stratabound Cu-Co deposits, while stratiform and vein-type deposits can be found in both the Nguba and Kundelungu Groups (Haest and Muchez, 2011). Several studies have highlighted the fluid evolution in the Katanga Copperbelt. In the Roan Group along the Lufilian arc, two main hypogene Cu-Co sulfide phases precipitated from hydrothermal fluids during early diagenesis and during late diagenetic to synorogenic stages (see El Desouky et al., 2009). In the Nguba Group, post-orogenic hydrothermal fluids have been recognized at Kipushi Cu-Pb-Zn (Heijlen et al., 2008). Microthermometric data of fluid inclusions from deposits in the Katangan foreland characterize the fluids responsible for syn- to- post orogenic mineralization in the Nguba and Kundelungu Groups (El Desouky et al., 2008a, b; Haest et al., 2009).

Copper mineralization is also found in different formations of the Kundelungu Group along the Lufilian arc, such as at Diyenge in the Kyandamu and Lusele formations, Kyaundji in the Lusele Formation, Shangoluwe in the Kanianga and Mongwe formations, Kamanyingo in the Kiubo and Sampwe formations. Presently, only the Shangoluwe Cu deposit located in the Kambove region has been investigated in detail (Mambwe et al., 2017a). The Kundelungu Group in the Lufilian arc has been poorly studied compared to the foreland and the metallogeny and the evolution of the hydrothermal fluids in these deposits is largely unknown. The aim of this newly started research project (on going in the Geodynamic and Geofluids Research Group at the KULeuven) provides multiple aspects of investigation: 1) define the geodynamic context of the mineralization based on the brittle structural deformation model of Kipata et al. (2013); 2) specify the fluid flow context with reference to the foreland (Haest et al., 2009; El Desouky et al., 2008a, b); 3) determine the petrography and mineral paragenesis; 4) define the nature and origin of the fluids in the Kundelungu Group; and 5) establish a possible correlation with the fluid migration through both Roan and Nguba groups (Dewaele et al., 2006; Mambwe et al., 2017b). The results of this research

will allow to characterize the fluid evolution and to propose a genetic model. Moreover, it can contribute to the exploration for new copper deposit in the African Copperbelt.

References

- Dewaele, S., Muchez, Ph., Vets, J., Fernandez-Alonzo, M. & Tack, L., 2006. Multiphase origin of the Cu-Co deposits in the western portion of the Lufilian fold-and-thrust belt, Katanga (Democratic Republic of Congo). *Journal of African Earth Sciences*, 46, 455-469.
- El Desouky, H., Muchez, Ph., Boutwood, A. & Tyler, R., 2008a. Postorogenic origin of the stratiform Cu mineralization at Lufukwe, Lufilian Foreland, Democratic Republic of Congo. *Economic Geology*, 103, 555-582.
- El Desouky, H.A., Muchez, Ph. & Tyler, R., 2008b. The sandstone-hosted stratiform copper mineralization at Mwitapile and its relation to the mineralization at Lufukwe, Lufilian foreland, Democratic Republic Congo. *Ore Geology Reviews*, 34, 561-579.
- El Desouky, H.A., Muchez, Ph. & Cailteux, J., 2009. Two Cu-Co sulfide phases and contrasting fluid systems in the Katanga Copperbelt, Democratic Republic of Congo. *Ore Geology Reviews*, 36, 315-332.
- Haest, M. & Muchez, Ph., 2011. Stratiform and vein-type deposits in the Pan-African Orogen in Central and Southern Africa: Evidence for multiphase mineralization. *Geologica Belgica*, 14, 23-44.
- Haest, M., Muchez, Ph., Petit, J.C.J. & Vanhaecke, F., 2009. Cu isotope ratio variations in the Dikulushi Cu-Ag deposit, DRC: Of primary origin or induced by supergene reworking? *Economic Geology*, 104, 1055-1064.
- Heijlen, W., Banks, D.A., Muchez, Ph., Stensgard, B.O.M. & Yardley, B.W.Y., 2008. The nature of mineralizing fluids of the Kipushi Zn-Cu deposit, Katanga, Democratic Republic of Congo: Quantitative fluid inclusion analysis using laser ablation ICP-MS and bulk crush-leach methods. *Economic Geology*, 103, 1459-1482.
- Kipata, M.L., Delvaux, D., Sebagenzi, M.N., Cailteux, J. & Sintubin, M., 2013. Brittle and stress field evolution in the Pan-African Lufilian and its foreland (Katanga, DRC): from orogenic compression to extensional collapse, transpressional inversion and transition to rifting: *Geologica Belgica*, 16, 001-017.
- Mambwe, P., Kipata, M.L., Chabu, M., Muchez, Ph., Lubala, R. T., Jébrak, M. & Delvaux, D., 2017a. Sedimentology of the Shangoluwe breccias and timing of the Cu mineralization (Katanga Supergroup, D. R. of Congo). *Journal of African Earth Sciences*, 132, 1-15.
- Mambwe, P., Milan, L., Batumike, J., Lavoie, S., Jébrak, M., Kipata, L., Chabu, M., Mulongo, S., Lubala, R.T., Delvaux, D. & Muchez, Ph., 2017b. Lithology, petrography and Cu mineralisation of the Neoproterozoic glacial Mwale Formation at the Shanika syncline (Tenke Fungurume, Congo Copperbelt; Democratic Republic of Congo): *Journal of African Earth Sciences*, 129, 898-909.

Origin of Cu mineralization in sedimentary breccias (Shangoluwe deposit, Democratic Republic of Congo): brittle tectonics and fluid flow related to the late to post-Lufilian orogeny

Pascal MAMBWE^{1,2}, Damien DELVAUX³, Louis KIPATA², Michel JEBRAK⁵, Alphonse KAPUTO⁴ & Philippe MUCHEZ¹

¹*KU Leuven, Department of Earth and Environmental Sciences, Celestijnenlaan 200E, B-3001 Leuven, Belgium*

²*University of Lubumbashi, Department of Geology, Lubumbashi, BP 1825, Democratic Republic of Congo*

³*Royal Museum for Central Africa, Department of Earth Sciences, Leuvensesteenweg 13B-3080 Tervuren, Belgium*

⁴*Gécamines, Département Géologique, Likasi, D.R. of Congo.*

⁵*Department of Earth Science and Atmosphere, University of Quebec, Montreal, Canada*

Corresponding author: p.mambwe@sciencesunilu.ac.cd

Key words: sediment-hosted Cu mineralization, fluid inclusion microthermometry, brittle tectonics, Lufilian arc, Katangan Supergroup

The Neoproterozoic Shangoluwe ore deposit in the Kambove region (Lufilian Arc, Katanga Region, R.D. Congo) is a particular Cu vein-type deposit situated in the Kundelungu Group of the Katangan Supergroup. This deposit consists of a succession of sedimentary breccias, with ferruginous and dolomitic breccias interbedded in both the Kanianga and the Mongwe formations, overlain by younger siliceous breccias. The sedimentary origin of these breccias is constrained on the basis of fault kinematic analysis (Kipata et al., 2013), quantitative analysis (see methodology of Jébrak, 1997, Bérubé & Jébrak, 1999) and a sedimentological investigation (Mambwe et al., 2017). In contrast, the main Cu-Co mineralization in the Katangan Supergroup along the Lufilian arc are hosted in the Roan Group (Cailteux et al., 2005; Muchez et al., 2008, Kampunzu et al., 2009).

Two hypogene phases of mineralization are described at the Shangoluwe Cu ore deposit. Phase I consists of disseminated diagenetic pyrite in the breccia clasts and interlayered beds (e.g. shale, siltstone, dolomite) and in the surrounding rocks of both the Kanianga and Mongwe formations (e.g. shale, sandy dolomitic shale, dolomitic shale and dolomite). Phase II is characterized by hypogene ore (pyrite, chalcopyrite, bornite and occasionally galena and sphalerite) which precipitated during later to post-orogenic stages (Mambwe, 2017). Veins with the ore minerals were studied by fluid inclusion microthermometry which evidence two main hydrothermal fluid phases. A first system of quartz – pyrite- chalcopyrite- malachite vein are related to the brittle tectonic stage 5 as defined by Kipata et al. (2013) which corresponds to a late orogenic (Lufilian) extensional collapse. The temperature of homogenization varies between 102° and 246° C and the salinity between 27.4 and 33 eq. wt.% NaCl. A second system consists of dolomite-pyrite-chalcopyrite veins related to the brittle stage 6 of Kipata et al. (2013) which corresponds to a post-

Lufilian transpressional inversion. It is coeval with Cu sulfides which precipitated in the both the fracture and the matrix of the sedimentary breccias. These Cu sulfides are occasionally associated to minor galena and sphalerite. Their temperature of homogenization ranges between 28 and 76°C and their salinity between 4.49 –22.38 eq. wt.% NaCl. The Cu sulfides are replacing or associated with azurite, chrysocola, cuprite, malachite, chalcocite, covellite, shattulite, native copper, goethite and hematite. The poorly sorted clasts, in situ fracturing of the clasts, faulting and folding favored trapping of the fluid in the sedimentary breccias. We conclude that the evolution of the Cu-mineralizing fluid in the Kundelungu Group at Shangoluwe along the Lufilian arc is controlled by its lithology and deformation.

References

- Bérubé, D. & Jébrak, M., 1999. High precision boundary fractal analysis for shape characterization. *Computers and Geosciences*, 5, 1059-1071.
- Cailteux, J.L.H., Kampunzu A.B., Lerouge, C., Kaputo, A.K., Milesi, J.P., 2005. Genesis of sediment-hosted stratiform copper-cobalt deposits, Central African Copperbelt. *Journal of African Earth Sciences* 42, 134-158.
- Jébrak, M., 1997. Hydrothermal breccia in vein-type ore deposits: A review of the mechanisms, morphology and size distribution. *Ore Geology Reviews*, 12,111-134.
- Kampunzu, A, B., Cailteux, J.H., Kamona, A.F., Intiomale, M.M. & Melcher, F., 2009, Sediment-hosted Zn-Pb-Cu deposit in the Central African Copperbelt: *Ore Geology Reviews*, 35, 263-297.
- Kipata, M.L., Delvaux, D., Sebagenzi, M.N., Cailteux, J., Sintubin, M., 2013. Brittle and stress field evolution in the Pan-African Lufilian and its foreland (Katanga, DRC): from orogenic compression to extensional collapse, transpressional inversion and transition to rifting. *Geologica Belgica* 16, 1-17.
- Mambwe, M.P., 2017. Sédimentologie et minéralisation cuprifère associée au Groupe du Kundelungu. Cas du gisement de Shangoluwe (Kambove, RDC). Inclusions fluides et contrôle tectonique. Unpublished Master Thesis, University of Lubumbashi, DRC, 144p.
- Mambwe, P., Kipata, M.L., Chabu, M., Muchez, Ph., Lubala, R. T., Jébrak, M. & Delvaux, D., 2017. Sedimentology of the Shangoluwe breccias and timing of the Cu mineralization (Katanga Supergroup, D. R. of Congo). *Journal of African Earth Sciences*, 132, 1-15.
- Muchez, Ph., Vanderhaeghen, P., El Desouky, H., Schneider, J., Boyce, A., Dewaele, S., Cailteux, J., 2008. Anhydrite pseudomorphs and origin of stratiform Cu-Co ores in the Katanga Copperbelt (Democratic Republic of Congo). *Mineralium Deposita* 43, 575-589.

Belgian clay geo-resources and their use for making compressed earth bricks

Lavie A. MANGO ITULAMYA¹, Frédéric COLLIN² & Nathalie FAGEL¹

¹ *AGEs - Argiles, Géochimie et Environnement sédimentaires, University of Liège, Belgium*

² *Géotechnique, Département ARGENCO, University of Liège, Belgium*

This study has two objectives: contribute to the knowledge of Belgian clays and evaluate their use for manufacturing of compressed earth block (CEBs). Nineteen Belgian clays formations were sampled in 56 sites and 135 samples were collected and analyzed. The analyzes focused on the determination of particle size, plasticity, nature and mineralogy, the main characteristics for assessing the suitability of the sediment to make CEBs. These analyzes allow to classify the sampled formations in three categories: clays that can be used unchanged to make CEBs (2 formulations), clays that are suitable for the manufacture of CEBs but require modification (13 formulations) and clays that are unsuitable to the manufacture of CEBs (4 formulations).

1. Introduction

Raw earth designate the soil used in construction with less transformations. Due to its ecological, economic and physical properties, it faces a renewed interest. This is reflected in Belgium by the appearance of local producers of raw earth materials. The objective of this research is the valorization of Belgian clay deposits for the manufacturing of raw earth bricks. Clays will be sampled, characterized and classified according to their ability for the manufacture of raw earth bricks, according to the technique of Compressed Earth Blocks (CEBs).

In several regions of Belgium, there are important clay formations, used for the manufacture of bricks, tiles, pottery, and also in the cement industry. The main clay deposits exploited in our country are Scheldt clays, Boom clays, Campine clays, Clays of Andenne and Condruz, Clays of Entre Sambre-et-Meuse, Ypresian clays, Landen clays, Herve clays, Aachen clays, Ethe clays, Wealdian clays, cover and alluvial silt and altered shale (Gulinck, 1958). These clays were the essential raw material used for this study.

2. Methodology

Field missions consisted in prospecting for clay deposits in 56 sites (Fig. 1), and representative sampling. The sampling criterion was based on the variability of materials and the representativeness of facies. Exploration, outcrop description, mapping of the deposits were achieved using classical prospecting surveys (manual auger borings, sampling on the forehead). A total of 135 samples were taken. Laboratory analyses covered the characterization of clay material sample during the prospecting campaign. The particle size of the samples was carried out by both sieving and wet laser granulometry. The plasticity or Atterberg limits was realized using the Casagrande dome. The nature of raw earth was determined by the combination of the values from the particle size, plasticity and methylene blue values. All these tests were done in the Geotechnology Laboratory and Argiles, Géochimie et Environnements sédimentaires, Laboratory of University of Liège.

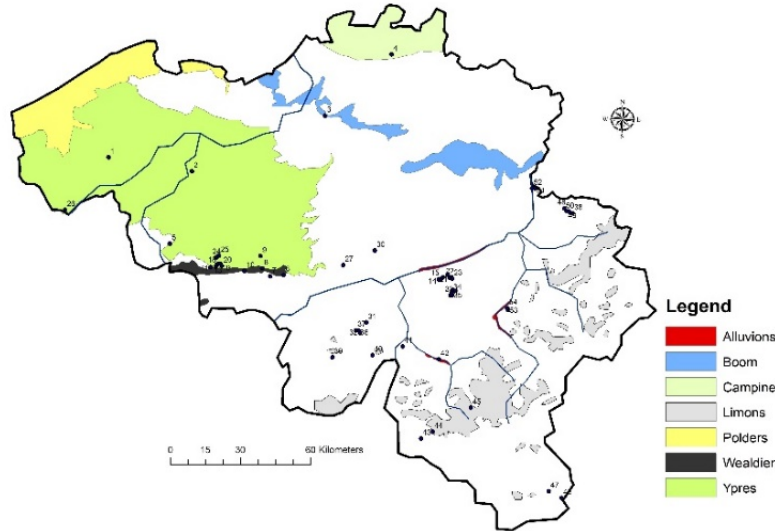


Figure 1. Location of sampled sites on the map of Belgian clay formations.

3. Results

The results allow to classify the studied raw clays in three categories (Table 1):

Categories	Formations	Description
A	Campine clays: Turnhout Member); Paleoalterations clays of Famennian schists	Acceptable material, good particle size distribution and good consistency
B	Scheldt clays; Campine clays: Rijkevorsel Member; Clays of Andenne and Condroz; Clays of Entre Sambre-et-Meuse; Boom Clays: Putte Member; Ypresian clays: Tielt Formation; Ypresian clays: Kortrijk Formation; Ypresian clays: Carnières Formation; Landen clays; Herve clays; Aachen clays; Wealdians clays; Ethe clays	Acceptable material but containing too much fine particles and requiring an addition of coarse particles (sand, gravel)
C	Silt-Loam; Paleoalterations clays of Devonian schists and sandstone; Paleoalterations clays of Ordovician schists; Ardennes kaolin	Clays with low consistency and having too much fines

Table 1. Classification of raw clay formations. A: clays that can be used unchanged to make CEBs; B: clays that are suitable for the manufacture of CEBs but require modification; C: clays that are unsuitable to the manufacture of CEBs (C category).

4. Conclusion and perspective

Here 19 clay formations have been characterized on the basis of particle size, plasticity, nature and mineralogy in order to evaluate their use for manufacture of compressed earth blocks (CEBs). The raw clay formations were classified in 3 categories according to their convenience to make CEBs: 4 of them are not suitable for making CEBs, 13 are acceptable, but require modification, and 2 can be used without modification. Larger amounts (300 kg) of clay were collected at 5 sites. The next

step will be the fabrication and characterization of Compressed Earth Bricks (CEBs) which will be characterized by the mechanical and hygrometric properties.

Reference

Gulinck M., 1958. Atlas de Belgique. Planche 39. Carrières. Bruxelles : Académie royale de Belgique, Comité national de Géographie, Commission de l'Atlas national.

The Q16-Maas field as geological buffer in a CCUS network

Bruno MEYVIS¹, Mariëlle KOENEN², Kris PIESSENS¹, Kris WELKENHUYSEN¹

¹ *Royal Belgian Institute of Natural Sciences, Geological Survey of Belgium, Jennerstraat 13, B-1000 Brussels, Belgium*

² *TNO, Princetonlaan 6, 3584 CB Utrecht, the Netherlands*

1. Introduction

The worldwide increased concern on climate change and related greenhouse gas emissions results in climate policies to reduce these emissions. In Europe, the industrial clusters surrounding the ports of Antwerp and Rotterdam form a hotspot of CO₂ emissions, which therefore aim to decrease their environmental impact (Port of Antwerp, 2018; Ros et al., 2014). CO₂ capture and storage (CCS) is a viable and necessary means of reducing emissions from large stationary sources; however, building a business case remains challenging. CO₂ capture and use (CCU) projects may provide the economic answer, but the limited scale generally inhibits deep emission cuts.

A CO₂ use network is currently operational in the Rotterdam harbour area by capturing CO₂ from two bio-ethanol plants (Shell Pernis and Alco), which is transported via pipeline (OCAP) towards greenhouses for boosting crop growth. These greenhouses have a seasonal variation in heat (high in winter) and CO₂ demand (high in summer). Several sources of both commodities are available: combined heat and power (CHP) installations produce both, but are not optimal because of the seasonal changes. Heat can also be produced with a regular boiler, or with geothermal energy. CO₂ can be supplied via the existing OCAP pipeline, or external CO₂ can be supplied via truck. The OCAP network currently supplies about 400 ktCO₂/y to the greenhouses but a discrepancy exists between supply and seasonal demand (Mikunda et al., 2015). Moreover, interruptions in supply force greenhouse farmers to buy (expensive) external CO₂ or fire up boilers or CHP's during summer to ensure plant growth.

2. Q16-Maas

The objective of the EU H2020 ENOS project (Enabling Onshore CO₂ Storage in Europe) is to build confidence on the onshore application of CCS technologies and the demonstration of the economic potential and societal relevance through several pilot cases. One of the pilot cases targets the currently producing Q16-Maas condensate field just offshore the Rotterdam harbour. The Q16-Maas reservoir consists of the Southwest dipping Solling Sandstone Member of the Upper Germanic Trias Group and Hardeggen Formation of the Main Buntsandstein Subgroup and is limited to the Northeast by faults. The caprock consists of the Solling Claystone Member and overlying clayey formations of the Upper Germanic Trias Group (Oranje-Nassau Energie, 2013). Production started in 2014 and was reduced in 2016 after water breakthrough (Oranje-Nassau Energie, 2018). A new side-track of the production well into the up-dip reservoir attic extracts the last hydrocarbons from the reservoir.

A concept for seasonal storage in the Q16-Maas field was developed to increase the efficiency and capacity of the OCAP network and to decrease CO₂ emissions by the greenhouses. The injection of CO₂ in winter and production in summer potentially solves the issue of the production and demand mismatch and provides security of supply. The ENOS project investigates the technical and economic viability of integrating such a geological buffer within the existing CO₂ network. To determine the applicability and uncertainties of the reservoir as a geological buffer, the effect of pressure changes due to alternating CO₂ injection and back-production, concentration of impurities, and changes of the reservoir properties due to CO₂ reactivity will be modelled. Moreover, the economic viability of such a geological CO₂ buffer will be investigated using the techno-economic simulator PSS (Fig 1, Piessens et al., 2017).

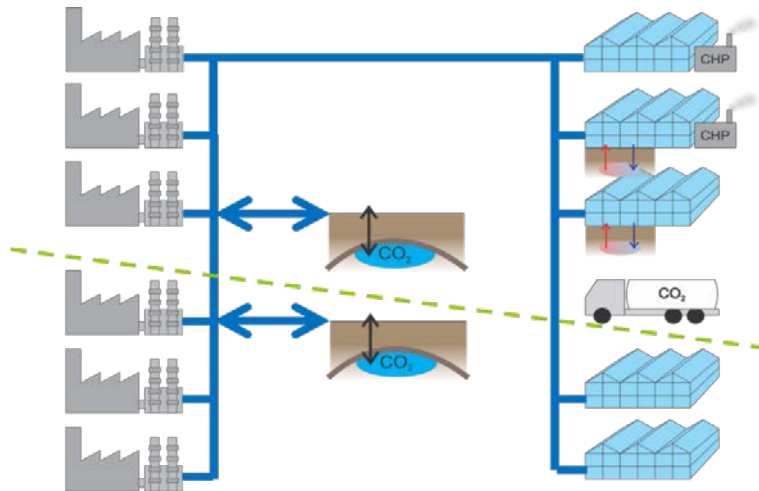


Figure 1. Simplified concept of the Q16-Maas case, as a base for PSS simulations (above green dashed line), with an example of potential extension of the CO₂ network with additional sources, greenhouses and buffer capacity.

In contrast with traditional techno-economic calculations, PSS simulates taking informed investment decisions, in this case by two independent actors: OCAP and the greenhouses. Decisions taken by one actor during the simulation will influence the other. Moreover, a trained analytical reservoir model will be incorporated in the simulation process to include the full reservoir characteristics and uncertainties in the techno-economic evaluation. The first and most important question to answer is if and under which conditions it is economic to introduce buffer storage in the Q16-Maas field, for both actors. An additional step is to determine the costs and benefits for including the buffer considering the reservoir constraints. This includes the influence on the CO₂ purchase cost by the greenhouses.

Simulations will also provide results on the potential expansion of the OCAP network, including new CO₂ sources and connection to additional greenhouses (Figure 1). Specifically for the greenhouses, preferential portfolios for heat and CO₂ delivery and its evolution over time will be generated. At the same time, the emission reduction from the greenhouses can be determined. Further expansion is possible by development of enhanced oil recovery or CCS projects in the North Sea oil and gas province. As such, Rotterdam could serve as a CO₂ hub with the additional advantage of the proximity of the Antwerp harbour, which can function as a supplier as well as a

potential user. The Antwerp petrochemical sector for example shows an increased interest in the use of CO₂ as a raw material in the production of for example urea and methanol (Alper & Orhan, 2017). The Q16-Maas project can provide the first business case to be developed and serve as a catalyser for the development of CC(U)S infrastructure in north-western Europe. Upscaling from current activities depends starts with correctly assessing the role of geology to buffer CO₂ production and demand.

References

- Alper E. & Orhan O.Y., 2017. CO₂ utilization: Developments in conversion processes. *Petroleum*, 3, 109-126.
- Mikunda, T., Neele, F., Wilschut, F. & Hanegraaf, M. 2015. A secure and affordable CO₂ supply for the Dutch greenhouse sector. TNO, 38 p.
- Oranje-Nassau Energie, 2013. Aanvraag Instemming Winningsplan Q16-Maas, 18 p.
- Oranje-Nassau Energie, 2018 <https://www.onebv.com/nl/project/q16-maas/> accessed on 27/04/2018.
- Piessens, K., Berenblyum, R., de Dios, C., Hladik, V., Koenen, M. & Welkenhuysen, K., 2017. Developing, testing and demonstrating onshore storage of CO₂: First results from the ENOS field sites. *European Geologist*, 44, p.6-10.
- Port of Antwerp, 2018. <http://www.portofantwerp.com/en/air-quality> accessed on 27/04/2018
- Ros, M., Read, A., Uilenreef, J. & Limbeek, J., 2014. Start of a CO₂ hub in Rotterdam: connecting CCS and CCU. *Energy Procedia*, 63, p.2691-2701.

Petrophysical characterization associated with lithotypes in tabular travertine geobody (case study from the Cakmak quarry, Turkey)

Zahra MOHAMMADI,¹ Mahtab MOZAFARI,² Cihan ARATMAN,^{1,3} Rudy SWENNEN¹

¹ *Department of Earth and Environmental Sciences, KU Leuven, Leuven, Belgium*

² *Natural and Experimental Tectonics Research Group, Department of Physics and Earth Sciences “Macedonio Melloni”, University of Parma, Italy*

³ *Department of Geological Engineering, Pamukkale University, Turkey*

1. Introduction and geological setting

Increased interest in continental carbonate reservoir characteristics relates to the relatively recent hydrocarbon reservoir discoveries offshore South America and offshore West Africa (the so-called Pre-salt deposits) (Carminatti et al., 2009). It has been reported that within the Pre-salt setting shrub-like fabrics developed within lacustrine settings (e.g. Carminatti et al., 2009; Wright, 2012; Saller et al., 2016) and that they also have been observed within the tabular geobody existing in the lowest part of Çakmak quarry (Denizli Basin, Turkey). Therefore, this Pleistocene tabular geobody was investigated for its reservoir characteristics based on an integrated petrophysical (poro/perm) and petrographical (optical microscopy, μ CT and medical CT) study.

2. Results

Field and petrographical observations of this tabular geobody displaying a sub-horizontal carbonate succession displaying nine dominant lithotypes reflecting an overall shrub flat and marsh pool depositional setting. The shrub flat strata consists mainly of dendritic shrub crust boundstone, pustular shrub grainstone, clotted micrite mudstone to boundstone and spongy boundstone. In contrast, the marsh pool environment is dominated by coated reed rudstone to boundstone, cryptalgal silty bioclast-rich bioturbated mudstone and peloidal grainstone to packstone. Other major lithotypes consist of coated grain- to packstone and pustular as well as radial shrub grainstone.

3. Interpretation and discussion

In the shrub flat facies, dendritic shrub and clotted micrite lithotypes exhibit uniform distribution of porosity and permeability with (poro/perm) mean values of 10.3% and 171 mD, and 5.7% and 13mD, respectively. The latter resulted from well-connected biomoldic and framework pore networks. In the marsh pool facies, the peloidal lithotypes show uniform distribution of poro/perm values (mean value of 15.3% and 149 mD) in relation to well-connected fenestral pore networks. The radial grainstone, cryptalgal silty bioclast-rich bioturbated mudstone, coated grain- to packstone and reed rudstone to boundstone, lithotypes are however characterized by a patchy distribution of poro/perm values which are highly attributed to unconnected vuggy and biomoldic pore networks. From a reservoir point of view, the permeability and porosity are slightly variable at sample scale but, in general, the shrub flat with more well-developed poro/perm values provides the best reservoir quality. In contrast, apart from peloidal lithotype, the marsh pool strata display relatively low reservoir quality.

References

- Carminatti, M., Wolff, B., Gamboa, L., 2009. New exploratory frontiers in Brazil. In: 19th World Petroleum Congress. World Petroleum Council.
- Saller, A., Rushton, S., Buambua, L., Inman, K., McNeil, R., Dickson, J. A. D., 2016. Presalt stratigraphy and depositional system in the Kwanza Basin, offshore Angola. AAPG Bulletin, 100, 1135 – 1164.
- Wright, V. P., 2012. Lacustrine carbonates in rift settings: the interaction of volcanic and microbial processes on carbonate deposition: Geological Society, London, Special Publications, 370, 39–47.

Collecting and organizing geological and mining data of the abandoned Monceau-Fontaine coal mine in order to assess geological resources

Mabeka NDONGALA¹, Fanny DESCAMPS¹, Nicolas GONZE¹, Sara VANDYCKE¹, Jean-Pierre K. TSHIBANGU¹

¹ *University of Mons, Mining Engineering Unit, 53 rue du Joncquois, 7000 Mons, Belgium.*

1. Introduction

Belgium has a long history of coal mining and gob gas drainage, especially in the Hainaut province. The closure of collieries during the late seventies and early eighties in the Charleroi region was the result of economic reasons rather than depletion of resources. Nowadays, independence in energetic supply for countries becomes an issue. Particularly in Belgium, a new interest is rising for abandoned coal mines as they may represent potential energetic resources for the future, even though these resources are criticized because of their impact on climate change. Modern software tools are under development since few decades to assess as accurately as possible geological resources. Such assessment requires high quality data for the geology (e.g., a wide range of borehole logs, cross-sections, geological maps, outcrop descriptions, etc.) as well as chemical, petrophysical and physico-mechanical parameters of coals in order to estimate residual gas reserves.

2. Available data

In this study, we focused on the Monceau-Fontaine coal mine (Charleroi District) in which a target area [16.4 km²] was selected in its southeast part. Because the colliery was one of the last active mines in the Hainaut province, more recent and numerous data were archived. First, the regional and local geology, even though complex has been widely studied. The area is within a highly disturbed zone of four main geological units (Tombe, Ormont, Carabinier and Centre or Poirier Massifs; Fig. 1) where more than a dozen of coal seams have been mined. Second, the mine experienced gas drainage from 1971 to 1990, with also several studies on the physical and chemical properties of coal: adsorption and desorption capacities of coal seams, porosities, permeability, and density. Particularly, we selected nine coal seams for which those data were available (Table 1).

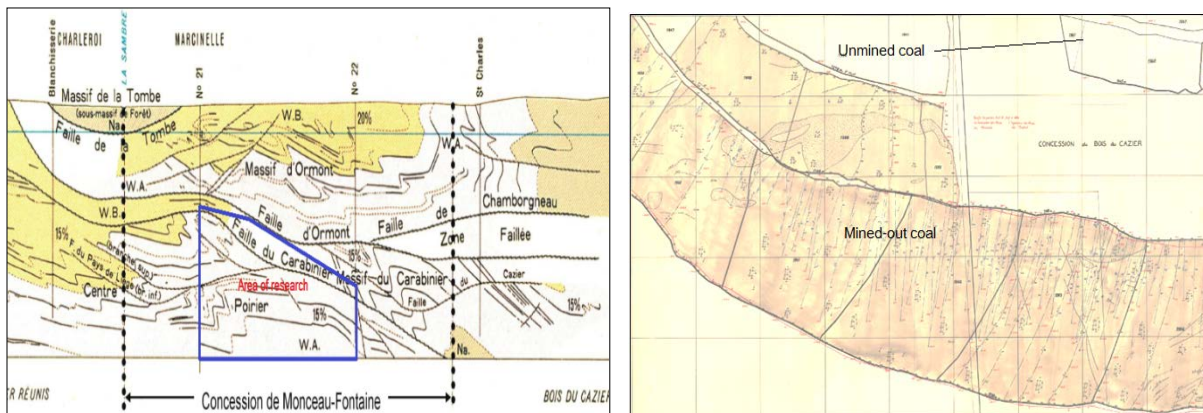


Figure 1 (Left): A typical N-S cross-section of the limits of the concession of Monceau-Fontaine at 35000 m to the east of Mons showing the target area (in black), the coal seams, the main geological structures setting and two shafts 21 and 22 (adapted from “Comité National de Géographie”, 1951). **(Right):** Detail of a plan view (11 Paumes) showing mined-out and unmined coal (adapted from SPW-DG03).

30 N-S vertical cross-sections drawn at a 1:5000 scale with a 100 m spacing and 3,000 meters of length each were collected. They give a general view on the shape of the coal seams over several kilometers and contain absolute and relative depth of seams and faults, and coordinates of the shafts (Fig. 2 – left). 86 plan views per coal seams were gathered. Drawn at a 1:1000 scale, they intended to report the evolution of mining process in a particular coal seam. They provide more precision on the structure of coal veins (dip and thickness), particularly in the areas between the N-S sections, but also report mined-out and unmined coal (Fig. 1 – right). However, plan views represent the situation at a given time and data may be missing (no full coverage of the target area).

Table 1. Chemical, petrophysical and physico-mechanical parameters of coal seams at the target area (Brych and Defourny, 1981; Defourny and Latour, 1980; Vandeloise, 1976, 1971).

Coal seam	Adsorbed CH ₄ content (m ³ /ton)	Desorbed CH ₄ content (m ³ /ton)	Permeability (mD)	Porosity (%)
4 Paumes	8.9 – 12.3	8.0 – 9.9	3.1 10 ⁻⁵ – 1.3 10 ⁻³ ; 0.12 – 0.27 (at 1250 m)	0.02 - 3
6 Paumes	10.2 – 24.15	12.0 – 12.9		
5 Paumes	5.0 – 12.0			
8 Paumes	6.5 – 12.4			
11 Paumes	6.5 – 12.5	12.9 – 16.0		
10 Paumes	9.4 – 21.6			
Anglaise	3.2 – 13.8			
Ahurie	3.2 – 13.8			
Gros Pierre	2.46 – 9.0			

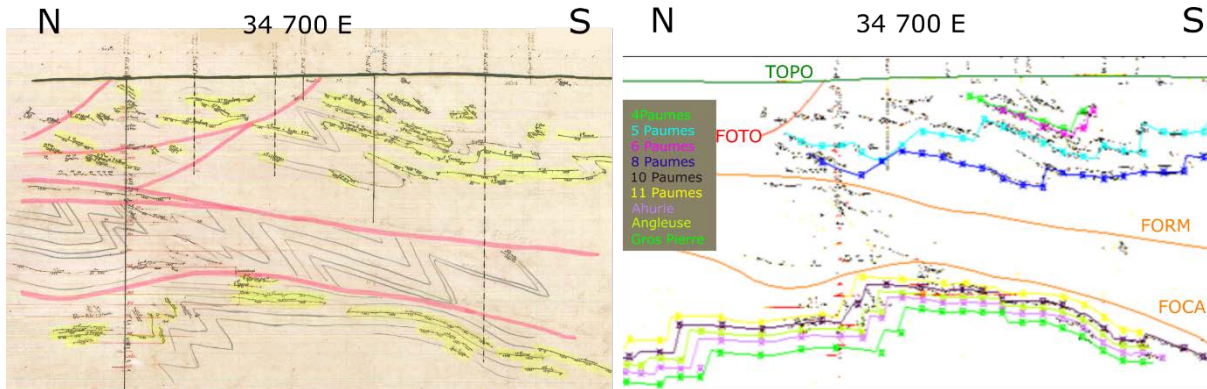


Figure 2 (Left): Vertical cross-section 34700E showing boreholes, faults, mined-out and unmined coal seams (modified after SPW-DG03); **(Right):** Digitized 34700 N-S vertical cross-section. FOTO, Fault of Tombe; FORM, Fault of Ormont; FOCA, Fault of Carabinier.

3. Organizing the data

Collected data were analyzed and processed to generate datasets that could help interpretation and understanding of the subsurface of the domain. Traces of coal seams and faults in N-S vertical cross-sections were digitized as polylines then smoothened, and named accordingly. A polyline dataset was then constituted for each feature (Fig. 2-right). On each plan view however, a number of points with known depths were also digitized, and an additional point dataset was generated for each coal seam from all plan views associated with the seam (Fig. 2-right).

References

- Brych J, Defourny P, 1981. Considérations sur les propriétés mécaniques du charbon. Contrat INIEX-FPMs-Rapport no 8. Faculté Polytechnique de Mons, Publication No 99, 40 p.
- Defourny P, Latour J-P, 1980. Considérations sur le comportement du charbon. Résultats d'essais sur échantillons soumis à des injections d'eau et d'azote. Contrat INIEX-FPMs – Rapport no 7. Faculté Polytechnique de Mons, Publication N0 95, 66 p.
- Comité National de Géographie, 1951. 1er Atlas de Belgique (1950-1972) v.1, planche 37.
- Vandeloise R., 1976. Le gisement et le dégagement du grisou. Recueils de recherches charbon. Rapport de synthèse 1969 – 1972/INEX. Rapport Final. Recueil no 56, Luxembourg, 134 p.
- Vandeloise R., 1971. Le gisement et le dégagement du grisou. Recueils de recherches charbon. Rapport de synthèse 1963 – 1968/INEX. Recueil no 5, Luxembourg, 48 p.

Evaluation of mineralogical and radiological data obtained at the geothermal plant in Mol, Belgium

Jente PAUWELS¹, Sonia SALAH¹, Stijn BOS², Valérie CAPPUYNS³

¹ *Belgian Nuclear Research Centre, SCK•CEN, Boeretang 200, BE-2400 Mol*

² *Flemish Institute for Technological Research, VITO, Boeretang 200, BE-2400 Mol*

³ *Catholic University of Leuven, KU Leuven, Oude Markt 13, BE-3000 Leuven*

1. Introduction

In the fall of 2015, a geothermal project was launched at the Balmatt site in Mol (Belgium) by drilling an exploration well in the Lower Carboniferous Limestones of the Campine Basin. This challenging project is coordinated by the Flemish Institute for Technological Research (VITO). The Carboniferous Limestones have an estimated extractable heat content of 13×10^{18} J (GEOHEAT-APP 2014) and are therefore seen as the most promising natural reservoir for a classical geothermal doublet in Belgium. As the tests performed on the well showed positive results, a second well was drilled in the spring of 2016, in order to create a full geothermal doublet. The formation water represents a Na(Ca)Cl brine with a total dissolved solids (TDS) content of approximately 165 g/L. Production temperatures up to 128°C are reached with formation pressures at a depth of 3300 m reaching 330 bars. Depending on the local geological and hydrogeological conditions, different elements, gases and naturally occurring radionuclides (NORs) are present in the fluid. Above the limestone reservoir, a geological layer with high thorium (Th) and uranium (U) contents is present and decay products, such as ²²⁸Ra and especially ²²⁶Ra were found enriched in the geothermal water. Their activity concentrations measured by gamma-ray spectrometry correspond to 8.5 ± 0.7 Bq/L and 95 ± 18 Bq/L, respectively (Vasile et al. 2017). These radionuclides may – influenced by changing pressure and temperature – accumulate/(co)precipitate in the future geothermal installation in form of different amorphous phases and/or minerals (e.g. lead-sulfide, barium-sulphate, etc.). Such so-called scales may become radioactive waste in case their concentrations exceed the exemption limits. Moreover, scaling may cause clogging of the injection well and parts of the surface installation (e.g. heat exchangers, pumps), which would drastically decrease the efficiency of the geothermal installation.

2. Status of the Balmatt project

Two wells have been drilled so far: MOL-GT-01-S1 which represents production well and MOL-GT-02 which corresponds to the injection well. MOL-GT-01-S1 reaches a depth of 3610 m while MOL-GT-02 reaches a depth of 3820m. The latter well is slightly inclined to the north-east as represented in Fig. 1 (Bos and Laenen 2017). A third well is in progress at the moment and is planned to be finished by the end of August 2018. This third well will also be a production well, located 1.5 km south of MOL-GT-01-S1 with an estimated depth of 4 km and a length of approximately 5 km. Some X-ray diffraction data on the reservoir rocks will be presented at the Geologica Belgica Conference. Moreover some preliminary geochemical calculation results will be shown.

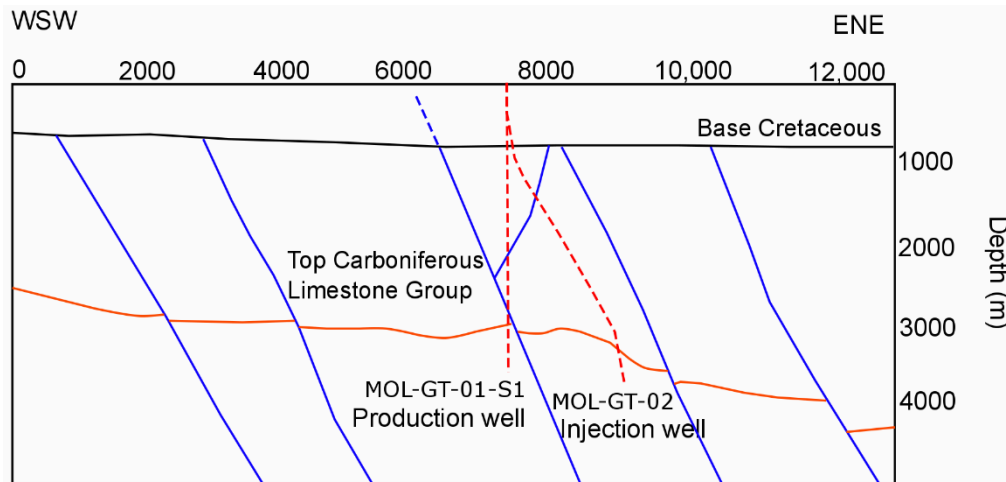


Figure 1. Structural WSW-ENE cross section through the Balmatt geothermal site with indication of already drilled wells MOL-GT-01 and MOL-GT-02

References

- Bos, S. & B. Laenen (2017) Development of the first deep geothermal doublet in the Campine Basin of Belgium. *European Geologist*, 43, 15-19.
- GEOHEAT-APP. 2014. Economische haalbaarheid van diepe en intermediaire geothermie voor het verduurzamen van de warmtevraag bij bouw- en renovatieprojecten (Economical feasibility of deep and intermediary geothermal energy in supplying sustainable heat for new building and renovation projects). VITO, Grontmij Nederland & TNO.
- Vasile, M., M. Bruggeman, S. Van Meensel, S. Bos & B. Laenen (2017) Characterization of the natural radioactivity of the first deep geothermal doublet in Flanders, Belgium. *Applied Radiation and Isotopes*, 126, 300-303.

Towards better exploitation of the shallow geothermal potential in the Brussels region

Estelle PETITCLERC¹, Xavier DEVLEESCHOUWER¹, Christian BURLET¹, Bertrand FRANCOIS², Pierre GERARD², Louis GAUDARE³, Mathieu AGNIEL³, Gust VAN LYSEBETTEN⁴

¹*Geological Survey of Belgium, Royal Belgian Institute of Natural Sciences, Jenner street 13, 1000 Brussels.*

²*Université libre de Bruxelles (ULB), Service BATir, Av F. Roosevelt 50 – CPI 194/02, 1050 Bruxelles.*

³*Bruxelles Environnement Gulledelle 100 - 1200 Bruxelles.*

⁴*Belgian Building Research Institute (BBRI), Av. P. Holoffe 21, 1342 Limelette .*

1. Introduction

With the public becoming increasingly aware of climate change, and with fossil energy sources running out, renewable energies are booming. Geothermal energy is among these new energy sources, and it is both emission free and inexhaustible. However, limited knowledge of ground conditions and lack of public awareness restrict the development of shallow geothermal systems in the Brussels Capital Region (BCR), despite the high potential of this technique in the area for heating, cooling, even seasonal energy storage of buildings and individual houses (Petitclerc et al., 2016). The BRUGEO project aims to facilitate accessibility and the efficient use of shallow geothermal energy in the Brussels region, especially for commercial and residential sectors. Thanks to Brussels ERDF (European Regional Development Fund) funding a consortium of all major actors in geothermal energy in the Brussels region were brought together (ULB, Bruxelles Environnement, BBRI, VUB, and GSB). In this four years project (2016-2020), specific actions promoting the geothermal potential of the BCR are addressed: 1- Collect existing data related to the knowledge on Brussels subsurface (geological, hydrogeological, and geothermal data) and consolidate them in a single database; 2- Conduct new laboratory and field tests in order to complete geological analyses in less explored areas that could have an attractive geothermal potential; 3- Map the geothermal potential of the BCR in order to evaluate the amount of energy that can be provided by or stored into the ground in any given place, depending on drilling depth and the geothermal system chosen (open and closed systems).

2. Geological database and 3D modelling

Nowadays, all geothermal systems in BCR are shallow systems, either closed (geothermal loop) or open (geothermal wells). While geothermal wells require the presence of an aquifer, geothermal loop fields can in principle be installed anywhere. However, the energy efficiency and the design of these two types of system depend crucially on the underground's characteristics. The lithology, the thickness, the saturation of the geological layers encountered below the surface have a strong influence on the design of the shallow geothermal systems. The Geological Survey of Belgium has created, during the last 7 years, a GIS based 2D-3D geological model of the underground of the BCR. This geological model has been progressively developed in the framework of several past projects (BUG, Hydrobrux, Hydroland, Cambier & Devleeschouwer, 2013) and lastly under the Brustrati3D project (Devleeschouwer et al., 2017). 9266 in-situ tests collected in and around the BCR (outcrops, drillings, piezometers, cone penetration tests, etc.) have been used to create an

ArcGIS project. The Brustrati3D model has allowed to generate interpolated top and base surfaces across the BCR for 19 geological layers representing the whole lithostratigraphic sequence from Quaternary to the Paleozoic basement. Different type of corrections were performed to establish a new geological model for the BCR. The following objective is to create a WebGIS portal for the BCR containing this 3D model in order to use it in other scientific projects.

3. New exploration in Brussels

An important exploration phase is included in the first two years of the BRUGEO project to acquire new data improving the geological and hydrogeological knowledge of BCR. Several in-situ parameters are measured by e.g. new piezometers implementation and monitoring, pumping tests, cores sampling, logging and enhanced thermal response tests (eTRT). These measurements are implemented as far as possible on future private projects by a win-win approach. The idea is to be grafted on existing projects to increase the data acquisition and to avoid purely exploratory drilling that are expensive and not used later for any geothermal exploitation. So far, the BRUGEO consortium has conducted two exploration drillings (La Cambre and Anderlecht) to assess the lithology, the structure, the groundwater flows, and geophysical properties of the Cambrian basement (Brabant massif). A third borehole is scheduled for 2019. In parallel, laboratory measurements are achieved to characterize the determinant thermal parameters of the Tertiary sediments and the Cambrian basement (Brabant Massif).

4. Mapping of the shallow geothermal potential

From all the subsurface data collected, the BRUGEO consortium aims at mapping the geothermal potential of the BCR. This web-based mapping, accessible to design offices, installers of geothermal systems, citizens, public and private stakeholders or regional and municipality administrations, will make it easier to switch to this clean and renewable source of energy. The web portal will consist of an interactive decision support and a design tool based on maps built thanks to the geoscientific 3D models. The amount of energy that can be provided by a geothermal system depending on the technique (i.e. closed loop or open loop systems) and the depth of the installation will be provided based on the geological setting of the place. On the other hand, from the demand in energy of a building, a first design of a geothermal system can be given. The environmental risks, constraints and legislation are other significant parameters that will be considered as they split the BCR into areas where the installation of geothermal systems is possible, restricted or forbidden. Currently, the first thermal conductivity maps have been developed. The final results are expected to be published on a web portal in the two coming years.

References

- BRUGEO website, <http://geothermie.brussels/en>
- Cambier, G. & Devleeschouwer, X., 2013. A GIS-based methodology for creating 3D geological models in sedimentary environment: application to the subcrop of Brussels. *Zeitschrift der Deutschen Gesellschaft für Geowissenschaften*, 164 (4), 557–567.
- Devleeschouwer, X., Goffin, C, Vandaele, J. & Meyvis, B., 2017. Modélisation stratigraphique en 2D et 3D du sous-sol de la Région de Bruxelles-Capitale. Projet n°2016B0512 de l'IBGE. Rapport final, 97 p.
- Petitclerc, E., Laenen, B., Lagrou, D. & Hoes, H., 2016. Geothermal Energy use, Country Update for Belgium. European Geothermal Congress 2016, Strasbourg, France, 19-24/09/2016, 9 p.

Understanding the Earth for the people that inhabit it: Belgian and Flemish institutes joining hands in the framework of GeoERA

Kris PIESSENS¹, Timothy N. DEBACKER², Griet HEUVELMANS³, Ben LAENEN⁴, Koen BEERTEN⁵, Christian BURLET¹, Marleen DE CEUKELAIRE¹, Pierre-Yves DECLERCQ¹, Cis SLEENTER³, Jan CORLUY³, Mieke DE CRAEN⁵, Sophie DECREE¹, Katrien DE NIL², Xavier DEVLEESCHOUWER¹, Helga FERKET², Matej GEDEON⁵, Eric GOEMAERE¹, Thomas GOOVAERTS¹, Vanessa HEYVAERT¹, Thierry LEDUC¹, Estelle PETITCLERC¹, Bart ROGIERS⁵, Yves VANBRABANT¹, Marleen VANDAMME², Koen VAN NOTEN¹, Jan WALSTRA¹, Kris WELKENHUYSEN¹

¹*GSB - Geological Survey of Belgium - Royal Belgian Institute of Natural Sciences, Jennerstraat 13, 1000 Brussels*

²*VPO - Bureau for Environment and Spatial Development, Koning Albert II-Laan 20, bus 8, 1000 Brussel*

³*VMM - Flanders Environment Agency, Koning Albert II-Laan 20, bus 16, 1000 Brussel*

⁴*VITO - Flemish Institute for Technological Research, Boeretang 200, 2400 Mol*

⁵*SCK•CEN Belgian Nuclear Research Centre, Waste and Disposal, Boeretang 200, 2400 Mol*

Societies rely on a secure, responsible and affordable supply of resources to meet their basic needs, in order to live life in a safe and healthy environment. The natural resources from the subsurface, i.e. groundwater, geo-energy and raw materials, represent essential elements in this provision. Safety from catastrophic events, such as those linked to earthquakes, or continuous ones, such as subsidence, can be improved by understanding the causes, frequency or rates of processes, and their impacts. These applied goals require a correct and intimate understanding of the regional geology.

While geological surveys and other organisations working on the subsurface were initially very much focussed on national supply of resources, issues such as environmental consequences have increasingly come to the forefront. Europe has now become the relevant scale when considering import or export of raw materials. This results in an increasing pressure to place regional knowledge in a cross-border or pan-European context.

To support cross-border, thematic research, the European Commission issued a call for an ERA-NET to which a consortium of 33 national and 15 regional organisations responded. An ERA-NET is a project that internally organises a competitive call for projects. In 2017, GeoERA officially started. After an internal call for project proposals, 15 projects were approved that receive about 30% top-up funding under H2020. The remainder of the resources comes from different sources of funding, totalling the budget to 30.3 M€ Projects are funded under the themes Geo-Energy, Raw Materials, and Ground Water. A fourth theme, Data Infrastructure, will realise the shared ambition of all projects to jointly store and publish their data on-line as an extension of country specific databases (e.g. DOV, Gisel).

The starting date of the GeoERA research projects granted funding is 1 July 2018, and the projects will run for three years. Belgian and Flemish institutes involved are: the Geological Survey

of Belgium (GSB), the Bureau for Environment and Spatial Development – Flanders (VPO), the Flemish Institute for Technological Research (VITO), Flanders Environment Agency (VMM) and the Belgian Nuclear Research Centre (SCK-CEN). Although not involved as official partner, the Geological Survey of Wallonia supports the initiative by means of data provision. The GSB is involved in seven projects, VITO, as linked third party of VPO in two projects, VPO itself in one project, and VMM in three projects of which two will be elaborated in close cooperation with SCK-CEN, the linked third party of VMM. Together with VPO-VITO, the GSB is coordinator of GeoConnect^{3d}, a strongly cross-thematic Geo-Energy project that aims to disclose geological information for policy support and subsurface management. Other funded Geo-Energy projects in which the GSB is involved are MUSE, a project on shallow geothermal energy in European urban areas, and HIKE, on induced hazards and impacts related to the exploitation of subsurface resources throughout Europe. Under the theme Raw Materials the GSB participates in Mintell4EU, which aims to improve the European knowledge base on raw materials, as well as in FRAME, that is designed to research the critical and strategic raw materials in Europe. For groundwater the GSB is directly involved in the HOVER project, mainly on data collection related to natural springs. VMM is also involved in HOVER, but in a work package on the distinction between anthropogenic and geogenic causes of groundwater contamination (especially how to deal with it in groundwater policy and management) with substances like arsenic. Moreover, VMM is, together with SCK-CEN, participating and leading a work package in two other Ground Water projects, namely VoGERA on investigating the vulnerability of shallow groundwater resources to deep subsurface energy-related activities, and RESOURces about harmonization of information about Europe's groundwater resources through cross-border demonstration projects. Finally, the GIP-P project, where the GSB is work package leader, will establish a common platform for organising, disseminating and sustaining the digital results of the GeoERA projects.

GeoERA is more than the occasional H2020 project. The combined efforts by the Belgian and Flemish institutes to engage in 10 different projects is a cooperative approach, with clear ambitions to demonstrate how cross-thematic research links can be set-up by different institutes, and how these can provide fruitful results for policy makers and other stakeholders. This is a notable effort in a project that is about establishing and demonstrating the added value of a European geological surveys research area, and finding how to optimally link regional, national and European efforts and interests.

Acknowledgements

This project has received funding from the European Research Council (ERC) under the European Union's Horizon 2020 research and innovation programme under grant agreement No 731166.

Geological Economics: Economics, Geology and Ecosystem Earth

Kris PIESSENS¹ & Tine COMPERNOLLE^{1,2}

¹*Geological Survey of Belgium - Royal Belgian Institute of Natural Sciences, Jennerstraat 13, 1000 Brussels.*

²*Departement of Economics - University of Antwerp, Prinsstraat 13, 2000 Antwerp, Belgium.*

1. Society and the destabilisation of the ecosystem Earth

An ecosystem consists of communities of interacting species and the physical environment on which they depend. Although it is well accepted that Earth consists of many different ecosystems, human societies much less readily recognize that Earth itself is an ecosystem, dependent on interacting species and consisting of finite resources (Vignieri & Fahrenkamp, 2018). Humans are part of this ecosystem, and have recently come forward as a dominant species in terms of their physical and biological impacts. These can mainly be related to waste production and land-use changes resulting from a rapid extraction of natural resources.

2. Geology fundamental to ecosystems and society

Geology determines, together with latitude, the external conditions of ecosystems. Indeed, geological processes have shaped the surface of the Earth through tectonic uplift, subsidence, and erosion, while plate tectonics determines the distribution of land and oceans. Volcanism, tectonic uplift, and the cycles of sedimentation, burial and metamorphism, determine which rocks surface, forming the primary substrate. Access to water depends on the hydrogeological cycle, which runs fast in the atmosphere and through surface waters, but also includes infiltration and buffering in aquifers, forming reliable and long-lasting sources of water.

In a similar way, also the carbon cycle spins fast in surficial gear, while the geological one is slow and fundamental. Part of the carbon bearing remains of life on Earth, such as carbonate shells or organic matter, were deeply buried and fossilised. This extraction of carbon from the atmosphere had a profound impact, reducing carbon dioxide to present-day levels. Compared to these natural processes, anthropogenic processes have immediate effects.

Humans have found a particular way to distinguish themselves very recently from other, contemporary life forms, in that they have established societies that rely on the ability to access and use geological resources.

3. The unsustainable basis for current society

Since humans learned to unlock geological resources at a large scale, population density increased and the impact since the industrial revolution has particularly been drastic.

Starting from the 20th century, the environmental impact and depletion of natural resources were identified as side effects of the free-market driven, unlimited growth-focussed economy. However, as the Earth and its resources are finite, the physical dimensions of the economy and the waste streams it produces cannot expand continuously. In contrast to more traditional economic theories, Ecological Economics is an economic discipline that gives a central position to the issue of scale. It aims to determine how large the physical dimensions of the economy should be, relative to the ecosystem that sustains it (Daly, 1992). This is challenging mainly because of the associated

uncertainties intrinsically linked to modelling highly complex systems and feedback loops between society and its environment. As a result, current assessments with regards to the optimal extraction of geological resources, often ignore scale and the distribution of costs and benefits within and across generations.

Geology as a discipline and the experience that geology has with uncertainties in geologically complex and poorly known systems, is a useful basis to reveal the intimate links between the Earth's natural resources and societal development.

4. Geology as the correct starting point

Traditional economic assessments are not designed for looking deep into the future, for example to compare an immediate gain of an activity (e.g. coal mining) with indirect costs to society that it may have in the future (e.g. long-term consequences of subsidence). Being flexible in handling time is one of the first elements to master for students in geology.

Equally well embedded and relevant is understanding how depth (as in distance) can change the nature of a problem. Two aspects are linked when considering depth. With depth, the amount of data and degree of understanding dramatically decreases, but also the degree to which the subsurface can be engineered to our needs. Already from a depth of several tens of meters, direct observations of the subsurface require drillings, but these are nearly point observations. Geophysical techniques may offer 2D or 3D visualisations, but are based on indirect data. With increasing depth, the effort for obtaining information increases rapidly. Hence, data generally becomes more sparse as depth increases. This is essential to understand resources and reserves, but also development of the subsurface, because the challenge of realising deep applications comes from two sides: information decreases, but also the degree to which we can adjust the subsurface to our needs through engineering diminishes. The subsurface will have to be largely accepted as is. Nevertheless, computing power has allowed to shift from qualitative understanding of the subsurface, towards quantitative verification or justification. Binding geology into economic evaluations has been done successfully, but mainly at project level to simulate or optimise project decisions of investors. The step towards interdisciplinary and system wide evaluations needed to analyse the complex interaction of societies and their environment is certainly unprecedented.

5. Theory to practice: Sustainable choices in the Campine Basin

To demonstrate an Ecological Economics approach to a practical case, the setting of the Campine Basin is chosen. As a geological unit, the Campine Basin can be used for storage of nuclear waste or CO₂ geological storage, it is being developed for deep hydrothermal energy production, and is in use for the seasonal storage of natural gas. Historically it has been mined for coal, with significant reserves remaining for potential future valorisation, and has potential for gas or oil shale. It is also an area with active groundwater production. The Campine Basin is certainly small compared to the potential subsurface demand, while large parts have only moderately been explored. This makes it a-priori challenging to estimate the impact radius of different subsurface activities, or their environmental economic and long-term effects. For this area, the construction of a model will be attempted using economic and semi-analytical geological techniques to integrate the economy, geology, and ecology into one realistic system. The model will integrate over a

decade of experience with simulating and forecasting highly uncertain systems. This interdisciplinary model for the Campine Basin then becomes the starting point for the actual analysis, which will ultimately allow to determine the optimal scale and ranking at which subsurface activities are developed. As such, geology will provide the expertise to handle system complexity in such a way that the development can be optimised from a societal point of view. This deeply engraining of geology into other disciplines is fundamental and opens completely new paths to scientifically based future policy. It is referred to as Geological Economics.

References

- Vignieri, S. & Fahrenkamp-Uppenbrink, J., 2017. Ecosystem Earth. *Science*, 356, 258-259.
- Daly, H. E., 1992. Allocation, distribution, and scale: towards an economics that is efficient, just, and sustainable. *Ecological Economics*, 6(3), 185-193.

Transforming waste into resources: inspirational cases from Flanders

Ruben SNELLINGS¹ & Peter NIELSEN¹

¹*Sustainable Materials Management, VITO, Boeretang 200, 2400 Mol; ruben.snellings@vito.be, peter.nielsen@vito.be*

The transition to a circular economy is one of the mega-trends identified by the European Commission. The transition to circularity would make our economy more sustainable, mitigate climate change and reduce depletion of the world's resources. At the same time it is expected that it would create local jobs and engender market robustness by a steady and multilateral supply of resources.

Moving away from the linear cradle-to-grave economy means keeping products and materials as long as possible at their highest level of intrinsic value. Reusing, repairing, refurbishing or remanufacturing of products should be encouraged, for instance by adopting eco-design principles that enable easy disassembly, by avoiding complex entanglement of materials and stop using toxic or hazardous materials that impair reprocessing (Fig. 1). Simultaneously, recycling at the material level should be intensified, not only end-of-life products should be recyclable, also industrial or municipal waste should be upcycled from waste-to-resource, or even from waste-to-product.

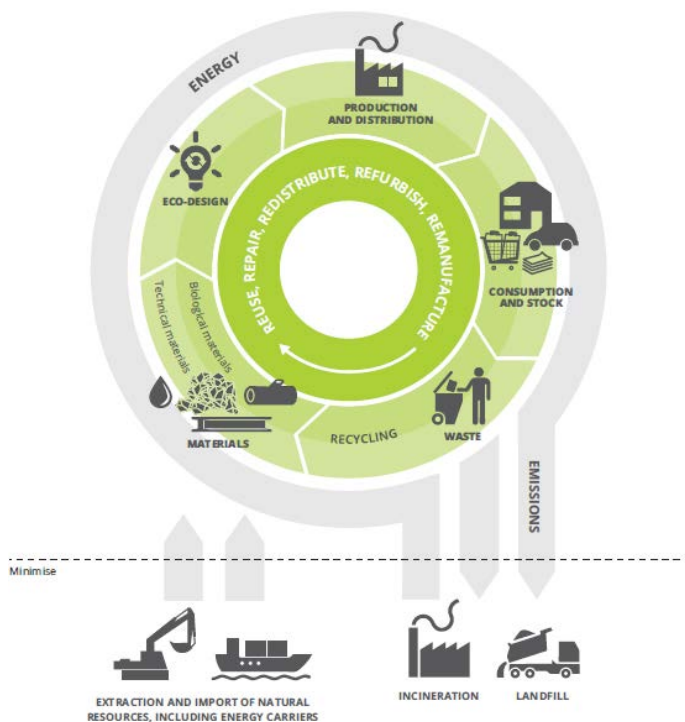


Figure 1. Materials flows in a circular economy. Material and product circulation in the inner circle is preferable over the more conventional recycling regime, or the cradle-to-grave paradigm depicted as the outer grey circle (Source: VITO).

As in any systemic change, the transition to a circular economy faces important challenges and barriers. Such barriers may be techno-economical, but may also be engrained in product standards or legislation. Bringing back extraction of raw materials to Europe will not only need compliance to strict environmental legislation, but will also require local social licenses to operate.

Flanders has made circular economy one of its strategic spearheads in its 2050 plan for economic development. Several factors indeed place Flanders, and in extension Belgium, in pole position to become a frontrunner. Close distances, dense transport infrastructure and well-developed industrial networks help building cases of industrial symbiosis, in which a residue of one industry becomes a resource for another. At the same time, innovation at centres of excellence and progressive waste management policy stimulated and facilitated inspirational cases of transforming waste into resources.

This contribution presents opportunities, challenges and creative solutions from large-scale projects that aim to valorize residues as new raw materials for a circular economy. A first case treats the recovery of valuable metals from ferrous slags or municipal solid waste incineration ashes combined with the valorization of the mineral fraction as building material using accelerated carbonation (Nielsen et al., 2017). In a second case, transformation of dredging sediments into cement substitutes using calcination technology is presented (Snellings et al., 2016). In a final third case, new processing technologies for concrete recycling are discussed.

References

- Nielsen, P., Baciocchi, R., Costa, G., Quaghebeur, M., & Snellings, R. 2017. Carbonate-bonded construction materials from alkaline residues. *RILEM Technical Letters*, 2, 53-58.
- Snellings, R., Cizer, Ö., Horckmans, L., Durdziński, P. T., Dierckx, P., Nielsen, P., & Vandewalle, L. 2016. Properties and pozzolanic reactivity of flash calcined dredging sediments. *Applied Clay Science*, 129, 35-39.

Geochemical fractionation of pegmatites from the Kabarore-Mparamirundi area (Burundi) as pathfinder to Sn-Ta-Nb pegmatites.

Denis TURIMUMAHORO^{1*}, Philippe MUCHEZ¹, Stijn DEWAELE^{2,3}, Niels HULSBOSCH¹ & Louis NAHIMANA⁴.

¹ *KU Leuven, Geodynamics and Geofluids Research Group, Department of Earth and Environmental Sciences, Celestijnenlaan 200E, B-3001 Leuven, Belgium.*

² *Department of Geology and Mineralogy, Royal Museum for Central Africa (RMCA), Leuvensesteenweg 13, 3080 Tervuren, Belgium.*

³ *Ghent University, Department of Geology, Ghent, Krijgslaan 281, S8, Belgium.*

⁴ *Université du Burundi, Faculté des Sciences, Département des Sciences de la Terre, B.P 2700 Bujumbura, Burundi.*

**denis.turimumahoro@student.kuleuven.be*

1. Introduction and geological setting

Located in northwestern Burundi in Central Africa, the Kabarore-Mparamirundi area forms part of the Sn-Ta-Nb-W-Au metallogenic province of the Mesoproterozoic Karagwe-Ankole Belt. This belt encompasses south Kivu and Maniema (DRC), Burundi, Rwanda, southwestern Uganda and northwestern Tanzania. It hosts significant Ta-Nb and Sn-bearing pegmatite intrusions associated with a Neoproterozoic tin granite generation (986 ± 10 Ma; SHRIMP U-Pb on zircon; Tack et al., 2010). In literature, the petro- and metallogenesis of pegmatites has been a controversial debate for decades (London, 2008). Varlamoff (1954) identified a regional mineralogical zonation of pegmatites in the Gatumba-Gitarama region of Rwanda (70 km from our study area) around the Gitarama pluton granite. A regional zonation is developed around a parental tin granite and the proximal pegmatites grade outwardly into biotite, two-mica and muscovite pegmatites. Rare-element (Nb-Ta-Sn) pegmatites occur most distal from the granite (Hulsbosch et al., 2014). Trace element modelling demonstrated that Rayleigh fractional crystallization governs this mineralogical and geochemical evolution from a granite source to common and eventually rare-element pegmatites (Hulsbosch et al, 2014).

The alkali metal concentration, i.e. K, Rb, and Cs, of dioctahedral micas are good indicators of the magmatic differentiation of pegmatites and are proxies for their mineralization potential (Černý et al., 1985). The aim of our study is to determine the degree of fractionation of the pegmatites of the Kabarore-Mparamirundi region and to correlate this fractionation with a regional mineralogical-geochemical zonation documented by Hulsbosch et al. (2013, 2014) around the granite pluton of Gitarama. The objective is to test if the trace element content of dioctahedral micas can be used as a vector tool for the exploration of mineralized or sterile pegmatites in the Kabarore-Mparamirundi area. Twenty-one muscovite samples from multiple pegmatite dykes from different localities in the area were analyzed for major, minor and trace elements by inductively coupled plasma optical emission spectrometry (ICP-OES) and inductively coupled plasma mass spectrometry (ICP-MS) respectively.

2. Results and interpretation

Concentrations of alkali metal elements (K, Rb, Cs) in muscovite vary in the range of 1450–7590 ppm for Rb, 40–1380 ppm for Cs and since K (in wt%) is a major element in muscovite it does not vary significantly within the samples (i.e between 9.9 and 10.3 wt%). The K/Rb and K/Cs ratios (in ppm/ppm) show a similar trend (Fig. 1). They range from 58 to 10 for K/Rb and from 2050 to 60 for K/Cs. According to the general model of fractional Rayleigh crystallization for the assessment of the regional differentiation mechanism of pegmatite zones around a parental granite, the model of Hulsbosch et al. (2014) is applied. The fractionation model states that the pegmatites close to the parental granite are the least fractionated whereas the distal pegmatites are the most fractionated. The modelled degree of crystallization of 78% - 99% crystallization suggests that the pegmatites of Kabarore-Mparamirundi region are highly differentiated. This fractionation interval corresponds to pegmatites of the muscovite zone and the Nb-Ta-Sn mineralized zone (Hulsbosch et al. 2014). Further studies are planned to petrographically and geochemically characterize the Gr5 parental granite from which these pegmatites are most probably derived.

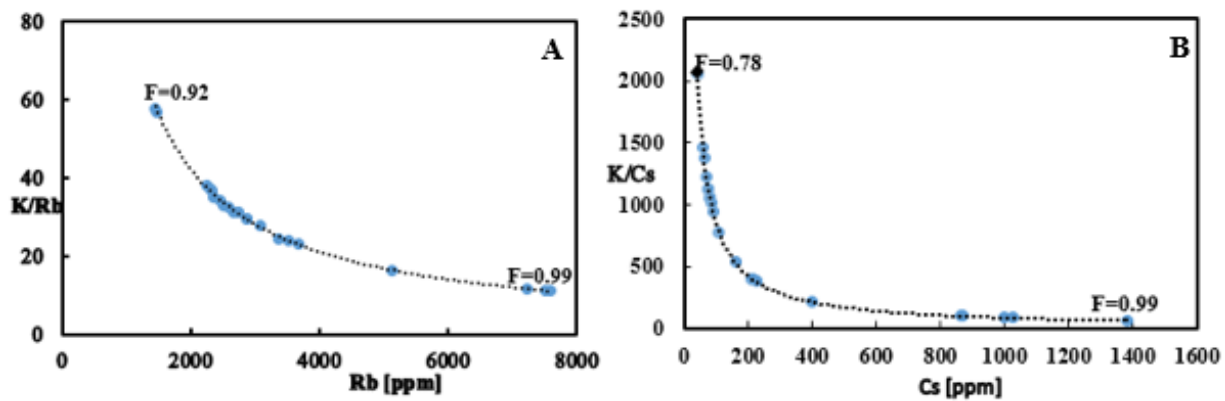


Figure 1. K/Rb vs Rb (A) and K/Cs vs Cs (B) plots of muscovite samples.

References

- Černý, P., Meintzer R. E. & Anderson A. J., 1985. Extreme fractionation in rare element granitic pegmatites: selected examples of data and mechanism. *Canadian Mineralogist*, 23, 381-421.
- Hulsbosch, N., Hertogen, J., Dewaele, S., André, L. & Muechez, P., 2014. Alkali metal and rare earth element evolution of rock-forming minerals from the Gatumba area pegmatites (Rwanda): Quantitative assessment of crystal-melt fractionation in the regional zonation of pegmatite groups. *Geochimica et Cosmochimica Acta*, 132, 349-374.
- Hulsbosch, N., Hertogen, J., Dewaele, S., André, L. & Muechez, P., 2013. Petrographic and mineralogical characterisation of fractionated pegmatites culminating in the Nb-Ta-Sn pegmatites of the Gatumba area (western Rwanda). *Geologica Belgica*, 16, 105-117.
- London, D. 2008. A petrologic assessment of internal zonation in granitic pegmatites. *Lithos*, 184-187, 74–104.
- Varlamoff, N. 1954. Répartition des types de pegmatites autour de la partie nord-ouest du grand massif granitique de Nyanza. *Annales de la société géologique de Belgique*, 78, 1-21.

Fracturation of Lower Carboniferous carbonates in the Namur-Dinant area as analogues to the Campine-Brabant Basin

Eva VAN DER VOET^{1,2,*}, Philippe MUCHEZ¹, David LAGROU², Ben LAENEN² & Rudy SWENNEN¹

¹ KU Leuven, Celestijnenlaan 200E, 3001 Leuven-Heverlee, Belgium

² VITO, Flemish Institute for Technological Research, Boeretang 200, 2400 Mol, Belgium

* eva.vandervoet@kuleuven.be; eva.vandervoet@vito.be

The Lower Carboniferous fractured and karstified limestones and dolostones of the Campine-Brabant Basin, located in northern Belgium, southern Netherlands and westernmost Germany, hold a great potential for geothermal energy. Since matrix porosity of the Lower Carboniferous carbonates is generally low, fractures are an important part of the reservoir. Therefore, the goal of this study is to assess the *mechanical stratigraphy* of the carbonates, addressing the relationships between lithologies and mechanical properties, such as fracture characteristics. These relationships will provide a better understanding of the fracture distribution which could be of value for the development of new geothermal systems.

Mechanical features were studied through cores and well logs of multiple boreholes in the Campine-Brabant Basin. However, these data are one dimensional and at a very limited scale. Therefore, outcrop analogues were selected to study the fracture networks in two dimensions and at a larger scale (several hundreds of meters wide and tens of meters high). Such similar Lower Carboniferous carbonate rocks are exposed in the southeastern part of Belgium. Three quarries were used for the analogue study: Marche-les-Dames (Tournaisian to lowermost Viséan dolostones), Beez (V2b thin-bedded limestones) and Moha (V2b thin-bedded limestones).

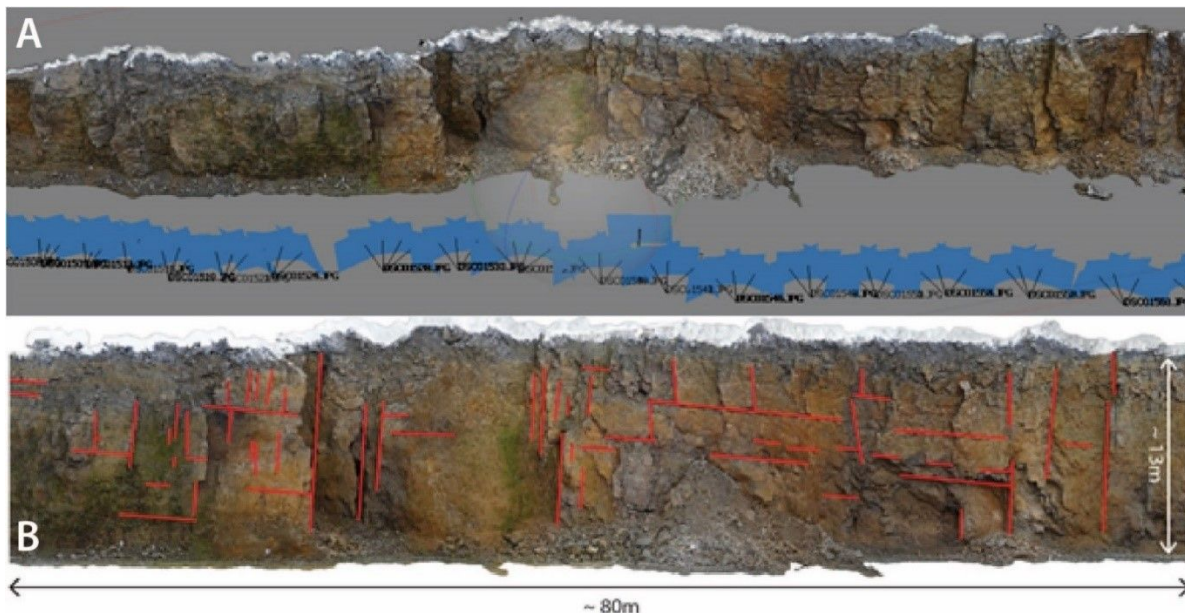


Figure 1. Two steps in the process of digitalizing fracture networks from outcrop walls. A) A 3D surface model is created from pictures of different positions, using the software Agisoft Photoscan.

B) An orthophoto of the outcrop is generated, on which open fractures and bedding planes are traced manually in Adobe Illustrator software.

Since the deformation history of the Namur-Dinant Basin is different from the evolution of the Campine-Brabant Basin, a strong selection was essential to end up with the best possible analogues. The selected outcrops contain Lower Carboniferous carbonates with similar lithologies, a sub-horizontal bedding (to eliminate obvious deformation differences), the largest possible rock surfaces, the least possible vegetation coverage and an amount of weathering that best accentuates the fractures. To a lesser extent, the stratigraphy played a role in the selection of analogues as well. Furthermore, by focusing on mechanical differences between units, the difference in structural evolution between the basin and the analogues is of minor importance. Photogrammetric analyses were performed on seven outcrops in three quarries (fig. 1). During this process a three-dimensional surface model of the quarry walls was made by combining several photographic images taken from different positions. From these 3D models, high resolution orthophotos were created, on which visible open fractures and bedding planes were traced. These digitalized fracture networks were used for statistical analyses.

Fracture patterns have been quantitatively studied on 2D walls, to identify different mechanical units. Clear differences in fracture frequency (m^{-2}), intensity (m/m^2) and topology (as an indication for connectivity) were found between dolostones and thin-bedded limestones. The Tournaisian dolostones generally have a low fracture frequency, intensity and connectivity, while thin-bedded limestones of the Neffe formation (V2b) contain denser and better connected fracture systems. The topology of the systems was also studied. Three different fracture node-types were identified (I=isolated, Y=abutting, X=crossing) and the ratios between these were plotted on a triangular diagram for the distinct outcrops (fig. 2; Sanderson & Nixon, 2015). Through this visualisation, the connectivities of the fracture systems could be compared to each other: the closer it plots to the Y-X line, the higher the connectivity. Thin bedded limestones appear to have better connected fracture networks than all dolostone outcrops.

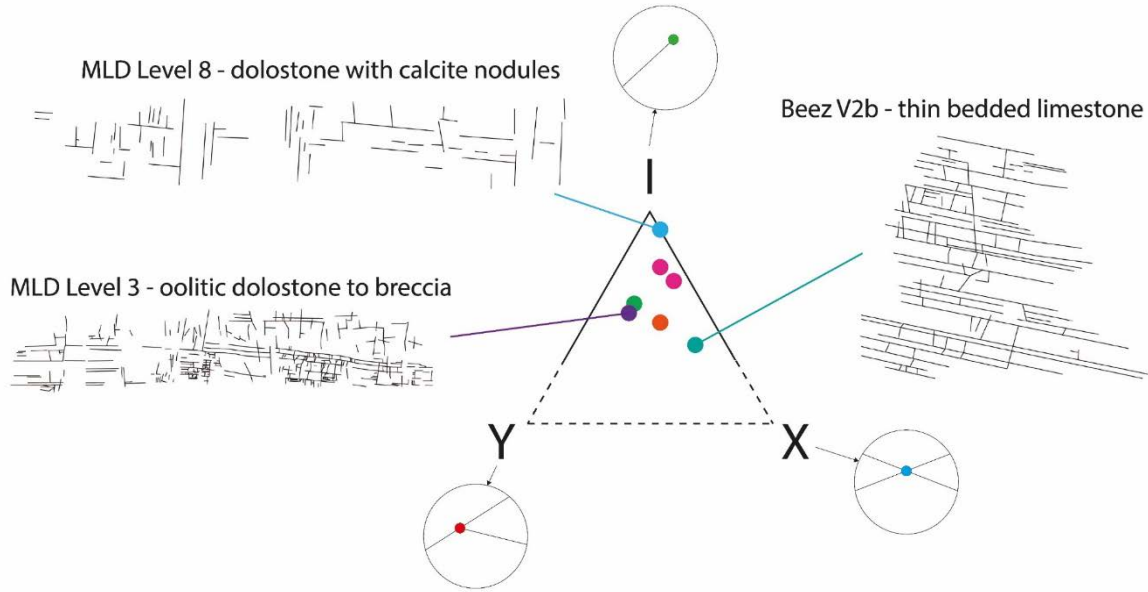


Figure 2. Triangular diagram showing the relative ratios between the isolated (I), abutting (Y) and crossing (X) nodes of the traces of the different outcrops, as an indication for the connectivity of the traces. After Sanderson & Nixon (2015). Abbreviation: MLD=Marche-les-Dames quarry.

The understanding of the mechanical behaviour of different lithological units will eventually support increasing the predictability of fracture systems and related reservoir quality.

Reference

Sanderson, D.J. & Nixon, C.W., 2015. The use of topology in fracture network characterization. *Journal of Structural Geology*, 72, 55-66.

Phyllosilicate Ar-Ar and Rb-Sr geochronology in the Gitarama-Gatumba area (Rwanda): an important Neoproterozoic influence in the Karagwe-Ankole Belt

Johanna VAN DAELE¹, Richard SPIKINGS², Peter ONUK³, Frank MELCHER³, Niels HULSBOSCH¹, Stijn DEWAELE⁴, Philippe MUCHEZ¹

1 KU Leuven, Geodynamics and Geofluids Research Group, Department of Earth and Environmental Sciences, Celestijnenlaan 200E, 3001 Leuven, Belgium

2 University of Geneva, Department of Earth Sciences, rue des Maraîchers 13, 1205 Geneva, Switzerland

3 Montanuniversität Leoben, Lehrstuhl für Geologie und Lagerstättenlehre, Peter-Tunnerstraße 5, 8700 Leoben, Austria

4 Ghent University, Department of Geology, Krijgslaan 281, S8, 9000 Ghent, Belgium

1. Introduction and geological setting

The Karagwe-Ankole Belt (KAB) is an orogenic belt in Central-Africa, situated between the Congo Craton (W) and the Tanzania Craton (E). At ~1375 and ~986 Ma, two S-type granite generations, termed the G1-G3 and G4 granites in Rwanda, respectively, intruded the Mesoproterozoic metasediments (Tack et al. 2010). The broader geodynamic context in which these magmatic intrusions and related early Neoproterozoic Nb-Ta, W and Sn ore deposits were emplaced is still a controversial topic. Currently, two contrasting tectono-magmatic models exist for the KAB during the Mesoproterozoic, i.e. an intracratonic versus an active margin setting (e.g. Tack et al. 2010; Debruyne et al. 2015). At the end of the Neoproterozoic, at ~550 Ma, a NS-oriented, Pan African overprint affected the KAB, caused by the amalgamation of Gondwana (Fernandez-Alonso et al. 2012). To clarify the timing of metamorphic and deformational events, an extensive geochronological survey of phyllosilicates from the Gitarama-Gatumba area, West Rwanda, was carried out by step-heating Ar-Ar and in-situ LA-ICP-MS Rb-Sr analyses.

2. Ar-Ar and Rb-Sr results

An Ar-Ar plateau age of 625±2 Ma is obtained for biotite from the rim of bedding-parallel quartz pods. Phyllosilicate pockets observed in inter-boudin quartz veins of a boudinaged pegmatite show Ar-Ar ages between 591±2 Ma (muscovite) and 567±2 Ma (biotite). The Rb-Sr phyllosilicate geochronology results of the Gitarama-Gatumba area can be subdivided into two age populations. First of all, a group of late Meso- to early Neoproterozoic ages (1082 – 893 Ma) can be distinguished. These are all ages of muscovite crystals from various geological contexts (e.g. G4-granite, mylonitized G1-G3 granite, crenulated muscovite schist) which show an extremely large uncertainty (~75 Ma, with an exception of 280 Ma), due to the limited intra-crystal variation in ⁸⁷Rb/⁸⁶Sr-ratio. Within error, the ages are contemporaneous, with an average of around 954 Ma. Second, a group of much younger, late Neoproterozoic to early Cambrian ages was observed, mostly for biotite, but in some cases also for muscovite. The muscovite ages vary between 609±140 and 526±86 Ma, the biotite ages between 531±3 and 486±5 Ma.

3. Discussion and conclusion

The oldest Rb-Sr age population (average of 954 Ma) can be linked to pervasive metasomatism associated with the G4 granite intrusions or regional cooling till below the muscovite Rb-Sr closure temperature (500 – 550 °C). This is reflected by the contemporaneous ages of multiple, petrographically different muscovite samples. A distinction between the two possibilities cannot be made. The oldest Ar-Ar biotite plateau age suggests the temperature had dropped to 300 – 350 °C by 625±2 Ma. However, Ar-Ar age spectra demonstrate that partial isotope resetting took place in inter-boudin phyllosilicate at 591±2 and 567±2 Ma. The youngest group of Rb-Sr ages also indicates that widespread recrystallization, mainly of biotite, took place at a later stage. This partial to complete resetting corresponds to the late Neoproterozoic hydrothermal activity in the area, which has been reported by Cahen et al. (1984) and others.

Unfortunately, the phyllosilicate geochronological data do not provide information on Mesoproterozoic deformation events. Nevertheless, the phyllosilicate ages of the Gitarama-Gatumba area indicate the occurrence of multiple important geological events in West Rwanda, and by extension in the Western Domain of the KAB, during the late Neoproterozoic to early Cambrian. Regional closure to temperature-driven diffusion was reached prior to 625±2 Ma, both for the Rb-Sr and Ar-Ar systems. Therefore, younger obtained ages record the occurrence of recrystallization due to local deformation and fluid circulation. These processes affected the phyllosilicates from shortly prior to the assembly of Gondwana in the east (around 550 Ma) till at a syn- to post-amalgamation stage.

References

- Cahen, L., Snelling, N., Delhal, J., Vail, J., Bonhomme, M., & Ledent, D., 1984. The geochronology and evolution of Africa. Oxford University Press, Oxford
- Debruyne, D., Hulsbosch, N., Van Wilderode, J., Balcaen, L., Vanhaecke, F., & Muchez, P., 2015. Regional geodynamic context for the Mesoproterozoic Kibara Belt (KIB) and the Karagwe-Ankole Belt: Evidence from geochemistry and isotopes in the KIB. *Precambrian Research*, 264, 82–97.
- Fernandez-Alonso, M., Cutten, H., De Waele, B., Tack, L., Tahon, A., Baudet, D., & Barritt, SD., 2012. The Mesoproterozoic Karagwe-Ankole Belt (formerly the NE Kibara Belt): The result of prolonged extensional intracratonic basin development punctuated by two short-lived far-field compressional events. *Precambrian Research*, 216–219, 63–86.
- Tack, L., Wingate, MTD., De Waele, B., Meert, J., Belousova, E., Griffin, B., Tahon, A., & Fernandez-Alonso, M., 2010. The 1375 Ma “Kibaran event” in Central Africa: Prominent emplacement of bimodal magmatism under extensional regime. *Precambrian Research*, 180, 63–84.

Pressure-temperature evolution during the Mesoproterozoic in the Western Domain of the Karagwe-Ankole Belt, Central-Africa

Johanna VAN DAELE¹, Niels HULSBOSCH¹, Alexander MONDELAERS¹, Stijn DEWAELE², Philippe MUCHEZ¹

¹ *KU Leuven, Geodynamics and Geofluids Research Group, Department of Earth and Environmental Sciences, Celestijnenlaan 200E, 3001 Leuven, Belgium*

² *Ghent University, Department of Geology, Krijgslaan 281, S8, 9000 Ghent, Belgium*

1. Introduction and geological setting

The Karagwe-Ankole Belt (KAB) is an important Mesoproterozoic orogenic entity in Central Africa, which covers Rwanda, Burundi and parts of the D.R. Congo, Tanzania and Uganda. Metasediments of this belt are intruded by two S-type granite generations, dated at ~1375 and ~986 Ma respectively, and numerous diorite intrusions (Tack et al. 2010). Additionally, abundant Nb-Ta, W and Sn ore deposits are present, of which a genetic link with the youngest granite generation has been established quantitatively (Hulsbosch et al. 2014, 2016; Van Daele et al. submitted). However, two contrasting tectono-magmatic models currently exist for the KAB during the Ectasian and Stenian period of the Mesoproterozoic era. In the first model, the area is interpreted as an intracratonic setting with anorogenic magmatism at 1375 Ma. The main compressional deformation took place around 1000 Ma and has been related to far field tectonics associated to the southern Irumide Orogeny (e.g. Tack et al. 2010). In the second model, an active continental margin at 1375 Ma is envisaged (e.g. Debruyne et al. 2015). According to this model, the 1 Ga granite magmatism is linked to the Rodinia amalgamation and indicates a renewed convergence and associated deformation. Information on the geodynamics is essential to get a more detailed understanding of the mineralization processes. This abstract presents the results of a detailed geothermobarometry study of the Mesoproterozoic metasediments in the Western Domain of the KAB. The study areas are located in West Rwanda, near the cities of Kibuye, Gitarama and Gatumba.

2. Results

Mineral growth in response to different metamorphic processes in the Kibuye-Gitarama-Gatumba (KGG) area were identified by thin section petrography. Garnet, staurolite and kyanite are part of the regional metamorphic mineral assemblage. In contrast, andalusite typically was observed in rocks affected by contact metamorphism. Additional granite contact-metamorphic effects are biotitization, muscovitization and occasionally silicification, while metasediments in close contact with diorites are intensely chloritized and sometimes contain hornblende. Metasomatism is widespread and intense in the metapelitic rocks, especially in the Gitarama-Gatumba area, and resulted in the crystallization of tourmaline, sericite, chlorite and chrysoberyl. The main retrograde effect is chloritization of biotite.

Fifteen representative samples have been selected for garnet-biotite, amphibole-plagioclase and chlorite geothermometry. The peak temperature of regional metamorphism was determined at ~540 °C, as evidenced by garnet-biotite and chlorite geothermometry of multiple samples from

different locations and geological contexts. A slightly higher temperature of ~570 °C was observed in amphibole-feldspar pairs in hornfels rock, interpreted as an effect of diorite contact metamorphism. Lastly, chlorite which formed due to metasomatism indicate a formation temperature of ~455 °C.

Pseudosection modelling confirmed the regional metamorphism temperature of ~550 °C. Garnet core and rim compositional data allowed to further constrain the pressure evolution. According to the modelling, peak metamorphic conditions were reached at ~9.5 kbar, after which isothermal decompression to ~8.5 kbar took place.

3. Interpretation and discussion

The Mesoproterozoic peak regional metamorphism in the KGG area is interpreted to be of upper greenschist facies (550 °C, 9.5 kbar), while the diorite intrusions locally induced lower amphibolite facies conditions (570 °C). Even during the Neoproterozoic metasomatism, the area was still affected by the circulation of high-temperature fluids (455 °C). The geothermometry data demonstrate that high temperature conditions prevailed in the KGG area for a significant time, which should be taken into account in future geochronological interpretations. Furthermore, the obtained P-T data and observed isothermal decompression indicate a typical clockwise, Barrovian-type P-T-path. Generally, such P-T path is the consequence of crustal thickening followed by thermal relaxation. The intermediate temperature and preliminary relatively high pressure values in the KGG area correspond more to an active margin setting than an intracratonic compression of the KAB during the Mesoproterozoic. However, the findings of this geothermobarometry study should be combined with geochronological data to reconstruct the geodynamic setting in more detail.

References

- Debruyne, D., Hulsbosch, N., Van Wilderode, J., Balcaen, L., Vanhaecke, F., & Muchez, P., 2015. Regional geodynamic context for the Mesoproterozoic Kibara Belt (KIB) and the Karagwe-Ankole Belt: Evidence from geochemistry and isotopes in the KIB. *Precambrian Research*, 264, 82–97.
- Hulsbosch, N., Boiron, M-C., Dewaele, S., & Muchez, P., 2016. Fluid fractionation of tungsten during granite–pegmatite differentiation and the metal source of peribatholithic W quartz veins: Evidence from the Karagwe-Ankole Belt (Rwanda). *Geochimica et Cosmochimica Acta*, 175, 299–318.
- Hulsbosch, N., Hertogen, J., Dewaele, S., André, L., & Muchez, P., 2014. Alkali metal and rare earth element evolution of rock-forming minerals from the Gatumba area pegmatites (Rwanda): Quantitative assessment of crystal-melt fractionation in the regional zonation of pegmatite groups. *Geochimica et Cosmochimica Acta*, 132, 349–374.
- Tack, L., Wingate, MTD., De Waele, B., Meert, J., Belousova, E., Griffin, B., Tahon, A., & Fernandez-Alonso, M., 2010. The 1375 Ma “Kibaran event” in Central Africa: Prominent emplacement of bimodal magmatism under extensional regime. *Precambrian Research*, 180, 63–84.
- Van Daele, J., Hulsbosch, N., Dewaele, S., Boiron, M-C., Piessens, K., Boyce, A., & Muchez, P., 2018. Mixing of magmatic-hydrothermal and metamorphic fluids and the origin of peribatholithic Sn vein-type deposits in Rwanda. *Submitt Ore Geol Rev*

The unexpected presence of supergene Cu-Pb-Ca-Zn-Fe arsenates and vanadates in Agoujgal Cu-mine (Anti-Atlas, Morocco).

Michèle VERHAERT¹, Lhou MAACHA², Atman MADI², Abdelaziz ELBASBAS², Mohamed ELHARKATY², Abdellah OUMMOUCH², Lahcen OUMOHOU², Johan YANS¹

¹ ILEE, Department of Geology, University of Namur, Rue de Bruxelles 61, 5000 Namur, Belgium. michele-alexandra.verhaert@unamur.be

² Managem Group, BP 5199, 20100 Casablanca, Morocco

A large number of copper deposits are located in the Moroccan Anti-Atlas, particularly at the contact between Precambrian inliers and Cambrian-Adoudounian cover formations. The Agoujgal deposit is located at the southeastern border of the Kerdous inlier, and has been managed by the mining company Managem for its copper (~1%) and silver (~30g/t) ore.

The ores are hosted by Adoudounian silts, sandstones, dolomites, dolomitic sandstones and limestones, and are located on the top of a strongly altered and weathered porphyritic granite and volcanoclastic series. The mineralization is composed of hypogene Cu(-Co-As-Pb-Zn) sulfides that underwent significant weathering, leading to the formation of successive generations of secondary minerals. Supergene minerals are observed as filling of fractures and geodic cavities of the host rock, as impregnations of the gangue, and as *in situ* replacement of the primary mineralization. The usual vertical sequence of weathered copper deposits is not observed at Agoujgal, which may be related to the varying altitude of the weathering front, in accordance with the fracturing and folding of the host rocks. However, the typical paragenetic profile (primary sulfides – secondary sulphides – oxidized minerals – iron oxides or *gossan*) is clearly recognized.

Pyrite and chalcopyrite are the main primary sulfides; bornite (Cu_5FeS_4), tennantite ($\text{Cu}_6\text{Cu}_4(\text{Fe}, \text{Zn})_2\text{As}_4\text{S}_{13}$), cobaltite (CoAsS), bismuthinite (Bi_2S_3), acanthite (Ag_2S), galena (PbS), arsenopyrite (FeAsS), matildite (AgBiS_2), sphalerite (ZnS), greenockite (CdS) and kobellite ($\text{Pb}_{22}\text{Cu}_4(\text{Bi}, \text{Sb})_{30}\text{S}_{69}$) are present in smaller proportions. The first step of weathering of chalcopyrite (and bornite) is the successive transformation in secondary sulfides such as bornite, chalcocite (Cu_2S), djurleite ($\text{Cu}_{31}\text{S}_{16}$) and covellite (CuS). By substituting chalcopyrite and bornite, chalcocite and djurleite form a typical *chickenwire* texture in which they are successively replaced by goethite and malachite (Fig. 1A).

The Cu-oxidized mineralization is much diversified, with carbonates (malachite, azurite), oxides (cuprite, tenorite, goethite), vanadates (mottramite ($\text{PbCu}(\text{VO}_4)(\text{OH})$), calcio-volborthite ($\text{CaCu}(\text{VO}_4)(\text{OH})$)), arsenates (conichalcite ($\text{CaCu}(\text{AsO}_4)(\text{OH})$), olivenite ($\text{Cu}_2\text{AsO}_4(\text{OH})$)), and sulfates (brochantite ($\text{Cu}_4\text{SO}_4(\text{OH})_6$)). These oxidized minerals, in which intergrowths are very common (Fig. 1B), most probably all precipitated within a short period of time. Arsenates are mainly found close to the altered and weathered granite of the basement, but are also observed in smaller amounts in the entire deposit. Conichalcite sometimes replaces a primary mineral of which only the shapes of the crystals remain (Fig. 1C). In some samples, mimetite ($\text{Pb}_5(\text{AsO}_4)_3\text{Cl}$) is weathered in a succession of various minerals including, among others, conichalcite, olivenite,

calcio-duftite ((Pb,Ca)CuAsO₄(OH)), mottramite, calcio-volborthite, Ca-Cu-, Ca-Zn-, and Ca-Fe-arsenates (Fig. 1D, 1E).

The proximity of Agoujgal granite probably enhanced the formation of hydrothermal polymetallic ores and later, the development of secondary minerals due to weathering. Base metals such as Cu, Pb, Zn, As, and V in the supergene minerals most probably derive from the primary sulfides and rocks. The arsenates result from the relative abundance of As-bearing minerals in the primary mineral association; tennantite is thought to be the most significant source of As. V is thought to be included in sulfides, such as galena and pyrite. During weathering, As and V are mobilized and recombined with available ions to be precipitated at favorable sites or barriers, such as the contact with the granite at Agoujgal. Vanadates, i.e. mottramite, preferably precipitate under low Eh and acidic conditions arising from sulfides weathering. Cation substitutions and solid solutions are common in arsenates, which might explain the abundance of mixed Ca-Cu-Zn-Fe arsenates at Agoujgal. For instance, conichalcite and calcio-duftite form a solid solution and are often replacing one another. The successive transformation of mimetite in calcio-duftite and later in olivenite is related to a rise of the Cu content; the inverse replacement of olivenite by calcio-duftite is associated with local pH rises. The presence of conichalcite or olivenite depends on geochemical parameters: conichalcite prefers basic pH and low Eh conditions, whereas olivenite precipitates from more acid fluids that are characterized with a lower Cu- activity.

Iron (hydr-)oxides show different forms: powdery, as pseudomorphs of pyrite, and botryoïdal. Hematite and goethite are mixed in all samples. Two generations of pyrite, one cubic and the other rhombododecaedral, are replaced by goethite and hematite in layers that follow the stratification (Fig. 1F). In these samples, goethite is observed at the center of the structures, and hematite at the edges, which could indicate dehydration processes. Late greenish Zn-calcite is cutting the entire sequence, sometimes leading to the formation of brecciated units.

Arsenates-bearing samples are rich in LREE, reaching ~900 ppm of La, ~1500 ppm of Ce, and ~500 ppm of Nd, which is consistent with the observation of monazite. Vanadates are slightly enriched in HREE, but values are not exceeding ~200 ppm. The As, Pb and Zn contents are particularly high for all the Agoujgal samples, and related to the presence of these elements in the primary (i.e. in sphalerite) and secondary (i.e. in smithsonite) mineralization. Arsenates are also rich in Bi (~1600 ppm) and Mo (~1000 ppm), and mottramite in Y (~1800 ppm).

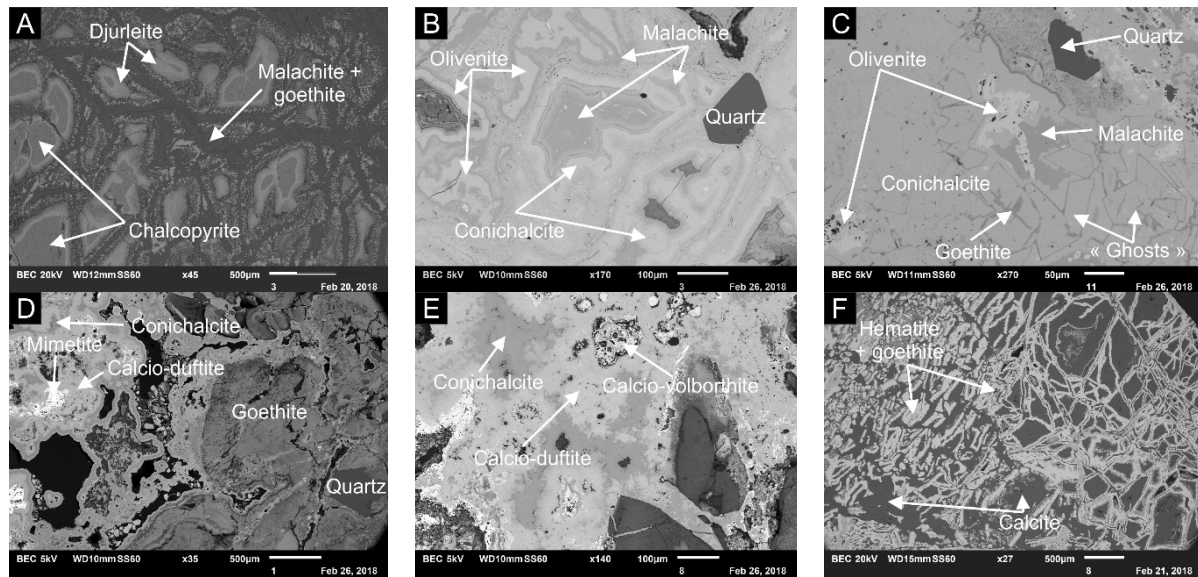


Figure 1. SEM photomicrographs in backscattered electrons mode.

Geothermal use of old mines: hydrogeological challenges for predicting efficiency and impacts

Olivier VOPAT^{1,2}, Philippe ORBAN¹, Serge BROUYERE¹ and Alain DASSARGUES¹

¹ *Hydrogeology & Environmental Geology, Urban & Environmental Eng., University of Liège, B52 Sart Tilman, 4000 Liège*

² *ABO-Group, Rue Haigniaux, 23, 5300 Namêche*

1. Introduction

Groundwater in flooded abandoned mines could be used for geothermal purposes using heat-pumps and an open loop involving pumping and re-injection. This kind of low temperature geothermal doublet belongs to the aquifer thermal energy storage (ATES) systems. Usually, hydraulic conductivity values of the considered rock zones have been significantly increased by mining exploitation. Therefore, these zones can be often considered as aquifers. In any case, accurate hydrogeological characterization of the old mined zones is needed to gain a minimum knowledge about these variably fractured rock zones together with the remaining network of shafts and galleries.

2. Hydrogeological and geothermal conditions in old mines

Depending on the type of abandoned mine, the true geometry of the interconnected network of open galleries and shafts can be highly complex (Figure 1). A high-velocity water flow is expected in this network, while low-velocity groundwater flow occurs in the permeable fractured and porous rocks. Logically, hot water is expected to be pumped in the deep parts of the open network, and cold water is expected to be re-injected in the shallower parts (i.e. in shallower galleries or fractured rocks).

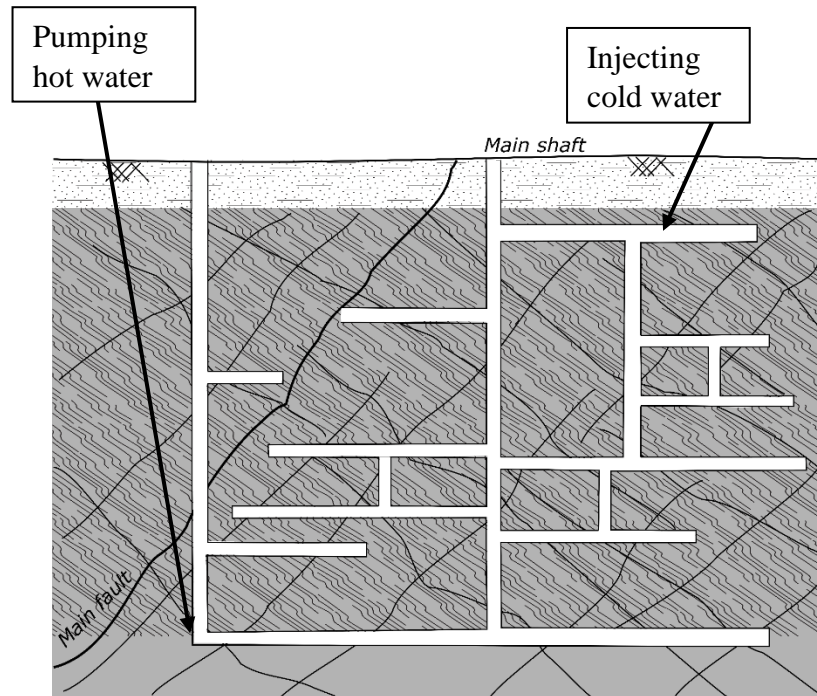


Figure 1. Schematic 2D vertical view of a simplified old mine network. In Belgium, old shafts could have been refilled with backfill materials, therefore it could be more efficient to drill new boreholes that directly reach the deep ancient open galleries for pumping hot water and reinjecting cold water (modified from Dassargues 2018).

3. Challenges and first results

Indeed, to assess the efficiency and the possible impacts of geothermal doublets in old mines, it could be critical to simulate the groundwater flow and associated temperature evolution in the pumping zones. Numerical simulations of such geothermal systems are not easy: variable density water flow and coupled heat transport must be simulated with a software allowing to describe accurately a combination of high-velocity ‘pipe-like’ water flows (in the galleries) and porous/fractured groundwater flow (in the rock matrix). The SUFT3D code allows to combine linear or distributed reservoirs to model groundwater flows in mine galleries and classical groundwater flow in the variably saturated equivalent porous surrounding media (Brouyère et al. 2009, Wildemeersch et al. 2010). Recent developments (Vopat 2017) allowed also to simulate the associated heat transfers using the similarities existing between solute and heat transport equations.

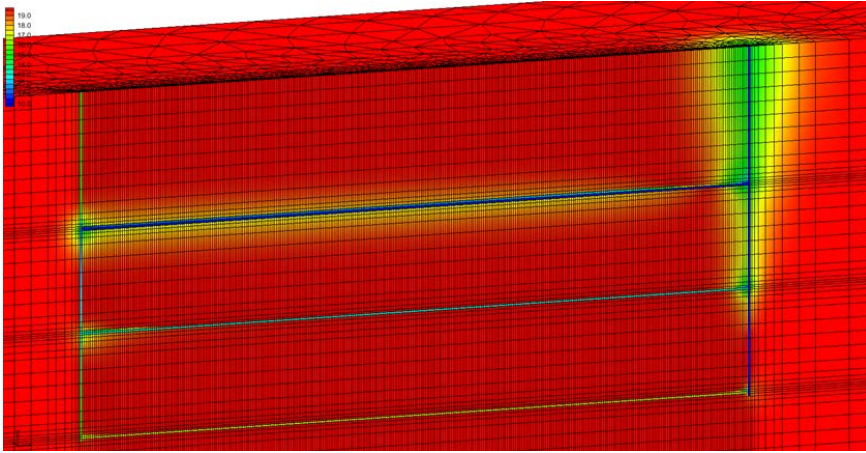


Figure 2. First results (using SUFT3D) showing the simulated stabilized (after 800 days) temperatures with a 130 m³/h pumping initially at 19°C at the bottom of the left shaft (at a 500m depth) and reinjection at 10°C at the top of the right shaft (results are shown for a $K_{\text{shaft}}/K_{\text{rocks}}$ ratio of 10^4 ; from Vopat 2017).

Results are showing clearly the differentiated temperatures as a consequence of heat/cold propagation in the galleries, shafts and the fractured rocks. Actual cases in relation with future projects, should thus be simulated taking the whole complexity/heterogeneity of the galleries network conjugated to the old mined rocks. Challenges will have still to be tackled in terms of characterization and numerical simulation with actual data. However, it is only on the basis of accurate predictions that the financial risk associated with such new geothermal systems could be assessed for further practical decisions.

References

- Brouyère, S., Orban, P., Wildemeersch, S., Couturier, J., Gardin, N. & Dassargues, A., 2009. The Hybrid Finite Element Mixing Cell Method: A New Flexible Method for Modelling Mine Groundwater Problems. *Mine Water & the Environment* 28(2): 102-114
- Dassargues, A., 2018. *Hydrogeology: groundwater science and engineering*. Boca Raton: CRC Press.
- Vopat, O., 2017. *Modélisation des caractéristiques hydrogéologiques liées à une exploitation géothermique d'anciennes mines*. Master Thesis. Engineering Faculty. ULiege, 115p.
- Wildemeersch, S., Brouyère, S., Orban, P., Couturier, J., Dingelstadt, C., Veschkens, M. & Dassargues, A., 2010. Application of the Hybrid Finite Element Mixing Cell method to an abandoned coalfield in Belgium. *Journal of Hydrology* 392 (3-4): 188-200.

Economic and environmental comparison of CO₂ storage and enhanced oil recovery project configurations in the North Sea

Kris WELKENHUYSEN^{1,2}, Tine COMPERNOLLE^{1,3}, Bruno MEYVIS¹, Michele MORETTI^{4,5}, Kris PIESENS¹, Pieter ROEFS³ & Rudy SWENNEN²

¹ *Geological Survey of Belgium – Royal Belgian Institute of Natural Sciences, Jennerstraat 13, 1000 Brussels, Belgium*

² *Department of Earth and Environmental Sciences, KU Leuven, Celestijnenlaan 200E, 3001 Heverlee, Belgium*

³ *Departement of Economics - University of Antwerp, Prinsstraat 13- 2000 Antwerp, Belgium*

⁴ *Centre of Environmental Sciences, Hasselt University, Agoralaan Building D - 3590 Diepenbeek, Belgium*

⁵ *University of Liege, Gembloux Agro-Bio Tech, Economy and Rural Development Unit, Passage des Déportés 2, 5030, Gembloux, Belgium*

1. Introduction

The EU has set ambitious goals on the reduction of CO₂ emissions into the atmosphere for limiting the effects of global warming. And while renewable alternatives are available in some cases, long-term storage of large quantities of produced CO₂ seems inevitable. Because the process of capturing, transporting and injecting CO₂ into a reservoir (CO₂ capture and storage, CCS) is costly and current revenues from the EU emission trading system (ETS) are insufficient to cover the expenses, the commercial deployment of CCS is delayed in Europe. A potential business case for CO₂ geological storage (CGS) is CO₂-enhanced oil recovery (CO₂-EOR), where CO₂ is used to drive out 5-15% additional oil after the application of primary and secondary recovery techniques. Within Europe, the North Sea is the main oil province with a high potential for CO₂-EOR. Earlier studies have concluded that off-shore CO₂-EOR projects are a viable business case, but no investments have been made yet. Moreover, adversaries of this technology often point out that CO₂-EOR is not a climate-friendly solution because its goal is to increase and lock-in fossil fuel production.

2. Economic and environmental analysis

To investigate the potential of CO₂-EOR, an integrated geological, techno-economic and environmental analysis is made of a potential candidate for EOR in the North Sea: the Buzzard oil field (Roefs et al., in press). A techno-economic spreadsheet calculation is made for different injection scenarios. The net present value (NPV) is calculated as the discounted cash flows over time. A full-sized coal-fired power plant is assumed, producing about 4 MtCO₂/y, of which the Buzzard field can accept 2.9 Mt/y for EOR. A second injection location in an aquifer is also assumed. The market scenario is chosen at an oil price of 50 €/bbl, and an ETS price at 5 €/t. In parallel, a life cycle assessment (LCA) is conducted to compare the environmental impact, considering emissions from the additional construction and operation of the capture plant and EOR operation. Results are expressed as the global warming potential (GWP). Four scenarios are considered: CO₂ capture and storage in an offshore aquifer; CO₂-EOR in the Buzzard field followed by emission into the atmosphere; CO₂-EOR and parallel aquifer storage; and CO₂-EOR and parallel aquifer storage, with a continuation of storage in the Buzzard field after the cease of oil production.

For the first time such an integrated economic and environmental analysis is made comparing CGS and EOR.

Results show that the scenario with only CGS has the lowest GWP (reference level for the other scenarios), but the NPV is negative (-800 M€) and thus does not provide a viable investment option. The scenario with only EOR has the highest NPV (>500 M€), but also has the highest GWP, 38% higher than the storage-only scenario. The results for the third and fourth scenario are very similar, with a GWP of 11% more than the storage-only scenario, and an NPV of 207 and 220 M€ respectively. This shows that CO₂-EOR can be a viable investment that, when combined with CO₂ storage, only has a minor additional environmental impact over a storage-only project. EOR can thus also serve as an enabler for CGS, with a widespread storage deployment when the necessary infrastructure is in place. It is also beneficial to use the depleted oil field for storage (fourth scenario) over aquifer storage (third scenario), because the necessary infrastructure is already present. From a sustainability perspective this also makes sense, as it allows for a more efficient use of geological resources.

3. Geo-economic simulation

The analysis shows that even at low oil and CO₂ prices, EOR projects can be viable. Since no projects are (soon becoming) operational, other factors are influencing the economic viability too. A more advanced geo-economic analysis is therefore performed with the PSS simulator from the point of view of an investor for the Buzzard field. In a more realistic approach, investment decisions are simulated, considering limited foresight generated by market and reservoir uncertainty. Results show that an increased hurdle rate results in a lower chance of a negative project value (Fig. 1, Welkenhuysen et al., *subm.*). A hurdle rate of 12% removes all project risk, but also eliminates potentially viable projects. At an oil price of 50 €/bbl, the threshold for EOR investment occurs at 0 €/tCO₂ (green dotted line; excluding capture cost). The discrepancy with the cost for capture is too much to be covered by the current CO₂ market price of around 15 €/t (June 2018). CO₂-EOR with or without CGS in the North Sea therefore does not come forward as commercially viable from this study, where, in comparison to state-of-the-art assessments, more realistic economic and geological uncertainties are used. It does, however, have strategic and environmental benefits compared to a situation where oil is imported into the EU. In that context, incentives to reduce the cost and/or risk could be justified. Future research will focus on the establishment of contractual agreements between the parties, including uncertainty in the environmental analysis, and the scarcity cost of storage capacity as a limited commodity will be taken into account.

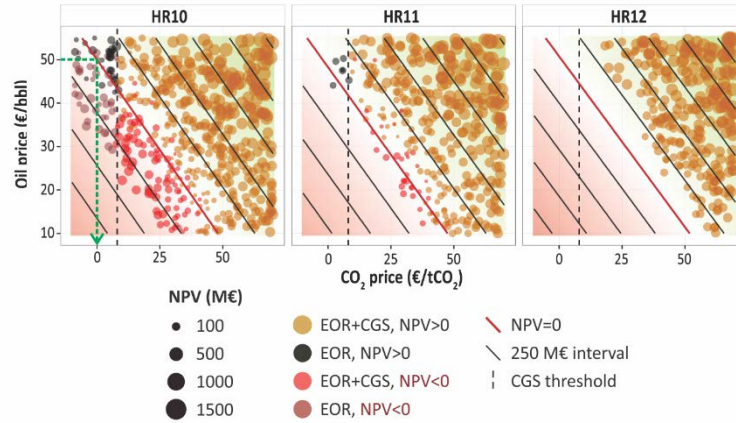


Figure 1. Results of the PSS IV simulation of the Buzzard field for different hurdle rates (HR10, HR11 and HR12). Negative project values are shown in red/brown. To the right of the dotted vertical threshold line are projects with CGS after the EOR phase.

References

- Roefs, P., Moretti, M., Welkenhuysen, K., Piessens, K. & Compennolle, T., in press. CO₂-enhanced oil recovery and CO₂ capture and storage: an environmental economic trade-off analysis. 13th Conference on Sustainable Development of Energy, Water and Environment Systems (SDEWES), Palermo, 2018.
- Welkenhuysen, K., Meyvis, B., Swennen, R., & Piessens, K., subm. Economic threshold of CO₂-EOR and CO₂ storage in the North Sea: a case study of the Claymore, Scott and Buzzard oil fields. International Journal of greenhouse Gas Control.

Petrographic study of gold mineralization in the Karagwe-Ankole belt (Byumba, Rwanda)

Sander WOUTERS¹, Stijn DEWAELE², Philippe MUCHEZ¹

¹ *KU Leuven, Department of Earth and Environmental Sciences, Celestijnenlaan 200E, B-3001 Leuven, Belgium*

² *Ghent University, Department of Geology, Krijgslaan 281, S8, 9000 Ghent, Belgium.*

1. Geological setting

The Mesoproterozoic Karagwe-Ankole belt (KAB) is a metallogenic province in Central Africa which is well known for hosting different types of granite-related rare metal (Nb, Ta, Sn, W) and also gold deposits (Fernandez-Alonso et al., 2012; Pohl & Günther, 1991). It extends from the eastern part of the Democratic Republic of Congo (DR Congo) into Burundi, Rwanda, northwest Tanzania and southwest Uganda. Previous studies demonstrated that the metal source for the Nb-Ta-Sn-W mineralization in pegmatites, greisens and peribatholithic quartz veins, are syn-to post orogenic early-Neoproterozoic leucogranites (Dewaele et al., 2011; Hulsbosch, et al., 2016), while the Central African orogenic gold mineralization has been related to fold-and-thrust belt formation (Koegelenberg et al., 2016). However, detailed knowledge of the metallogenic source, evolution and age of the Au mineralization in the KAB is largely missing (Pohl et al., 2013). Therefore, the metallogenic study of KAB Au occurrences forms an excellent opportunity to investigate the contribution of magmatic, metamorphic and water-rock interaction processes related to mineralization in an orogenic belt.

2. Methodology & results

The Byumba gold deposit, situated in the north of Rwanda, was selected for study due to its comparable position in the Mesoproterozoic metasedimentary stratigraphy and structural trend as the well-studied W- and Sn-deposits, allowing a straightforward comparison. From this location, a total of 9 boreholes (± 1800 m) were logged and sampled with the aim to determine the structural setting and timing of ore deposition and the origin and evolution of the mineralizing fluids. Core logging was carried out with special attention to lithological variations, alteration, deformation structures, different vein generations and their relation to the ore grade.

The general lithology is comprised of alternations of sand- to siltstone, with organic-rich shale, which host multiple quartz vein generations. These quartz veins contain varying amounts of chlorite, carbonate and pyrite. Several meter-thick shear zones were identified that are characterized by the occurrence of C'-type shear bands. These shear zones are heavily chloritized and host several deformed quartz veins which are parallel to the foliation. Thin and polished section petrography of the samples reveals the presence of pervasive chloritization, some sericitization, silicification, carbonitization and multiple pyrite generations which are associated with some minor sulfides.

3. Paragenetic sequence of veining and mineralization

A first bedding-parallel quartz vein generation has been folded and is interpreted to predate tectonic deformation. A second and third generation of quartz veins occur in the hinge zones of folds and in faults, respectively. They can be associated with massive pyrite, together with some smaller

irregular chlorite-rich veins inside the fold hinges. Quartz veins belonging to a fourth generation developed parallel to the cleavage and are sometimes boudinaged. These quartz veins do not always follow the bedding, but crosscut sandstones at an angle of 45°-60°, giving them a sigmoidal geometry. At least two distinct sigmoidal vein generations have been recognized. The first generation of these veins is filled with quartz, chlorite and sericite, and is crosscut by a generation consisting of quartz and Fe-rich carbonate. As expressed by these sigmoidal veins and shear zones, a distinct phase of shearing post-dates folding and cleavage development, characterized by silicification and intense chloritization. Preliminary results, based on the ore grade distribution, suggest that gold mineralization at Byumba could have been emplaced during this phase. Finally, cm to m-thick massive quartz veins crosscut the folds, cleavage and all former quartz generations. Often these veins contain fragments of the host-rock and are thus related to a brecciation phase.

Multiple pyrite generations are present in the metasediments. Many of the early pyrite generations are anhedral and contain chalcopyrite blebs. A pre-deformation origin is evidenced by the presence of quartz-filled pressure shadows around these pyrites. Younger, more euhedral, pyrite is associated with pyrrhotite. Many of the later pyrite generations are related to folding and shearing and the associated veining. Notably, a generation of large euhedral pyrites is clearly associated with, but post-dates, the late carbonitization phase associated with shearing.

An important secondary gold enrichment phase is present, as evidenced by the high ore grade associated with oxidation/reduction zone boundaries. The primary gold hosting phases have not yet been directly observed by the used petrographic techniques. However, with the help of different analytical techniques like FEG-EPMA, LA-ICP-MS and ChemScan, the hosting phase(s) of this 'invisible' gold will be identified in the future.

References

- Dewaele, S., Henjes-Kunst, F., Melcher, F., Sitnikova, M., Burgess, R., Gerdes, A., Fernandez-Alonso, M., De Clercq, F., Muchez, P., Lehmann, B., 2011. Late Neoproterozoic overprinting of the cassiterite and columbite-tantalite bearing pegmatites of the Gatumba area, Rwanda (Central Africa). *Journal of African Earth Sciences*, 61, 10–26.
- Fernandez-Alonso, M., Cutten, H., De Waele, B., Tack, L., Tahon, A., Baudet, D., & Barritt, S. D., 2012. The Mesoproterozoic Karagwe-Ankole Belt (formerly the NE Kibara Belt): The result of prolonged extensional intracratonic basin development punctuated by two short-lived far-field compressional events. *Precambrian Research*, 216–219, 63–86.
- Hulsbosch, N., Boiron, M. C., Dewaele, S., & Muchez, P., 2016. Fluid fractionation of tungsten during granite-pegmatite differentiation and the metal source of peribatholithic W quartz veins: Evidence from the Karagwe-Ankole Belt (Rwanda). *Geochimica et Cosmochimica Acta*, 175, 299–318.
- Koegelenberg, C., Kisters, A. F. M., & Harris, C., 2016. Structural controls of fluid flow and gold mineralization in the easternmost parts of the Karagwe-Ankole Belt of north-western Tanzania. *Ore Geology Reviews*, 77, 332–349.
- Pohl, W., & Günther, M. A., 1991. The origin of Kibaran (late Mid-Proterozoic) tin, tungsten and gold quartz vein deposits in Central Africa: a fluid inclusions study. *Mineralium Deposita*, 26, 51–59.
- Pohl, W. L., Biryabarema, M., & Lehmann, B., 2013. Early Neoproterozoic rare metal (Sn, Ta, W) and gold metallogeny of the Central Africa Region: a review. *Applied Earth Science*, 122, 66–82.

Petrography and geochemistry of Cu-Zn VMS deposits of the Troodos ophiolite, Cyprus

Nina ZARONIKOLA¹, Vinciane DEBAILLE¹, Sophie DECREE², Ryan MATHUR³, Ioulia GEORGIADOU GAVRILOVIC⁴ & Christodoulos HADJIGEORGIOU⁴

¹ *Laboratoire G-Time, Universite Libre de Bruxelles, Brussels, Belgium*

² *Royal Belgian Institute of Natural Sciences, B-1000 Brussels, Belgium*

³ *Juniata College, 1700 Moore Street, Huntingdon, Pennsylvania 16652, USA*

⁴ *Geological Survey Department, 1 Lefkonos Street, 2064 Strovolos, Lefkosia, Cyprus*

Ophiolites are fossil oceanic crust that has been uplifted above sea level after subduction (Moore and Jackson, 1974). For that reason, they offer one of the easiest ways to study the oceanic crust. Notably, seawater related hydrothermal fluids circulations and subsequent alteration are likely amongst the most important mechanisms that modify the trace element budget of the oceanic crust and influence the recycling of trace elements in subduction zones. The above mentioned mechanism can lead to very large ore deposits, due to the mobilization and accumulation of some elements such as metals (Cu, Zn, Au...).

The Troodos ophiolite is generally considered as a volcanogenic massive sulfide (VMS) with primary massive sulfides, such as chalcopyrite, pyrite and sphalerite (USGS, 2017), which are partly affected by supergene alteration and hydrothermal alteration (e.g., Parvaz, 2014). Supergene alteration leads to the enrichment of the mineralization in Cu, with a paragenesis of secondary sulfides (chalcocite, covellite, bornite...; e.g. Pantazis, 1978) that differs significantly from the primary massive sulfide mineral assemblage.

To be more precise, the sulfides that can be found in the Troodos ophiolite, are divided into three zones (Constantinou and Govett, 1973). The first part is the upper part of the VMS with >40% of S, dominated by pyrite with some chalcopyrite and covellite in fractures. The second part corresponds to the medium part composed of pyrite-quartz assemblage and with 30<S<40%; and the last is the lower stockwork part with <30% of S. Copper makes up to 2.5 % of those deposits (Constantinou and Govett, 1973). In addition to the above sulfides, seafloor alteration of the VMS deposits has contributed to the formation of submarine gossans (highly weathered and oxidized Fe-rich rocks), which are enriched in Au at Troodos (Herzig et al., 1991).

We will present the petrography and the geochemistry of the VMS deposits from different regions/mines of the Troodos ophiolite. Notably, we plan using non-traditional stable isotopes like Cu and Zn to investigate the origin of fluids that circulated within the Troodos ophiolite and led to primary and secondary Cu-bearing sulfide deposits.

References

- Constantinou, G. & Govett, G. J. S., 1973. Geology, geochemistry, and genesis of Cyprus sulfide deposits. *Economic Geology*, 68 (6): 843-858.
- Herzig, P. M., Hannington, M. D., Scott, S. D., Maliotis, G., Rona, P. A., & Thompson, G., 1991. Gold-rich sea-floor gossans in the Troodos Ophiolite and on the Mid-Atlantic Ridge. *Economic Geology*, 86(8), 1747-1755.

Moore, E.M & Jackson, E.D., 1974. Ophiolites and oceanic crust. *Nature*, v.250, p.136–139.

Pantazis, T.M., 1978. Cyprus evaporites. D.A. Ross, Y.P. Neprochnov et al. *Init. Rep. DSDP*, 42 (2): 1185–1194.

Parvaz, 2014. Oxidation Zones of Volcanogenic Massive Sulphide Deposits in the Troodos Ophiolite, Cyprus: Targeting Secondary Copper Deposits (Phd Thesis). University of Exeter, p.326.

USGS, 2017. Descriptive model of Cyprus massive sulfide.

Theme 5

Hydrology and environmental geology for the future

Seawater intrusion in coastal areas of arid and semi-arid regions

Nawal ALFARRAH^{1,2} & Kristine WALRAEVEN¹

¹Laboratory for Applied Geology and Hydrogeology, Department of Geology, Ghent University. Krijgslaan 281 S8, Ghent 9000, Belgium. *nawalr2003@yahoo.com & kristine.walraevens@ugent.be

²Geology Department, Az Zawiyah University, Az Zawiyah, Libya.

The exploitation of groundwater resources is of high importance and has become very crucial in the last decades, especially in coastal areas of arid and semi-arid regions. The coastal aquifers in these regions are particularly at risk due to intrusion of salty marine water. One example is the case of Tripoli city at the Mediterranean coast of Jifarah Plain, North West Libya. Libya has experienced progressive seawater intrusion in the coastal aquifers since the 1930s because of its ever increasing water demand from underground water resources. Tripoli city is a typical area where the contamination of the aquifer in the form of saltwater intrusion is very developed. Sixty-four groundwater samples were collected from the study area and analyzed for certain parameters that indicate salinization and pollution of the aquifer. The results demonstrate high values of the parameters Electrical Conductivity, Na⁺, K⁺, Mg²⁺, Cl⁻ and SO₄²⁻, which can be attributed to seawater intrusion, where Cl⁻ is the major pollutant of the aquifer. The water types according to the Stuyfzand groundwater classification are mostly CaCl, NaCl and Ca/MgMix. These water types indicate that groundwater chemistry is changed by cation exchange reactions during the mixing process between freshwater and seawater. The intensive extraction of groundwater from the aquifer reduces freshwater outflow to the sea, creates drawdown cones and lowering of the water table to as much as 25 m below mean sea level. Irrigation with nitrogen fertilizers and domestic sewage and movement of contaminants in areas of high hydraulic gradients within the drawdown cones probably are responsible for the high NO₃⁻ concentration in the region.

Clays in drilling muds: technical considerations and environmental implications

Samira BABA HAMED¹ & Nathalie FAGEL²

¹ *Université des Sciences et de la Technologie d'Oran – Mohamed Boudiaf, USTO, Algérie, Laboratoire de rhéologie, transport et traitement des fluides complexe; samira.babahamed@univ-usto.dz*

² *Université de Liège, Département de Géologie, UR AGEs - Argiles, Géochimie et Environnements sédimentaires.*

Clays provide great benefits in the petroleum industry; they are used as additives in the composition of drilling muds. The choice of clay depends on the nature of geological strata, and has a direct impact on the drilling speed, its safety and its cost. As additives in drilling fluids, clays require specific physico-chemical characteristics to adapt optimally to the most varied drilling conditions, in compliance with economic and environmental constraints. Bactericide is the most polluting components in drilling mud. In this study, two water based muds formulations with clay and weighting material were tested; we investigated the effect of different products in order to obtain ecological drilling muds. The raw clays were characterized using X-ray diffraction; these clays enhance the viscosity of drilling muds. The rheology of those formulations was determined. The samples take into account the environmental field as well as the proximity of the groundwaters and constitute a non-polluting alternative for ecological drilling muds.

1. Introduction

The swelling of clay formations may be responsible for several disorders during oil drilling, with economic consequences. Onaisi et al, (1994) consider that the main disorders encountered are the instability and widening of the wall of the wellbore and stem distortion during drilling. In extreme cases, it could result in the collapse of the well and so its closure. If the area is potentially productive, it is recommend to drill in the vicinity of the first drilling in order to keep the same characteristics initially determined (drilling muds, depth). Dzialowski et al (1998) reported that shale makes up to 75 percent of all drilled formations worldwide and that over 90% of the instability challenges arise in shale formations. Disorders caused by swelling clays in wells oil companies are estimated at \$ 500 million per year in United States as argued by Oort et al (1996). This study is motivated by problems encountered in directional drilling as collapse of wells, falling cuttings, well instability, and loss of fluid through the porous formations so favor the pollution of formations.

2. Material and methods

As a result of clay characteristics, technical and environmental, the petroleum industry use clay as the main constituent of drilling fluids, the studied water based muds formulations are compliant with American petroleum institute (API) standards. In the first step, two clays were studied, and their mineralogical compositions were determined using X-ray diffraction. Secondly, the tested clays were compared with High Mod Prima (HMP), initially characterized by Baba Hamed and Belhadri (2009) and used in water based mud. Finally, rheological characterization of samples was measured by a rheometer.

3. Results and discussion

Figure 1 shows XRD patterns of clays used in drilling muds. In practice, bentonite is used for freshwater mud and attapulgite for saturated salt mud.

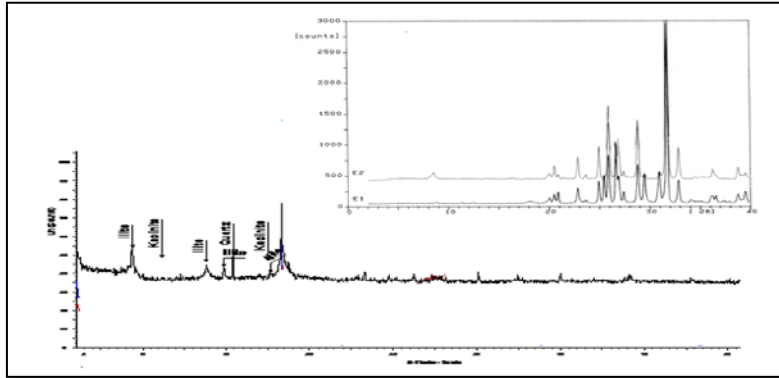


Figure 1. XRD diffractions for reference clay and clays used in drilling fluids.

The three rheological Herschel–Bulkley parameters were derived according to standard methodology, using non-linear regression with a numerical package in order to find rheological behaviour for sample based clay and sample based weighting. As shown in fig. 2, the main difference between the two tested formulations concerns the value of yield stress and consistency index. These parameters affect the flow conditions in the drilling tool. Yield stress is defined as the minimum shear force required providing flow and is mainly due to the nature of additives. Nasser and James (2007) claimed that the shear stress represents the macroscopic manifestation of the shear strength of inter particle forces in a network and its microstructure.

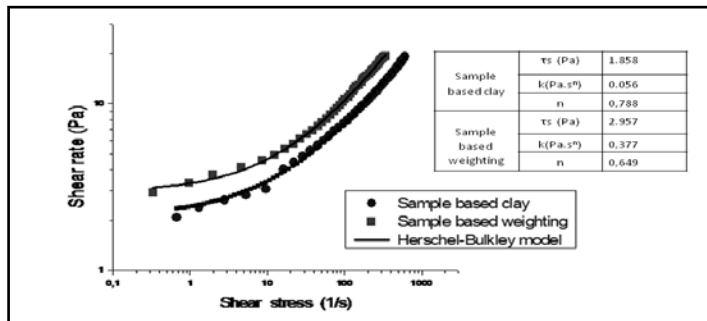


Figure 2. Flow curves for two formulation of drilling muds.

4. Conclusion

Clays used in this study are natural minerals and non-toxic. However, their capacity for water retention loaded with chemicals additives can make them potentially harmful to the environment. The clay based formulations have the ability to increase viscosity and maintain the cuttings in suspension, consequently improve the hole cleaning.

References

- Onaisi, A, Durand, C. & Audibert, A., 1994. Role of hydration state of shales in borehole stability studies. *Eurock* 275–284.
- Dzialowski, A. Hale A. & Mahajan, S., 1998. Lubricity and wear of shale: Effects of drilling fluids and mechanical parameters. *Society of Petroleum Engineers* 25730 (1998).
- Van Oort, E., Hale, A.H. & Mody F.K., 1996. Transport in shales and the design of improved water based shale drilling fluids. *SPE, Drilling and Completion*, 137–146.
- Baba Hamed, S. & Belhadri, M., 2009. Rheological properties of biopolymers drilling fluids. *Journal of Petroleum Science Engineering* 67 - August 2009. ISSN 0920-4105.
- Nasser, M.S & James, A.E., 2007. Effect of polyacrylamide polymers on floc size and rheological behaviour of kaolinite suspensions. *Colloids and Surfaces A: Physicochemical and Engineering Aspects*, Volume 301, Issues 1-3, 5 311-322.

Water balance of Beles Basin

Ashebir SEWALE BELAY^{1,2}, Seifu A. TILAHUN³, Michael M. MOGESs³, Mekete DESSIE³, Enyew ADGO⁴, Jan NYSSSEN⁵, Margaret CHEN⁶ & Kristine WALRAEVENS⁶

¹ *School of Earth Sciences and Blue Nile Water Institute, Bahir Dar University, Ethiopia.*

² *Laboratory for Applied Geology and Hydrogeology, Department of Geology, Ghent University, Belgium.*

³ *School of Civil & Water Resources Engineering, Bahir Dar University, Ethiopia.*

⁴ *Department of Natural Resource, Bahir Dar University, Ethiopia.*

⁵ *Department of Geography, Ghent University, Ghent, Belgium.*

⁶ *Department of Hydrology and Hydraulic Engineering, Faculty of Engineering, Vrije Universiteit Brussel, Belgium.*

The Beles basin is one of the least studied basins in Ethiopia, which is attributed to scarcity of data, poor distribution of hydro-meteorological stations and poor quality of available data. In addition, the Beles basin is characterized by a heterogeneous and complex geological setting with artificial and possibly natural and inter-basin water inflows from the Tana basin that makes the Beles basin complex to study. Despite this knowledge gap, huge irrigation and hydropower project activities are under development. Understanding the groundwater - surface water interaction and dynamics of the water system of this basin based on appropriate data will help to establish water management plans to avoid erroneous water use practices. In Beles basin, since April 2017, 4 river discharge measuring stations (2 on Main Beles and 2 on Gilgel Beles river), 18 groundwater monitoring stations (4 automatic and 14 manual) and 5 meteorological stations (rainfall and temperature) have been installed. Some preliminary results show that rainfall, temperature, groundwater response with precipitation, are highly spatially variable within the basin. There are high discharge springs along the water divide with Tana which hint to inter-basin flow. Intake flow data from Lake Tana-Beles hydropower project show that there is a gradual increase of artificial surface water transfer from Tana basin to Beles basin since the hydropower started operating in 2011. The recently developed small scale irrigation practice in the upper Gelgel-beles also creates new ecohydrology such as wetlands. The Great Ethiopian Renaissance Dam (under construction) will impound the lower reaches of Beles basin. For the better understanding of the Beles basin water balance, additional hydrometric stations will be installed, rating curves for the river discharge measuring stations will be developed, the geological map will be updated using field and remote sensing data, water points (wells and springs) will be inventoried and water will be sampled and analyzed both on site and in the laboratory to understand water dynamics within the basin.

Hydrogeochemical characteristics of shallow groundwater in volcanic rock aquifer systems in the western and northern flanks of Mount Meru, Tanzania

George BENNETT^{1,2}, Kristine WALRAEVENS¹, Jill VAN REYBROUCK¹, Laura SEGERS¹, Ceven SHEMSANGA², Mary KISAKA^{3,4}, Matthieu KERVYN⁴ & Karen FONTIJN⁵

¹ *Laboratory for Applied Geology and Hydrogeology, Ghent University, Krijgslaan 281 S8, 9000 Ghent, Belgium. * George.Bennett@UGent.be*

² *College of Earth Sciences, University of Dodoma, P.o.Box 11090, Dodoma, Tanzania.*

³ *Department of Geology, University of Dodoma, Tanzania.*

⁴ *Department of Geography, Vrije Universiteit Brussel, Belgium.*

⁵ *Department of Earth Sciences, University of Oxford, United Kingdom.*

In the Arusha volcanic region in northern Tanzania, within the western branch of the East Africa Rift Valley, water shortage is common and much of the surface water carries unacceptable levels of dissolved fluoride hence groundwater is the main source of drinking water. Unfortunately the quality of groundwater in this region also is very poor due to high fluoride content as a result of natural contamination from surrounding geological environment, leading to dental and skeletal fluorosis among the local population (Ghiglieri et al., 2012; McKenzie et al., 2010).

35 groundwater samples (from 15 springs and 20 wells) were collected and analysed for chemical properties. Preliminary results obtained from analyses show contrast in pH, electrical conductivity (EC), total dissolved solids (TDS) and F⁻ concentration across the study area, with some significant spatial patterns for water samples from springs where pH, EC, TDS and F⁻ concentration increase with decrease in elevation. Sodium (Na⁺) and bicarbonate (HCO₃⁻) are the dominant ions hence the main water type in this area is NaHCO₃ type water as represented in Fig. 1 (Piper, 1944).

High values of F⁻ (up to 41.2 mg/l) were recorded. The groundwater pH varies from 6.97 to 8.11, the EC varies from 439 to 3500 µS/cm, the TDS varies from 336 to 2781 mg/l. Na⁺ and HCO₃⁻ are ranging from 75.7 to 711.5 mg/l and from 188.49 to 1342 mg/l respectively. The concentration of fluoride in the groundwater varies from 3.87 to 41.2 mg/l. In all 35 groundwater samples, F⁻ exceeds the WHO limit (1.5 mg/l), whereas the 97 % (34 samples) are above the Tanzanian limit (4 mg/l). The only sample with lower F⁻ value (3.87 mg/l) than the Tanzanian limit is from a hand dug well in the western flank of Mount Meru.

High fluoride concentrations are linked to high sodium contents and pH, and low Ca²⁺ concentrations. The weathering of Na-rich volcanic rocks increases pH which in turn triggers the dissolution of CO₂. The dissolution of CO₂ increases HCO₃⁻, which at high pH is producing CO₃²⁻, causing oversaturation in the groundwater compared to calcite, and leading to the precipitation of this mineral. This precipitation lowers the Ca²⁺ concentration in solution and leads to a sub-saturation with respect to fluorite in the system. As a result, fluorite will dissolve and an increase in F⁻ concentration is observed (Coetsiers et al., 2008).

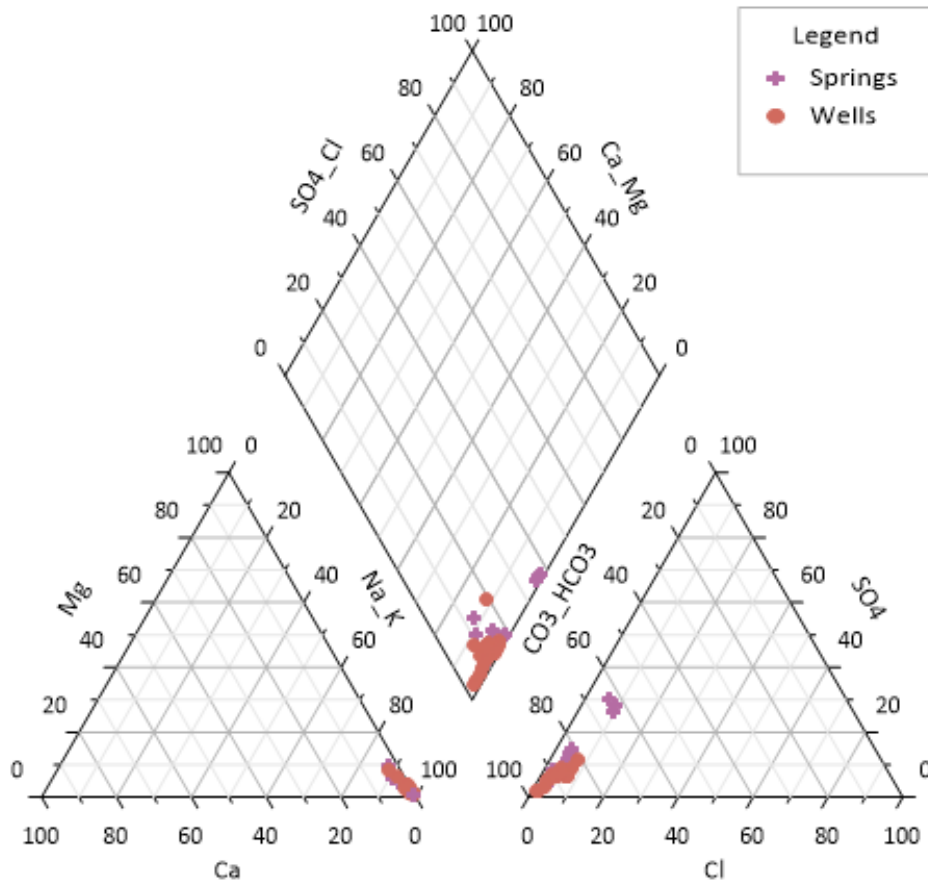


Figure 1. Piper diagram with classification of major ions from groundwater samples taken from springs and hand dug wells in the western and northern flanks of Mount Meru, Tanzania.

References

- Coetsiers, M., Kilonzo, F. & Walraevens, K., 2008. Hydrochemistry and source of high fluoride in groundwater of the Nairobi area, Kenya. *Hydrological Sciences Journal*, 53(6), 1230–1240. doi: 10.1623/hysj.53.6.1230.
- Ghiglieri, G., Pittalis, D., Cerri, G. & Oggiano, G., 2012. Hydrogeology and hydrogeochemistry of an alkaline volcanic area: the NE Mt. Meru slope (East African Rift – Northern Tanzania). *Hydrology and Earth System Sciences*, 16, 529–541. doi: 10.5194/hess-16-529-2012.
- Mckenzie, M., Mark, B.G., Thompson, L.G., Schotterer, U. & Lin, P.N., 2010. A hydrogeochemical survey of Kilimanjaro (Tanzania): implications for water sources and ages. *Hydrogeology Journal*, 18, 985–995.
- Piper, A.M., 1944. A graphical interpretation of water analysis. *Transactions American Geophysical Union*, 25, 914–928. doi: 10.1029/TR025i006p00914.

Groundwater assessment and its dynamics in Mekelle Outlier: Preliminary results, N. Ethiopia

Gebremedhin BERHANE¹, Nawal ALFARRAH², Tesfamichael GEBREYOHANNES¹, Abdelwassie HUSSIEN¹, Miruts HAGOS¹, Kassa AMARE¹ & Kristine WALRAEVENS²

¹ *School of Earth Sciences, Mekelle University, P.O. Box 1202, Mekelle, Ethiopia. *gmedhin_berhane@yahoo.com*

² *Laboratory for Applied Geology and Hydrogeology, Ghent University, Krijgslaan 281-S8, B-9000 Ghent, Belgium.*

Globally, water is an increasingly scarce resource requiring careful economic and environmental planning and management. In developing countries (like Ethiopia) the situation is exacerbated by rapid population growth, land degradation/erosion and urbanization. Demand of water for domestic use, agriculture and industrial purposes has been escalated and is being escalated. Groundwater resources have become the main source of water supply for various purposes including domestic, industry and agriculture. Initially, Mekelle City (in the northern Ethiopia, East Africa) has been supplied since 1998 with groundwater mainly from Aynalem well field, which is situated about 5 km south east of the City. It was reported that the groundwater level in the Aynalem well field is declining with time. This paper provides preliminary results of groundwater assessment and its dynamics in terms of groundwater level. To understand the causes and to have better insights of the situation, a four year collaborating research project with VLIR-UOS, Mekelle University and UGent was launched in 2016. In the framework of this project, a groundwater monitoring network using five data loggers was established to understand the effect of abstraction and temporal dynamics of the groundwater level. To complement the results from the data loggers, intensive geological mapping, manual groundwater level measurement and water sampling and analysis were carried out. The results show that groundwater dynamics or fluctuation in relation to recharge and abstraction or exploitation are captured in the automatic groundwater level measuring device (data loggers) installed in the study area. In addition Micro-Dam Reservoirs (MDR) (e.g. Arato) have also shown a recharging effect to the shallow aquifer. This unintentional recharge from MDRs lead for the shallow wells become more sustainable in terms of water availability and groundwater level dynamics which is a positive impact to the local community and the environment. The preliminary results gathered so far show that the aquifer system in Mekelle area is very sensitive to meteorological events and changes. Water chemistry analyses indicate an elevated sulfate and calcium content, attributed to the local geology of the area (presence of gypsum and limestone). These further indicate the need for accurate hydrogeological data and overall understanding of the system in relation to abstraction and climatic changes.

Investigation of zero-valent iron nanoparticle transport for groundwater remediation by means of lab-scale flow experiments.

Benjamin K. BLYKERS¹, Tim DE KOCK¹, Tom BULTREYS¹, Johan DE GRAVE¹ & Veerle CNUUDE¹

1 Department of Geology, Faculty of Sciences, Ghent University, Krijgslaan 281/S8, 9000 Ghent, Belgium.

1. Introduction

The use of nanoparticles zero-valent iron (nZVI) is one of the most recent and promising techniques for groundwater remediation (Crane & Scott, 2012). nZVI successfully reduces pollutants such as chlorinated hydrocarbons (e.g. PCE, TCE and DDT) and transforms a variety of dissolved metals into an insoluble form fixed to the rock, thereby reducing their ecological impact according to the following removal mechanisms: reduction, adsorption, (re)oxidation, co-precipitation and precipitation (Almeelbi & Bezbaruah, 2012; Lin et al., 2018; O'Carroll et al., 2013; Stefaniuk et al., 2016).

The purpose of this research was to know whether the nZVI suspension moves unrestrained through the soil or whether (part of) the nZVI is retained in the soil and if so, where this retention occurs. To answer these research questions, lab-scale flow experiments were conducted in which barium was chosen as pollutant. Inductively Coupled Plasma – Optical Emission Spectrometry (ICP-OES) was used to measure the barium and iron content in the fluids and X-ray Computed micro-Tomography (μ CT) to investigate the composition and location of possible precipitates of barium and nZVI.

2. Material and methods

A sand pack was used as soil model. As such, all occurring reactions can be ascribed to be reactions of barium with nZVI.

The nZVI product selected for all the experiments was Nanofer 25S, provided by Nano Iron, s.r.o. It contains 20 % nZVI and a mixture of 80 % water and polyacrylic acid. Untreated nZVI particles would oxidize and agglomerate before reaching the contaminant, strongly reducing the efficacy and mobility of the particles. Therefore, nZVI was mixed with carboxymethylcellulose (CMC) in equal amounts to provide electrostatic and steric repulsion between the particles, reducing the aggregation and increasing the reactivity and mobility of nZVI in the soil.

In the flow experiments, first a barium solution was drawn through the sand pack, followed by a CMC-nZVI mixture. Ultimately, the sand pack was flushed with distilled water. The outflow was sampled in small volumes equal to two pore volumes of the sand pack and analyzed with ICP-OES. The sample holder for the sand pack is shown in Fig. 1A. Glass beads and a mesh were placed below and on top of the 3-cm long pack to obtain an even flow through it. The direction of flow was upwards.

After the experiment, the sand pack was scanned with μ CT to determine whether and where iron (and/or barium) compounds were precipitated.

3. Results and discussion

Fig. 1B shows the evolution of both barium and iron concentration in the outflow of the flow experiment with respect to the total drawn volume. The delay in the concentration decrease is related to the fact that the fluids first flow through the entire setup before reaching the outlet. The decrease in barium concentration upon CMC-nZVI injection is much more abrupt than the decrease in iron concentration upon the injection of distilled water. This illustrates the nZVI's tendency to be retained in the soil. An additional explanation for this retention is the difference in viscosity: a less viscous fluid (barium solution or water) is more easily displaced by a more viscous fluid (CMC-nZVI) than vice-versa, in which case 'viscous fingering' can occur: the water passes through the sand pack along a 'preferential flow path', only slightly affecting the rest of the CMC-nZVI. The difference in viscosity between the barium solution and the CMC-nZVI has impeded the interaction between the two fluids, resulting in a negligible amount of barium being removed from the solution. The μ CT analysis showed that in the pore space, more X-rays were absorbed towards the bottom of the sand pack. This is probably due to retained iron particles, as the chemical analysis of the outflow has ruled out the presence of the barium. This indicates that the iron particles are very susceptible to gravitational forces and that a substantial amount of iron is retained in our model, although no barium was coprecipitated with the nZVI.

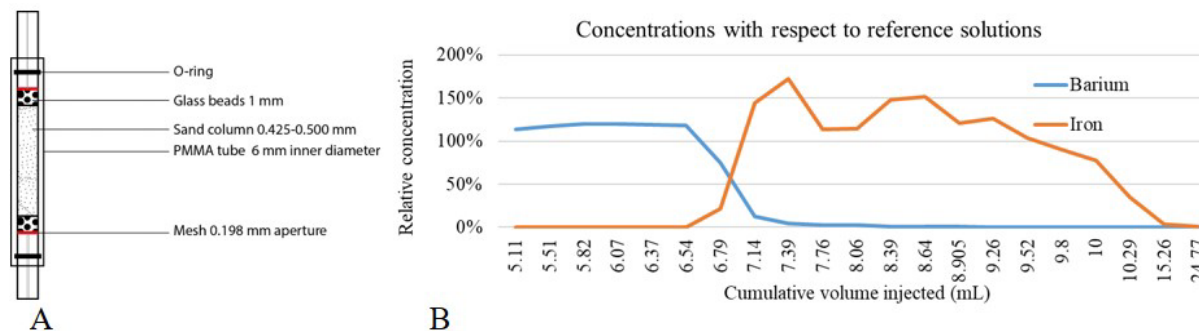


Figure 1. A: Schematic setup of sample holder. B: Evolution of barium and iron concentrations in the outflow of the flow experiment.

4. Conclusion and further research

Barium should be immobilized by nZVI, but in these flow experiments the difference in viscosity has led to very limited interaction between barium solution and CMC-nZVI. Although the setup used in this research is only a simplification of reality, it reveals hitches that also occur in the field. In future research, the setup should be improved and these obstacles overcome for a more efficient application of nZVI in groundwater remediation.

References

- Almeelbi, T. & Bezbaruah, A., 2012. Aqueous phosphate removal using nanoscale zero-valent iron. *Journal of Nanoparticle Research*, 14(7).
- Crane, R.A. & Scott, T.B., 2012. Nanoscale zero-valent iron: Future prospects for an emerging water treatment technology. *Journal of Hazardous Materials*, 211–212, 112–125.

- Lin, K.S., Mdlovu, N.V., Chen, C.Y., Chiang, C.L., Dehvari, K., 2018. Degradation of TCE, PCE, and 1,2-DCE DNAPLs in contaminated groundwater using polyethylenimine-modified zero-valent iron nanoparticles. *Journal of Cleaner Production*, 175, 456–466.
- O'Carroll, D., Sleep, B., Krol, M., Boparai, H., Kocur, C., 2013. Nanoscale zero valent iron and bimetallic particles for contaminated site remediation. *Advances in Water Resources*, 51, 104–122.
- Stefaniuk, M., Oleszczuk, P., Ok, Y.S., 2016. Review on nano zerovalent iron (nZVI): From synthesis to environmental applications. *Chemical Engineering Journal*, 287, 618–632.

The Balmatt project: Deep geothermal energy from the Dinantian in Mol-Donk

Stijn BOS¹, Ben LAENEN¹, David LAGROU¹, Virginie HARCOUET-MENOU¹ & Matsen BROOThAERS¹

¹ VITO, Flemish Institute for Technological Research, Boeretang 200, BE-2400 Mol, Belgium.

In 2010, VITO initiated a new 2D seismic campaign covering the area between Turnhout, Herentals and Mol. Although the seismic data could be tied to the Poederlee well (30W371), which reaches the top of the Dinantian at 1,481 mbs, uncertainty about top reservoir interpretation was in the order of several 100s of m. This uncertainty resulted mainly from correlation of the top Dinantian seismic reflector over the faults down-throwing to the E between Poederlee and Mol. The seismic data pointed towards the presence of the Dinantian at depths between 2.8 and 3.8 km at Mol.

A prospect was defined, targeting the Dinantian near a fault that affected the Chalk Group and older strata, potentially improving hydraulic properties of the reservoir. A drilling location for a vertical exploration well towards the fault zone and the possibly fractured carbonate rocks was found at the Balmatt brownfield site that VITO acquired in Mol-Donk. Proving the potential of geothermal energy at this location and converting the brownfield into a greenfield with a geothermal power and heating plant, is in line with the sustainability goals of VITO.

In September 2015 exploration well MOL-GT-01 was spudded. This well was both financed by VITO and the Flemish government. Additionally, NIRAS co-funded the first section up to the base of the Cenozoic for their research in the field of nuclear waste storage.

The well architecture was designed with an anticipated top of the Dinantian at 2.8km true vertical depth (TVD). However, the reservoir was encountered some 370 m deeper than foreseen. This led to drilling technical issues which resulted in a side-track, MOL-GT-01-S1, that reached the Dinantian at a depth of 3,175 m. The carbonates were drilled with a 6" bit down to 3,610 m and completed with a 5" slotted liner. Well MOL-GT-01-S1 was completed in January 2016 and subsequently tested for its production capacity. While drilling the 6" section total mud losses were encountered, therefore indicating the presence of transmissivity in the Dinantian. The production test confirmed this with a calculated productivity index PI of 4-5 m³/h/bar and production temperatures up to 128 °C.

The formation water is a Na(Ca)Cl brine with 165 g/l tds. Na⁺ and Cl⁻ sign for 90% of the dissolved ions. Besides, the water contains minor amounts of Ca²⁺, Mg²⁺, K⁺, and SO₄²⁻. Downhole water samples reveal a pH of 5.4. The fluid is slightly reducing (redox potential SHE; 141-152 mV at 20 °C) and contains 800 mg/l dissolved Fe. The gas content is about 2.5 Nm³ of gas per m³ of formation water. The main component is CO₂ (75–80 Vol%). Besides, minor amounts of CH₄ (8-11%), N₂ (2-4%) and H₂ (11%) are present.

Based on the test results, VITO decided to drill a 2nd well from the same location. Well MOL-GT-02 was spudded in March 2016 and was drilled with an inclination up to 40° in order to reach a distance from MOL-GT-01-S1 of at least 1.5 km at the top of the Dinantian. MOL-GT- 02 was deviated towards the NE, parallel to the seismic line MH10-04 and targeting the reservoir in a more pristine area, not influenced by faults, to minimise the risk of fault activation when injecting large amounts of water. The well was drilled without major drilling technical issues. Again, the top of the Dinantian was found some 200 m deeper (at 3.3 km TVD) than predicted. MOL-GT-02 reached its final depth in July 2016 at 4,341 m along hole (3,830 mTVD). The well drilled through

530 mTVD of limestones and dolostones and was completed with a 7” slotted liner The well was tested for its injection capacity in September 2016, resulting in an injectivity index II of 1.5-2 m³/h/bar.

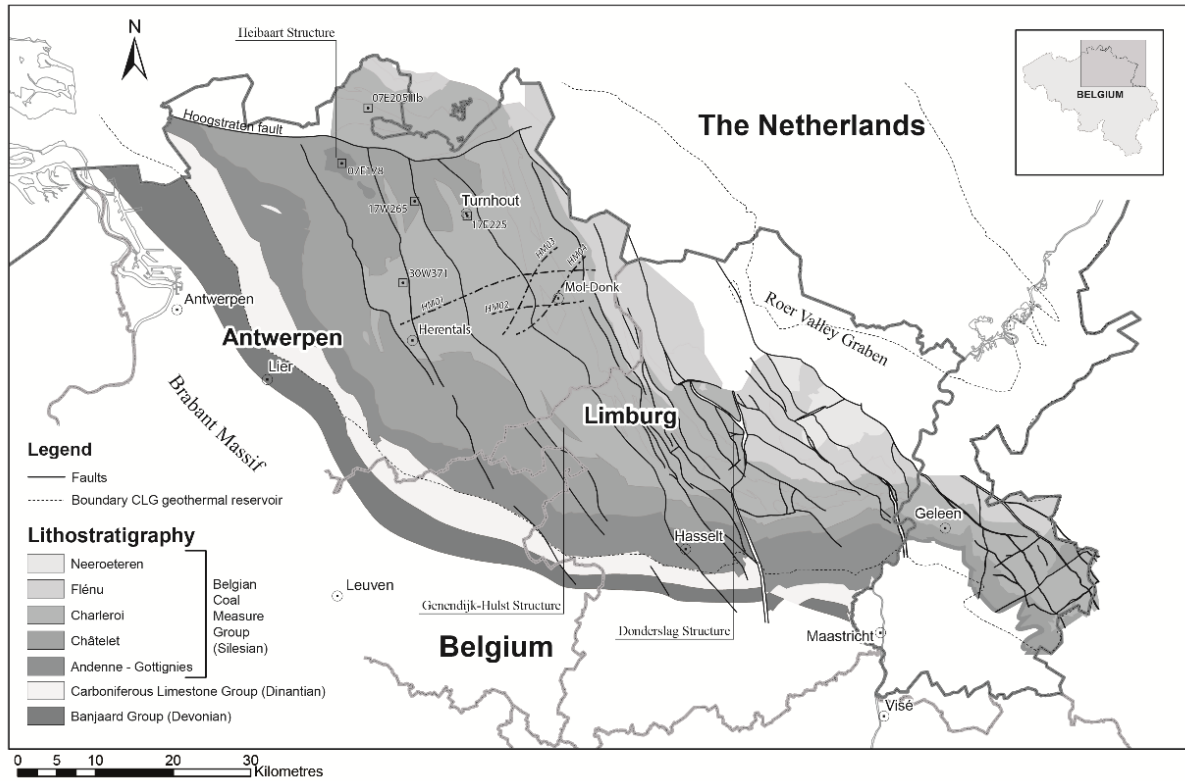


Figure 1. Palaeozoic subcrop map of the Campine Basin (compiled after Langenaeker, 2000; and Patijn & Kimpe, 1961). The map shows the location of the Balmatt -site at Mol, offset wells used to define the Balmatt geothermal project and the geometry of the 2D seismic survey of 2010.

Based on the test data, the design for the geothermal plant was made. Surface equipment will run at an operational pressure of 40 bar in order to avoid degassing of the brine and the need to evacuate CO₂ and CH₄ into the atmosphere.

The initial thermal power output of the geothermal plant will be about 8-9MW since the return temperature is as high as 80 °C. This high return temperature is imposed by the existing high temperature heating grid already in place on the location. Connecting low temperature heating networks that could go as low as 30 °C, would double the thermal output. With regard to this addition of extra low temperature heating networks, VITO has already started drilling a 3rd well, MOL-GT-03, which is intended to become a 2nd production well. MOL-GT-03, spudded in December 2017, is targeting the same fault zone as MOL-GT-01-S1, although now in a SE direction at 1.6km distance to MOL-GT-01.

Next to the production target in the Dinantian, MOL-GT-03 also has an exploration goal since it is planned to drill into the underlying Devonian. These strata have never been drilled at large depths (>4 km) in Flanders. At shallower depths, e.g. in the Loenhout area (see Figure 1), these layers have shown losses while drilling, indicating promising reservoir conditions. Drilling

of well MOL-GT-03, which will have its final total depth around 4.3 km TVD and a total length of almost 5 km, is supposed to take until July 2018.

References

- Bos, S. & Laenen, B., 2017. Development of the first deep geothermal doublet in the Campine Basin of Belgium. *European Geologist*, 43:16-20.
- Langenaeker, V., 2000. The Campine Basin: Stratigraphy, structural geology, coalification and hydrocarbon potential of the Devonian to Jurassic. *Aardkundige Mededelingen*, 10:1-142.
- Patijn, R.J.H. & Kimpe, W.F.M., 1961. De kaart van het Carboonoppervlak, de profielen en de kaart van het dekterrein van het zuid-Limburgse mijngebied en Staatsmijn Beatrix en omgeving.

Approach of a regional heavy metal pollution caused by non-ferrous industry in the Campine area of Belgium

Jan BRONDERS¹, Ilse VAN KEER¹, Ingeborg JORIS¹, Nele DESMET¹, Johan PATYN¹, Johan VOS¹, Piet SEUNTJENS¹ & Eric FIERENS²

¹ VITO, Flemish Institute for Technological Research, Boeretang 200, 2400 Mol, Belgium. * jan.bronders@vito.be

² OVAM, Flemish Waste Agency, Stationsstraat 110, 2800 Mechelen, Belgium.

1. Abstract

A spatially distributed model was used to calculate the fate of Zn and Cd pollution in soil, groundwater and surface water in the surroundings of former and actual sites of non-ferro industries in the Belgian-Dutch Campine Area. Several scenarios including the reference situation, autonomous evaluation and various remediation measures were taken into account. According to the modelling results the impact of the proposed remediation measures was less pronounced at a regional scale and more effective locally. Related to the status of the (ground)water bodies, the used methodology enables the authorities to evaluate, prioritize, plan and invest in land management resulting in a better future status of the water bodies.

2. Introduction

The Campine region, located in the north-eastern part of Flanders (Belgium) and the south-eastern part of the Netherlands, is polluted with heavy metals due to the former activities of non-ferro industry smelters. The observed soil, ground and surface water pollution of mainly zinc and cadmium, has a regional character and covers an area of 700 km². The observed average regional groundwater concentrations range between 500 – 3000 µg/l for Zn and are up to 20µg/l for Cd. As a result of the studies being carried out in the area since 1995, a good overview is obtained related to the source, the fate and the risks of the pollution. This resulted in a holistic modelling approach including remedial actions and protective measures. The EU Water Framework Directive (WFD) obliges the EU member states to monitor and evaluate the status of their water bodies. The developed hydrogeological model allows to interpret the evolution of the pollution in ground and surface water as function of time, taking the into account the effect of the remedial actions, and to interpret the status of the water bodies.

3. Methodology

A spatially distributed coupled model, based on a multiple site deposition model, HYDRUS-1D and MODFLOW, was used to calculate the fate of Zn and Cd pollution in soil and (ground)water. Input parameters include land use, atmospheric deposition data, soil type and soil concentrations, and the geology and hydrogeological parameters of the aquifer system.

Leachate concentrations and concentrations in groundwater were calculated as function of time and location. Subsequently, metal fluxes from the groundwater system to the surface water were calculated. Different scenarios including the actual reference scenario, autonomous evolution and the impact of remediation measures were distinguished. The types of measures taken into account are 1) hydrodynamic measures (pumping) at the different (non-ferro industrial) sites, 2) drainage (pumping) in certain areas in the region, 3) implementation of draining systems along rivers in (highly) polluted areas, with or without additional infiltration of water and 4) excavation of contaminated topsoil and zinc ashes.

4. Results and discussion

For each of the scenarios the modeling results in 1) the reconstruction of historical deposition of Zn and Cd in space and time, 2) concentration maps of Cd (Fig. 1) and Zn, present in the leachate from the unsaturated zone to the shallow groundwater, for different time periods and as a function of remedial actions, and 3) calculated Cd (Fig. 2) and Zn fluxes from groundwater to the affected surface water. The generated output enables to evaluate the effect of the different measures proposed on the quality and quality evolutions of the ground- and surface water bodies present in the study area.

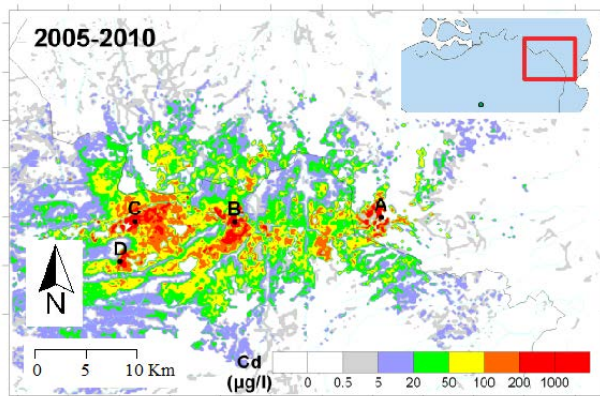


Figure 1. Concentration map of Cd in leachate in 2005 (Joris et al. 2014).

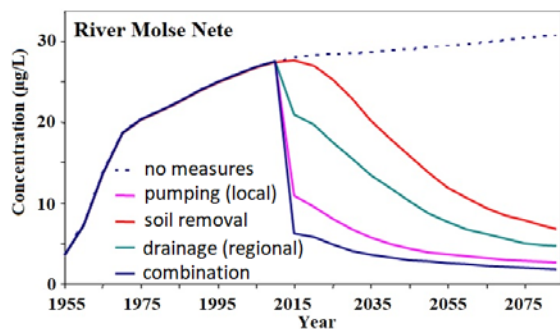


Figure 2. Calculated concentration of Cd in surface water based on polluted groundwater discharging (draining) to the river Molsse Nete for a selection of remedial action.

5. Conclusion

Modelling results indicate that for the diffuse contamination, remediation measures are not very effective or not feasible on a regional scale. Effective actions were only recommended at or near the industrial sites itself. The only significant measure to reduce loads entering the river systems is the instalment of groundwater abstraction wells in zones where higher discharge of polluted groundwater to the rivers is present. It was also concluded that the status of the considered water

bodies is not expected to significantly change before 2027. If no remedial actions are taken, improvement of the water quality at a regional scale is, even at the end of this century, not visible.

The modelling and future data collection will be used to follow the status of the water bodies. This will allow to identify if improvement (positive trend) is present or if at some places more effort (actions) is needed to reduce the pollutant flow towards receptors such as local rivers.

Acknowledgement

This project was financially supported by the Flemish Waste Agency, OVAM and Interreg project BeNeKempen (partnership between Campine Active Soil Management [AbdK] and the Public Waste Agency of Flanders [OVAM]) BeneKempen.

Reference

Joris, I., Bronders, J., van der Grift, B. & Seuntjens, P., 2014. Model-based Scenario Analysis of the Impact of Remediation Measures on Metal Leaching from Soils Contaminated by Historic Smelter Emissions. *Journal of Environmental Quality*, 43(3), 859-868.

Theme 6

Biotic and climatic evolution and paleoenvironments through time

Depositional reconstruction of Quaternary continental carbonates in Tunceli Region (East of Turkey)

Gamze KARVAR¹, Cihan ARATMAN^{2, 3}, Calibe Koç TASGIN¹ & Rudy SWENNEN³

¹ Engineering Faculty, Department of Geological Engineering, Fırat University, Turkey.

² Engineering Faculty, Department of Geological Engineering, Pamukkale University, Turkey.

³ Geodynamic and Geofluids Research Group, Department of Earth and Environmental Sciences, KU Leuven, Belgium.

This study aims to infer the paleoenvironmental conditions related to Quaternary microbialites and tufa carbonates, present in Tunceli region located between Ankara-Erzincan and Assyrian suture zones in the East Anatolian Plate of Turkey. Deep or shallow alkaline, bicarbonate-rich fluids of around 30 °C in temperature (Oztufekci et al., 2018) had been circulated through such a compressional zone, being driven by NW-striking dextral strike-slip faults. These fluids drained into bedrocks that serve to determine the regional flow regime, precipitating the reservoir carbonates which overlie unconformably Miocene-Pliocene pyroclastic rocks, Miocene limestones, Eocene flysh deposits and Permian marbles (Fig. 1).

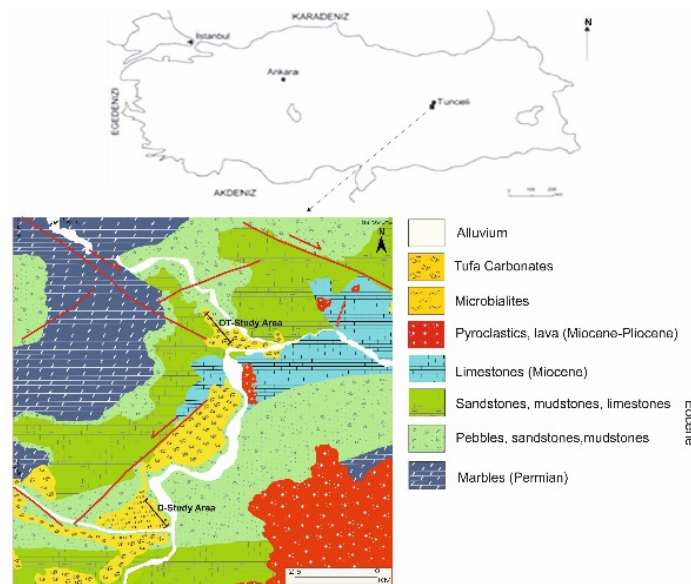


Figure 1. Generalized geological map indicating the studied areas at the Tunceli region (modified from Oztufekci et al., 2018).

They consist in the north of up to 10 m thick tufa deposits and to about 30 m thick microbialites in the south. The microbialites and tufa deposits crop out along the Dinar valley and the Munzur valley, respectively. The microbialites comprise mainly of the 40 cm thick domal non-oncoidal stromatolite lithotype and the domal oncoidal stromatolite lithotype. They are commonly characterized by the alternation of the concave to convex-shaped continuous wavy calcite laminae, fibrous to massive in texture, and micritic laminae of chironomid larvae pores. These laminae create the rhythmic layering, and also in domal oncoidal stromatolite occur closely associated with small dome-shaped microbial filaments. This layering also occurs as surrounding tube-shaped tree trunks having several cm in diameter or macrophytes in the domal oncoidal stromatolite lithotype. The latter comes over the basal alluvial conglomerates, about 4 m thick, with a sharp erosional boundary, being interbedded upward with the massive cross-bedded oolitic carbonate sands and

grey- to pinky-coloured fascicular and massive wackestone to packstone lithotype. On the one hand, tufa deposits differentiate from the microbialite by microsparite wackestone to packstone, phyto boundstone covered by massive shrubby grainstone lithotypes. The ICP-OES elemental analyses were applied both to microbialites and to tufa deposits to elucidate the varying environmental conditions from microbialites to tufa precipitation. The mean value of Ba (69.7 ppm), Na (157.6 ppm), S (1102 ppm) and Sr (796 ppm) elements for the Dinar microbialites is higher than those for Munzur tufa deposits, hence indicating the formation of high-energy low-gradient ramp-type margins of the lacustrine environment where high evaporation and subaerial exposures developed. The heavy element compositions (As, Co, Cr, Cu, Li, Ni, Pb, Rb, Ti, V, Zn) gained in the Munzur tufa deposits are much higher, compared to Dinar microbialites deposits. Between them, high Cr values ranging 1 ppm to 161 ppm point out that CO₂-origin fluid forming Munzur tufa deposits should interact partially with ultramafic bedrocks. However, these tufa deposits might be closely precipitated by shallow- to- hydrothermal fluids which reside in karstic limestones according to the plot of Ba versus Sr values. On the one hand, high Sr values ranging 389 ppm to 2090 ppm in the Dinar microbialites suggests that hydrothermal fluids were enriched in Sr element due to the dissolution and reprecipitation of carbonate minerals into drainage mafic or granitic bedrocks. In addition, these carbonates are differently clustered in this plot, and exhibit a positive trend with the increasing Sr and Ba values (Fig. 2). It is very interesting that such a trend has never been indicated in Teboul's (2016) combined Ba and Sr plot. Besides, these continental carbonates tectonically should indicate the central part of a large strike-slip basin (Platt and Wright, 1991).

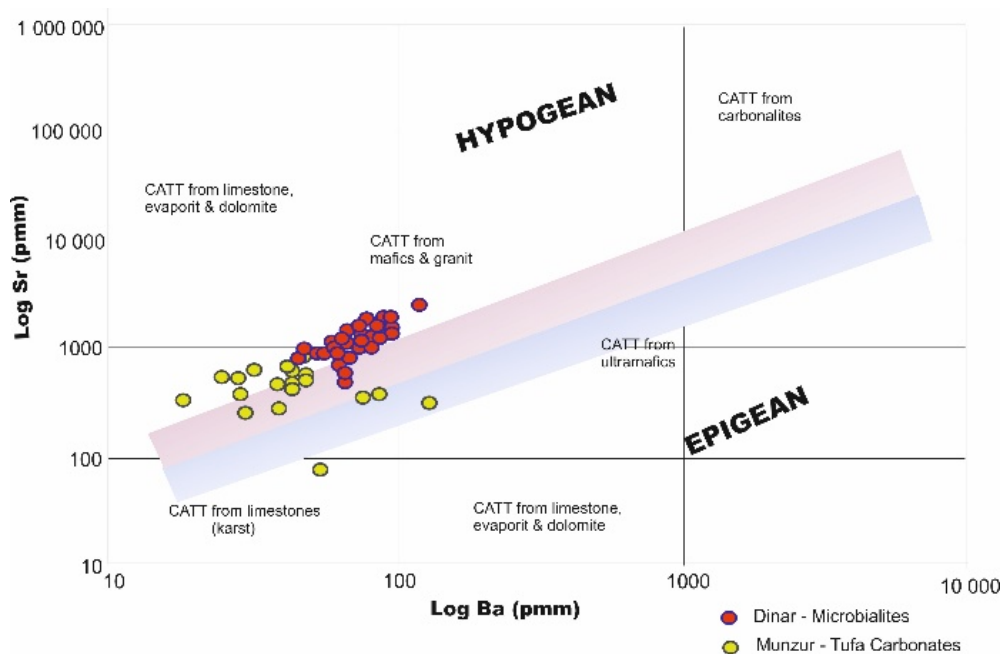


Figure 2. Geochemical plot of Sr and Ba elements at the Tunceli continental carbonates. Notice that the data of this study were superimposed on the plot of Teboul et al. (2016).

References

- Öztüfekçi Önal, A., Sançar, T. & Önal, A., 2018. Mineral waters in Munzur and Pülümür valley (Tunceli): Preliminary results, 8. Geochemistry Symposium, Abstracts Book.
- Platt, N.H. & Wright, V.P., 1991. Lacustrine Facies Analysis. Edited by Anadon, P., Cabrera, LI., Kelts, K. In: Lacustrine carbonates: facies models, facies distributions and hydrocarbon aspects. Special Publication International Association of Sedimentologists, 13, 57-74.
- Teboul, P.-A., Durllet, C., Gaucher, E.C., Virgone, A., Girard, J.-P., Curie, J., Lopez, B. & Camoin, G.F., 2016. Origins of elements building travertine of tufa: New perspectives provided by isotopic and geochemical traces, *Sedimentary Geology*, 334, 97-114.

Reconstructing Holocene water table dynamics from small-scale buried depressions in NE Belgium: pedological, lithological and botanical evidence

Koen BEERTEN¹, Wouter VAN DER MEER², Arno GRADE^{3,*}, Koen HEBINCK⁴ & Miel SCHURMANS⁴

¹ *SCK•CEN Belgian Nuclear Research Centre, Waste and Disposal, Engineered and Geosystems Analysis, Boeretang 200, 2400 Mol, Belgium.*

² *Biax Consult, Hogendijk 134, 1506 AL Zaandam, the Netherlands.*

³ *SCK•CEN Belgian Nuclear Research Centre, Waste and Disposal, Boeretang 200, 2400 Mol, Belgium (now at ONDRAF/NIRAS, Kunstlaan 14, 1210 Brussels, Belgium.*

⁴ *VUhs archeologie, De Boelelaan 1105, 1081 HV Amsterdam, Nederland.*

Hydro(geo)logical systems are routinely described using state variables (groundwater head or river discharge), obtained from instrumental observations which cover a time period of a few decades only. This time window is too short to capture the full variability of a hydrological system that might be expected under different boundary conditions and driving forces (climate and land use change). In an attempt to extend this time window, we present preliminary results of an integrated study of small-scale buried depressions (buried fens) in the northeastern Belgian sand belt, aiming at deciphering the observed archive in terms of water table dynamics. Several proxies were used to estimate the elevation of the past groundwater table, including podzol soil morphology, texture and depositional style of the sediments in the depressions, and their palynological content. Age control was derived from OSL dating of quartz and radiocarbon dating of plant remains.

The depressions, studied through shallow trenching, are located on an interfluvium reaching several meters above the adjacent valley bottom. Their size varies between 100-5000 m², while they are between several dm up to 2 m deep (relative to the ancient surface). We observe the following: (1) soil horizon morphology (hydromorphic soil features) and peat development are related with depression depth, (2) peat in the deepest depression contains pollen of aquatic plants, (3) the pollen content reflects alternating periods of eutrophic and oligotrophic conditions, and (4) the subsequent sandy infill shows sedimentological features typical for deposition in a standing water body.

Combining the evidence from proxies with age control leads to the following water table reconstruction: (i) an initial phase of podzol soil formation and landscape stabilization under drainage conditions that were sufficiently good to allow the soil to be formed, and (ii) a subsequent phase during which the deepest depressions were permanently filled with water to allow peat to be developed and drifting sand to be deposited in a standing water body.

As a preliminary conclusion we put forward that the rising water table which was initiated at the latest around ca. 3000 years ago is probably a combined effect of climate and land use change (less evapotranspiration due to lower temperatures and different vegetation). Furthermore, the correlation between proxy characteristics on the one hand, and fen depth on the other hand strongly suggests that the observed water table fluctuations reflect groundwater table dynamics. Overall, we find second-order sub-millennial variations superimposed on a first-order supra-millennial signal.

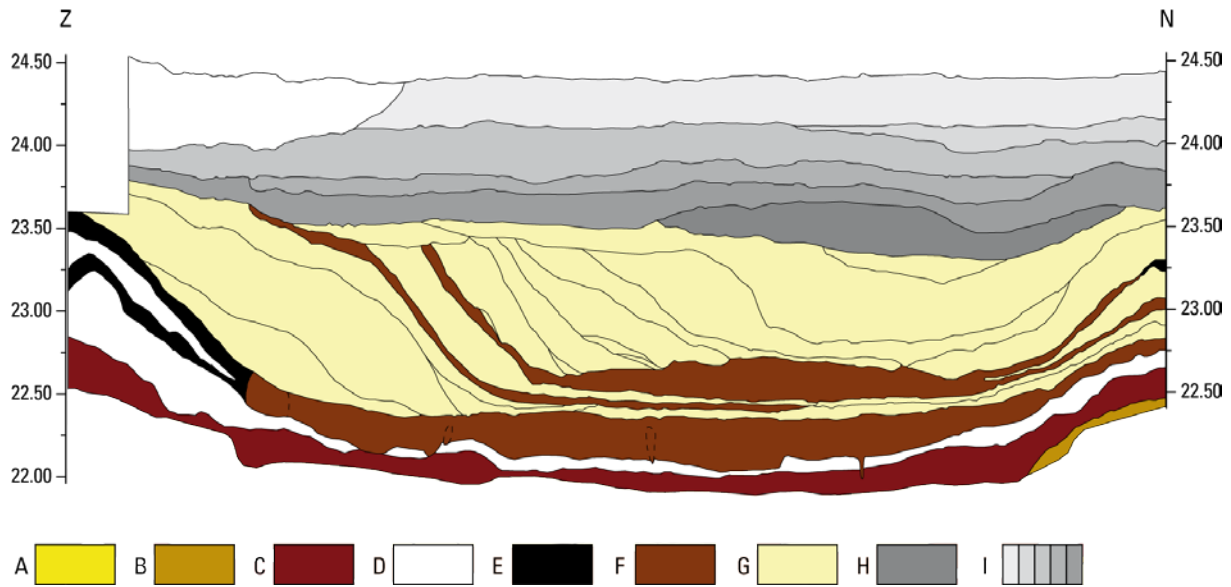


Figure 1. Photograph and drawing of a cross-section through the deepest depression. A = podzol C-horizon, B = podzol BC-horizon, C = podzol B-horizon, D = podzol E-horizon, E = podzol A-horizon, F = peat, G = drift sand, H/I = agricultural soil.

From Ediacaran to Devonian - The Great Early-Middle Palaeozoic Biodiversification as a 'Half-Horst' Model

Alain R. M. BLIECK

ULille, Campus Cité Scientifique, Faculté des Sciences & Technologies, bâtiment SN5 (Sciences de la Terre), Blvd. Paul Langevin, F-59655 Villeneuve d'Ascq cedex, France; alain.blieck@univ-lille.fr, alain.blieck@yahoo.fr

Geobiological developments of end-Proterozoic-Phanerozoic life on Earth are traditionally described and/or interpreted as a series of rises, 'plateaus', falls, crises, (r)evolutions & whatsoever. A reappraisal of the Ediacaran to Mid-Palaeozoic portion of this story-telling is proposed. Most recent data and/or re-analyses of palaeobiologic databases as, e.g., the PaleoBiology Database, show that (1) life on Earth suffered of hundreds of common 'small', 'medium' & 'wide' crises all along its duration [what has been known for long], (2) ordinary, 'normal destiny' of all individuals, species, ecosystems... is death [*idem*], (3) the 'Cambrian Explosion' began in the Ediacaran, (4) it is continued with the GOBE (Great Ordovician Biodiversification Event), (5) the latter does peak in Early Devonian time or GEBE (Great Eodevonian Biodiversification Event *sensu* Blieck, 2015, 2017), (6) this is part of a Palaeozoic Plateau that ends with the Permian/Triassic crisis, (7) the latter does correspond to a 'two shot' crisis, (8) the Early Triassic, post-crisis recovery did not exist because palaeontologists find more & more evidence of 'normal' life during this time slice, (9) this is followed by a near-continuous Meso-Cenozoic, logarithmic-like, rise (or MCR) until the Present, (10) the Mesozoic/Cenozoic, aka the K/T, boundary & crisis was not that important &, in any case, just an 'ordinary' event, with the now classical case of dinosaurs survived by birds, (11) latter MCR is still on way, (12) there is no rationality in thinking that this will soon end, & (13) the so-called '6th Extinction' which would be operating nowadays, is a pure 'view of the spirit'. I thus propose to replace the now traditional biodiversity curve for the Ediacaran to Devonian by a 'Half-Horst' one as an anamorphic model that needs (i) not being discarded, (ii) being 'filled' with additional data, & (iii) being statistically re-analysed with a new open mind. This programme needs multi-disciplinary collaborations in order to reach a multi-factor numerical model that, in turn, will be included within a new palaeobiological model for Earth Life inside a renovated theory of biological evolution such as the 'Phylo-Evo-Devo-Eco-Etho-Geo-Bio' one being in progress. 'This is another story' as everybody may imagine.

References

- Blieck A. 2015. An Early Devonian peak of biodiversity: the case of heterostracan vertebrates. In Mottequin B., Denayer J., Königshof P., Prestianni C. & Olive S. (eds), IGCP 596 – SDS Symposium: Climate change and biodiversity patterns in the Mid-Palaeozoic (Sept. 20-22, 2015, Brussels). Strata, Série 1: communications, 16: 16-17; Assoc. Strata, Gaillac (France).
- Blieck A. 2017. Heterostracan vertebrates and the Great Eodevonian Biodiversification Event - an essay. In Mottequin B., Slavik L. & Königshof P. (eds), Climate change and biodiversity patterns in the mid-Palaeozoic (IGCP 596 – SDS Symposium MPBCC, Brussels, 20-22 Sept. 2015). Palaeobiodiversity and Palaeoenvironments: 97(3): 375-390, 7 fig.; Senckenberg Gesellschaft für Naturforschung & Springer-Verlag, Berlin Heidelberg; DOI:10.1007/s12549-016-0260-1.

Stratigraphical, palaeoecological and geochemical consequences resulting from the ostracod study close to the Frasnian / Famennian boundary in the type region for the definition of these two stages

Jean-Georges CASIER

O.D. Earth and Life History, Royal Belgian Institute of natural Sciences, Vautier street 29, B-1000 Brussels, Belgium; casier@naturalsciences.be

The small bivalve crustacean ostracods are certainly the best fossil group useful to reconstruct palaeozoic environments. Their great abundance (they grow by ten or so moltings!), their great diversity and presence in all kind of niches in aqueous environments, from fresh to hypersaline waters, and from high altitude on continents to deep settings in oceans at the very least presently, are the principal reasons. In the marine realm ostracods lived in the upper part of soft sediments, on the bottom, on plants, and some species are nekto-benthic or nekto-planktonic. The principal environmental factors influencing their distribution are the salinity, temperature, nature of substrate, oxygen content, food supply and water motion. Their mode of preservation (carapaces or dissociated valves of adults and instars, sorted valves and carapaces, stacked valves etc.) provides also valuable information on palaeoenvironments. Their study in the type region for the definition of the Frasnian and Famennian stages has lithostratigraphical, chronostratigraphical, palaeoecological and geochemical consequences.

1. Lithostratigraphical consequences

Owing to the parachronology established on entomozoid ostracods, we can state that the Matagne Fm. is composed of two temporally distinct beds (or members) in the Dinant Synclinorium. A diachronic relationship is not supported by the zonation established on that group of ostracods. The first bed (or lower member) cropping out in the vicinity of Frasnes, Mariembourg and Boussu-en-Fagne, never exceeds the *reichi* Zone of the zonation based on entomozoid ostracods, and the second bed (or upper member) recognized north notably in the Neuville railway section, straddles the boundary between the *splendens* Zone and the *sigmoidale* Zone. These two beds or members reflect similar environmental conditions as *e.g.* is the case for the Late Frasnian Lower and the Upper Kellwasser Horizons, in the Kellerwald, Germany. In reality, the stratotype of the Matagne Fm. located along the Mariembourg-Nismes railway section, exposes only the base of its first bed (or member).

At Senzeille, 5.5 m of blackish to bluish shales containing some decalcified nodules separate the Matagne Fm. and the former “Senzeille Assise”. This bed corresponds to the unit “G” of Gosselet (1877), and contains in its upper part the historic Fr/Fa boundary (*Ibid.*). In 1995, Bultynck and Martin proposed to include these “transition” shales in the base of the Senzeille Fm. as an informal member. Ostracods support this proposition: in the lower member of the Senzeille Fm., although not *in-situ*, they are indicative of semi-restricted water conditions whereas in the upper member they are indicative of true marine conditions. The historic Fr/Fa boundary of Gosselet (1877) located in the upper part of this lower member corresponds in reality to this change.

2. Chronostratigraphical consequence

The position of the Fr/Fa boundary in the southern border of the Dinant Basin corresponds probably to the boundary between the *splendens* Zone and the *sigmoidale* Zone of the zonation based on entomozoid ostracods. This boundary is located in the upper part of the second bed or member of the Matagne Fm., at a minimum of 3 m below the base of the Senzeille Fm.. At this level the recovery of the nekto-benthic entomozoid ostracods belonging to the Myodocopid Mega-Assemblage is recorded.

3. Palaeoecological consequences

The ecological study of ostracods proves that the paroxysmal phase of the late Devonian mass extinction is related to a period of hypoxia of marine waters followed and probably linked to a regression close to the Fr/Fa boundary. The hypoxia is marked by the occurrence of the Myodocopid Mega-Assemblage and its acme corresponds to the *splendens* Zone/*sigmoidale* Zone boundary of the parachronology based on entomozoid ostracods. Myodocopid ostracods in “butterfly” position are also indicative of the absence of activity on the sea-floor. The sea-level fall is attested by the occurrence of ostracods indicative of semi-restricted water conditions in several sections, and particularly at Sinsin where stacked valves due to very small waves related to the lap of the water are observed. This fauna has been mobilized periodically, most likely by the seismic activity. However the abnormal great abundance of particularly well preserved dissociated valves of adults and instars indicates a deposition very close to the shore at Hony as it is the case in some other localities (Sinsin, Lambermont) in the southern border of the Dinant Synclinorium. At Senzeille this fauna is more disseminated and consequently indicates a greater distance from the shore. Thus for ostracods, factors linked to global tectonic regime are the most important explaining the Late Devonian mass extinction.

4. Geochemical consequence

Glassy spherules believed to be of impact origin have been reported close to the Fr/Fa boundary in the Hony section (Claeys & Casier, 1994). Later, a geochemical study for trace and major elements was made to test the possibility of an Ir anomaly associated to this spherule layer (Claeys *et al.*, 1996) but no significant positive anomaly was detected. Nevertheless the geochemical analysis showed that chalcophile elements increased close to the Fr/Fa boundary. These increase were interpreted as evidence of a reduction of oxygen content of the sea water during the deposition of the investigate shales (*Ibid*). However the presence of silicified valves and carapaces of ostracods close to the Fr/Fa boundary in the Hony section gives in reality evidence for an intense circulation of bottom water during the diagenesis of sediments. This may explain both the increase of chalcophile elements and the absence of a significant iridium anomaly at this level.

Note that the microtektite-like glass found at Hony are not contemporaneous of those found previously in the Senzeille section (Claeys *et al.*, 1992). These latter are in reality in the base of the second member of the Senzeille Fm. and the progressive recovery of the micro and megafauna after the Fr/Fa bioevent was totally accomplished by this time.

References

- Casier, J.-G., 2017. Ecology of Devonian ostracods: application to the Frasnian/Famennian boundary bioevent in the type region (Dinant Synclinorium, Belgium). *Palaeobiodiversity and Palaeoenvironments*, 97, 3, 556-564. DOI 10.1007/s12549-017-0278-z.
- Casier, J.-G., in press. Ostracod across the Frasnian/Famennian boundary (Devonian) in the Hony railway section (southern border of the Dinant Synclinorium, Belgium) - Geochemical consequences. *Palaeobiodiversity and Palaeoenvironments*. DOI 10.1007/s12549-018-0321-8.
- Claeys, P., Casier, J.-G. & Margolis S., 1992. Microtektites and Mass Extinctions: Evidence for a Late Devonian Asteroid Impact. *Science*, 257, 1102-1104.
- Claeys, P. & Casier, J.-G., 1994. Microtektite-like impact glass associated with the Frasnian-Famennian boundary mass extinction. *Earth and Planetary Science Letters*, 122, 303-315.
- Claeys, P., Kyte, F., Herbosch, A. & Casier, J.-G., 1996. Geochemistry of the Frasnian-Famennian boundary in Belgium: mass extinction, anoxic oceans and microtektite layers, but not much iridium? *Special Paper of the Geological Society of America*, 307, 491-504.
- Gosselet, J., 1877. Quelques documents pour l'étude des Schistes de Famenne. *Annales de la Société géologique du Nord*, 4, 303-320.

***Campanile giganteum* (Lamarck 1804) from the middle Lutetian (~45 Ma) Paris Basin: a potential seasonality archive?**

Alexander CLARK¹, Johan VELLEKOOP^{1, 2}, Niels de WINTER², Philippe CLAEYS^{1,2}, Peter STASSEN^{1,3} & Robert P. SPEIJER¹

¹ Department of Earth and Environmental Sciences, KU Leuven, Celestijnenlaan 200E, B-3001 Heverlee, Belgium.

² Earth System Science, Vrije Universiteit Brussel, Pleinlaan 2, B-1050, Brussels, Belgium.

³ Directorate Earth and History of Life, Royal Belgian Institute of Natural Sciences, Vautierstraat 29, B-1000 Brussels, Belgium.

Fossil gastropod shells have often been used as paleoenvironmental and paleoclimatic archives (Andreasson & Schmitz 1996, Huyghe et al. 2015). Usually, stable carbon and oxygen isotopes, $\delta^{13}\text{C}$ and $\delta^{18}\text{O}$ respectively, and the incorporation of elements such as Sr and Mg, are used to reconstruct variations in paleotemperature and seasonality. However, most of the commonly used gastropod species only have lifespans of a few years. In this study, a *Campanile giganteum* (Lamarck 1804) specimen from the Lutetian of Fleury-la-Rivière (Paris Basin, France) was examined for its potential to reconstruct climate conditions during the middle Eocene. With an estimated lifespan of ~20 years, this extremely large species might provide an exceptionally long record of seasonal variations in temperature and salinity. A comparison to the nearest living relative, *Campanile symbolicum* (Iredale 1917), suggests that both taxa live at sublittoral depths in subtropical climates (Houbrick 1981).

Cathodoluminescence microscopy was performed on our specimen to evaluate the extent of diagenetic alteration. No significant alterations were found, illustrating the excellent preservation of carbonates at the Fleury-la-Rivière locality. Micro-X-Ray-Fluorescence line scanning was used to determine elemental concentrations in the columellar and parietal walls. Measuring along the columella of the gastropod yielded accurate results, indicating its potential as a future method of examination in long-living gastropods. Correlations between carbonate $\delta^{13}\text{C}$ and $\delta^{18}\text{O}$ values of the parietal wall segments and the corresponding elemental ratios of Sr/Ca (Fig.1) and Ba/Ca illustrate their potential as seasonality proxies. A possible paleoproductivity proxy using Sr/Ca and $\delta^{13}\text{C}$ was inferred. Our analyses also revealed a possible species-specific incorporation of Mg and Cl. A model for the growth of *C. giganteum* is proposed based on the growth of modern gastropod shells (Tojo & Ohno 1999).

This reveals the potential future use of carbon and oxygen isotopes incorporated into the secondary whorl infills as a paleotemperature archive after the main shell growth has stopped. Paleoclimatologically, it was found that the modern Red Sea represents a possible analogy to the Paris Basin in the middle Eocene. Using stable carbon and oxygen isotopes, mean annual seawater temperatures between 22°C and 23°C were reconstructed, with a range of $\pm 5^\circ\text{C}$ depending on the temperature calibration used. This is comparable to other ranges found for the middle Eocene of the Paris Basin (Andreasson & Schmitz 1996, Huyghe et al. 2015) and confirms the potential use of the geochemical composition of *C. giganteum* species as a paleotemperature and paleoseasonality proxy.

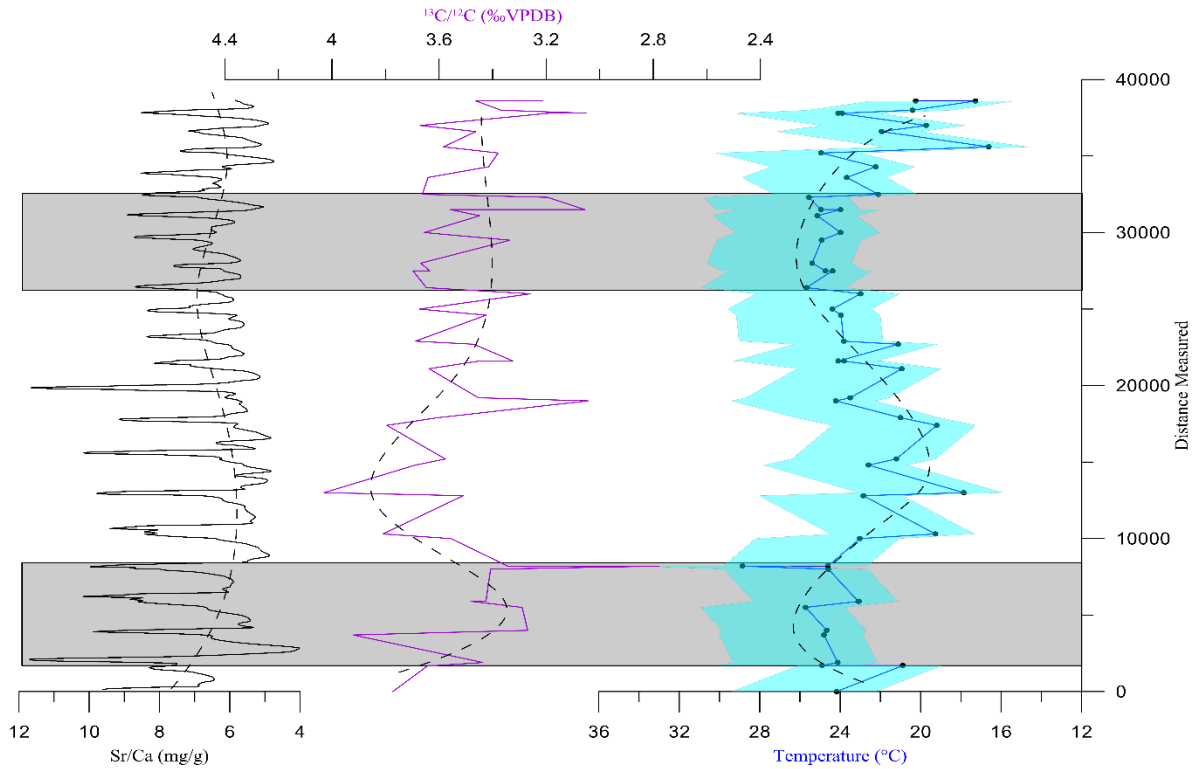


Figure 1. Temperature (based on $\delta^{18}\text{O}$), Sr/Ca and $\delta^{13}\text{C}$ ratios showing seasonality. The light grey areas represent summers while the white areas reflect other seasons. The dotted lines are manual fits of the data.

References

- Andreasson, F.P. & Schmitz, B., 1996. Winter and summer temperatures of the early middle Eocene of France from *Turritella* $\delta^{18}\text{O}$ profiles. *Geology*, 24, 1067-1070.
- Houbrick, R.S., 1981. Anatomy, Biology and Systematics of *Campanile symbolicum* with reference to adaptive radiation of the Cerithiacea (Gastropoda: Prosobranchia). *Malacologia*, 21, 263-289.
- Huyghe, D., Lartaud, F., Emmanuel, L., Merle, D. & Renard, M., 2015. Palaeogene climate evolution in the Paris Basin from oxygen stable isotope ($\delta^{18}\text{O}$) compositions of marine molluscs. *Journal of the Geological Society*, 172, 576-587.
- Tojo, B. & Ohno, T., 1999. Continuous growth-line sequences in gastropod shells. *Palaeogeography, Palaeoclimatology, Palaeoecology*, 145, 183-191.

Palaeoecology of the Upper Tournaisian “Petit Granit”: much more than crinoids!

Julien DENAYER¹ & Laurent DEBOUT¹

*1 EDDy Lab – Université de Liège. *julien.denayer@uliege.be*

The Tournaisian stage (Lower Carboniferous) is considered as the golden age of crinoids. In S Belgium, upper Tournaisian crinoidal limestones – “Petit Granit” – are known in the Condruz area (Ourthe Formation) and in the Soignies area (Soignies Member) where tens of quarries expose the crinoidal facies. Despite its apparent monotony, five crinoidal and peloidal microfacies are identified throughout the formation, and the size and preservation of the crinoid columnals vary vertically and laterally. The encrinite deposited as amalgamated tempestites that accumulated under the fair-weather wave base. An estimation of the carbonate production rate in both sedimentation areas was calculated based on geological and biological hypothesis. A value of c. 1200 cm³/m².y is proposed for the Ourthe Fm. The crinoid density was lower in the HSA (Hainaut Sedimentation Area) possibly due to its deeper situation, as also suggested by the dominance of packstone microfacies. An isopachs map shows that the Ourthe Formation thins westwards and northwards, with a maximal thickness in the Ourthe valley area. The local variation of thickness is tentatively interpreted by variations in subsidence due to synsedimentary block faulting.

The modern taxonomy of crinoids is based on the morphological characters of the crown (calyx, arms) but complete calyxes are extremely rare in the “Petit Granit” due to hydrodynamic disarticulation. Hence, the parataxonomy based on the morphology of columnals, developed by Moore & Jeffords (1968), was used on disarticulated crinoid columnals in thin sections. Though not perfect, this analysis provides a good rough approach of the diversity. It reveals an unexpectedly diverse crinoidal meadows where several genera and species co-existed. The identified crinoid taxa are of several size class and were seemingly distributed following a vertical tiering model to maximise the capture of food particles from the water column.

Beside the crinoids, the fauna was dominated by suspension feeders (brachiopods, bryozoan, sponges, tabulate and rugose corals) adapted to a weakly-agitated environment and a relatively soft ground. The trilobites and palaechinids were the dominant benthic macrophages, the latter being known as a predator of crinoids. Rare nektonic predators were occasional dwellers of the crinoidal meadows (holocephalan chondrychthian, actinoceratoids, palaechinids and trilobites) shows that the ecosystem was relatively complex despite a simple appearance. Moreover, it witnesses the recovery of the marine environment after the collapse of the reefal ecosystem at the end of the Devonian, when the echinoderms became the dominant carbonate producer in neritic environments.

References

Moore, R.C. & Jeffords, R.M., 1968. Classification and nomenclature of fossil crinoids based on studies of dissociated parts of their columns. University of Kansas, Paleontological Contributions, Echinodermata, 9, 1-86.

An Eifelian story of reefs and reef builders: the Belgian case re-investigated

Julien DENAYER

*EDDy Lab – Université de Liège. *julien.denayer@uliege.be*

The Eifelian is well exposed in southern Belgium where it displays facies ranging from stromatoporoid biostromes (SW) to outershell fine siliciclastics to proximal redbeds (NE). The carbonate factory started already in the Late Emsian with the deposition of mixed siliciclastic-bioclastic units, progressively purer as the transgression progressed. There is no reef *sensu stricto* in these St-Joseph and Eau Noire formations but local accumulation of tabulate corals and stromatoporoids acknowledges the occurrence of environmental conditions suitable for their growth. The oldest reef in the Devonian of Belgium is the “premier biostrome” of the Couvin Formation (Fm) (Foulerie member (Mbr), Bultynck, 1970, fig. 1): a succession of <1m-thick autobiostrones with lamellar stromatoporoids and tabulate corals, stabilising crinoidal rudstones. Rugose corals are uncommon: some fasciculate colonies of *Sociophyllum* and rare solitaires. Up-section, these beds are often made of broken skeleton suggesting higher hydrodynamic conditions, and appear as parabiostromes. This first complex is c. 15-20 m-thick in Villers-la-Tour and Couvin and covered with mostly bioclastic beds. The “deuxième biostrome” comprises a 50-m-thick succession of c. 1-m-thick parabiostromes with large domal and bulbous stromatoporoids, massive tabulate corals and heliolitids with abundant large solitary corals (*Mesophyllum*, *Cystiphyllum* and *Acanthophyllum*). Each parabiostrome is separated from the next one by 10-20 cm of bioclastic argillaceous limestone beds. The upper part of the Foulerie Mbr comprises mostly bioclastic, often dolomitised limestone displaying a shallowing-upwards trend. It is rich in fauna, including brachiopods, large solitary rugosa, delicate ramose tabulate corals and tubular stromatoporoids. The “troisième biostrome”, exposed in the Abîme Cliff of Couvin comprises several thin stromatoporoid biostromes and two thicker parabiostrome made of large bulbous stromatoporoids and tabulate corals. These biostromes alternates with “lagoonal” limestone made of debris of fasciculate tabulate and rugose corals and of tubular stromatoporoids, in a fine-grained matrix. The Couvin Fm is overlaid by the shales and calcareous shales of the Jemelle Fm in which are developed small (c. 300 m-large, 150 m-thick) bioherms in Macon, Salles, Bourlers, Couvin and Nismes. These lense-like bioherms are made of lamellar and massive stromatoporoids covering crinoidal gravel, passing to framestone of tabulate corals still rich in crinoids, with some large colonies of the rugose coral *Cyathophyllum*. This succession is regarded as the “classical Couvinian” (Bultynck, 1970; Godefroid, 1968).

Eastwards, between Petigny and Nismes, the Foulerie Mbr disappears and is replaced by the siltstone and shale of the Vieux-Moulin Mbr (Dumoulin & Coen, 2008), possibly along a synsedimentary fault. The Abîme Mbr disappears as well but in a continuous manner between Nismes and Givet. In Nismes, the member includes the same thin stromatoporoids-tabulate corals biostromes alternating with fine-grained facies but the main biostrome is replaced by a c. 20-m-thick bioherm made of fasciculate coral framestone and stromatoporoid coverstone with abundant fauna. Several smaller biostrome and coral beds cover it and the succession is capped by a *Spongophyllum* bed that can be traced to Olloy eastwards. Whereas the limestone member thins progressively (160 m in Nismes, 60 m in Olloy, 45 m in Vierves, < 30 m in Mazée), the biostrome

is replaced by argillaceous limestone (Vierves) then by calcareous siltstone (Foisches). East of Olloy, this unit is considered as a different member, the name Vierves Mbr is proposed.

After the local disappearance of limestone facies in the Meuse valley (probably the deepest part of the basin), limestone re-appears in Fromellennes with argillaceous facies. In Dion, the siliciclastic Vieux Moulin Mbr displays surprising facies with the development of small (c. 350 m-long, c. 50 m-thick) biohermal lenses made of lamellar stromatoporoids and fasciculate rugose corals. This reef is covered by shales and siltstones passing upwards to dark argillaceous limestone that possibly corresponds to the Abîme Mbr. Between Wancennes and Pondsôme, an anomaly in thickness of the “Couvin Fm” was noted by Dumoulin & Blockmans (2008) and on their geological map. This anomaly is due to the development of a massive bioherm c. 3 km-long and 250 m-thick laterally to the Vieux Moulin and Vierves members. This reef starts with large lamellar stromatoporoids stabilising lenses of crinoidal gravel extremely rich in brachiopods, gastropods, trilobites and tabulate corals. It passes upwards to a framestone of ramose tabulate and fasciculate rugose corals with stromatoporoids then to a framestone comprising large bulbous stromatoporoids and heliolitids in the reef crest. The upper part of the reef, reef crest excepted comprises a rich and very diverse coral fauna with large solitary (*Cystiphyllum*, *Mesophyllum*, *Acanthophyllum*, *Stringophyllum*), fasciculate (*Fasciphyllum*, *Lyriellasma*, *Dendrostella*, *Sociophyllum*, *Thamnophyllum*) and massive rugose corals (*Spongophyllum*, *Xystriphyllum*, *Beugniesatsraea*) together with massive and ramose tabulate corals. The top of the reef is not exposed but it seems to be very clear-cut, suggesting an emersion (sequence boundary?) before deposition of the shaly Jemelle Fm. The bioherm is again replaced by the siliciclastics of the Vieux Moulin Mbr east of Wancennes. However, a c. 40-m thick unit of bedded dark limestone with tabulate corals and stromatoporoids persist up to Wellin with an increasing dolomitisation eastwards.

In Wellin another abnormality is developed in the Jemelle Fm where small bioherms in the upper part of the formation evolved into massive crinoidal limestone with stromatoporoids yielding an abundant coral fauna (Coen-Aubert et al., 1991). East of Wellin, the Eifelian succession is dominated by the siliciclastic Jemelle and Lomme formations with some rare occurrences of thin corals and stromatoporoids beds that can be traced from the Jemelle area up to the Aisne valley.

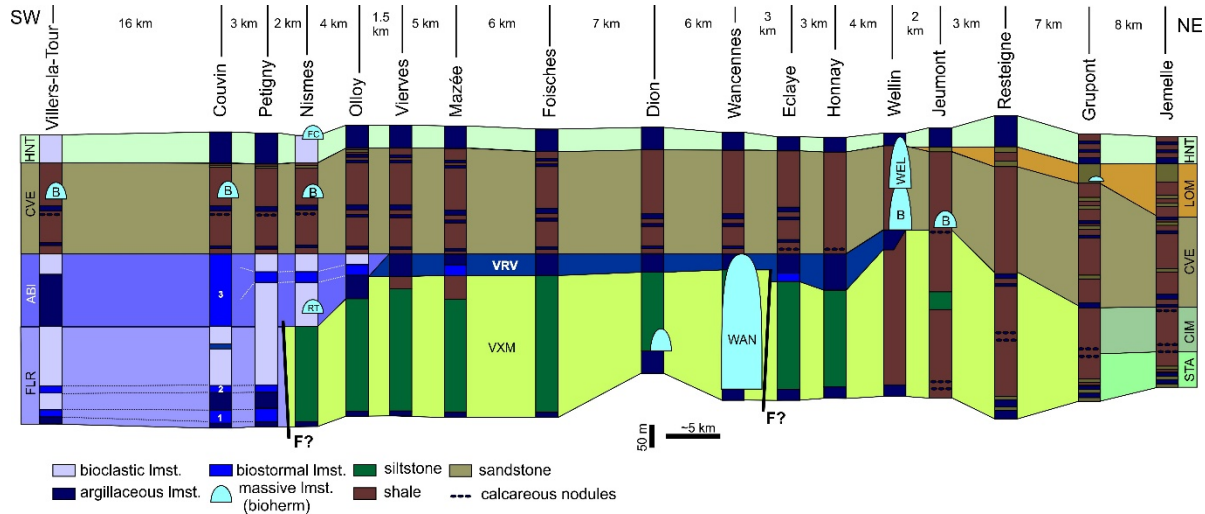


Figure 1. Lateral facies changes between Villers-la-Tour and Jemelle. Modified from Dumoulin & Blockmans (2008) with additions from Bultynck (1970), Godefroid (1968), Coen-Aubert et al. (1991). Legend: ABI: Abîme Mbr (Couvin Fm), B: Bioherm (Jemelle Fm), CIM: Cimetière Mbr (Jemelle Fm), CVE: Chavées Mbr (Jemelle Fm), FC: Fondry des Chiens bioherm, HNT: Hanonet Fm, LOM: Lomme Fm, RT: Roche Trouée bioherm, STA: Station Mbr (Jemelle Fm), VXM: Vieux Moulin Mbr (Jemelle Fm): WAN: Wancennes bioherm, WEL: Wellin bioherm (Formation X in Coen-Aubert et al., 1991); F?: putative synsedimentary fault; 1-3 in Couvin section: 1st, 2nd and 3rd biostrome of Bultynck (1970).

References

- Bultynck, P., 1970. Révision stratigraphique et paléontologique (brachiopodes et conodontes) de la coupe type du Couvinien. Mémoires de l'Institut géologique de l'Université de Louvain, 26, 1-150.
- Coen-Aubert, M., Mamet, B., Prétat, A. & Tourneur, F., 1991. Sédimentologie, paléoécologie et paléontologie des calcaires crinoïdiques au voisinage de la limite Couvinien-Givetien à Wellin (bord sud du Synclinorium de Dinant, Belgique). Mémoire pour servir à l'explication des cartes géologiques et minières de la Belgique, 31, 1-61.
- Dumoulin, V. & Coen, M., 2008. Carte géologique de Wallonie : Olloy-sur-Viroin – Treigne (58/5-6). Carte au 1/25000 et sa notice explicative, 103 p.
- Dumoulin, V. & Blockmans, S., 2008. Le passage latéral entre les formations de Couvin et de Jemelle (Eifelien) au bord sud du Synclinorium de Dinant (Belgique): Introduction du Membre du Vieux Moulin-Formation de Jemelle. *Geologica Belgica*, 11, 25-33.
- Godefroid, J., 1968. Contribution à l'étude du Couvinien entre Wellin et Jemelle (bord sud du bassin de Dinant). *Mémoire de l'Académie royale de Belgique, Classe des Sciences*, 13, 1-79.

Shelf ecosystems prior and during the PETM along the US Atlantic Coastal Plain

Monika DOUBRAWA¹, Peter STASSEN^{1,2}, Linde VANLOOK¹, Marci M. ROBINSON³ & Robert P. SPEIJER¹

¹ Department of Earth and Environmental Sciences, KU Leuven, Belgium.

² OD Earth and History of Life, Royal Belgian Institute of Natural Sciences, Belgium.

³ US Geological Survey, Eastern Geology and Paleoclimate Science Center, Virginia, US.

During the early Paleogene, Earth's climate was characterized by a long-term warming trend that was punctuated by short-term global warming events known as hyperthermals. These climate events are recognized by negative $\delta^{18}\text{O}$ and $\delta^{13}\text{C}$ excursions, and environmental perturbations, with the Paleocene-Eocene Thermal Maximum (PETM) being the most pronounced one. The PETM in the subsurface of the US eastern coastal plains is marked by the widespread distribution of fine-grained sediments, probably related to a regional intensification in river outflow, contrasting with the Paleocene sediment-starved setting. Recent stable isotope data show an additional small, but distinct, $\delta^{13}\text{C}$ excursion in a more clayey interval below the onset of the PETM, coined the POE, or "pre-onset excursion" (as represented in Fig. 1.) The relationship with the PETM is still unclear, but the POE may indicate that latest Paleocene climate was not as stable as previously assumed, but exhibited a more gradual change towards the PETM onset.

Our study focuses on the recognition of paleoenvironmental changes prior to the PETM, using various drill cores retrieved from the US Atlantic Coastal Plain. The South Dover Bridge (SDB) core serves as the reference site, as the Paleocene-Eocene transition is stratigraphically confined by nannoplankton zones, and the POE and PETM are lithologically well-expressed in respectively the top part of the Paleocene Aquia Formation and the Marlboro Clay. In addition, the SDB site is presumed to be situated in a shallow marine setting near the paleo-Potomac River outflow system in a comparable setting as the New Jersey Coastal Plain, thus allowing for an insight into regional variations in the hydrological cycle (Self-Trail et al., 2012). Here we present our preliminary interpretation of paleoenvironmental changes during the late Paleocene and earliest Eocene, as expressed in the biotic, geochemical and lithological records.

Three main biofacies are presented based on the relative abundances of four recognized benthic foraminiferal species associations. Biofacies A is present in the upper Paleocene glauconitic fine sands. This biofacies contains a mixture of the foraminiferal Ia association, consisting of e.g. *Epistominella minuta* and *Paralabamina lunata*, and the Ib association of *Anomalinoidea midwayensis* and *Cibicidoides alleni*. Both are associated with a middle neritic depositional setting and stable, well-oxygenated oligo- to mesotrophic bottom water conditions. This biofacies includes the POE, marked by more silty sediments and a negative stable carbon excursion at SDB. It is hypothesized that the POE corresponds to a regional pulse in fluvial sediment discharge preceding the PETM. The second Paleocene biofacies (B), which is characterized by increased abundances of *E. minuta* and *P. lunata*, is present in the interval between the top of the POE and the base of the PETM. These species indicate an episodic supply of organic flux to the sea floor in the aftermath of the POE. Across the onset of the PETM, the diversity of the foraminiferal fauna decreases noticeably, pointing towards a drastic

change of living conditions. Biofacies C is restricted to the PETM and therefore reflects the specific environmental conditions associated with the widespread deposition of the Marlboro clay. This biofacies contains characteristic PETM-related foraminiferal association III such as *Anomalinoidea acutus* and *Pulsiphonina prima*. Other associated taxa, e.g. *Bulimina virginiana* or *Spiroplectinella laevis* are also considered more stress-tolerant species (association II), and were already present during the Paleocene. Similar to the New Jersey Coastal Plain setting (e.g. Stassen et al., 2015), the global warming conditions resulted in an intensified fluvial influence of the region, causing annual to periodically dysoxic bottom water conditions. Remarkably, the topmost PETM foraminiferal assemblage indicates sustained high food levels and increasing oxygen levels, related to a decrease in river-induced stratification. This tendency towards more silty and less clayey sediments is linked to renewed bottom current activities and winnowing, although sediment accumulation rates remained high. As comparable regional data on the POE, PETM and younger intervals become available, we will be able to establish the strength of river influence, paleodepth variations and distance to shore during the latest Paleocene and earliest Eocene.

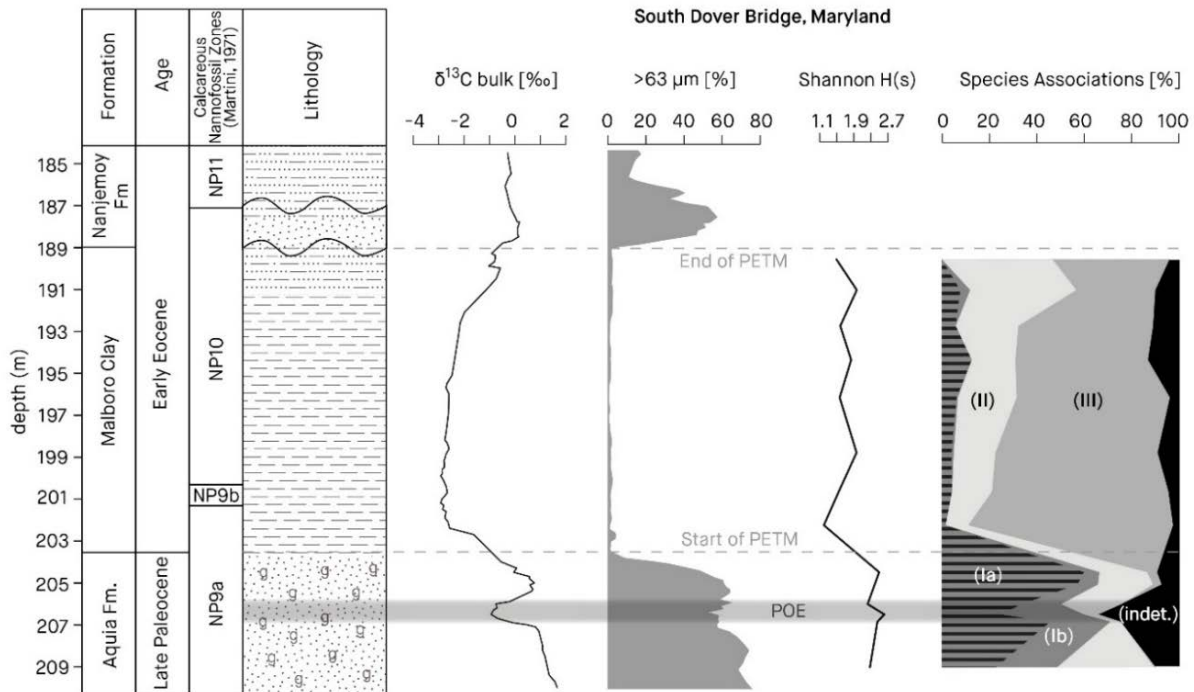


Figure 1. $\delta^{13}\text{C}$ bulk carbonate (Self-Trail et al., 2012), grain size ($>63\ \mu\text{m}$) and foraminiferal abundance data (species associations I (a+b), II and III, black: undetermined individuals and least abundant species) across the Paleocene-Eocene boundary. Gray interval corresponds with POE, dashed lines indicate beginning and end of the PETM interval.

References

- Self-Trail, J. M., D. S. Powars, D. K. Watkins & G. A. Wandless, 2012. Calcareous Nannofossil Assemblage Changes across the Paleocene–Eocene Thermal Maximum: Evidence from a Shelf Setting. *Marine Micropaleontology*, 92–93, 61–80.
- Stassen, P., E. Thomas & R. P. Speijer, 2015. Paleocene-Eocene Thermal Maximum environmental change in the New Jersey Coastal Plain: benthic foraminiferal biotic events. *Marine Micropaleontology*, 115, 1–23.

Geochemical record of Lake Jeinimeni and environmental variability over the last centuries in Northern Chilean Patagonia

Nathalie FAGEL¹, Pablo PEDREROS², Denisse ÁLVAREZ², Isabel BILLY³, Philippe MARTINEZ³, Sabine SCHMIDT³, Frédéric BOULVAIN⁴, Olivier NAMUR⁵ & Roberto URRUTIA²

¹ AGEs – Geological department, University of Liège, Belgium.

² EULA Aquatic Systems Research Unit, University of Concepcion, Chile.

³ UMR EPOC, Université de Bordeaux, France.

⁴ Pétrologie sédimentaire, Département de Géologie, Université de Liège, Belgium.

⁵ KU Leuven, Department of Earth and Environmental Sciences, Leuven, Belgium.

1. Introduction

The precipitation regime in southern South America evidences strong correlations with the general atmospheric circulation. Located in the mid-latitude 30-60°S belt, Patagonia is comprised between two main circulation systems, the Intertropical Convergence Zone to the North and the Antarctic Convergence Zone to the South (Moy et al., 2009). Its present climate is therefore influenced by both tropical and polar oscillation modes mainly the El Niño-Southern Oscillation (ENSO) and the Antarctic Oscillation. For the last decades, paleoclimate studies in Patagonia have emphasized climate variability strongly controlled by the latitudinal position and intensity of the Southern Westerly Wind over the Holocene (Gilli et al. 2005). Precipitation variations derived from different paleoclimate proxies and archives were used to reconstruct the evolution of SWW, in term of wind intensity and latitudinal position over the Holocene (Lamy et al. 2010). According to vegetation distribution, SWW were probably located southwards (45-50°S) during the early Holocene. The wind belt started to migrate northwards during the middle Holocene and reached their modern position in the late Holocene. This latitudinal migration is responsible for the Late Holocene higher climate variability in Patagonia (Markgraf et al. 2013). In this study XRF core scanner geochemical profile of a lacustrine sediment core was used to evaluate the environmental and/or climate variability of Northern Chilean Patagonia over the last centuries.

2. Sediment material and age

The lake Jeinimeni (46°5'S, 72°W) is located in a natural reserve in the region of Chile Chico. The lake lays in NW Patagonia, an area characterized by cold and steppic conditions with less than 300 mm by year of precipitation, mainly as snow (annual average 286 mm ± 106 over 1958-1980, WMO data from Chile Chico weather station). The core (161 cm long) was collected with an UWITEC gravity corer in 2014 at a water depth of 60 m. The sediment is terrigenous with a low organic matter content (mean 2.5%, C/N 16.7) of allochthonous origin. Visual descriptions and Scopix radiographies show that the sediment is finely laminated, made by light brown clayey silts and fine sands with a few centimetric coarser layers. Magnetic susceptibility highlights the presence of a 5 mm-thick tephra layer in the upper part of the core. A second less marked tephra is evidenced by visual observation and is currently being confirmed by glass shard separation. Those two tephra may correspond to recent eruptions of the Hudson volcano (1991, 1972AD). Such

interpretation is consistent with the age model based on ^{210}Pb and ^{137}Cs data and demonstrates that the upper 17 cm of the core covers the last century with an average sedimentation rate of 1.3 mm/yr. The laminated structure of the sediment, confirmed by thin section observation, is consistent with an annual deposition at least for the upper part of the core.

3. Geochemical results and interpretation

A multivariate statistical analysis of the raw XRF data was run using the R software 3.5.0. The principal component analysis (PCA) evidences 4 principal components. The first component PC1 composed by Al, Si, Ti, K, Y and Fe represents 47% of the variance. The second component PC2 is explained by Ca and Sr and corresponds to 10 % of the variance. According to the sample distribution in the PC1-PC2 factor map PC2 is controlled by the main tephra layer. The tephra-free PCA allows to decipher three groups of samples (Fig.1). The first group plots close to PC1 axis, it corresponds to the argillaceous Al-rich layer. The second and third groups are distributed along the PC2 axis lead by Zr and Rb. The second group covaries with Zr and Rb. They coincide with plurimillimetric sandy-layers and probably represent flood-like events related to heavy rains. The third group of samples is made by a few pluricentimetric sandy and gravely layers that interrupt the background sedimentation. They correspond to massive erosional events due to watershed perturbation. The evolution of PC1/PC2 ratio probably record flood-like events, bringing to the lake variable detrital supplies according to the precipitation rate.

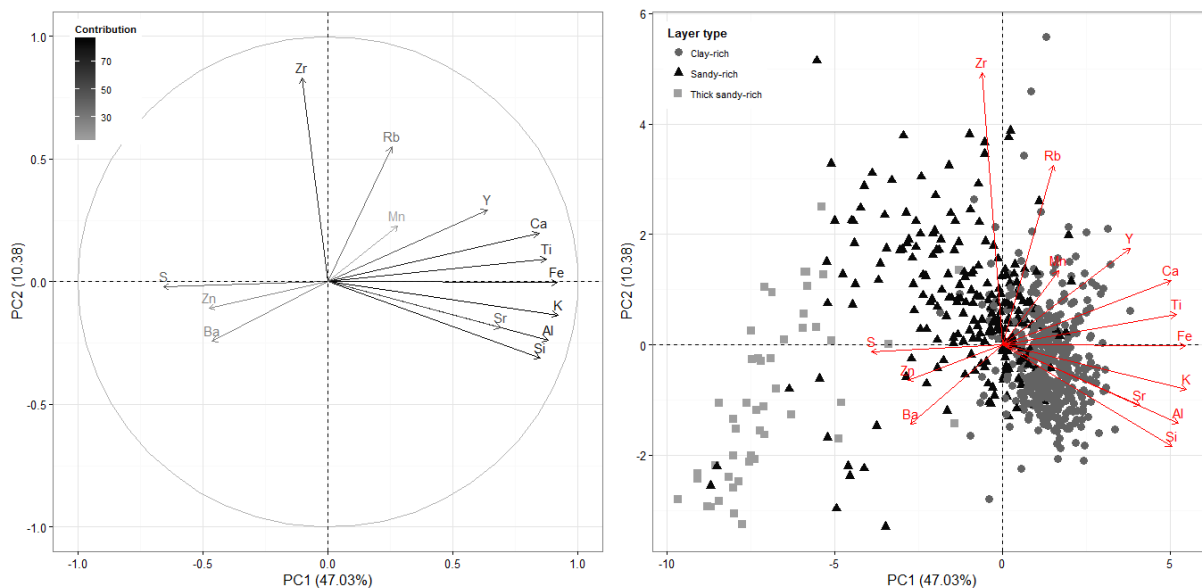


Figure 1. PCA results on XRF core scanner data performed at 2 mm of resolution.

4. Conclusion and further studies

Our study site, the Lake Jeinimeni, allows to document environmental and climate variability in Patagonia over the last centuries. By combining sedimentological and geochemical proxies the lacustrine sequence reveals recurrent coarse detrital supplies attributed to floods. Lamination counting (in progress) will confirm the varve character of the sediment deposition model. The time-

series flood record will be compared with regional paleoclimate reconstructions derived from Patagonian archives to decipher between local and regional climate influences - This research is funded by WBI-Chile cooperation project.

References

- Gilli, D. Ariztegui, F. Anselmetti, J. McKenzie, V. Markgraf, I. Hajdas & McCulloch R., 2005. Mid-Holocene strengthening of the southern westerlies in South America - sedimentological evidences from Lago Cardiel, Argentina (49°S). *Global & Planetary Change* 49, 75-93.
- Lamy, F., Kilian, R., Arz, H., Francois, J.-P., Kaiser, J., Prange, M., & Steinke, T., 2010. Holocene changes in the position and intensity of southern westerly wind belt. *Nature Geoscience* 3, 695-699.
- Margraf V., Iglesias V. & Whitlock C., 2013. Late and postglacial vegetation and fire history from Cordón Serrucho Norte, northern Patagonia. *Palaeogeography, palaeoclimatology, palaeoecology*, 371, 109-118
- Moy C., Moreno P. I., Dunbar R., Kaplan M. R, Francois J., Villalba R. & Haberzettl T., 2009. Climate change in southern South America during the last two millennia. In *Past climate variability in South America & surrounding regions*, 353-393, Springer, Dordrecht.
- Villalba R., 1994. Tree-ring and glacial evidence for the Medieval Warm Epoch and the Little Ice Age in southern South America. *Climatic Change* 26, 183-197.

Evolution of the Cretaceous shot-necked plesiosaurians

Valentin FISCHER¹, Roger B. J. BENSON², Nikolay G. ZVERKOV³, Laura SOUL⁴, Maxim S. ARKHANGELSKY⁵, Olivier LAMBERT⁶, Ilya M. STENSHIN⁷, Gleb N. USPENSKY⁸, Patrick S. DRUCKENMILLER⁹, Hilary F. KETCHUM¹⁰ & Nathalie BARDET¹¹

¹ *Evolution & Diversity Dynamics Lab, UR Geology, Université de Liège. B18, 14 allée du 6 août, 4000 Liège, Belgique.*

² *Department of Earth Sciences, University of Oxford, Oxford OX1 3AN, UK.*

³ *Lomonosov Moscow State University, Leninskie Gory 1, GSP-1, Moscow 119991, Russia*

⁴ *Department of Paleobiology, Smithsonian Institution, P.O. Box 37012, Washington DC 20013-7012, USA.*

⁵ *Ecological Faculty, Saratov State Technical University, Politekhnickeskaya Ul. 77, Saratov 410054, Russia.*

⁶ *Earth and History of Life O.D., Royal Belgian Institute of Natural Sciences, 29 Rue Vautier, 1000 Brussels, Belgium.*

⁷ *I.A. Goncharov Ulyanovsk Regional Natural History Museum, Boulevard Novyi Venets 3/4, Ulyanovsk 432000, Russia.*

⁸ *Natural Science Museum, Ulyanovsk State University, Ulitsa L. Tolstogo, 42, 424320 Ulyanovsk, Russia.*

⁹ *University of Alaska Museum and Department of Geosciences, University of Alaska Fairbanks, 907 Yukon Drive, Fairbanks, AK 99775, USA.*

¹⁰ *Oxford University Museum of Natural History, Parks Road, Oxford OX1 3PW, UK.*

¹¹ *CR2P CNRS-MNHN-UPMC Paris 6, Département Origines et Evolution, Muséum National d'Histoire Naturelle, CP 38, 57 rue Cuvier, 75005 Paris, France.*

Plesiosauria is the most diverse and probably the most disparate clade of secondarily aquatic tetrapods. The adaptive landscape of plesiosaurians has been often summarised to two global morphotypes: one for short-necked forms (pliosauromorphs) and one for long-necked forms (plesiosauromorphs). ‘Pliosauromorphs’ and especially pliosaurids are iconic marine reptiles that dominated marine ecosystems during the Jurassic and the Cretaceous. These giant predators met their demise during the early Late Cretaceous but the final chapter of their long evolutionary history remains barely documented. Prompted by the discovery of a peculiar and very well preserved new taxon from Russia (Figure 1), we compute the evolution of pliosaurid disparity from their Early Jurassic radiation to their Late Cretaceous extinction. Despite a patchy Early Cretaceous fossil record, we show pliosaurids reached their maximal disparity during the Hauterivian-Barremian interval, suggesting a strong Early Cretaceous recovery from the apparently low phenotypic disparity of Late Jurassic pliosaurids. By using cladistic and morphological data, we show that pliosaurids have repeatedly converged with another group of short-necked plesiosaurians, Polycotylidae, demonstrating a more complex evolutionary history than their traditional representation as gigantic apex predators of Mesozoic marine ecosystems suggests. The extinction of pliosaurids during the Turonian (early Late Cretaceous) and polycotylids at the KT boundary

are both preceded by a marked contraction of their disparity, similar to the trajectory documented in ichthyosaurs, another successful marine reptile clade that disappeared during the Cretaceous.

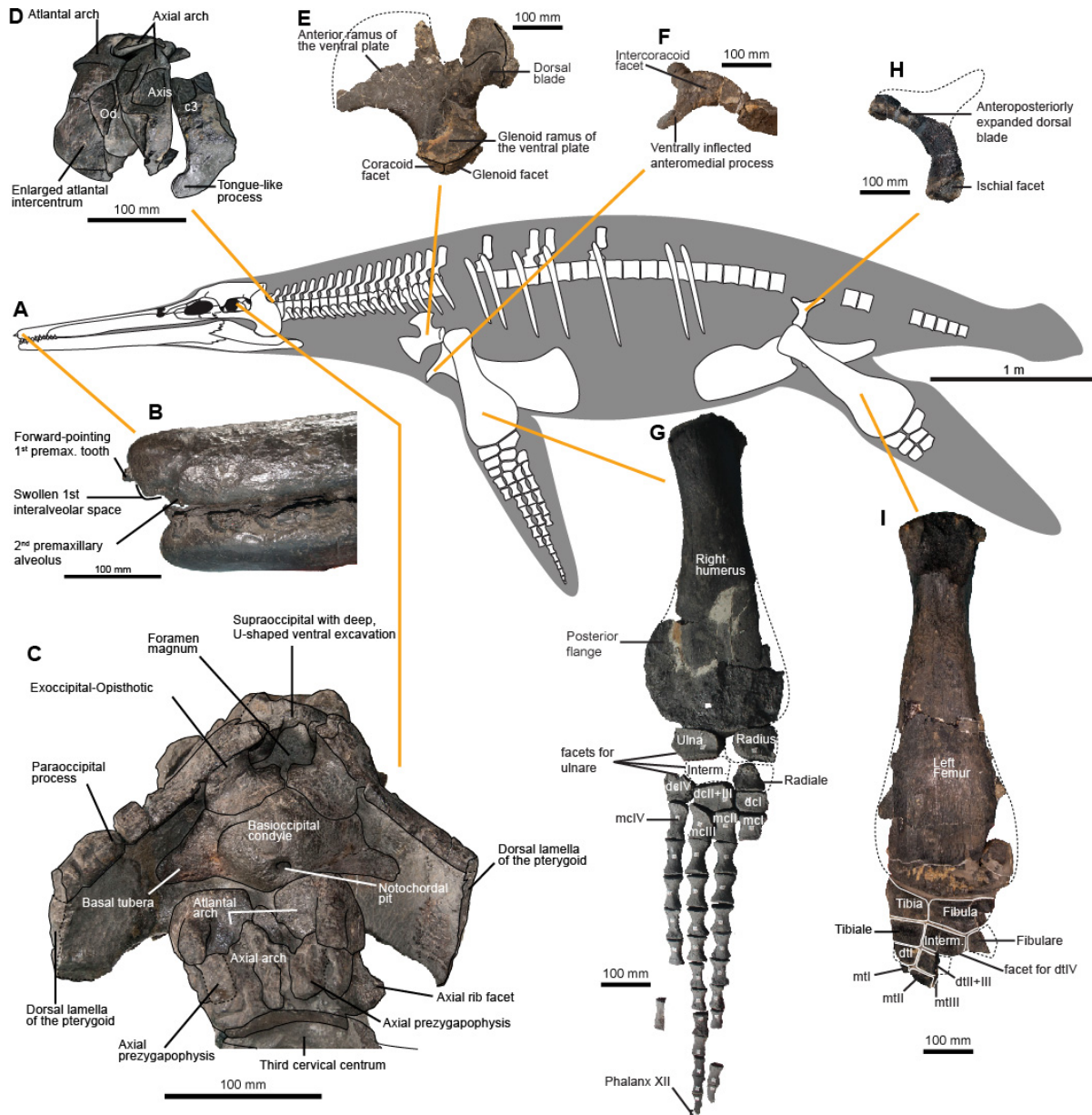


Figure 1. Morphology of the holotype of *Luskhan itilensis* (YKM 68344/1_262) from the Hauterivian of western Russia.

Sedimentary evolution of the Sagara coastal area in Japan and its potential to preserve extreme wave deposits

Philipp KEMPF¹, Ed GARRETT^{1,2}, Osamu FUJIWARA^{3,4}, Yusuke YOKOYAMA⁵, Vanessa M.A. HEYVAERT^{1,6}, Marc DE BATIST⁶ and the QuakeRecNankai Team

¹ *Royal Belgian Institute of Natural Sciences, OD Earth and History of Life, Geological Survey of Belgium, Jennerstraat 13, 1000 Brussels, Belgium.*

² *Department of Geography and Institute of Hazard, Risk and Resilience, Durham University.*

³ *Geological Survey of Japan, National Institute of Advanced Industrial Science and Technology, Japan.*

⁴ *Geoinformation Service Center, Institute of Earthquake and Volcano Geology.*

⁵ *Atmosphere and Ocean Research Institute, University of Tokyo, Japan.*

⁶ *Renard Centre of Marine Geology, Department of Geosciences, Ghent University, Krijgslaan 281, 9000 Ghent, Belgium.*

1. Introduction

Japans Pacific coast towards the Nankai Trough experienced a Holocene sea level highstand. The vertical displacement of the shoreline dominated the sedimentary evolution of coastal areas. These are the same coastal areas, which are now targeted by geoscientists, because recent events have highlighted the importance of coastal sedimentary records in assessing tsunami risk. After the unexpectedly large impact on the coastal regions of northern Japan during the 2011 Tōhoku earthquake and tsunami, the Central Disaster Management Council of the Japanese Cabinet Office specifically included the necessity to pay more attention to evidence from geological records to seismic risk assessment guidelines. This was introduced as a direct response to the disastrous Fukushima-Daiichi reactor melt-downs and the successful prevention of a similar disaster at the Onagawa nuclear power plant, where the Coastal Engineering Committee was aware of historical and geological evidence of the CE 869 Jōgan tsunami and advised to build accordingly. On the coast along the Nankai Trough similar insight before the next great tsunami could prevent death and infrastructural damage.

2. Setting

The Nankai-Suruga subduction zone is the destructive plate boundary between the overriding Eurasian Plate and the subducting Philippine Sea Plate. The relative motion of 40-55 mm yr⁻¹ on average causes extreme earthquakes to occur on the Nankai megathrust. The lowlands of Sagara are located on the coast of the easternmost section of the Nankai-Suruga subduction zone, the so-called Tōkai region. Historical and geological evidence exist for megathrust earthquakes from at least six earthquakes in 684 CE (Tenmu or Hakuho), 1096 (Eichō), 1361 (Shōhei), 1498 (Meiō), 1707 (Hōei) and 1854 (Ansei), which ruptured beneath the study area (Ando, 1975; Garrett et al., 2016). Our aim is to reveal the coastal sedimentary evolution of the Sagara coastal and, if possible, identify traces of overwash events in the sedimentary record and possibly expand the tsunami record in the region.

3. Methods

We collected cores of the Sagara floodplain in two field campaigns in 2016 and 2017. All cores were split, sedimentologically described, analyzed with a multi sensor core logger using a gamma ray attenuation density sensor, a magnetic susceptibility point sensor and a spectrophotometer. Most cores were additionally scanned with a medical X-ray computer tomography scanner. The results of these analyses were used to identify 17 different lithofacies, which comprise several facies associations from various environments ranging from continental to paralic. Age control is achieved through radiocarbon dating of calcareous fragments and plant remains.

4. Results

Five up to 11 m long cores show that mud is dominant in the early- to mid-Holocene. Four core-transects of 3 m long cores show that fluvial processes dominate at the base and evolved towards mostly mixed and mud-dominated floodplain sub-environments. This fits the general coastal history of the region. The area of the Sagara lowlands was submerged by the Jomon Transgression, which led to a sea level highstand in the early- to mid-Holocene. During this time the accommodation space left by the transgression was filled with first estuarine sediments, which then transitioned into a tide-dominated deltaic complex evidenced by firstly muds, and then flaser beds and other fluvial sediments. At present, long-shore coastal currents and riverine input are the two dominant sediment supplies in the greater sedimentary system.

Preliminarily, we identified only two potential extreme wave deposits, however, their occurrence is limited to a small area in the record. Precise age control is not yet available for the two extreme wave deposits. However, the deposits will be most likely from the last 1200 years BP. The low abundance of extreme wave deposits contrasts expectations, as historical documents give evidence for numerous large tsunamis in the area. Human activity, dynamic fluvial processes and shoreline displacement are probably the limiting factors to the preservation potential of sandy sheets deposited by extreme wave events, which appears to be a common problem along the entire Nankai coast. Further investigations may reveal how much each process contributes to the problem.

In the general sedimentary record, XRF-scanning data show low abundance of sulphur (S) in the upper part, which we interpret as low marine influence. The sulphur count across suspected extreme wave beds remains low, too, which may indicate that these layers despite their sedimentary characteristics are not of marine origin or, if they are of marine origin, that they have lost their sulphur chemical signature that would be expected from marine water.

Scatter electron microscopy on the sand of the potential extreme wave deposits shows a complete lack of biogenic skeletal remains, like diatoms, foraminifera or ostracods. The grains are mostly quartz and are angular with fresh surfaces and edges. Again, this could be due to a non-marine origin of the sandy deposits or it could be that the ~700 m between the core sites and the present-day coastline are enough to remobilize enough material from the onshore area that the clear marine signature is lost along the way. There are examples that would contradict this interpretation (e.g. Kelsey et al., 2005), however, others have found the same marine signature depletion after significant onshore transport (Kempf et al., 2015).

Despite being common among extreme wave deposits, none of the mentioned characteristics can be exclusively linked to extreme wave deposits. The sharp lower contact that suggests an erosive surface and the gradually upward increasing bioturbated mixture of sand and mud are indicating rapid transport and deposition with the typical post-depositional processes that lead to altered and bioturbated sandy sheets, as it is described for many extreme wave deposits elsewhere.

Acknowledgements

PK et al. acknowledge the Belgian Federal Science Policy Office (BELSPO) for funding the QuakeRecNankai project.

References

- Ando, M., 1975. Source mechanisms and tectonic significance of historical earthquakes along the Nankai trough, Japan. *Tectonophysics* 27, 119–140.
- Garrett, E., Fujiwara, O., Garrett, P., Heyvaert, V.M.A., Shishikura, M., Yokoyama, Y., Hubert-Ferrari, A., Brückner, H., Nakamura, A., De Batist, M., 2016. A systematic review of geological evidence for Holocene earthquakes and tsunamis along the Nankai-Suruga Trough, Japan. *Earth-Science Reviews* 159, 337–357.
- Kelsey, H.M., Nelson, A.R., Hemphill-Haley, E., Witter, R.C., 2005. Tsunami history of an Oregon coastal lake reveals a 4600 yr record of great earthquakes on the Cascadia subduction zone. *Geological Society of America Bulletin* 117, 1009–1032.
- Kempf, P., Moernaut, J., Van Daele, M., Vermassen, F., Vandoorne, W., Pino, M., Urrutía, R., Garrett, E., De Batist, M., 2015. The sedimentary record of the tsunami caused by the 1960 Great Chilean Earthquake in two coastal lakes on Chiloé Island, Chile. *Sedimentary Geology* 328, 73–86.

Geochemistry of *Nummulites* as a proxy for the Eocene paleotemperature evolution in the Southern North Sea Basin: an Ypresian test case

Lise MARTENS¹, Peter STASSEN^{1,2}, Etienne STEURBAUT^{1,2} & Robert P. SPEIJER¹

¹ Department of Earth and Environmental Sciences, KU Leuven, Celestijnenlaan 200E, B-3001 Heverlee, Belgium.

² Directorate Earth and History of Life, Royal Belgian Institute of Natural Sciences, Vautierstraat 29, B-1000 Brussels, Belgium.

The early Eocene period is characterized by sudden and brief climate variations, recognized as short-term hyperthermals, which are superimposed on the gradual warming trend that culminated in the Early Eocene Climatic Optimum (EECO). The regional environmental conditions during these periods of varying temperature and sea level under greenhouse conditions are recorded in the Ypresian (56 - 47.8 Ma) sediments in Belgium. Here we present the shallow marine temperature evolution towards the EECO based on the geochemical composition of nummulites. These larger benthic foraminifera (LBF) are absent in the clayey Orchies Member of the Kortrijk Formation (Fm.) but appear abruptly as monospecific assemblages in the aftermath of a hyperthermal, suggesting an environmental threshold. The lowermost incursion, represented by *Nummulites involutus* (Baccaert, 2017), is recorded in the nearshore fine sands of the Mons-en-Pévèle Fm. (nannoplankton zones NP11-12). Renewed deposition of a basin-wide clayey unit (Aalbeke Member of the Kortrijk Fm.) marks the regional disappearance of this species. This pre-EECO LBF fauna is replaced by *Nummulites aquitanicus* in the Egem sands of the Hyon Fm. (zone NP12), which represents renewed deposition in a broad shallow marine embayment during the EECO. We hypothesize that these LBF dispersals into the North Sea Basin are controlled by pulses of northward migration during warmer periods and by species-specific environmental thresholds.

At the moment, nummulites are still an underutilized source of detailed paleoclimate data, despite their potential as high-resolution archives of annual to seasonal temperature variations (Evans et al., 2013). These temperature reconstructions are based on the Mg-incorporation into the calcareous tests, by using the Mg/Ca (mmol/mol) ratio and a recently proposed Mg/Ca_{LBF}-temperature calibration (Evans et al., 2018). The use of Mg/Ca as a paleotemperature proxy solves the limitations of traditional oxygen isotope paleothermometry, which depends on two unknown values: temperature and regional $\delta^{18}\text{O}_{\text{sw}}$. We tested the effect of a) preservation (dissolution and recrystallization), b) natural variability and c) cleaning methods on the geochemical record of LBF to assess their potential as a paleotemperature proxy.

Nummulites within the Mons-en-Pévèle and Hyon Formations occur regularly in outcrops, but are also common in drill cores. Our geochemical analyses and SEM observations of different preservation states indicate that taphonomic alterations by partial dissolution and recrystallization resulted in significantly lower Mg/Ca and Sr/Ca ratios, which renders unrealistically low temperatures. This post-depositional decrease in the Mg-content is a general feature of the tested outcrop material. Nonetheless, the majority of analyzed specimens retrieved from the Kester core (Mons-en-Pévèle Fm.) and the Ampe section (Hyon Fm.) show reliable Mg/Ca data (range of 60 to 85 mmol/mol) with higher Sr/Ca content (> 1.75 mmol/mol). These results indicate a gradual increasing trend of the mean annual temperature, starting from 15°C (pre-EECO) to > 30°C during the peak of the EECO (Fig. 1).

To estimate the size-dependent effect on the geochemical signal of individual specimens, we used a set of well-preserved nummulites derived from a single layer, thus excluding any

taphonomic alteration and paleoclimate variations. Our results indicate that smaller specimens (radius < 2.5 mm) show a natural variability in their mean temperature signal. Larger specimens represent periods of continuously higher seawater temperatures and partially overlap with the observed variability within the smaller ones. This can bias the temperature reconstructions to higher values if the dimensions of individual specimens are not taken into account. Geochemical cleaning steps are widely used to remove elements that are related to contamination by detrital particles, organic matter, and iron- and manganese-rich oxyhydroxide coatings on the test surfaces. Traditional foraminiferal cleaning protocols were applied, which include multiple ultrasonication steps, and additional oxidative and reductive cleaning methods. The results indicate that Mn/Ca and Fe/Ca, two commonly used indicators of contamination, can be successfully removed with the oxidative and reductive cleaning methods. However, these more intensive and hazardous procedures are avoidable as no significant effect on the Mg/Ca-signal of the calcareous tests was detected.

Based on these observations, we conclude that the geochemistry of nummulites can be applied as a proxy for the Eocene paleotemperature evolution within the North Sea Basin. Further integration of high-resolution geochemical data of all nummulites-bearing levels with other biotic, geochemical and lithological data will give an explanation for the collapse of one species and its replacement by another on a NW European scale, linking their distribution and evolution to the Eocene climate development.

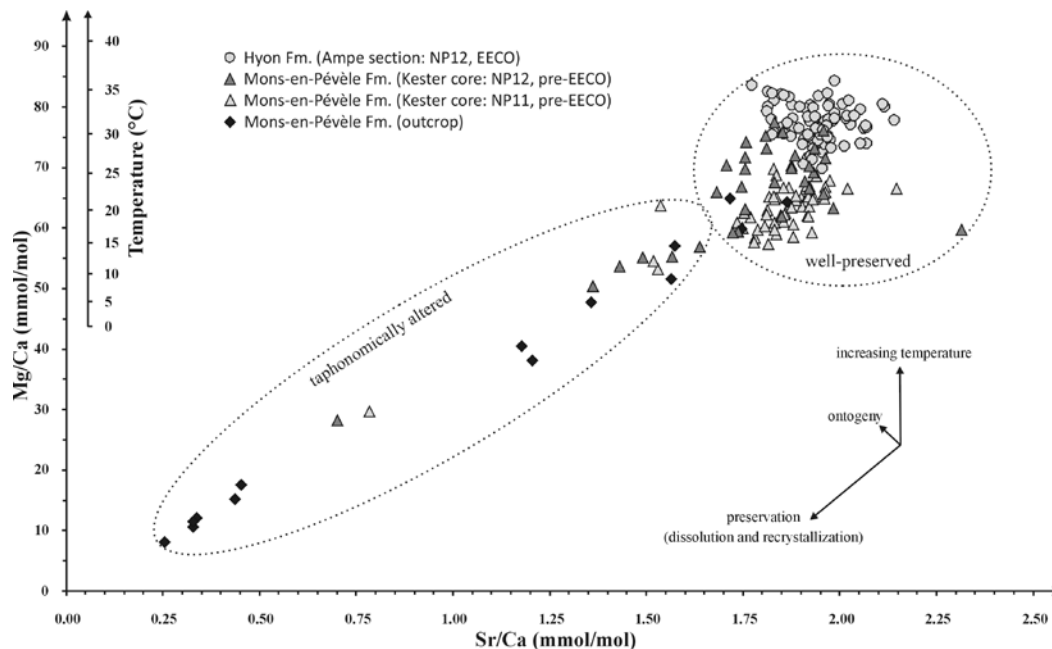


Figure 1. Sr/Ca – Mg/Ca element data and the approximate trajectories of different processes impacting Mg/Ca and Sr/Ca content in nummulites.

References

- Baccaert, J., 2017. First record of Nummulites involutus Schaub in the Early Eocene of Belgium: a taxonomic-ecologic approach. *Memoirs of the Geological Survey of Belgium*, Vol. 63, 48 p.
- Evans, D., Müller, W., Oron, S. & Renema, W., 2013. Eocene seasonality and seawater alkaline earth reconstruction using shallow-dwelling large benthic foraminifera. *Earth and Planetary Science Letters*, 381, 104-115.
- Evans, D., Sahoo, N., Renema, W., Cotton, L.J., Müller, W., Todd, J.A., Saraswati, P.K., Stassen, P., Ziegler, M., Pearson, P.N., Valdes & P.J., Affek, H.P., 2018. Eocene greenhouse climate revealed by coupled clumped isotope-Mg/Ca thermometry. *Proceedings of the National Academy of Sciences*, 115, 1174-1179.

A stratigraphic re-evaluation of the Maaseik Member

Johan MATTHIJS

*VITO, Flemish Institute for Technological Research, Boeretang 200, BE-2400 Mol, Belgium;
johan.matthijs@vito.be*

1. Introduction

The second version of the geological 3D model for the subsurface of Flanders (Matthijs et al., 2013), ordered by the Flemish Government (<http://dov.vlaanderen.be>), was finished by VITO in 2013. For the Neogene-Paleogene Period the model was made on formation level. Since then it is being revised and detailed on member level. Therefore approximately a thousand boreholes with geophysical measurements were lithostratigraphically interpreted and documented in a geodatabase. During this process it was noticed that the geophysical signatures of the Maaseik Member and the upper part of the Gelinden Member were quite alike. These members belong to different formations straddling the Thanetian-Selandian boundary (i.e. the Hannut and Heers Formations). Hence a correlation of geophysical borehole measurements was made between the type-sections of both lithostratigraphic units.

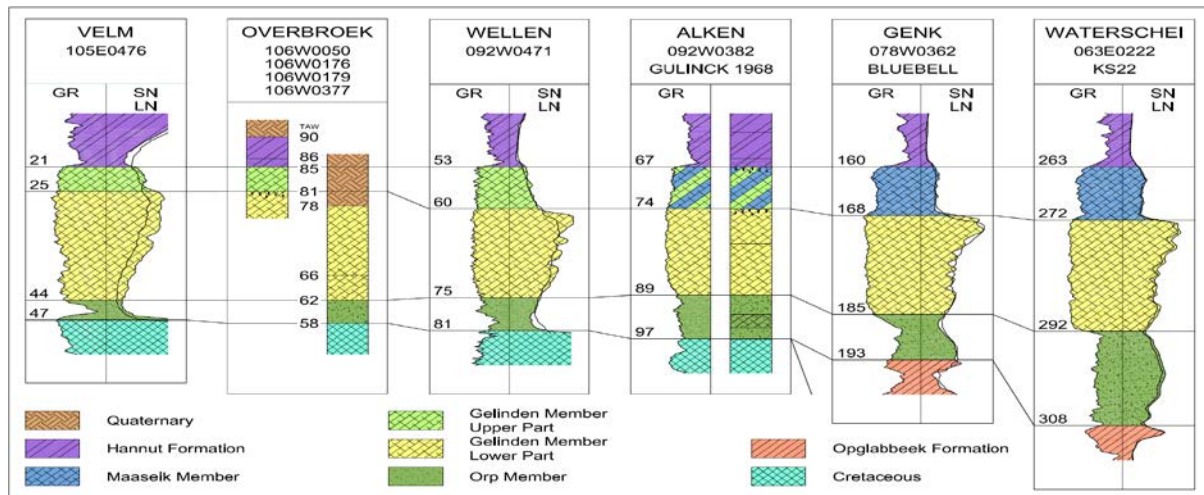
2. Stratigraphy

The Maaseik Member was introduced by Steurbaut (1998) as the pale grey marly clay between 263.5m and 272m depth in the cored Waterschei borehole, which serves as type-section. It is overlain by dark grey stiff clay of the Waterschei Member (Hannut Formation). The transition between both members is sharp. The Maaseik Member is underlain by marl of the Gelinden Member. The contact consists of a burrowed hardground, which has been recognized in several other locations. Based on biostratigraphic analyses Steurbaut (1998) attributed the Maaseik Member to nannofossil zone NP6, gave it an early Thanetian age and made it the lowermost member of the Hannut Formation. The Gelinden Member (Heers Formation) was introduced by Dumont (1850). The marl was exposed in several quarries near the village of Heers (Rutot & Van den Broeck, 1884). The Thewis quarry in Overbroek serves as type-section. It shows about 7m of marl, overlain by 1m of green glauconitic sand with pebbles at the base (Overbroek Horizon) and 4m of grey siliceous limestone of the Lincent Member (Hannut Formation). The contact is sharp. The Gelinden Member itself can be subdivided into an upper part of about 4m consisting predominantly of pale grey slightly clayey marl and a lower part consisting mainly of hardened white marl (Fig. 19 in Gullentops, 1963). In between both parts two bioturbated horizons are observed (Parent, 1972). Based on biostratigraphic analyses on samples taken by Schumacker-Lambry in 1978, Hooyberghs et al. (1999) attributed the upper part of the Gelinden Member to nannofossil zone NP6 and gave it a Selandian age.

3. Correlation

In the Waterschei borehole several geophysical parameters were measured in open hole. For correlation purposes, as there are none available in the Overbroek quarry, geophysical

measurements of the nearby Velm borehole were used as a proxy. The regional correlation of these measurements connecting both type-sections reveals the Maaseik Member to be a lateral more clayey equivalent of the upper part of the Gelinden Member. The natural gamma ray and electrical resistivity signatures indicate the upper part of the Gelinden Member gradually becoming less calcareous and more clayey to the north, hence morphing into the Maaseik Member. Prior to deposition of this unit a stop in sedimentation, probably due to the hinterland being a peneplain, resulted in a burrowed hardground. Renewed tectonics with uplift of the Brabant Massif brought on erosion of freshly exposed Cretaceous sediments. The new source material, possibly calcareous and clayey marl of the Beutenaken Member of the Gulpen Formation, was more clayey than before. Difference in density and sedimentary behaviour of calcareous and clayey particles resulted in calcareous marl being deposited near the coast in the south (upper part of the Gelinden Member), clayey marl being transported further into the basin and marly clay being deposited in the north (Maaseik Member).



4. Conclusion

Signature and correlation of geophysical borehole measurements, biostratigraphy (Sturbaut, 1998; Hooyberghs et al., 1999), the amount of reworked Cretaceous coccoliths (Fig. 2 in Sturbaut, 1998; Fig. 4 in Deckers & Matthijs, 2017) and regional occurrence (Fig. 3.12 in Sturbaut, 2015) indicate the Maaseik Member having a closer relationship to the Heers rather than the Hannut Formation. We thus propose to maintain the name as such, but to reclassify the Maaseik Member to the Heers Formation as a lateral more clayey equivalent of the upper part of the Gelinden Member. As a consequence the existing boundary surface between the Hannut and Heers Formations will be adjusted in the revised geological 3D model. Furthermore the sequence stratigraphic position of the Maaseik Member, as being a part of the first third order Thanetian depositional sequence Th1 (Sturbaut, 1998; Vandenberghe et al., 2004), can no longer be maintained and should to be re-evaluated.

References

- Deckers, J. & Matthijs, J., 2017. Middle Paleocene uplift of the Brabant Massif from central Belgium to the southeast coast of England. *Geological Magazine*, 154(5), 1117-1126.
- Dumont, A., 1950. Rapport sur la carte géologique du Royaume. *Bulletins de l'Académie royale des Sciences, des Lettres et des Beaux-Arts de Belgique*, 16 (2) (1849), 351-373.
- Hooyberghs, H., Jutson, D. & Moorkens, T., 1999. Microfossils of the Heers Formation (Middle Paleocene) of N.E. Belgium. *Biostratigraphy, depositional and climatic-hydrographic setting*. *Aardkundige Mededelingen*, 11, 29-44. Leuven, Belgium.
- Gullentops, F., 1963. Etude de divers facies quaternaires et tertiaries dans le Nord et l'Est de la Belgique. 6e Congrès International de Sedimentologie, Belgique et Pays-Bas, 20 p.
- Matthijs, J., Lanckacker, T., De Koninck, R., Deckers, J., Lagrou, D. & Broothaers, M., 2013. Geologisch 3D lagenmodel van Vlaanderen en het Brussels Hoofdstedelijk Gewest - versie 2. VITO-rapport, 2013/ETE/R/43, 23 p.
- Parent, W., 1972. Tereinstudie en laboratoriumstudie van de mergels van Gelinden. Ongepubliceerde Licentiaatsverhandeling, KU Leuven: 92 p.
- Rutot, A. & Van den Broeck, E., 1884. Explication de la feuille de Heers. Musée royal d'Histoire Naturelle de Belgique, Service de la Carte Géologique du Royaume, 136p.
- Steurbaut, E., 1998. High-resolution holostratigraphy of Middle Paleocene to Early Eocene strata in Belgium and adjacent areas. *Paleontographica, Abt A*, 247, 91-156.
- Steurbaut, E., 2015. Het Paleoceen. *In: Borremans, M. (ed). Geologie van Vlaanderen*. Gent, Belgium.
- Vandenberghe, N., Van Simaëys, S., Steurbaut, E., Jagt, J.W.M. & Felder, P.J., 2004. Stratigraphic architecture of the Upper Cretaceous and Cenozoic along the southern border of the North Sea Basin in Belgium. *Netherlands Journal of Geosciences*, 83 (3), 155-171.

Weathering pattern of Messinian *Lithothamnium* limestones: implication about paleoclimatic conditions

Meriem L. MOULANA^{1,4}, Meriam EL OUAHABI², Frédéric BOULVAIN³, Mostefa GUENDOOUZ⁴ & Aurelia HUBERT-FERRARI¹

¹ Department of Geography, University of Liege, Allée du VI Août 2, 4000 Liège, Belgium

² UR Clay, Sediment Geochemistry and Environment (AGEs), Department of Geology, Agora Quarter, Building B18, Allée du VI Août, 14, Sart-Tilman, University of Liège, B-4000, Belgium.

³ Sedimentary Petrology, University of Liege, B20, Agora Quarter, Allée du VI Août, 12, 4000 Liege, Belgium.

⁴ Faculty of Earth Sciences, Geographical and Territorial Planning, University of Science and Technology Houari Boumediene, (USTHB), El Alia, BP 32, Bab Ezzouar, 16111 Algiers, Algeria.

Limestones are prevalent in Algeria. These formations have been affected by a range of weathering, dissolution and recrystallization processes since their deposition, dependant of the paleoclimatic conditions they sustained. These transformations also affect the potential hazard that these karstic terrains represent. We focus here on the Boukadir Region situated at the foot of the Ouarsenis Mountain (Fig. 1). The region comprises the Ouarsenis northern piedmont composed of ~15° north dipping *lithothamnium* limestones of the Messinian period that rest unconformably upon blue marls of the upper Miocene, and to the south the E-W striking lower Chlef Basin filled by Pliocene-Quaternary sediments and flooded by the Chlef River. The *Lithothamnium* carbonates rocks form a major deep aquifer in the basin. The basin is crossed along its southern edge by the Relizane strike-slip fault. In June 1988, there was a large collapse sinkhole of 60 m in diameter and 35 m deep that occurred along the national road RN4 near the southern edge of the basin (Ourabia & Bennallal, 1989). Drilling shows that the sinkhole can be associated to *Lithothamnium* limestones that were covered by more than 61 m of sediments at that location. No other sinkhole formed since this accident.

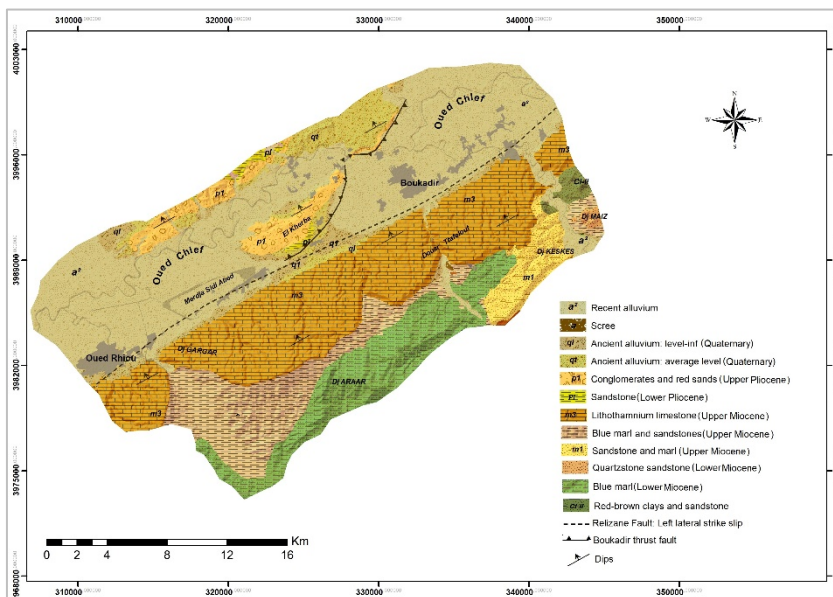


Figure 1. Geological map of the study area.

In this study we investigate the weathering pattern of the *Lithothamnium* limestones to unravel the likelihood of the development of large sinkholes in this formation. Boreholes and quarries show that the Messinian calcareous limestones of the Boukadir region are deeply weathered and partly recrystallized; the weathering affects its entire thickness, reaching a maximum of 200 m. This weathering pattern is not visible a few kilometres more to the east, in limestones having a similar origin.

To unravel the specific paleoclimatic conditions that these limestones sustained, we combine field work and on selected samples, petrographic thin section and mineralogical (XRD) analysis and SEM observations. Field work in quarries and in the wadi shows that the *Lithothamnium* limestones are composed of altering sandstone-rich beds with a calcareous cement and bioconstructions-rich beds. In addition, there is a marked difference between, at the surface, the dense recemented limestone carapace (calcrete) with a thickness reaching 4 m in the quarries and the calcareous tuff below. The formation of this calcrete top layer, is a common feature in the Mediterranean area and can be related to Quaternary climates in the region. At the surface, dissolution features and meters scale open caves are visible. In the calcareous tuff in the quarry, an in depth weathering with recrystallization features and small-scale dissolution conduits are visible. The results of mineralogical (XRD) analysis reveal that Boukadir limestones are mainly calcite with variable amount of quartz and dolomite. The thin sections observations reveal large heterogeneity in the texture, dissolution features, pedogenic structures and micritic recrystallized cement (Fig. 2). Part of this weathering pattern may be attributed to the paleoclimatic conditions that prevailed shortly after the deposition of these carbonate-rich rock at the end of the Messinian Period.

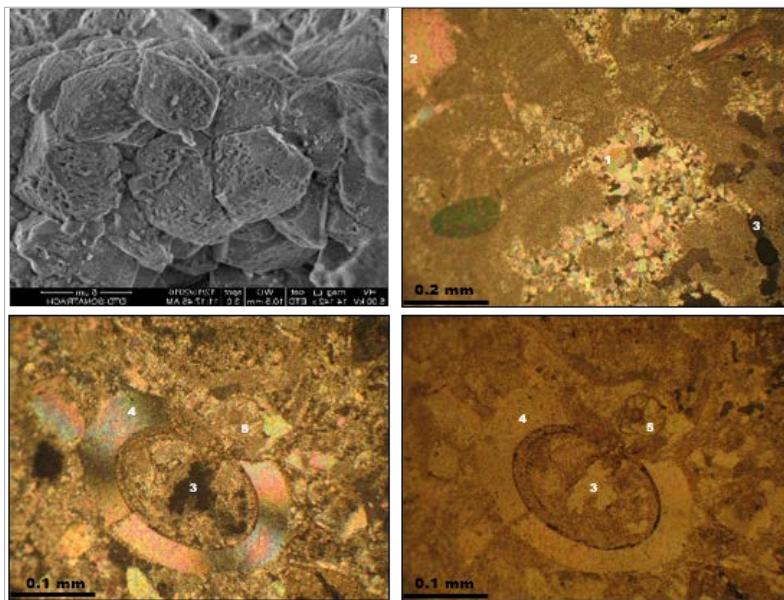


Figure 2. Analyses on *Lithothamnium* limestones. Top left: Scanning electron microscope (SEM) image showing weathered calcite crystal; Top right: Thin section (see meaning of numbers below); Bottom: Thin section under polarized light (left) and under reflected light (right). Numbers on thin sections: 1- recrystallization of the micritic cement. 2- calcite. 3- porosity. 4- recrystallized shell; 5- recrystallized planktonic foraminifera.

References

- Brives, A., 1911. Explanatory note for the 1: 50,000 geological map of Charon.
 Ourabia, K. & Benallal, K., 1989. Report of the collapse of RN4. Central Laboratory of Public Works, 01-03.

Landslide and turbidite records reveal a 2 kyr history of frequent seismic shaking in Eklutna Lake, Alaska

Nore PRAET^{1*}, Jasper MOERNAUT², Maarten VAN DAELE¹, Elke VANDEKERKHOVE¹, Tim COLLART¹, Philipp KEMPF^{1,3}, Peter HAEUSSLER⁴ & Marc DE BATIST¹

¹ *Renard Centre of Marine Geology, Ghent University, Krijgslaan 281 (S8 WE13), 9000 Ghent, Belgium. *Nore.Praet@ugent.be*

² *Institute of Geology, University of Innsbruck, Innrain 52, 6020 Innsbruck, Austria.*

³ *Geological Survey of Belgium, Royal Belgian Institute for Natural Sciences, Jennerstraat 13, 1000 Brussels, Belgium.*

⁴ *U.S. Geological Survey, Anchorage, 4210 University Drive, Anchorage, AK 99508, United States.*

On 27 March 1964, a M_w 9.2 megathrust earthquake ruptured an 800-km-long segment of the Alaska-Aleutian Subduction Zone (in south-central Alaska), representing the largest measured earthquake in North America. In order to better understand the recurrence pattern of such large earthquakes in that region, we studied the sediments of Eklutna Lake, a proglacial lake located in the area affected by the 1964 earthquake. We used a combination of high-resolution seismic stratigraphy (3.5 kHz), multibeam bathymetry (50 kHz) and sediment cores (~8-17 m).

Seismic profiles and bathymetric maps reveal 15 lacustrine landslide deposits caused by the 1964 megathrust earthquake. We also identified a series of older landslide deposits in the subsurface, which we infer to result from multiple, coeval slope failures, and can thus be attributed to past seismic shaking.

Sediment cores in five sites show a varved “background” sedimentation that is frequently interrupted with earthquake- and flood-triggered turbidites. We constructed an event stratigraphy (earthquake or megaflood) by performing a statistical outlier study of varve thickness data. As distinguishing between flood- and earthquake-triggered turbidites in proglacial clastic lakes is not always straightforward, we measured a selection of variables including grain size parameters, spatial distribution and reflectance data for each turbidite at every coring site. We performed a principal component analysis and a clustering algorithm on (pre)historical turbidites to ascertain the seismic origin of the turbidites. The principal component analysis allows us to explain which variables account for most of the variability, while the k-means clustering provides an objective classification of the events based on their similarity. These statistical methods represent a powerful tool for distinguishing between earthquake- and flood- triggered turbidites in future studies.

A continuous 2250-year varve chronology together with seven ¹⁴C ages provide a robust age framework for our paleoseismic records of landslides and turbidites. The resulting time series shows that the paleoseismic records not only reveal information on large megathrust earthquakes, but also on earthquakes generated by surrounding fault systems. Unraveling the different seismic sources and their characteristic recurrence intervals will be crucial for understanding the seismic hazard of southern Alaska and, in particular, the more densely populated city of Anchorage.

Sedimentological study of the Ypresian carbonate platform in Tunisian Atlas and south Pyrenean foreland basin

Mouna RACHDI^{1,2,*}, Frédéric BOULVAIN¹ & Mohamed SOUSSE²

¹ *Laboratoire de pétrologie sédimentaire, B20, Université de Liège, B-4000, Liège, Belgium.*

² *Université de Tunis El Manar, Faculté des sciences de Tunis, UR11ES15, Tunisia.*

* *mouna.rachdi@doct.ulg.ac.be / rachdi.mouna@yahoo.fr*

The sedimentation varied from north to south of the Tethyan domain during the Ypresian. The purpose of this work is to understand the behavior of the Ypresian carbonate platforms in two different tectonic systems. Northern Tunisia is characterized by a distensive tectonic context. Ypresian sediments are represented by nummulitic limestones to the south. Toward the north, the deposits are formed by an open marine sedimentation represented by white micritic and pelagic limestones. Southern France is characterized by a compressive tectonic system and sediments varies from proximal deposits, represented by miliolid-rich facies, to the open marine sedimentation represented by nummulitic limestones. Six cross sections was logged (four in North East Tunisia and two in Southern France). Microscopic studies of thin sections allowed us to describe a range of microfacies and establish a detailed sedimentological study. Paleoenvironmental models are based on the identification of 10 microfacies in France and 5 microfacies in Tunisia.

In northern Tunisia, facies were set up in a progressive ramp model with a transition zone, the shallow-water deposits represent 'small barriers' filled with small and robust *Nummulites*. Nummulites becomes more broad and flat in the pelagic facies in open marine deposits. The microfacies distribution in the most distal environments represent globigerinid- and radiolarian-rich mudstones. The microfacies varied from: a) laminated globigerinid-rich mudstone. There are contributions of juvenile nummulites, which are transported to the deepest environments during regressions. b) wackestone and packstone with globigerinids, radiolarians, small nummulites, ostracods and mollusc debris. c) wackestone and packstone, locally globigerinid- rich packstone associated with echinoderms debris, well individualized nummulites, ostracods and sea urchin radioles. Platform facies is formed by glauconious wackestone and packstone, rich in nummulites, discocyclines and red algae. Locally, patch reef facies is identified, represented by a packstone and grainstone with corals, debris of nummulites and algae, ostracod debris and globigerinids.

In southern France the deposition model is different, it is rather a reef platform that tends towards deepening. Microfacies varied from lagoonal deposit to open marine sedimentation. Shallowest microfacies was composed by: a) packstone and grainstone rich in miliolids and oolitic packstone and grainstone. b) Alveolinid-rich packstone and grainstone, and c) the nummulitic platform was composed by nummulitic wackestone and packstone.

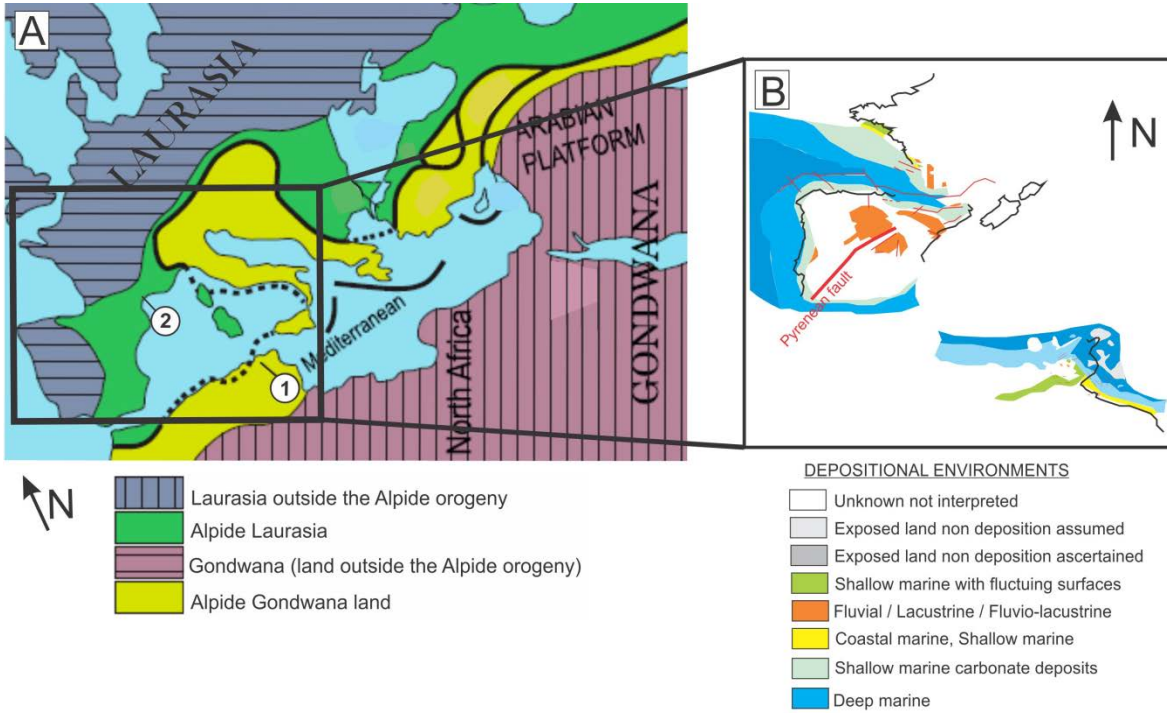


Figure 1. A) Paleogeographic map of the Tethyan domain during the Ypresian. B) Depositional environments during the Ypresian in the Tunisian and Pyrenean basins.

Foraminiferal response to early Eocene climate variability in the North Sea Basin

Peter STASSEN^{1,2}, Etienne STEURBAUT^{1,2} & Robert P. SPEIJER¹

¹ Department of Earth and Environmental Sciences, KU Leuven, Celestijnenlaan 200E, B-3001 Heverlee, Belgium.

² Directorate Earth and History of Life, Royal Belgian Institute of Natural Sciences, Vautierstraat 29, B-1000 Brussels, Belgium.

The early Eocene greenhouse world was marked by multiple transient hyperthermal events, of which the Paleocene-Eocene Thermal Maximum (PETM) was the most prominent. The biotic impact of the less prominent hyperthermals following the PETM has been primarily studied in deeper water setting, while documentation of the foraminiferal responses in shallower shelf settings is still quite sparse, hampering the assessment of potential variability in marine ecosystem responses to Eocene global warming events. We present the lithologic, biotic and geochemical expression of these events in the Kallo reference core, located in northern Belgium. This core represents an extensive and almost complete record of the classical Ypresian Clays, deposited at the southern shelf edge of the North Sea Basin. Our stable isotope records, based on benthic foraminifera and bulk organic material, reveal a succession of carbon isotope excursions (CIE), correlatable to the deep-sea records of DSDP Site 550 (Gulf of Biscay) and ODP Site 1263 (Walvis Ridge). They are accordingly labelled H1 to P? (in accordance to the Ypresian astronomical time scale, Westerhold et al., 2017) and integrated within the holostratigraphic data of the Ypresian Clays (e.g. Steurbaut, 2006).

In this mid shelf setting, these CIE's correspond to distinct variations in lithology and characteristic foraminiferal assemblage changes (Figure 1). The occurrence of only agglutinated foraminifera in the basal layers, corresponding to the Lower Orchies Member (Mbr.), is linked to stagnant bottom waters in an enclosed basin. During the H1-CIE (ETM-2), a lowermost incursion of planktic foraminifera coincides with the permanent establishment of calcareous benthic foraminiferal faunas, indicative of intensified basin ventilation. This transgressive interval (Middle Orchies Mbr) is also characterized by elevated sediment accumulation rates. In the aftermath of the H1-CIE, correlatable with the top of the Upper Orchies Mbr., a more diverse benthic foraminiferal fauna appears and planktic foraminifera become consistently present (see Steurbaut et al., 2016 for subdivision of the Ieper Group).

Fully marine conditions were established during the deposition of calcareous silty to fine sandy clays (Roubaix Mbr), which is also marked by reduced sediment accumulation rates. Major regional biotic events are recorded during the K-CIE (ETM-3), recognizable by an influx of *Subbotina patagonica* and an acme of *Asterigerina bartoniana kaasschieteri*. The latter is considered indicative of deposition in a shallow tropical sea and may thus represent a basin-wide expansion of its habitat. In addition, transient blooms *Uvigerina* species seem to correspond to these minor CIE's, suggesting increased organic fluxes to the sea floor. Planktic foraminiferal abundances rapidly decline after the L-CIE and the basin becomes sediment-starved as indicated by multiple levels enriched in glauconite.

The onset of the Early Eocene Climatic Optimum (EECO) coincides with the basin-wide deposition of a transgressive clayey sediment (Aalbeke Mbr.) and renewed bottom water stagnation, resulting in a complete absence of benthic foraminifera. Carbon isotope excursions in the bulk organic record indicate a relationship with the M- and N-CIE's for this interval, as defined on foraminifera in the deep-sea record. The succeeding siltier levels (Kortemark Mbr.) contain a

References

- Steurbaut, E., 2006. Ypresian. In: L. Dejonghe (Editor), Current status of chronostratigraphic units named from Belgium and adjacent areas. *Geologica Belgica*, 9: 73-93.
- Steurbaut, E., De Ceukelaire, M., Lanckacker, T., Matthijs, J., Stassen, P., Van Baelen, H. & Vandenberghe, N., 2016. Lithostratigraphy of the Ieper Group, 76 p.
- Westerhold, T., Röhl, U., Frederichs, T., Agnini, C., Raffi, I., Zachos, J.C. & Wilkens, R.H., 2017. Astronomical calibration of the Ypresian timescale: implications for seafloor spreading rates and the chaotic behavior of the solar system? *Climate of the Past* 13, 1129-1152.

An acme of the dinoflagellate cyst *Palynodinium grallator*, Gocht, 1970; a marker for the late Maastrichtian warming event at Northern mid-latitudes?

Johan VELLEKOOP^{1,2}, Appy SLUIJS³ & Robert P. SPEIJER¹

¹ Division of Geology, KU Leuven, 3001 Heverlee, Belgium.

² Analytical and Environmental Geochemistry (AMGC) VUB, B-1050 Brussels, Belgium.

³ Marine Palynology & Palaeoceanography, Utrecht University, 3508 TA Utrecht, Netherlands.

The Late Maastrichtian Climatic Optimum (LMCO; 66.4-66.1 Ma), likely related to a large volcanic outpouring phase of the Deccan Traps large igneous province (Ravizza & Peucker-Ehrenbrink, 2003), was characterized by a 3-7 degrees warming of sea-surface temperatures in the last ~350 kyrs of the Cretaceous (Schoene et al., 2015; Barnett et al., 2018; Woelders et al., 2018). Our dinoflagellate cyst (dinocyst) records suggest that in the North Atlantic and European mid-latitudes, dinoflagellate communities responded strongly to this warming event (Fig. 1). Stable, normal marine dinocyst assemblages generally characterize the interval before the LMCO. The onset of the warming is marked by a transition to assemblages that are alternatingly dominated by one or two specific dinocyst taxa. At widespread sites such as the New Jersey paleoshelf, the North Sea Basin, Denmark and Poland, an acme of the dinocyst taxon *Palynodinium grallator* occurs within the LMCO. At its peak abundance, *P. grallator* typically represents >50% of the assemblages, in some samples even >80% of the assemblage. This acme is characterized by a 2 to 10 fold increase in concentration of dinocysts in cysts/gram. This increase in concentration of dinocysts is caused by the additional input of *P. grallator*, as the concentrations of other dinocyst taxa (in cysts/gram) remain relatively stable, ruling out condensation as the mechanism causing the observed high concentrations of dinocysts. Instead, the peak abundances of *P. grallator* reflect massive production of dinoflagellate cysts. The palynological records from the New Jersey paleoshelf illustrate that the *P. grallator* acme occurs during peak warmth, as recorded by $\delta^{18}\text{O}$, Mg/Ca and TEX₈₆ paleotemperature records (Vellekoop et al., 2016; Woelders et al., 2018; Fig. 1). Accordingly, assemblages characterized by a dominance of *P. grallator* appear to be a marker for the end-Cretaceous warming event throughout the Northern mid-latitudes. This dinoflagellate response to the LMCO was likely triggered by the combination of higher sea-water temperatures and more thermally-stratified seas, which may have resulted in higher growth rates and longer-lasting annual bloom windows.

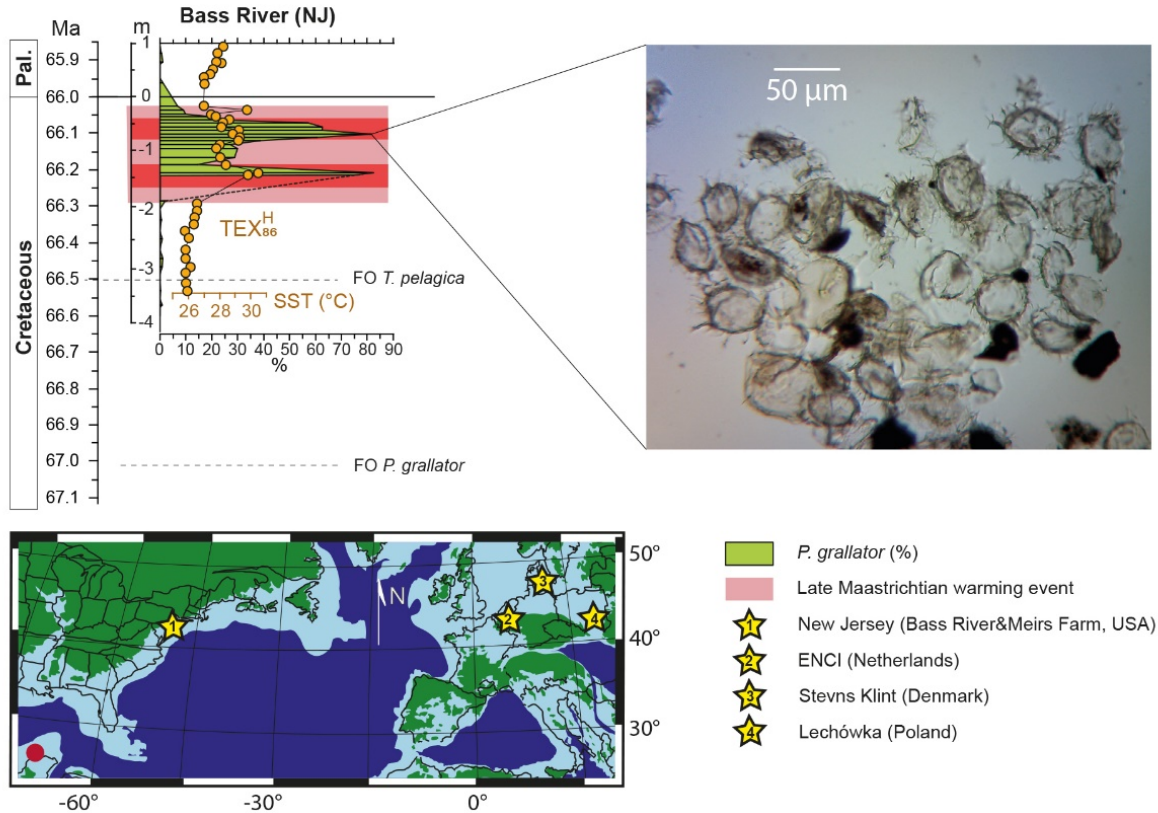


Figure 1. *Palynodinium grillator* acme at Bass River.

References

- Barnet, J.S.K., Littler, K., Kroon, D., Leng, M.J., Westerhold, T., Röhl, U. & Zachos, J., 2018. A new high-resolution chronology for the late Maastrichtian warming event: Establishing robust temporal links with the onset of Deccan volcanism. *Geology* 46(2): 147-150.
- Ravizza, G. & Peucker-Ehrenbrink, B., 2003. Chemostratigraphic evidence of Deccan volcanism from the marine osmium isotope record. *Science* 302(5649):1392–1395.
- Schoene, B., Samperton, K.M., Eddy, M.P., Keller, G., Adatte, T., Bowring, S.A., Khadri, S.F.R. & Gertsch, B., 2015. U-Pb geochronology of the Deccan Traps and relation to the end-Cretaceous mass extinction. *Science* 347(6218):182–184.
- Vellekoop J., Esmeray-Senlet, S., Miller, K.G., Browning, J.V., Sluijs, A., van de Schootbrugge, B., Sinningh-Damsté, J.S. & Brinkhuis, H., 2016. Evidence for Cretaceous-Paleogene boundary bolide “impact winter” conditions from New Jersey, USA. *Geology* 44(8):619–622.
- Woelders, L., Vellekoop, J., Weltje, G.J., de Nooijer, L., Reichart, G.-J., Peterse, F., Claeys, P. & Speijer, R.P., 2018. Approach for robust multi-proxy paleotemperature reconstructions, using late Cretaceous temperature records as a case study. *Earth and Planetary Science Letters*, *accepted manuscript*.

Progressive increase in organic-matter burial and preservation from the “Weissert” event to the Faraoni event in Umbria-Marche (central Italy)

Sébastien WOUTERS¹, Johann SCHNYDER², Sara SATOLLI³, Mathieu MARTINEZ⁴, Frédéric BOULVAIN¹, Thomas GOOVAERTS⁵, Bruno MEYVIS⁵ & Xavier DEVLEESCHOUWER⁵

¹ University of Liège, Sedimentary Petrology, Boulevard du Rectorat, 15, B20, Sart-Tilman, 4000 Liège, Belgium.

² Sorbonne Universities, UPMC-Univ. Paris 06, CNRS, Institut des Sciences de la Terre (ISTeP), UMR 7193, 4 Place Jussieu, 75005 Paris, France.

³ University “G. D’Annunzio” of Chieti-Pescara, Department of Engineering and Geology, Via dei Vestini 31, 66100, Chieti, Italy.

⁴ University of Rennes, CNRS, Geosciences Rennes, UMR 6118, 35000 Rennes, France

⁵ Royal Belgian Institute of Natural Sciences, O.D. Earth and History of Life, 29 rue Vautier, 1000 Brussels, Belgium.

The Cretaceous experienced several Oceanic Anoxic Events (or OAEs). Anoxia in these events is indicated by deposits of black shales, enriched in organic matter (OM) compared to the layers below and above, strong carbon isotope perturbations, often with a negative excursion at the onset of the OAEs followed by a positive excursion, and concentration of redox-sensitive trace-elements (RSTE) (Baudin & Riquier 2014). Considered to be the earliest Cretaceous OAE (Baudin & Riquier, 2014), the Faraoni level is a short event first defined in the late Hauterivian sections of the Umbria-Marche Apennines (Cecca et al. 1994). It presents black shales enriched in OM with high concentrations of RSTE, but lacks an important positive $\delta^{13}\text{C}$ excursion (Baudin & Riquier, 2014). This event follows the “Weissert” event, a ca. 2.3 million year carbon isotope perturbation event taking place during the late Valanginian-early Hauterivian (Sprovieri et al. 2006). This latter event is not considered to be an OAE, as anoxia indicators such as RSTE high concentrations or OM-rich layers are not observed at least in the western Tethys (Westermann et al. 2010).

In order to link those two seemingly opposite events, sections of Late Valanginian to Early Barremian age were studied in the Umbria-Marche Apennines, Italy. Lesser magnitude black shales preceding the Faraoni level were identified. They were correlated in two sections using magnetostratigraphy (Fig. 1). Rock-Eval and palynofacies analyses reveal that they are part of a longer-term trend of increased organic matter preservation and burial. In the black shales this is hinted by a progressive increase of total organic carbon (TOC) content, of the hydrogen index (HI), and by increasingly better preserved amorphous organic matter (AOM) towards the Faraoni level (Fig.1). This increase starts in the upper part of the M5n magnetochron. This is coeval with an increase in mercury concentration interpreted to be due to volcanic activity that was measured among others in the Bosso section (Charbonnier et al., 2018). Palaeoenvironmental differences between the Bosso and Frontone sections are shown by differences in palynomorphs and in organic matter preservation, and by the presence of slumps found in Frontone only.

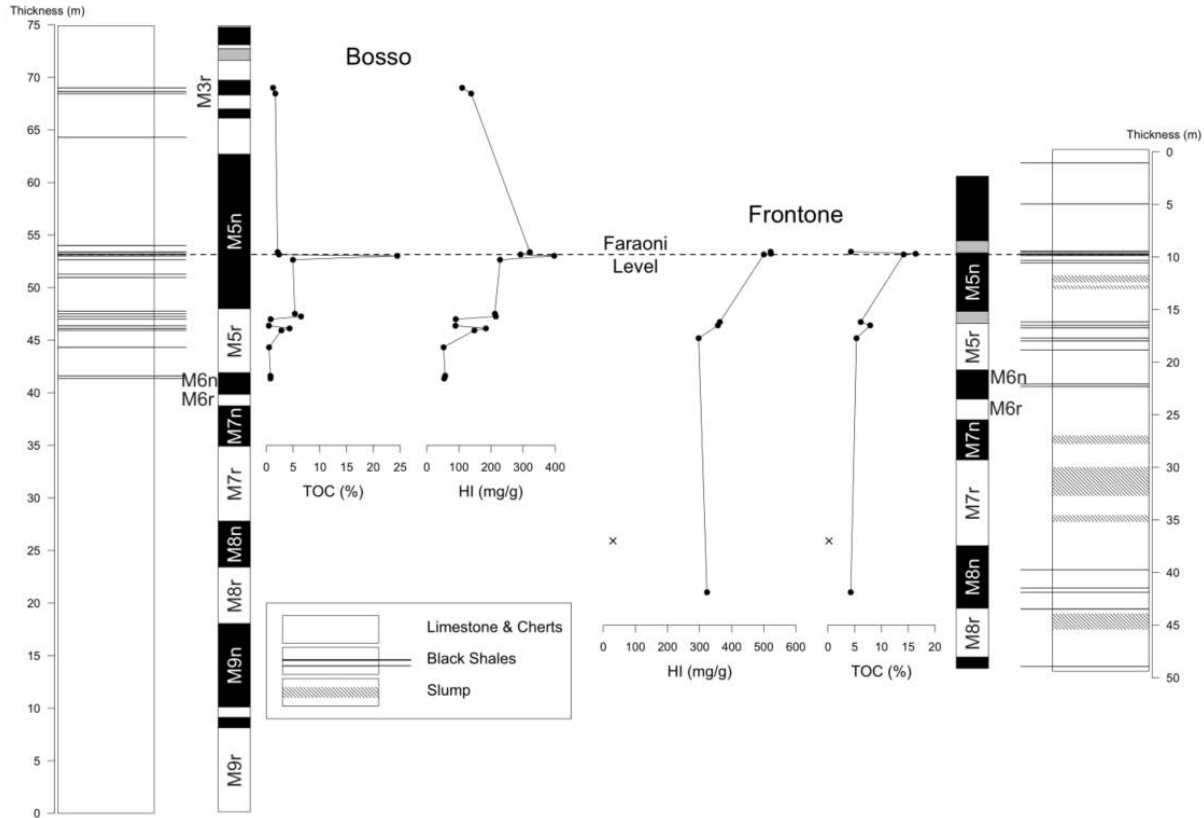


Figure 1. Synthetic litholog of the Bosso and Frontone sections, with magnetostratigraphy and Rock Eval results (TOC & HI). The cross is for a limestone sample, all others are black shales.

References

- Baudin, F. & Riquier, L., 2014. The Late Hauterivian Faraoni ‘Oceanic Anoxic Event’: An Update. *Bulletin de La Société Géologique de France*, 185, 6, 359-77.
- Cecca, F., Marini, A., Pallini, G., Baudin, F. & Begouen, V., 1994. A guide level of the uppermost Hauterivian (Lower Cretaceous) in the pelagic succession of Umbria Marches Apennines (Central Italy): the Faraoni level, *Rivista Italiana di Paleontologia e Stratigrafia*, 99, 4.
- Sprovieri, M., Coccioni, R., Lirer, F., Pelosi, N. & Lozar F., 2006. Orbital Tuning of a Lower Cretaceous Composite Record (Maiolica Formation, Central Italy). *Paleoceanography*, 21, 4.
- Westermann, S., Föllmi, K.B., Adatte, T., Matera, V., Schnyder, J., Fleitmann, D., Fiet, N., Ploch, I. & Duchamp-Alphonse S., 2010. The Valanginian $\delta^{13}\text{C}$ Excursion May Not Be an Expression of a Global Oceanic Anoxic Event. *Earth and Planetary Science Letters*, 290, 1-2, 118-31.
- Charbonnier, G., Godet, A., Bodin, S., Adatte, T. & Föllmi, K. B. 2018. Mercury anomalies, volcanic pulses, and drowning episodes along the northern Tethyan margin during the latest Hauterivian-earliest Aptian. *Palaeogeography. Palaeoclimatology. Palaeoecology*.

Theme 7

Lessons to be learned from geoarchaeology

Drowned landscapes of the Belgian Continental Shelf: implications for northwest European landscape evolution and preservation potential for submerged heritage

Maikel DE CLERCQ^{1,*}, Tine MISSIAEN², David G. MORENO², Mieke MATHYS³ & Marc DE BATIST¹

¹*Renard Centre of Marine Geology, Department of Geology, Ghent University, Krijgslaan 28, building S8, B-9000 Gent*

²*Flanders Marine Institute, InnovOcean site, Wandelaarkaai 7, warehouse 48, B-8400 Ostend*

³*International Marine & Dredging Consultants N.V., Van Immerseelstraat 66, B-2018 Antwerp*

*Corresponding author: maikel.declercq@ugent.be

Keywords: Belgian Continental Shelf, southern North Sea, Quaternary, incised-palaeovalleys, stratigraphy, palaeogeography.

For a long period it was considered that the Quaternary sedimentary record of the Belgian Continental Shelf (BCS) was well understood and needed no further attention. However, recent research (De Clercq, 2018; De Clercq et al., 2018; Mathys, 2009) demonstrates that these now drowned landscapes have a much more complicated architecture, comprising of marine, estuarine, coastal, intertidal and fluvial environments, often separated from each other by erosive boundaries. The main driving factors behind the preservation/deposition of this wide range of environments are climate change, glacio-isostasy and sea-level fluctuations, which in turn control the palaeogeographic evolution of northwest Europe.

The unique tectonic position of the BCS between the depositional southern North Sea and the erosive area of the Dover Strait left strong imprints in its preserved record (as erosion in the top of the Paleogene and preservation/erosion within the Quaternary record) that prove to be important for unravelling the palaeogeographical evolution of northwest Europe. Here, we provide a summary of the current stratigraphical and chronological frameworks and provide an overview of the landscape changes preserved in the sedimentary environments of the BCS for the last two glacial-interglacial cycles.

The oldest geomorphic imprints preserved in the stratigraphic record date back to the Penultimate Glacial and are related to the final opening of a glacio-isostatic upwarped remnant Elsterian (MIS 12) land bridge between East Anglia and Belgium-southwest Netherlands. This upwarped area experienced a lag in the Last Interglacial (MIS 5e; Eemian) sea-level rise impacting the development of the southern North Sea at the time. This is demonstrated by the transition of wave- to tide-dominated estuaries along the Eemian palaeoshoreline during the Early-Middle Eemian transition. While Early Glacial global sea levels were already on the decline the former upwarped zone was now also subsiding sustaining high sea levels within the area of the southern North Sea. Climate fluctuations during the following Pleniglacial resulted in the formation of a single merged ice-sheet across the North Sea Basin during the Early and Late Pleniglacial (MIS 4 and 2; 70 ka glaciation and Last Glacial Maximum). This ice mass expansion and its related glacio-isostatic

adjustment impacted the drainage network across northwest Europe in such a way that it routed most of its water down to the southern North Sea and the English Channel. The possible formation of ice-marginal lakes and their subsequent drainage had a major impact on downstream landscapes. This is demonstrated by the presence of far-travelled clasts encountered on the BCS that originate from the Scottish Grampian Highlands and the British East Coast suggesting such a north-south transportation route took place (Dusar, 2014; Dusar et al., 2016). During the Late Glacial period aeolian wind-driven activity resulted in the development of sand ridges. The development of the so-called Maldegem-Stekene sand ridge is believed to be the sole cause of the palaeo-Scheldt River deflection from Ghent-Zeebrugge-Ostend to Ghent-Antwerp, however the impact of glacio-isostasy and how big its role may have been during this deflection has never been accounted for. The final Holocene drowning of the BCS resulted in a dynamic palaeoshorline and the development of a back-barrier environment protected by barrier islands until its final present configuration (Mathys, 2009).

Next to their own sedimentary characteristics some of the aforementioned deposits and landforms provide fossil material and provide additional information of the various palaeoenvironments of the time (interglacial vs. glacial fauna, terrestrial vs. aquatic species, freshwater vs. marine biota) and provide information about possible archaeological preservation (e.g. Cohen et al., 2017). Evidence from the North Sea, such as the Brown Bank and the Eurogeul navigation channel, demonstrate that concentrations of faunal remains appear to be in the same areas as the archaeological remains and provide the first clues as to where archaeological material may be preserved within the wide suite of preserved palaeoenvironments on the BCS. These results have for the first time ever been visualised in archaeological and palaeontological potential maps.

References

- Cohen, K.M., Westley, K., Erkens, G., Hijma, M.P., Weerts, H.J.T., 2017. The North Sea. In Flemming C., Harff J., Moura D, Burgess A., Bailey G.N (eds.), *Submerged Landscapes of the European Continental Shelf*, John Wiley & Sons, Ltd., Oxford, United Kingdom. DOI: 10.1002/9781118927823.ch7.
- De Clercq, M., 2018. *Drowned landscapes of the Belgian Continental Shelf: implications for northwest European landscape evolution and preservation potential for submerged heritage*. Published Ph.D Thesis. Ghent University, 331 p.
- De Clercq, M., Missiaen, T., Wallinga, J., Zurita Hurtado, O., Versendaal, A., Mathys, M., De Batist, M., 2018. A well-preserved Eemian incised-valley fill in the southern North Sea Basin, Belgian Continental Shelf - Coastal Plain: implications for northwest European landscape evolution. *Earth Surface Processes and Landforms*. DOI: 10.1002/esp.4365.
- Dusar, M., 2014. *Lithology of gravel deposits at the seabed East of the Westhinderbank*, Royal Belgian Institute for Natural Sciences, Brussels, Belgium.
- Dusar, M., Pieters, M., Van Haelst, S., De Clercq, M., Goethals, H., De Ceukelaire, M., Heyvaert, V., 2016. Pleistocene gravels on the Belgian offshore investigated for the composition and provenance, towards a reassessment of the transport models. In 5th International Geologica Belgica Meeting 2016.
- Mathys, M., 2009. *The Quaternary geological evolution of the Belgian Continental Shelf, southern North Sea*. Unpublished Ph.D Thesis. Ghent University, 382 p. <https://biblio.ugent.be/publication/716421>.

Antimony as a raw material in metal and vitreous materials making: from the Bronze Age to the Roman period

Sarah DILLIS¹, Alicia VAN HAM-MEERT^{1,2}, Patrick DEGRYSE^{1,3}

¹ *KU Leuven, Department of Earth and Environmental Sciences, Celestijnenlaan 200E, B-3001 Leuven, Belgium*

² *Analytical, Environmental and Geo-Chemistry, VUB, Pleinlaan 2, 1050 Brussels, Belgium*

³ *Leiden University, Archaeology, Van Steenis building, Einsteinweg 2, 2333 CC Leiden, The Netherlands*

1. Attestations of antimony in the archaeological record

Antimony has a long history of use in metallurgy and glass making. The first attestation of Cu-Sb alloys dates to the 5th millennium BC (e.g. Nahal Mhisar), while its widespread adoption started around 3500 BC (Hauptmann, 2007). Metallic antimony objects are reported in Mesopotamia (e.g. Tello, Tell Leilan, Assur, Hasanlu, Carchemish) and more abundantly in the southern Caucasus (e.g. Chambarak, Brili) from 3000 BC onwards (Moorey, 1999). Sb was also commonly used in glass production, either as an opacifier in coloured glass from the Late Bronze Age onwards, or as decolouriser in colourless glass from the Hellenistic period onwards (Henderson, 2013; Shortland, 2012). Nevertheless, many questions pertain on the geographical location and nature of Sb extraction and on the nature of its adoption in several technological processes. This research intends to identify the primary origin of the Sb raw materials used and to compare the origin of these mineral resources used for the glass craft with the development of metallurgy in order to reveal an interrelation of these two industries.

2. Mineralogical, geochemical and isotopic analysis

In this study, a mineralogical and chemical characterisation of different Sb-rich ores from various regions is performed by XRD, SEM-EDS and ICP-OES to find possible elemental chemical traces. Additionally, for provenancing purposes, antimony and lead isotopic analysis using MC-ICP-MS have been developed (Lobo et al., 2012; 2013; 2014; Degryse et al., 2015). For high antimony content samples this procedure is in process of being redeveloped.

3. Case study: Caucasus

The region of the Caucasus yield a significant amount of metallic antimony objects such as beads, jewellery and small cast objects, and has suitable deposits, such as Gornaya Racha (Georgia) of which it is known that exploitation started at least in the 17th century BCE (Chernykh, 1992), just before the start of glass production and not too distant from the region where the earliest, Sb-rich glass was potentially made (e.g. Tell Rimah, Tell Brak and Nuzi). This makes the Caucasian region an interesting case study to combine geological, geochemical and archaeological data.

4. Results

Archaeological artefacts from the LBA cemeteries of Brili and Chalpirogrebi were sampled and analysed. EPMA analysis show some preliminary results considering a different ore use (see figure 1).

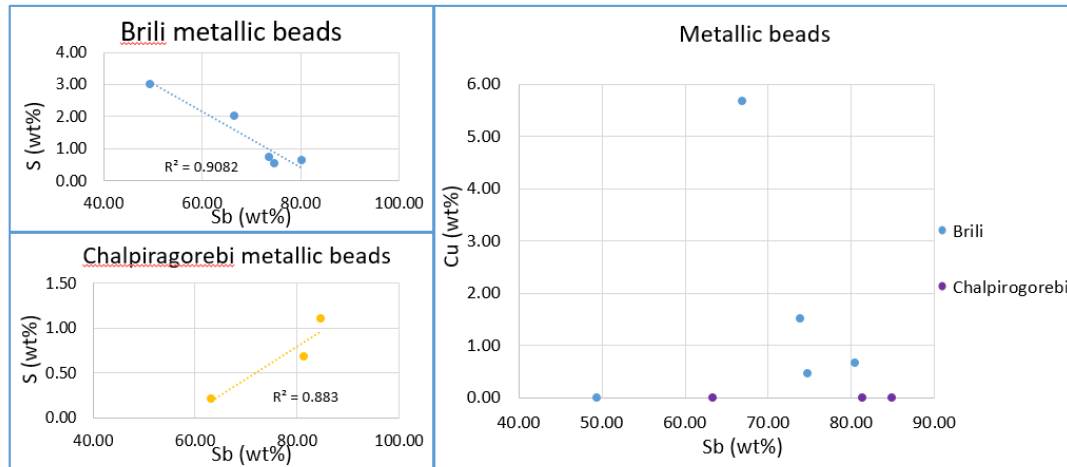


Figure 1. The different relation between S and Sb for the Sb metallic beads of Brili and Chalpiragorebi, as well as the presence of Cu only in the Brili beads indicates to the use of a different antimony source and/or technology. It points to the use of tetrahedrite for the Brili beads, considering the association of Cu, and to the use of stibnite for the Chalpiragorebi beads.

References

- Chernykh, E. N., 1992. *Ancient Metallurgy in the USSR: the Early Metal Age*. Cambridge: Cambridge University Press.
- Degryse, P., Lobo, L., Shortland, A., Vanhaecke, F., Blomme, A., Painter, J, Gimeno, D. et al., 2015. Isotopic Investigation into the Raw Materials of Late Bronze Age Glass Making. *Journal of Archaeological Science* 62. Elsevier Ltd: 153–60. <https://doi.org/10.1016/j.jas.2015.08.004>.
- Hauptmann, A., 2007. *The Archaeometallurgy of Copper: Evidence from Faynan, Jordan*.
- Henderson, J., 2013. *Ancient Glass: An Interdisciplinary Exploration*. Cambridge: Cambridge University Press.
- Lobo, L., Devulder, V., Degryse, P. & Vanhaecke, F., 2012. Investigation of natural isotopic variation of Sb in stibnite ores via multi-collector ICP-mass spectrometry – perspectives for Sb isotopic analysis of Roman glass, *Journal of Analytical Atomic Spectrometry*, 27 (8), 1304-1310.
- Lobo, L., Degryse, P., Shortland, A. & Vanhaecke, F., 2013. Isotopic analysis of antimony using multi-collector ICP-mass spectrometry for provenance determination of Roman glass, *Journal of Analytical Atomic Spectrometry*, 28, 1213-1219.
- Lobo, L., Degryse, P., Shortland, A., Eremin, K., & Vanhaecke, F., 2014. “Copper and Antimony Isotopic Analysis via Multi-Collector ICP-Mass Spectrometry for Provenancing Ancient Glass.” *Journal of Analytical Atomic Spectrometry* 29 (1): 58–64. doi:10.1039/c3ja50303h.
- Moorey, P. R. S., 1999. *Ancient Mesopotamia Materials and Industries: The Archaeological Evidence*. Oxford: Clarendon.
- Shortland, A. J., 2012. *Lapis Lazuli from the Kiln: Glass and Glassmaking in the Late Bronze Age*. Vol. 2, *Studies in Archaeological Sciences*. Leuven: Leuven university press.

Update of the natural building stone atlas for Belgian Limburg

Roland DREESEN^{1,2,3}, Michiel DUSAR² & Frans DOPERÉ⁴

¹ *Gallo-Roman Museum Tongeren*

² *Royal Belgian Institute of Natural Resources – Geological Survey of Belgium*

³ *Department of Historical Archaeology, Ghent University*

⁴ *Research group Archaeology KU Leuven*

The inventory of historical building stones in monuments of Belgian Limburg, first edited in 2001 was a milestone in building stone research (Dreesen et al., 2001). It was the first comprehensive survey of natural building stone use in a large area and linked typology to both geological origin and time and place of application in the built environment. Description of the different stone types is essentially based on visual features (texture, fossils, sedimentary structures, colour, alteration, format and traces of stone cutting techniques), but petrography based on analysis of thin sections comes as a support to substantiate the depositional environment and mode of lithification, helps to explain colour, physical parameters and weathering, and provides clues for provenance studies. Observations are assembled in a GIS-supported database. The geological characterisation allowed to define the lithostratigraphical level and to locate potential quarry sites based on the geological map for all rock types described. Equal attention was given to rare and abandoned rock types as to the common and commercial ones. This approach led to the discovery of unusual local building stones. This way, a geodiversity component is added to the cultural heritage values of the inventoried monuments. Over 35 different stone species were inventoried in historical monuments of Belgian Limburg and described in great detail. The resulting petrographical atlas provides a powerful identification and decision tool in restoration. A large part of this heritage is indeed very fragile; especially indigenous building stones are threatened. Hence, the purpose of this book is to contribute to a better understanding and conservation of an authentic and irreplaceable heritage.

Meanwhile and covering a 20 years' time span, the natural building stone inventory continued and expanded over Flanders and neighbouring areas, both by adding random observations and more detailed observations in the framework of heritage conservation and restauration works. This already resulted in a technical manual on historical building stones in Flanders and Brussels (Dusar et al., 2009). The inventory gradually expanded to include the interior of buildings, the vernacular building heritage, road pavements and garden architecture. More attention was directed to replacement stones and to contemporary buildings making deliberate use of natural stone. Over this period the number of inventoried buildings in Belgian Limburg has risen by 50%, the number of natural building stone records by 70%, also the number of rock type descriptions increased by over 50%, as part of an active nation-wide database developed at the Geological Survey of Belgium and maintained by the Geo-collections unit at the Royal Belgian Institute of Natural Sciences. Even more significant is the improved insight in the natural variability of building stones, resulting in greater specification of their geographical provenance and stratigraphic assignment. Also the traces left on the building stones by the stonemasons tools allowed refined dating of medieval buildings constructed between the 11th to 16th centuries (Doperé, 2018).

More data and better knowledge incited to revise the Limburg atlas. In the new edition, about 55 different rock types are described, among which new variants (e.g. Roosburg Block of Maastricht stone), distinctive types (e.g. Vechmaal tauw and Elst tauw have a very different geological history), hitherto unrecorded occurrences (e.g. Lede stone in Limburg) and new rock types, e.g. Berggrind-ijzerzandsteen (a ferruginous sandstone extracted from a soil horizon in the Lower Pleistocene gravel deposit). Stone types, which were initially grouped in the first edition, are now described separately, e.g. the Ardennian Early Devonian sandstones or the French Jurassic and Cretaceous limestones. The relationship between ‘Roman sandstones’, recycled from Roman ruins in the area around Tongeren, and Coal Measures sandstones is now firmly established. Special attention is given to the Roman use of building stones, resulting from recent data obtained from in situ archaeological observations within the Civitas Tungrorum, a former Roman administrative district encompassing the whole of Limburg (Dreesen & Vanderhoeven, 2017). Finally, geological city walks are added for Hasselt, Tongeren, Sint-Truiden, and the connection between architectural heritage and the already existing geological biking tours is emphasised (Dusar & Dreesen, 2009).

Consequently, the updated natural building stone atlas for Belgian Limburg maintains its naturalistic approach but reinforces even more the link between geology and building history. It highlights the regional geodiversity, which distinguishes Limburg from the other Flemish provinces and provides a better tool for the conservation of this mixed natural – cultural heritage.

References

- Doperé, F., 2018. Dater les édifices du Moyen Âge par la pierre taillée. Editions Safran. Collection Précisions 4, 540 p.
- Dreesen, R., Dusar, M. & Doperé, F., 2001. Atlas Natuursteen in Limburgse monumenten, Provincie Limburg, 294 p.
- Dreesen, R., Dusar, M. & Doperé, F., in press. Atlas Natuursteen in Limburgse monumenten, 2e herziene druk, Provincie Limburg.
- Dreesen, R. & Vanderhoeven, A., 2017. Romeins gebruik van natuursteen in de provincies Limburg. In: Quist, W. & Tolboom, H.-J (red.): Natuursteen in Limburg, natuursteen uit Limburg. Delftdigitalpress, 61-93.
- Dusar, M. & Dreesen, R., 2009. Geodiversiteit weerspiegeld in historische monumenten: Vlaamse natuursteenlandschappen als geotoeristische trekpleister. Geological Survey of Belgium Professional Paper, 305, 79-100.
- Dusar, M., Dreesen, R. & De Naeyer, A., 2009. Natuursteen in Vlaanderen, versteend verleden. Kluwer Renovatie & restauratie, 562 p.

Historical glazes (14th-16th century CE) characterization for the development of adapted restoration materials in Morocco

Meriam El OUAHABI¹, Mouhssin EL HALIM^{1, 2}, Lahcen DAOUDI², Laurie SCAFF³, Leila REBOUH^{3, 4}, Valérie ROUSSEAU³, Catherine COOLS³ Frédéric HATERT⁵, Nathalie FAGEL¹

¹*UR Argile, Géochimie et Environnement sédimentaires (AGEs), Département de Géologie B.18, Sart-Tilman, Université de Liège, Belgium.*

²*Laboratoire des Géosciences et Environnement, Université Cadi Ayyad, Faculté des sciences et techniques Guéliz, Marrakech, Morocco.*

³*Ecole supérieure des Arts Saint-Luc de Liège, 41 Bd de la constitution, B-42000, Liège. Belgium.*

⁴*Lab for User Cognition & Innovative Design, Faculté des Sciences Appliquées B. 52, Sart-Tilman, Université de Liège, Belgium.*

⁵*Laboratory of Mineralogy, Département de Géologie B.18, Sart-Tilman, Université de Liège, Belgium.*

Keywords: Historical ceramics, glaze chemistry, restoration materials

Historical Islamic monuments are impressive by their artistic and fascinating architecture, and many of them therefore belong to the UNESCO world cultural heritage. Particularly, in Morocco the historical monuments are carefully decorated with arranged glazed ceramic pieces, called “zellige”, giving the buildings their typical and colorful appearance. The glaze performs a dual role in the decoration and protection of the surface. Unfortunately these architectural monuments lose their impressive appearance, when the glazed tiles are damaged and the glazes are chipped off (Fig.1). Through time, the influence of climate, water and environmental pollution can cause deterioration of the building materials and contribute to the chipping of the tile glazes (Tite *et al.*, 2016, Gradmann, 2016). Unfortunately this damage affects many historical buildings worldwide, and restoration of glazes becomes urgent to save the brilliant facades from irreversible destruction. In Morocco, eight sites located in the imperial cities Fez and Marrakech, were classified as world heritage by UNESCO in the sixties. Since then, restoration campaigns are being undertaken to preserve the former architecture of these monuments. However, two recent restoration campaigns undertaken in Marrakech have been unsuccessful, because of the weakness of the tiles used.

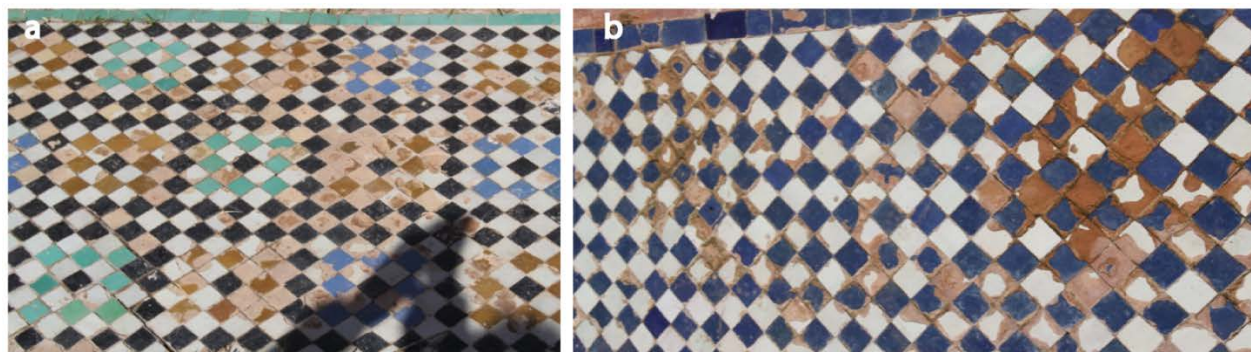


Figure 1. Appearance of current damaged ceramic on the Saadian tombs (a) and the El Badi Palace (b).

This study aims to characterize the glazes of the main historical buildings (14th-16th century CE) in the Marrakech area with the purpose of developing adapted restoration materials. This study will contribute to selecting the most appropriate glaze composition for restoration purposes. To address this issue, a total of 156 glaze samples were taken. Among these, 27 samples are original to different buildings in the Marrakech and Fez area (Saadian tombs, Bahia Palace, El Badi Palace and Medersa Ben Youssef, 14th to 16th c. CE), 11 samples are assumed to belong to a 1st restoration phase, 18 samples are assumed to belong to a 2nd restoration phase and 97 samples are derived from recent traditional zellige production.

The glazes were carefully observed under a binocular to identify any damage affecting the surface of the sherds. The glaze color was determined using a Konica Minolta CM-700d spectrophotometer. Non destructive XRF devices (Thermo Fisher Scientific© Niton XL3t GOLDD) were used to determine the chemical composition of the glaze. Mineralogical phases of different color of glazes were carried out using a BrukerD8-Advance diffractometer with copper anticathode.

From 14th to 16th century CE, in Marrakech area, the ceramists use a mixture of clay, sand and flux agents to manufacture glazes. The chemical composition did not highlight obvious correlation between the colors of the glazes and their compositions, except for the green colored glaze. The latter contains copper and sporadic chromium as a colorant. The historical glazes are lead glazes with Pb contents from 37 to 56%, opacified with Sn in the range 4–18%. Our results are in agreement with the composition of Islamic glazes in the Mediterranean area in general, and in Southern Spain in particular (e.g. Molera et al., 2001, Gradmann, 2016). This technology is taken up from the Roman and Byzantine imperia and then continued during the medieval Islamic culture in Morocco. The use of lead as flux, in association with alkalis, promotes the expansion properties during firing and increases the hardness of the tile and makes the color more clear. Furthermore, the glaze appears thicker with a more brilliant color, due to the high diffraction index of lead glass (Tite et al., 1998). In recent glazes, however, a decrease in lead amount is observed for the two restorations phases, reflecting the weakness of the glazed tiles mainly with the lack of any substituent of flux agent (Fig. 2a).

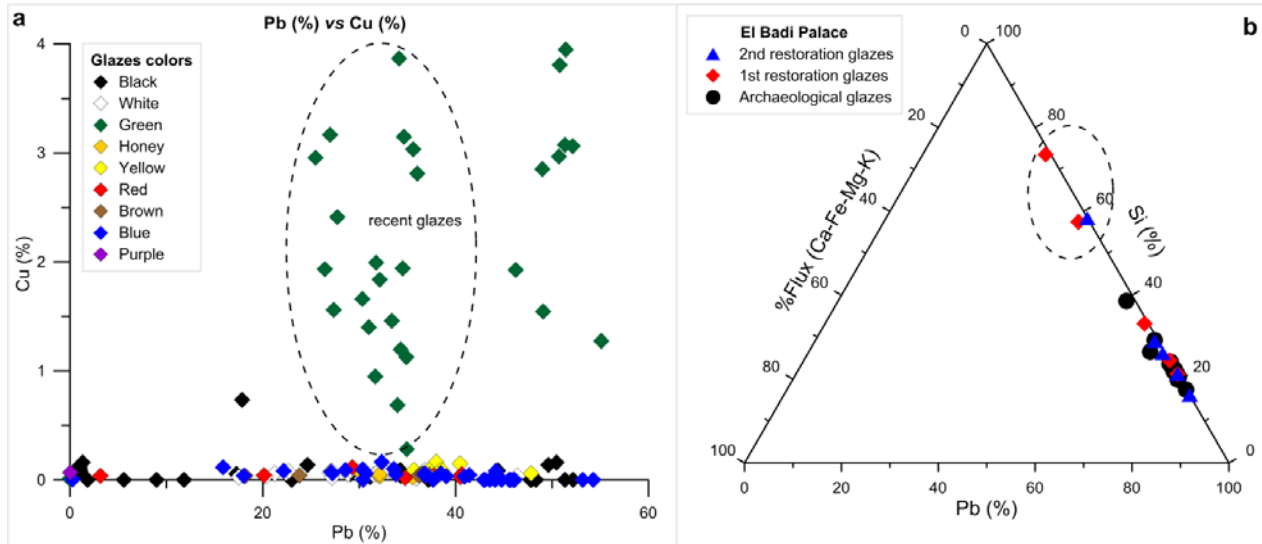


Figure 2. (a) Pb and Cu content of the colored glazes. The green glaze contains Cu mixed with lead. Also noted is a decrease in Pb content in the recent glazes. (b) Ternary diagram Pb-Si-flux (Ca-Fe-Mg-K) indicating the decrease of Pb amount used for restoration of the El Badi Palace. This reduction of Pb is not associated with any supply of flux, implying the partial melting at low firing temperature and then the weakness of the glazed tile.

References

- Gradmann, R., 2016. Analysis of Historical Islamic Glazes and the Development of a Substitution Material. PhD thesis, Institute of Geography and Geology Department of Geodynamics and Geomaterial Research, Julius Maximilians University Würzburg, Germany. <https://opus.bibliothek.uni-wuerzburg.de>.
- Molera, J., Vendrell-Saz, M., & Pérez-Arantegui, J., 2001. Chemical and textural characterization of tin glazes in Islamic ceramics from Eastern Spain. *Journal of Archaeological Science*, 28, 331-340.
- Tite, M. S., Shortland, A. J., Schibille, N., & Degryse, P. 2016. New data on the soda flux used in the production of Iznik glazes and Byzantine glasses. *Archaeometry*, 58, 57-67.
- Tite, M. S., Freestone, I., Mason, R., Molera, J., Vendrell-Saz, M., & Wood, N., 1998. Lead glazes in antiquity-methods of production and reasons for use. *Archaeometry*, 40(2), 241-260.

Characterisation and weathering of flint from prehistoric sites in NW Belgium

Géraldine FIERS^{1*}, Éva HALBRUCKER², Tim DE KOCK¹, Brecht LAFORCE³, Philippe CROMBÉ², Veerle CNUDDE¹

¹ *Pore-scale Processes in Geomaterials Research Group (PProGRess)/UGCT, Department of Geology, Ghent University, Belgium*

² *Research group Prehistory of Europe, Department of Archaeology, Ghent University, Belgium*

³ *X-ray Microspectroscopy and Imaging group (XMI), Department of Chemistry, Ghent University, Belgium*

1. Introduction

In most regions of Europe, flint was by far the most important raw material for the production of stone tools during the Stone Age. Because tools made from organic material (e.g. bones, antler, wood) are rarely preserved in the archaeological record, our knowledge about the Stone Age is predominantly based on the study of stone tools. Flint is a sedimentary rock composed of micro-to cryptocrystalline quartz and often contains mineral impurities such as carbonates, clay minerals, iron and manganese oxides. Due to its formation process, flint is defined by a wide variety of internal structures, chemical variations and impurities. Moreover, alteration processes cause additional chemical and structural changes making the study of this material even more complex. Archaeological artefacts often display alteration features, which are frequently expressed as patination or burning. These alteration features complicate the analysis of use-wear traces, which are microscale damages on the surface of a stone tool caused by its use (Semenov & Thompson, 1964), by partial or complete obliteration of these traces (Levi Sala, 1986; Burroni et al., 2002). Therefore, altered artefacts are regularly discarded from the functional analysis of lithic tools. By not incorporating these artefacts, our understanding of the investigated assemblages is biased. To gain more insight about stone tool use by prehistoric man, it is essential to study partially weathered use-wear traces. Hence, it is important to investigate how the flint characteristics influence their weathering behaviour, and what the impact is on the preservation of prehistoric use-wear traces on flint artefacts.

2. A multi-methodological approach

The selection of the flint raw materials involved in our project is based on lithic finds excavated at various prehistoric sites along the Scheldt river assumed to be made of raw material found in these areas (Fig. 1). The materials selected for this study are all located in the western part of Belgium and neighbouring regions of France and the Netherlands. The material characteristics and alteration features were studied using a combination of traditional techniques, such as macroscopic descriptions, optical microscopy and X-ray fluorescence. Beside these traditional characterization techniques, high-resolution X-ray computed tomography, or micro-CT (Cnudde & Boone, 2013), was used in this research providing 3D information of internal structures of flint, and is moreover used to investigate laboratory alteration processes, i.e. chemical weathering (patination) and burning.

Figure 1. Regional map of Belgium and surrounding regions indicating the sampled outcrop locations of raw materials (dark green dots) and archaeological sites along the Scheldt river (red dots). The green areas indicate Cretaceous outcrops in Belgium.



3. Characterization of raw materials and weathering

The combination of above mentioned techniques allowed for a complete mineralogical, chemical and structural characterisation of the different flint variants. Macroscopic descriptions based on visible properties provided a good basis in flint characterisation. Further mineralogical and structural determination was achieved by microscopic analysis using optical microscopy and micro-CT. Thin section analysis revealed the microcrystalline quartz matrix and, depending on the flint variant, different types of inclusions such as spherulithic chalcedony, fossil and non-fossil calcite, other remnants of fossils, etc. The mineralogical analysis was complemented by geochemical analysis using X-ray fluorescence. Micro-CT provided valuable 3D information regarding internal structures among the different variants, e.g. distribution and size of higher-density particles (mainly remnants of fossils and high-density minerals). Additionally, natural patination surfaces and burning features were characterized using the same techniques with the aim to compare these to simulated alterations in future experiments. This methodology, applied to the different flint variants, will provide a good understanding of the development of these alteration processes.

4. Conclusion

The raw material characteristics affect all the main processes lithic tools undergo, i.e. tool production, tool use and weathering, and therefore these characteristics influence the information that can be interpreted from a stone tool. By studying the flint characteristics, which influence use-wear development, as well as the alteration processes, which affect the preservation of flint tools, their impact on the preservation of use-wear traces are investigated.

References

- Burroni, D., Donahue R. E., Pollard, A. M & Mussi, M., 2002. The Surface Alteration Features of Flint Artefacts as a Record of Environmental Processes. *Journal of Archaeological Science*, 29 (11), 1277-1287.
- Cnudde, V. & Boone, M. N., 2013. High-resolution X-ray computed tomography in geosciences: A review of the current technology and applications. *Earth-Science Reviews*, 123, 1-17.
- Levi Sala, I., 1986. Use wear and post-depositional surface modification: a word of caution. *Journal of Archaeological Science*, 13, 229-244.
- Semenov, S. A., & Thompson, M. W., 1964. *Prehistoric Technology: An Experimental Study of the Oldest Tools and Artefacts from Traces of Manufacture and Wear*. London: Cory, Adams and Mackay.

Stylistic study of a tondo portraying Charles V supported by isotope fingerprinting (alabaster) and thin-section petrography (black marble)

Laurent FONTAINE^{1a}, Géraldine PATIGNY^{1b}, Judy DE ROY^{1c}, Jana SANYOVA^{1a}, Wolfram KLOPPMANN²

¹ KIK-IRPA, Royal Institute for Cultural Heritage (a. Laboratories, b. Documentation, c. Conservation-Restoration), Parc du Cinquantenaire/Jubelpark 1, 1000 Brussels, Belgium

² BRGM, Bureau de Recherches Géologiques et Minières (French Geological Survey), Avenue Claude-Guillemain 3, 45060 Orléans, France

1. Introduction

Last year, the Royal Institute for Cultural Heritage led an interdisciplinary research on an outstanding work of art from a private collection: a tondo portraying Charles V made up of a bas-relief in alabaster stuck on a circular plate in black marble (Figs 1-2), enclosed in a gilded oak frame (not shown here). Besides the restoration, a thorough stylistic research was carried out to find the true provenance of the tondo. The two previous art-historical studies had provided contradictory results; one attributing the work to an Italian sculptor (Alfonso Lombardi) in 1533, and the other to a sculptor of the Low Countries among the attendants of Jacques Du Broeucq, around 1540-1545.



Figure 1. Front view of the tondo (Ø 30.2 cm)
© KIK-IRPA, Brussels (cliché X101345).



Figure 2. Back view of the tondo
© KIK-IRPA, Brussels (cliché X101348).

In parallel with the new stylistic study, an identification of the alabaster and the black marble was conducted, since the geological origin of these materials could give key information about the execution place of the tondo. The white adhesive between the bas-relief in alabaster and the plate in black marble was also investigated.

2. Materials and Methods

Two mm-size fragments (ca. 20 mg) were sampled at the back of the alabaster part, after taking apart the whole piece for restoration. Since the provenance of alabaster cannot be determined by examination with the naked eye or optical microscopy, a multi-stable isotope analysis was performed at BRGM by continuous flow isotope ratio mass spectrometry (CF-IRMS) and thermal ionization mass spectrometry (TIMS), according to the analytical protocol described in the pilot study of Kloppmann et al. (2014). The recently published article of Kloppmann et al. (2017) provides a robust geochemical framework for provenancing alabaster by isotope fingerprints of sulphur, oxygen and strontium (S, O, Sr). A flake of the support in black marble was taken for identification by thin-section petrography. The white adhesive was analysed by SEM-EDX.

3. Results

Both sulphur/oxygen and sulphur/strontium isotope ratios (Fig. 2) conclusively indicate that Charles V's head was manufactured with English alabaster from the East Midlands (UK). The use of English alabaster is in agreement with the 16th-century commercial practices in the Low Countries (Dubelaar, 2009). Petrographic examination of the plate shows a compact limestone with a mudstone texture which can be identified as Belgian black marble from Dinant. This marble knew a flourishing period during the Renaissance (De Ceukelaire et al., 2014). The white adhesive consists of a gypsum-based mortar (plaster of Paris mixed with marble powder).

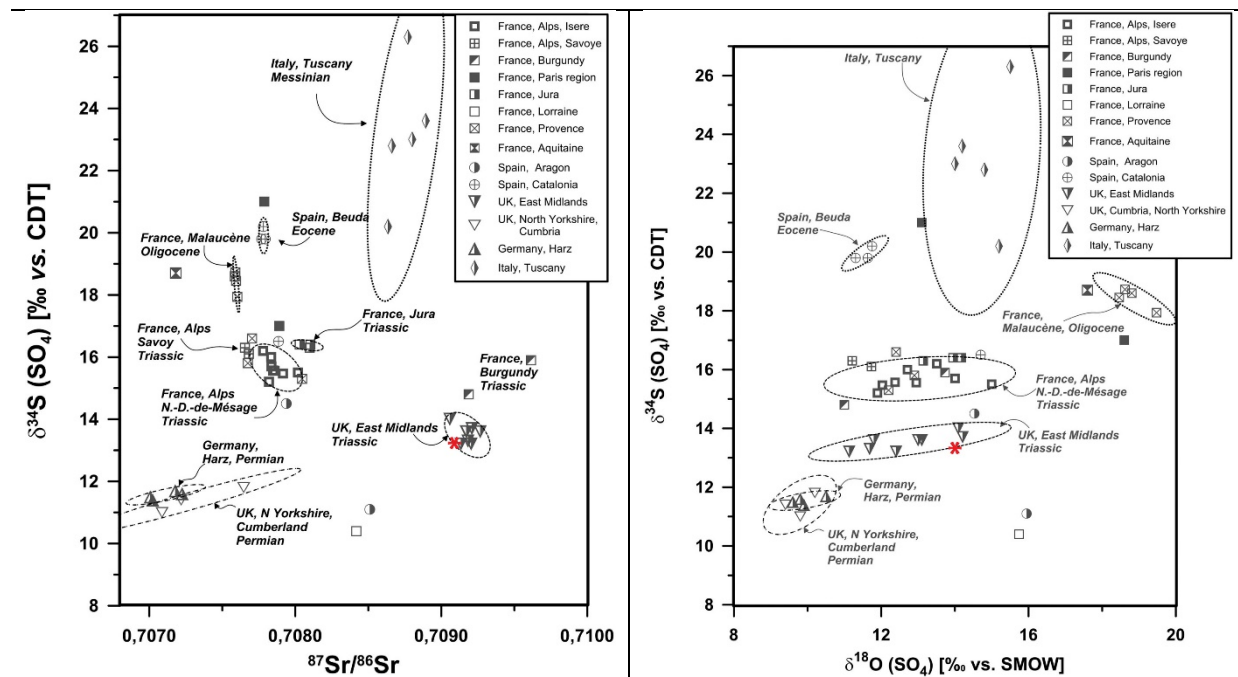


Figure 2. $\delta^{18}\text{O}$ and $^{87}\text{Sr}/^{86}\text{Sr}$ versus $\delta^{34}\text{S}$ ratios of historical alabaster quarries in France, England, Spain, Italy and Germany, after Kloppmann et al. (2017). The star (*) stands for the analysed alabaster.

4. Conclusion

The association of English alabaster (East Midlands) and Belgian black marble (Dinant) rules out an Italian provenance for the tondo and supports the conclusions of the current stylistic study which

suggests that it was made in the Low Countries towards 1560-1570 by people from the entourage of the medallists Leone Leoni and Jacques Jonghelink, who both worked for Charles V's court in Brussels. Most likely the tondo was manufactured in Mechelen, the second production centre of English alabaster after Nottingham and surroundings in the UK.

5. References

- De Ceukelaire, M., Doperé, F., Dreesen, R., Dusar, M. & Groessens, E., 2014. Belgisch marmer. Academia Press, 292 p.
- Dubelaar, W., 2009. Albast uit Nottingham: geologie, winning en verspreiding in de Lage Landen. Tijdschrift GEA, 42, 72-77.
- Kloppmann, W., Leroux, L., Bromblet, P., Guerrot, C., Proust, E., Cooper, A.H., Worley, N., Smeds, S.-A. & Bengtsson, H., 2014. Tracing Medieval and Renaissance Alabaster Works of Art Back to Quarries: A Multi-Isotope Approach. *Archaeometry*, 56 (2), 203-219.
- Kloppmann, W., Leroux, L., Bromblet, P., Le Pogam, P.-Y., Cooper, A.H., Worley, N., Guerrot, C., Montech, A.T., Gallas, A.M. & Aillaud, R., 2017. Competing English, Spanish, and French alabaster trade in Europe over five centuries as evidenced by isotope fingerprinting. *Proceedings of the National Academy of Sciences of the United States of America*, 114 (45), 11856-11860.

Lime-earth in China: From traditional to modern and contemporary times

Changxue SHU¹, Koenraad VAN BALEN², Jan ELSESEN³

¹ *KU Leuven. Department of Architecture and Raymond Lemaire International Centre.*

² *KU Leuven, Department of Civil Engineering, Building materials and technology section and Raymond Lemaire International Centre.*

³ *KU Leuven, Department of Earth and Environmental Sciences, Division of Geology.*

1. Sanhetu: The ignored historical facts

The study starts with a recent investigation into the first-hand rare sources from the engineers working in modern China (1840-1949). The sources reveal, surprisingly, that the traditional cementitious material Sanhetu 三合土 was largely used in modern engineering projects as a substitute for cement concrete at a time cement supply was insufficient. This challenges historians' mainstream idea that cement dominated the modern construction in China.

Traditional Sanhetu (literally Tri-mixture earth) was a mixture of slaked lime, local earth and sands (sands were absent sometimes). The mixture of lime, powder of ceramics, and crushed stones was also found in tombs of Ming Dynasty (1368-1644). It is said that sticky-rice juice, cattle blood, straw, rice vinegar, and Tung oil (Tung oil) were added into lime mortar at times. As binder and plaster, Sanhetu was widely used with brick, tile, and stone in irrigation dams, banks, foundations, floors, walls, and roofs in ancient China.

The modern rediscovery of Sanhetu--so called "Chinese (lime) concrete" or "lime-earth concrete" by western engineers--was closely linked to foundations and hydraulic works which requested hydraulic binder. The modern composition included slaked lime and local earth, too; the local earth often meant loess or so-called "yellow earth" in North China and "red earth" in South China. Pozzolans were sands, or crushed granite, or pulverized tiles and bricks; residue of burned coal-balls were also used for extra strong mortar. All the ingredients were of diverse origins. In 1901-30, lime-earth concrete became a subject in all the major engineering societies of China (Shanghai Society of Engineers and Architects; Association of Chinese and American Engineers; Chinese Engineering Society).

The engineers observed very different hardness of the various lime-earth fills, and often associated it with sources of earth. The durability of lime-earth mixture was studied by tests and by observation of existing structures in different localities of China. Theoretical studies were conducted, too, in terms of the hardening mechanism, conditions, preparing methods and recipes. References were given to the noted contributions from Louis-Joseph Vicat, Joseph Aspdin, Clément-Louis Treussart, Edwin C. Eckel, Quincy A. Gillmore, and etc. They also referred to successful cases of ancient China and Europe like Roman Pozzuoli, French Gaize, Dutch Taras, and Santorino earth, and modern projects in India and Egypt.

2. New questions

Geologists or chemists did not engage in building accurate, scientific knowledge of Sanhetu. Nearly no specific laboratory study was conducted for their hydraulic properties. Little attention was paid to the diverse origins of calcined lime, which might invalidate the tested results because

of clay impurities in the limestone source that could give hydraulicity. Most of the time, the engineers were interested in comparing lime-earth mixture with other lime-sand and cement-based materials in terms of structural strength and stability.

A special black earth K'an tze tu 矸子土 from West Hills coal mines in Beijing was noted. It was procured by pulverising a soft stone generally known as "earthstone." (Van der Veen 1921: 14) Today, K'an tze tu is still used in the Forbidden City for consolidating roof tiles, repairing golden-brick pavements, and etc. There has been very few serious studies on the K'an tze tu mortar regardless its remarkable architectural uses.

Characters of the modern lime-earth mixture and their present conditions are unknown, neither are the sources. Have the lime-earth structures stood modern usage over time? Would be there a sustainable future for them? The currently available materials: 1) source of K'an tze tu is sampled; 2) recorded recipes of lime-earth mixture; 3) identifying the modern lime-earth materials and structures. 2) and 3) can be partly achieved by literature review and fieldwork. The authors propose a new methodology by combining laboratory work, Geoarchaeological and architectural methods to study model samples based on defined recipes.

References

- Ehlers, J.H., 1924b. Chinese engineering materials. *Journal of the Association of Chinese and American Engineers* (Abbrev. *J. Assoc. Ch. Am. E.*), 5(8), 9-23.
- Elsen, J., Mertens, G. & Snellings, R., 2011. Portland cement and other calcareous hydraulic binders: history, production and mineralogy. *European Mineralogical Union Notes in Mineralogy* 9(1), 441-79.
- Hutson, J., 1925. Irrigation works on the Min River. *J. Assoc. Ch. Am. E.*, 6(7), 10.
- Mertens, G., 2009. Characterisation of historical mortars and mineralogical study of the physico-chemical reactions on the pozzolan-lime binder interface (published PhD thesis, ISBN 978-90-8649-285-5), KU Leuven, Leuven.
- Callebaut, K., 2000. Characterisation of historical lime mortars in Belgium: Implications for restoration mortars (PhD thesis), KU Leuven, Leuven.
- Lai, D.L., Wu, J. & Xu, S.B., 2016. *History of Modern Chinese Architecture*, vols. 1-5. Beijing: China Architecture and Building Press.
- Lane, E.W., 1929. Hydraulic lime for masonry construction in China. *J. Assoc. Ch. Am. E.*, 10(1), 19-34.
- Lane, E.W., 1930. Controlling floods in China. Century-old fight against the rampages of the Yellow River. *J. Assoc. Ch. Am. E.*, 11(Dec 1930), 32-40.
- Mayne, C. & Carter, W.J.B., 1903. Foundations in Shanghai. *Shanghai Society of Engineers and Architects. Proceedings of the Society and Report of the Council 1902-03*, 3, 83-107.
- Miao, J.S., Li, X.Y., Cheng, R.K. & Lu, B.S., 1981. A Preliminary Investigation of Cementing Materials used in Ancient China. *Journal of the Chinese Silicate Society*, 9(2), 234-40.
- Shi, K.H., 1925. Discussion on the use of lime Sanhetu in major constructions. *Journal of the Chinese Engineering Society*, 1(2), 148-49.
- Smith, C.A.M., 1926. Testing construction materials used in the Orient. *J. Assoc. Ch. Am. E.*, 7(2), 41-48.
- Van der Veen, H., 1921. Lime-earth fill and lime mortar. *J. Assoc. Ch. Am. E.*, 2(2), 13-17.
- Wiggin, T.H., 1920. Discussion on lime-earth fill and lime mortar. *J. Assoc. Ch. Am. E.*, 1(3), 12-22.

Provenancing Pre-Colonial Pottery in the Lesser Antilles

Anneleen STIENAERS¹, Patrick DEGRYSE^{1,2}, Corinne HOFMAN² & Bert NEYT¹

¹ KU Leuven, Department of Earth and Environmental Sciences, Celestijnenlaan 200E, B-3001 Leuven, Belgium

² University of Leiden, Einsteinweg 2, 2333 Leiden.

There is an extensive research tradition of Caribbean pre-colonial ceramics in general and archaeometric work in the region specifically (e.g. Journal of Caribbean Archaeology Special Volume 2008, Pavia et al. 2013). However, since many previous studies display an in-depth focus on a specific site or island, it is important to start looking at the broader regional picture. In this respect, this study seeks to contribute to this overarching effort of HERA/Nexus by establishing an archaeometrical baseline for the investigation of precolonial ceramics across 11 islands of the Lesser Antilles using a combination of thin section petrography and geochemistry (XRF and ICP-OES). In this way, 23 petrographic and chemical groups were identified for the 11 islands and 255 thin sections under investigation as can be seen on figures 1 and 2 and table 1. When combined with archaeological information, we can conclude that 15 groups were probably produced and used locally on the island where they were excavated while 8 groups display evidence of exchange across different islands of the Lesser Antilles and/or the mainland. This wide-encompassing study in space and time not only provides a solid baseline for further archaeometrical investigations of ceramics of the region, but can also be regarded as an interesting additional body of evidence for studies highlighting other aspects of the ceramic repertoire of the Caribbean.

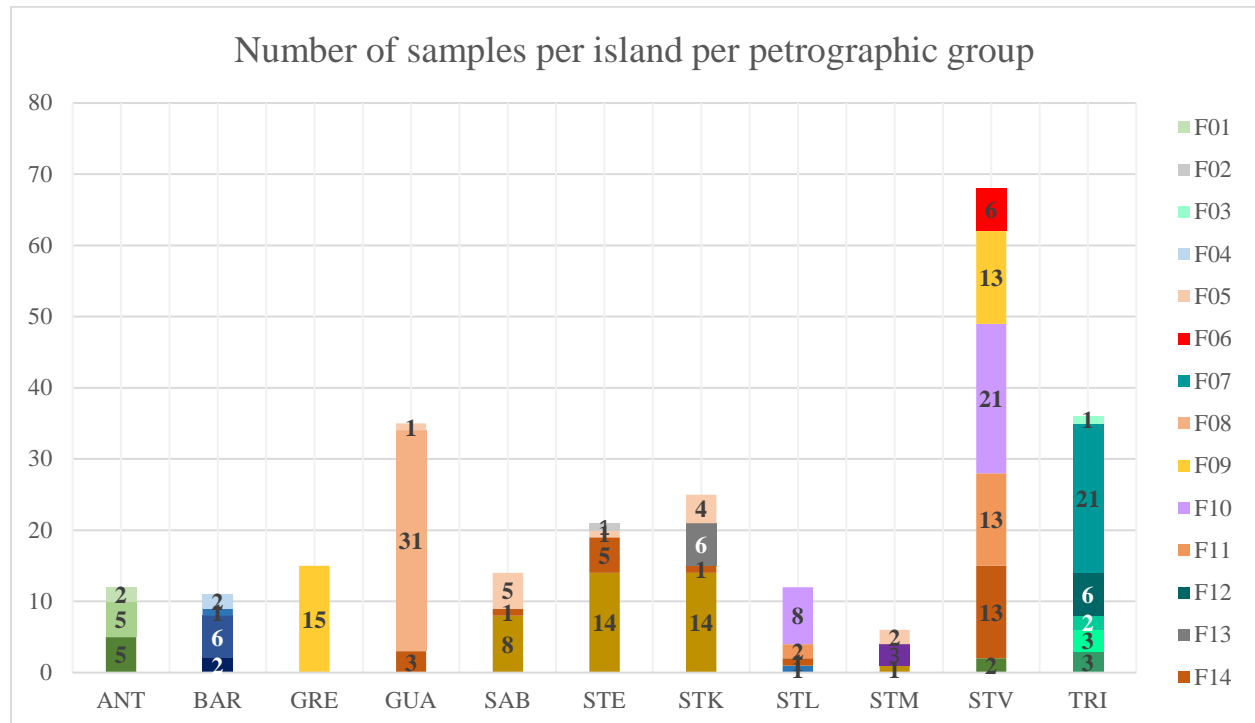


Figure 1. Number of samples per island per petrographic group.

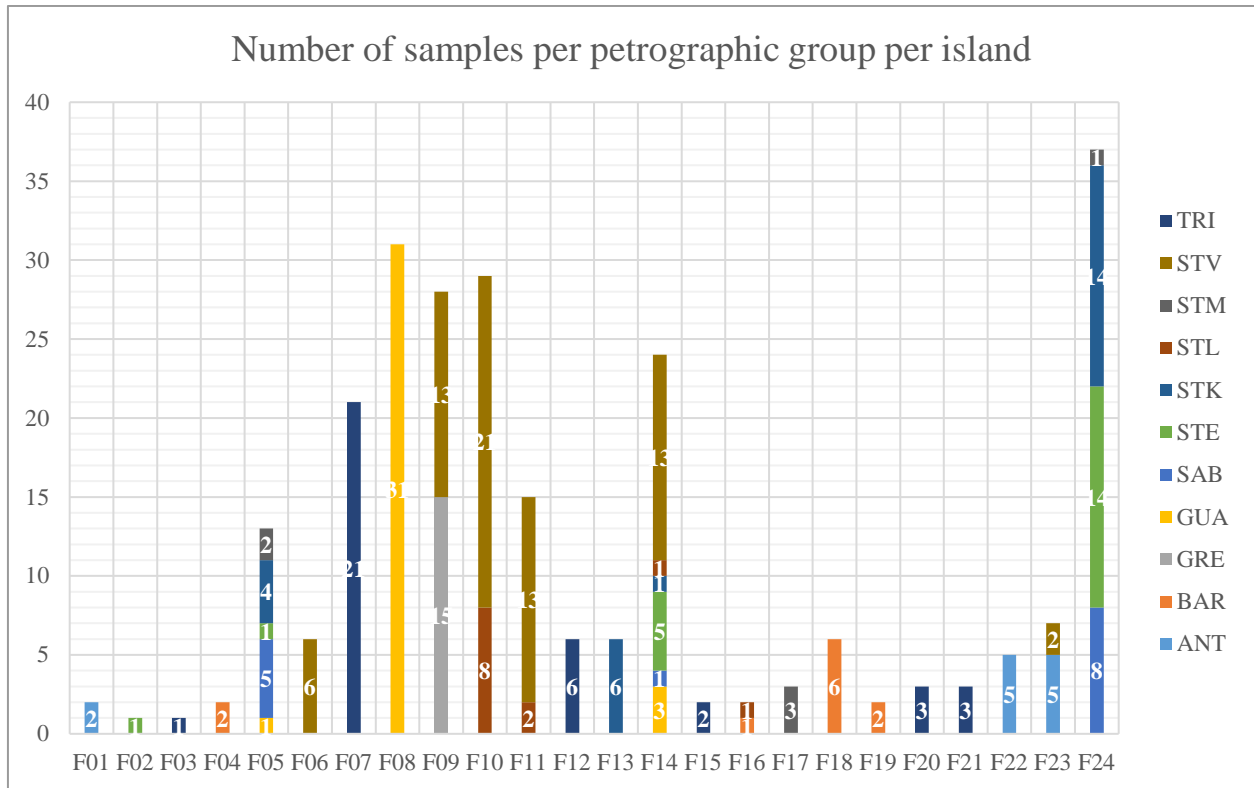


Figure 2. Number of samples per petrographic group per island.

F	Group Name	F	Group Name
F01	Calcareous volcanic with fine opaque grains	F13	Plagioclase and amphibole
F02	Calcareous volcanic	F14	Plagioclase and clinopyroxene
F03	Caraipé	F15	Plagioclase and quartz
F04	Coral and calcareous clay	F16	<i>Porous Volcanic</i>
F05	Fine-grained igneous	F17	Quartz and granite
F06	Granodiorite	F18	Quartz sand
F07	Grog	F19	Radiolarian clay
F08	Heterogeneous clay matrix and few inclusions	F20	Shells
F09	Mafic volcanic with hornblende	F21	Sponge spicules
F10	Mafic volcanic with quartz chunks	F22	Volcanic with fine opaque grains and few inclusions
F11	Mafic volcanic without quartz	F23	Volcanic with fine opaque grains and few inclusions
F12	Micaschist and quartzite	F24	Volcanic with very poor sorting

Table 1. Overview of the 23 petrographic groups. F16 was originally included as a separate group but later reclassified as outliers within existing groups.

References

Pavia, J., Marsaglia, K. & Fitzpatrick, S., 2013. Petrography and Provenance of Sand Temper within Ceramic Sherds from Carriacou, Southern Grenadines, West Indies. *Geoarchaeology* 28, 450-477.

Sasanian lead coins – elemental and isotopic analysis

Alicia VAN HAM-MEERT^{1,2}, Frederik RADEMAKERS¹, Philippe CLAEYS², Rika GYSELEN³, Bruno OVERLAET⁴, Patrick DEGRYSE^{1,5}

¹ KU Leuven, Department of Earth and Environmental Sciences, Celestijnenlaan 200E, B-3001 Leuven, Belgium

² Analytical, Environmental and Geo-Chemistry, VUB, Pleinlaan 2, 1050 Brussels (Belgium)

³ Groupe pour l'étude de la civilisation du moyen-orient, CNRS, 13 Rue Fondant, 91440 Bures-Sur-Yvettes (France)

⁴ Ancient Near East and Iran, Royal Museums of Art and History, Jubelpark 10, B-1000 Brussels (Belgium)

⁵ Universiteit Leiden, Faculty of Archaeology, Archaeological Sciences, Einsteinweg 2 2333 CC Leiden (Netherlands)

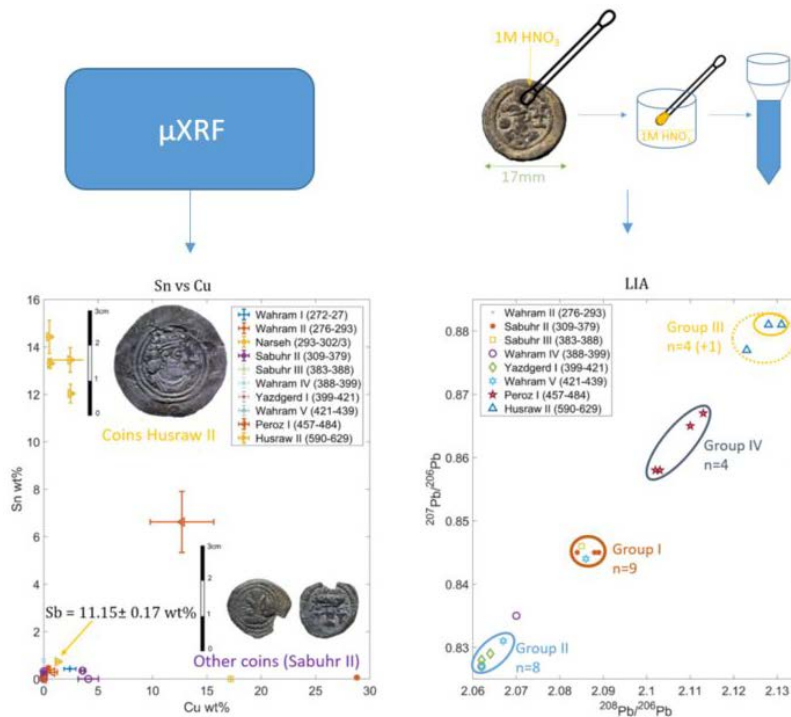


Figure 1: Graphical abstract

The Sasanian Empire started under the rule of Ardašīr I in 224 CE. Prince of Fars, a province in the south of the Parthian empire, he rapidly expanded his domination over Iran. Under the subsequent Sasanian kings, the empire reached from Mesopotamia in the West, to the Indus in the East. This empire lasted until the 7th century CE, when the Arab Conquests changed the geopolitical situation of the region. During its existence the borders of the empire moved mainly as a consequence of on-going war, first with the Roman and later the Byzantine Empire. At its maximal extension, it also included the Caucasus in the North and most of the Near East and parts of Egypt and Yemen. The Sasanians also controlled part of the silk road, making them a people with access

to materials, skills and knowledge from all around the ancient world. As such, their material culture influenced - and was influenced by - many surrounding cultures.

The present paper presents elemental and lead isotopic data on lead coins from the Sasanian empire. These are remarkable as the number of published lead coins (from private and museum collections) remains very limited (176) (Gyselen and Mochiri, 2017). A significant assemblage of which (37) are treated in this paper. The role of these coins in the economy is still debated. The elemental analysis of the coins revealed important changes in composition through time, with a movement from lead-rich copper coins to copper-rich lead coins.

No lead isotope analysis of Sasanian coins has been published so far. Furthermore, this paper proposes a new sampling method for lead isotopic analysis. It is non-invasive and provides results which comply with classical sampling methods.

This elemental and isotopic analysis showed there was an overall continuity in the elemental composition, with only a few exceptions. There are 4 different isotopic groups. The groups are period-bound rather than mint-bound. This points towards a centralised control of raw material supply and coin quality, in turn indicating that these coins were used as money.

References

Gyselen, R., Mochiri, M.I., 2017. Une collection de monnaies Sassanides de billon, de cuivre et de plomb, 26 Res Orientales XXVI, 9-106.

Speleothems as chronostratigraphic tool in archaeological cave sites, the Mishin Kamik (Bulgaria) cave site.

Sophie VERHEYDEN^{1,2}, Elena MARINOVA³, Stefanka IVANOVA⁴, Wim VAN NEER^{1,5} and Maria GUROVA⁴.

¹ *Royal Belgian Institute of Natural Sciences - Earth and History of Life. Rue Vautier 29, 1000 Brussels, Belgium.*

² *The Belgian Science Policy Office - BELSPO. Ass researcher at the AMGC- VUB.*

³ *State Office for Cultural Heritage Baden-Württemberg. Referat 84.1/ Laboratory for Archaeobotany, Fischersteig 9, 78343 Geienhofen-Hemmenhofen. Germany.*

⁴ *National Institute of Archaeology and Museum, Bulgarian Academy of Sciences, 2 Saborna Street, 1000 Sofia, Bulgaria.*

⁵ *Center for Archaeological Sciences, Katholieke Universiteit Leuven, Celestijnenlaan 200E, B-3001 Heverlee – Leuven, Belgium.*

1. Introduction

The Balkan Peninsula is known as the ‘Balkan’ or ‘Danubian’ corridor, one of the important routes for SE-NW Human migrations and dispersal. New fieldwork, particularly in these regions can strengthen our insights in the chrono-cultural succession of Human occupation and dispersal, and related palaeoenvironmental context. The Mishin Kamik cave site, situated westward in the northern Stara Planina mountain range provides such opportunity. The sedimentological study and U-series dating of speleothems in the Mishin Kamik Cave offers a well-constrained chronological framework for the archaeological findings in the cave as well as palaeo-environmental information for the cave site.

2. Localisation

The Mishin Kamik Cave opens at 463 masl and ~30 m above a small tributary of the Ogosta river (a tributary of the Danube) in the western part and northern foothills of Stara Planina (Balkans) Mountains. The cave develops in Upper Jurassic to Lower Cretaceous bioconstructed and micritic limestones (Angelov et al. 1995). A porch of four by four meters, nowadays closed by a door, gives access to an approximately 300m long gallery of similar dimensions. The galleries are filled with detrital material, mostly unsorted, covered by calcite flowstones at several places. Between 2013 and 2016 four trenches were excavated in the cave under auspices of the National Institute of Archaeology and Museum, Bulgarian Academy of Sciences (NIAM-BAS) leading to the observation of a rich paleontological series in trench one and indications of human presence in trenches two and four and potentially in trench one. (Ivanova et al. 2014; Gurova et al. 2016). The study and dating of speleothems was started in order to provide a more constrained chronology for the cave site as well as indications for its palaeo-environmental evolution.

3. Samples and methods

A 66 cm high stalagmite (MK-stm-1) was sampled in 2014 at ~80 meters from the entrance and at approximately 15 meters from trench 1. The sampled MK-stm-1 stalagmite was halved along the growth axis and the surface was polished with Silica Carbide-paper. A petrographic study was done with a binocular. 20 subsamples of ~300 mg were taken for ²³⁸U/²³⁰Th dating. In addition, six samples from calcite crusts from trenches one to four were taken for ²³⁸U/²³⁰Th dating in the

trenches. Uranium and thorium analyses were performed with a Thermo-Scientific Neptune-Plus multi-collector inductively coupled plasma mass spectrometer (MC-ICP-MS) at the Isotope Laboratory at Xi'an Jiaotong University, China. Uncertainties were calculated at 2s level and ages were corrected assuming an initial $^{230}\text{Th}/^{232}\text{Th}$ atomic ratio of $4.4 \pm 2.2 \times 10^{-6}$ (Cheng et al., 2013 and references herein).

4. Results and discussion

The 66 cm long MK-stm-1 stalagmite is composed of white, yellow to dark-brown calcite and displays several important sedimentological changes. It was deposited between 200 ka and recent. A first regular deposition occurred between ~215 and ~208 ka (MIS 7c) and was followed by a detrital phase that partially filled the cave site between 208.1 ± 2.1 ka and 170.2 ± 0.9 ka, suggesting cold conditions with episodes of important rain or ice melting. Calcite deposition recovered slowly after 170 ka with less important interruptions. Between 138.5 ± 0.5 ka and 135.6 ± 0.5 ka, an important change in growth axis and rate occurred with possibly a speleothem breakage of unknown origin. Rapid speleothem deposition occurred between 135 and 133ka (MIS6). Strangely, stalagmite growth decreased during the presumably better conditions of MIS5 since between 133.8 ± 0.5 ka and 114.7 ± 0.5 ka only a very whitish powdery and porous carbonate was deposited covering the floor around the stalagmite and above trench one. The stalagmite continued its growth afterwards until 85.6 ± 3.8 ka, after which another powdery calcite layer was deposited on, and around the speleothem and most probably also above trench one. The last very thin layers of the speleothem are of Holocene age. The dating of the speleothems in the cave constrain the age of the paleontological and archaeological findings in trench one before the deposition of the thick powdery carbonate layer, thus at least before ~ 115 ka. The calcite crust in trench one that corresponds to the crust embedding a complex of bear skulls and bones inside this trench give an age close to 130 ka which suggest a minimum age for the bear complex of ~130 ka, while the crust underneath the bear complex was dated ~250 ka, indicating a maximum age for the bear complex. The 'calcitic crusts' in the upper part of trenches two and four, dated between ~130 and 120 ka, are clearly well preserved thin flowstones covering the underlying sediments and indicating the existence of a palaeosurface close to nowadays during MIS 5e (~130 to 120 ka) in the cave.

5. Conclusions

Speleothems are powerful tools to constrain the chronology of cave findings there where in these environments the stratigraphic correlation remains difficult due to the complex cave sedimentology. The study of the Mishin Kamik speleothems revealed an age of at least 115ka and possibly of at least 130 ka for the paleontological and archaeological findings in the cave as well as a maximum age of 250 ka for the bear complex.

References

- Angelov, V., Hajdutov, I., Yanev, S., Tronkov, D., Sapunov, I., Tchumachenko, P., Tsankov, T., Popov, N., Dimitrova, R., Nikolov, T., Aladzhoa-Hrischeva, K. & Filipov, L., 1995. Geological map of Bulgaria in scale 1:100 000; Map part: Belogradchik, Sofia, KGMR Geology and Geophysics GmbH.
- Gurova, M., Ivanova, S., Krumov, I., Spassov, N., Hristova, L. & Dojare, K., 2015. Investigations at Mishin Kamik Cave. Archaeological discoveries and excavations in 2016. Sofia, 32-34. (in Bulgarian).
- Ivanova, S., Krumov, I., Spassov, N., Hristova, L., Makedonska, J., Gurova, M. & Strait, D., 2014 Excavations at the cave Mishin Kamik, Tchiprovska. Archaeological discoveries and excavations in 2014. Sofia, 31-34. (in Bulgarian).

INDEX OF AUTHORS

ADGO Enyew	208
ADRIAENS Rieko	82
AGNIEL Mathieu	172
ALFARRAH Nawal	204,211
ALVAREZ Denisse	239
AMANN-HILDENBERAND Alexandra	134,148
AMARE Kassa	211
ARATMAN Cihan	128,165,222
ARKHANGELSKY Maxim	242
BABA HAMED Samira	205
BAELE Jean-Marc	84,86,132
BARBIER Christian	55
BARDET Nathalie	242
BARRIÈRE Julien	48,50
BASTIAENS Jan	30
BECK Christian	40
BECKERS Arnaud	40
BEERTEN Koen	30,174, 225
BEJARANO-URREGO Leidy	55
BENNETT George	209
BENSON Roger	242
BERHANE Gebremedhin	211
BERTIER Pieter	114,117,134
BEUNON Hugues	60
BEYSSAC Olivier	132
BIBENTIYO Toussaint Mugaruka	35,47
BILLY Isabel	239
BISDOM Kevin	134
BLIECK Alain R. M.	227
BLOCKMANS Sabine	136
BLYKERS Benjamin	212
BOLLE Olivier	71,77,79
BOS Stijn	170,215
BOULVAIN Frédéric	125,142,239,252,255,262
BOURDET Julien	142
BOUSSEN Slim	153
BRANCART Joost	110
BRASSINES Stéphane	130
BREULS Ton	144
BRONDERS Jan	218
BROOHAERS Matsen	88,215
BROUYERE Serge	193
BRUGGEMAN Christophe	148
BRUNEEL Yaana	130

BUFFEL Pieter	33
BULS Nico	110
BULTREYS Tom	212
BURLET Christian	52,57,172,174
BUSCH Andreas	114,134
CALUWAERTS Steven	37
CAPPUYNS Valerie	170
CASIER Jean Georges	228
CAUDRON Corentin	50
CHARLET Frederic	43,134
CHARLIER Bernard	62
CHEN Margaret	208
CHI FRU Ernest	140
CHOUABBI Abdelmadjid	140
CLAEYS Philippe	63,65,75,231,283
CLARK Alexander	231
CNUUDE Veerle	90,114,212,274
COBERT Corentin	84,132
COLLART Tim	254
COLLIN Frédéric	159
COMPERNOLLE Tine	176,196
COOLS Catherine	271
CORLUY Jan	138,174
COUMONT Valentin	71
CROMBÉ Philippe	274
CROONENBORGHES Thibauld	55
CROSDALE Peter	142
D'OREYE Nicolas	48
DA SILVA Anne-Christine	142
DAOUDI Lahcen	271
GUILBERT Daphne	37
DASSARGUES Alain	193
DAWSON Sue	93
DE BATIST Marc	40,244,254,265
DE CEUKELAIRE Marleen	174
DE CLERCQ Maikel	265
DE CLERCQ Pierre-Yves	32
DE CRAEN Mieke	103,106,146,174
DE GRAAFF Sietze	63,65,75
DE GRAVE Johan	212
DE KOCK Tim	37,90,212,274
DE KONINCK Roel	138
DE NIL Katrien	138,174
DE ROUCK Tinne	138

DE ROY Judy	276
DE SCHAEZTEN Caroline	33
DE WINTER Niels	75,231
DEAN Marcella	138
DEBACKER Timothy	88,122,174
DEBAILLE Vinciane	201
DEBOUT Laurent	233
DEBRET Baptiste	60
DECKERS Jef	88,110
DECLERCQ Pierre-Yves	55,174
DECRÉE Sophie	132,174,201
DEGRYSE Patrick	267,281,283
DÉHAIS Thomas	63,65,75
DEKONINCK Augustin	136
DELABY Serge	54
DELLE PIANE Claudio	142
DELVAUX Damien	35,67,157
DEMOULIN Alain	40,45
DENAYER Julien	233,234
DEPREZ Maxim	90
DERAUW Dominique	55
DESBOIS Guillaume	103,106
DESCAMPS Fanny	167
DESCHUTTER Geert	90
DESMET Nele	218
DESSIE Mekete	208
DEVLEESCHOUWER Xavier	32,125,172,174,262
DEWAELE Stijn	67,69,155,181,186,188,199
DEWITTE Olivier	35,47
DIAB Hamida	140
DILLE Antoine	35,47
DILLIS Sarah	267
DIOT Hervé	79
DIRIX Katrijn	112
DJOUDEH Hocine	142
DOPERE Frans	269
DOSTER Florian	134
DOUBRAWA Monika	237
DOUCET Luc-Serge	60
DREESSEN Roland	269
DROUGKAS Anastasios	55
DRUCKENMILLER Patrick	242
DUPONT Nicolas	43
DUSAR Michiel	144,269

DUTRIEUX Adeline	71
EL HALIM Mouhssin	271
EL OUHABI Meriam	252,271
ELBASBAS Addelaziz	190
ELHARKATY Mohamed	190
ELSEN Jan	146,279
ENGEL Max	93
ESSGHAIER GAIED Mohamed	153
EVERAERTS Michel	43
FAGEL Nathalie	96,153,159,205,239,271
FERKET Helga	88,174
FERNANDEZ-ALONSO Max	67
FIERENS Eric	218
FIERS Géraldine	274
FINK Reinhard	134
FISCHER Valentin	242
FONTAINE François	96
FONTAINE Laurent	276
FONTIJN Karen	209
FRANCOIS Bertrand	172
FREDERICKX Lander	146
FUJIWARA Osamu	244
GALLAND Olivier	110
GANEROD Morgan	71
GANZA Gloire Bamulezi	35,67
GARRETT Ed	93,244
GAUDARE Louis	172
GEBREYOHANNES Tesfamichael	211
GEDEON Matej	174
GEIGER Sebastian	134
GEORGIADOU GAVRILOVIC Ioulia	201
GERARD Pierre	172
GODERIS Steven	63,65,75
GODERNIAUX Pascal	43
GOEMARE Eric	174
GONZE Kevin	43
GONZE Nicolas	167
GOOLAERTS Stijn	98,125
GOOVAERTS Thomas	125,174,262
GOUWY Sofie	125
GRADE Arno	225
GROVE Timothy	62
GUENDOZ Mostefa	252
GUROVA Maria	285

GYSELEN Rika	283
HADJ HASSINE Seif Ben	114
HADJIGEORGIOU Christodoulos	201
HAEST Pieter	100
HAEUSSLER Peter	254
HAGOS Miruts	211
HALBRUCKER Eva	274
HARCOUET-MENOU Virginie	215
HATERT Frédéric	96,136,271
HAVENITH Hans-Balder	45
HAYEN Roald	55
HEBINCK Koen	225
HERBOSCH Alain	122
HEUVELMANS Griet	174
HEYVAERT Vanessa	93,174,244
HOCQUET François-Philippe	55
HOFMAN Corine	281
HOLLIS Cathy	128
HOLLIS Dave	110
HOLOHAN Eoghan	110
HOLTZ Francois	62
HONTY Miroslav	146
HUBERT- FERRARI Aurelia	40,50,72,252
HULSBOSCH Niels	69,181,186,188
HURST Sheryl	134
HUSSIEN Abdelwassie	211
HUYBRECHTS Roel	100
HUYSMANS Marijke	100,103,106
ILOMBE Guy Mawe	35,67
IVANOVA Stefanka	285
JACOPS Elke	148
JACQUES Dominique	151
JACQUES Diederik	103,106
JANSSENS Nick	148
JAUBERT Jacques	52
JEBRAK Michel	157
JORIS Ingeborg	218
KALIKONE Christian Buzera	35,67
KAMATE KALEGHETSO Ephrem	72
KAMPMAN Niko	134
KAPUTO Alphonse	157
KARVAR Gamze	222
KASKES Pim	63,65,75
KASSE Cornelius	30

KAUFMANN Olivier	43
KEMPF Philipp	93,244,254
KERVYN François	35,48,50,72
KERVYN Mathieu	35,110,209
KETCHUM Hilary	242
KIPATA Louis	155,157
KISAKA Mary	209
KLOPPMANN Wolfram	276
KOENEN Kris	162
KROOSS Bernhard	117,134,148
LACQUEMENT Frédéric	84
LAENEN Ben	174,183,215
LAFORCE Brecht	274
LAGHMOUCH Mohamed	67
LAGROU David	144,183,215
LALOY Eric	103,106
LAMBERT Olivier	242
LECOCQ Thomas	52
LEDUC Thierry	174
LEMMENS Laurent	103,106
LEVASSEUR Severine	114
LIDSTONE Andy	134
LITTKE Ralf	148
MAACHA Lhou	190
MAALLA Imen	153
MADI Atman	190
MAES Norbert	114,148
MAKITO Evelyne Safari	35
MAMBWE Pascal	155,157
MANGO ITULAMYA Lavie Arsène	159
MARINOVA Elena	285
MARTENS Lise	247
MARTIN Frank	43
MARTIN Thierry	43
MARTINEZ Mathieu	262
MARTINEZ Philippe	239
MATHUR Ryan	201
MATHYS Mieke	265
MATTHIJS Johan	249
MATTIELLI Nadine	60
MELCHER Frank	186
MERTENS Gilles	82
MESTDAGH Thomas	30
MEYLEMANS Erwin	30

MEYVIS Bruno	162,196,262
MICHELIERS Caroline	48
MISSIAEN Tine	265
MOERNAUT Jasper	254
MOGESS Michael	208
MOHAMMADI Zahra	128,165
MOINE Bertrand	60
MONDELAERS Alexander	188
MONIÈ Patrick	136
MONSIEURS Elise	35
MONTALBANO Salvatrice	77
MORENO David	265
MORETTI Michele	196
MORTIER Jan	122
MOULANA Meriem Lina	252
MOZAFARI Mahtab	165
MREYEN Anne Sophie	45
MUCHEZ Philippe	69,151,155,157,181,183,186,188,199
MUGISHO Espore	67
MUGUNGA Gustave	48
MUKOKYA Yogolelo	67
MUSHAMALIRWA Toussaint	67
NACER Djamel-Eddine	140
NAERT Martijn	33
NAHIMANA Louis	181
NAMUR Olivier	62,71,72,77,239
NDONGALA Makeba	167
NEEFS Ben	119
NEYT Bert	281
NIELSEN Peter	179
NILA Alex	110
NYSSSEN Jan	208
NZOLANG Charles	67
ONUK Peter	186
OP DE BEECK Sander	75
ORBAN Philippe	193
OTH Adrien	50
OUMMOUCH Abdellah	190
OUMOHOU Lahcen	190
OVERLAET Bruno	283
OZKUL Mehmet	128
PAPATHEODOROU George	40
PAREDIS Bram	108
PATEL Tasnim	93

PATIGNY Géraldine	276
PATYN Johan	218
PAUWELS Jente	170
PEDREROS Pablo	239
PETITCLERC Estelle	172,174
PIESSENS Kris	57,119,162,174,176,196
PILATE Pascal	96
POPPE Sam	110
PRAET Nore	254
RACHDI Mouna	255
RADEMAKERS Frederik	283
RAMANAÏDOU Erick	142
REBOUH Leila	271
REZAEYAN Amirsaman	114
ROBINSON Marci	237
ROCHEZ Gaëtan	136
ROEFS Pieter	196
ROGIERS BART	103,106,174
ROMBAUT Bernd	88,112
ROUSSEAU Valérie	271
SAFARI Evelyne	67
SAKELLARIOU Dimitris	40
SALAH Sonia	170
SANYOVA Jana	276
SATOLI Sara	262
SCAFF Laurie	271
SCHMIDT Sabine	239
SCHNYDER Johann	262
SCHURMANS Miel	225
SEEMANN Timo	114,148
SEGERS Laura	209
SEUNTJENS Piet	218
SEWALA BELAY Ashebir	208
SHEMSANGA Ceven	209
SHIMONI Michal	55
SHÖN Isa	93
SHU Changxue	279
SINTUBIN Manuel	151
SLENTER Cis	174
SLUIJS Appy	260
SMETS Benoît	35,48,72
SMIT Jan	75
SMOLDERS Erik	130
SNELLINGS Ruben	179

SNIPPE Jeroen	134
SOUL Laura	242
SOUSSI Mohamed	255
SPEIJER Robert	231,237,247,257,260
SPIKINGS Richard	186
STANJEK Helge	117
STASSEN Peter	231,237,247,257
STENSHIN Ilya	242
STEURBAUT Etienne	247,257
STEYAERT Lore	48
STIENAERS Anneleen	281
SUBIRA Josué	50
SWENNEN Rudy	103,106,128,148,165,183,196,222
SYAVULISEMBO Adalbert	48
SZCZUCINSKI Witold	93
TASGIN Calibe Koç	222
TAYLOR Rochelle	128
THÜNS Nicolai	117
TILAHUN Seifu	208
TODD Andrew	142
TRIANAFYLLOU Antoine	84
TRIPSANAS Efthymios	40
TSIBANGU Jean-Pierre	167
TURIMUMAHORO Denis	181
URAI Janos	103,106
URRUTIA Roberto	239
USPENSKY Gleb	242
UYSAL Tonguç	142
VAN BAELEN Hervé	100
VAN BALEN Koen	55,279
VAN DAELE Johanna	186,188
VAN DAELE Maarten	254
VAN DAMME Marleen	100,138,174
VAN DE WAUW Johan	100
VAN DER MEER Wouter	225
VAN DER VOET Eva	183
VAN GOMPEL Gert	110
VAN HAM MEERT Alicia	267,283
VAN HERREWEGHE Samuel	33
VAN HOEY Stijn	100
VAN KEER Ilse	218
VAN LAER Liesbeth	130
VAN LYSEBETTEN Gust	172
VAN NEER Wim	285

VAN NOTEN Koen	52,119,174
VAN REYBROUCK Jill	209
VAN ROOIJ David	30
VAN ROSSUM Paul	134
VANBRABANT Yves	57,174
VANDEKERKHOVE Elke	254
VANDER AUWERA Jacqueline	71,72,77,79
VANDIJCK Ruben	63
VANDYCKE Sara	167
VANLOOK Linde	237
VANMAERCKE Matthias	47
VANMEIRHAEGHE Jan	122
VELLEKOOP Johan	231,260
VERHAERT Michèle	190
VERHEYDEN Sophie	52,57,285
VERNIERS Jacques	122
VERSTRYNGE Els	55
VOPAT Olivier	193
VOS Johan	218
WALRAEVENS Kristine	204,208,209,211
WALSCHOT Luck	144
WALSTRA Jan	32,55,174
WAZI Robert	67
WELKENHUYSEN Kris	57,162,174,196
WELTJE Gert Jan	108,123
WILKINSON Camilla	71
WILLIAMSON Paul	88
WOUTERS Sander	199
WOUTERS Sébastien	262
WYNANTS Marc Aurèle	125
YANS Johan	136,190
YOKOYAMA Yusuke	244
ZARONIKOLA Nina	201
ZIHMS Stephanie	134
ZVERKOV Nikolay	242

